Electro-reflectance in conducting thin films in the infra-red

ELECTRO - REFLECTANCE IN CONDUCTING THIN FILMS IN THE INFRA - RED

Author: John N. Avaritsiotis

Supervisor: Dr. R. P. Howson

Submitted for Ph.D. degree of

Loughborough University of Technology

Date of submission 1976

"ἐὰν ᾖς φιλομαθὴς, ἔσῃ πολυμαθής"

Ἰσοκράτης

"If you love learning, you will soon be full of learning"

Isocrates

Greek Rhetorician, 436 - 338 B.C.

CONTENTS

ACKNOWLEDGEMENTS

The author wishes to express his gratitude to his supervisor, Dr R. P. Howson, for his helpful guidance, constant encouragement, and keen interest.

The author also wishes to express his gratitude to:

a) Stathatos Foundation for the award of a postgraduate scolarship, and

b) Science Research Council for the award of a grant which enabled him to set up the apparatus for the electro-reflectance measurements.

Further acknowledgement is due to Professor K. L. Chopra for a long conversation in connection with thin-film fabrication techniques and the optical properties of GeTe films.

Thanks are due to Thorn Lighting Co (Leics) for the preparation of tin-doped indium oxide films, and Plessey Co Ltd (Towcester) for the donation of a variety of sputtered, tin-doped indium oxide films and a tin-doped gallium arsenide wafer.

Finally the author wishes to express his gratitude to his wife, Rea, for her constant encouragement.

LIST OF PRINCIPAL SYMBOLS

C	Capacitance
c	Velocity of light
d	Film thickness
E	Electric field amplitude
e	Electronic charge
I	Intensity
K	Propagation constant
k	Extinction coefficient
ℓ	Thickness of the enhanced layer
m_e	Electron mass
m_r^*	Free carrier relative mass (scalar)
m_r	Free carrier effective mass
N	Free carrier concentration
n	Refractive index
q	Free carrier charge
R	Reflectance
r	Fresnel's reflection coefficient
V	Voltage
Y	Optical impedance
δ	Phase angle
ε_o	Permitivity of free space
ε_L	Lattice dielectric constant
Θ	Angle
λ	Wavelength
λ_p	Plasma wavelength
μ	Optical mobility
μ_o	Permeability of free space

ν	Wavenumber
τ	Free carrier relaxation time
Φ	Angle
ω	Angular frequency
ω_p	Plasma frequency

C H A P T E R 1

INTRODUCTION

It is well established that when the surface of a conducting material contains an excess charge created by an external electric field, a modulation of the reflectance spectrum occurs. Electric-field modulation techniques of the reflectivity are used for a) the elucidation of optical structure associated with critical points [Cardona (1969)] and b) the study of modulation effects of intraband transitions near the plasma frequency [Seraphin (1972)].

There exists an essential difference between the former and latter concept : The former one is known as the Franz - Keldysh effect [Keldysh (1958)] and is concerned with the effect of strong electric fields on the optical properties of insulating or semiconducting materials in spectral regions where $\omega \gg \omega_p$, whereas the latter is associated with free carrier effects. Due to the nature of the experimental techniques employed the Franz - Keldysh effect is observed when the penetration depth of the radiation is less than the depth of the perturbation, whereas the effect, associated with intra - band transitions, is observed when the depth of perturbation is very much less than the penetration depth of the incident radiation.

However, the same term (ELECTRO-REFLECTANCE) has been used for both of these effects. Most electro-reflectance experiments have been carried out in the visible and UV parts of the electromagnetic spectrum. Axe and Hammer (1967), however are the only research workers who observed a qualitative modulation peak in the IR and in the vicinity of the reflectance plasma edge of Ge and tin - doped GaAs. Large absorption corrections were required due to the absorption by the saturated methanol - NaCl electrolyte solution used. Their results were not reproducible, but indicate that a rather large effect should be expected.

The scope of the work reported here was to extend ER studies associated with free electron effects into the near IR and obtain valuable quantitative results in order to develop and evaluate a microscopic theory.

The theory proposed is analysed in Chapter 2. The effect of the free carrier parameters on the magnitude and shape of the ER spectrum is studied. A summarized verification of the calculated results is given for the visible and ultraviolet spectral regions. Chapter 3 includes the experimental techniques employed to measure quantitatively the ER spectra of various materials, in the near IR. The ER spectra of GeTe films are given in Chapter 4 for both Internal and External Reflection Spectroscopy. Chapter 5 includes the experimental and calculated results for SnTe films for both IRS and ERS.

Chapter 6 describes the theoretical and experimental ER spectra of tin-doped indium oxide films and a comparative study of D.C. sputtered and Chemically (CVD) fabricated films.
Also it was found necessary to develop a computer technique for the evaluation of the Drude - model parameters from reflectivity data around the plasma edge. The features and limits of the technique are discussed in Appendix D.

Finally, Chapter 7 summarizes the results of the investigation and indicates fruitful areas of further research.

REFERENCES

1. Cardona M."Modulation spectroscopy", Solid State Physics, Suppl. 11, Academic Press,1969.

2. Keldysh L.V.,Soviet Physics JETP 34, 788 (1958).

3. Seraphin B.O. Modulated Reflectance Chapt.4, "Optical Properties of Solids" edit. by Abelès North Holland Co. 1972.

CHAPTER 2

THEORY

2.1 Introduction

Several semi - empirical models have been developed for the explanation of the electroreflectance effect in metals.

Hansen andProstak, (1967) proposed that when an electric field is applied across the surface of the sample the free electron concentration of the metal is changed. The shift in the free electron concentration causes a change in the plasma frequency ω_p, where:

$$\omega_p^2 = \frac{N e^2}{m_r^* \; m_e \; \varepsilon_o \; \varepsilon_L}$$

In other words a rigid - shift of the plasma edge is assumed. The rigid shift model yields an electro - reflectance spectrum which simply is a normalized first - derivative of the reflectivity with respect to wavelength. So, for a metal like silver, which exhibits a pronounced reflectivity minimum at about $0.325 \; \mu m$, peaks of both signs should occur in the electro - reflectance spectrum. McIntyre (1973), however, experimentally showed that the spectral response of $\Delta R / R$ for silver exhibits only one peak at the vicinity of the reflectivity minimum.

The above model was subsequently refined by Hansen and Prostak (1968). They proposed that the optical constants of the metal are shifted along the energy axis, by the same fraction that ω_p is shifted, by the application of a low - frequency electric field on the surface of the metal. However , a plasma frequency shift does not induce a uniform shift of the real and imaginary part of the dielectric constant, along the energy axis. The shift is not rigid but varies with the photon energy ,

and generally is a rather complicated function of photon energy. Thus, the model employed by Hansen and Prostak would be practically applicable only over very narrow frequency intervals, i.e. when $\omega \simeq$ constant.

McIntyre and Aspnes (1971) proposed a model based on a first - order approximation for the reflectance change of a two - phase system produced by the generation of a thin intermediate (transition) region of thickness $d << \lambda$, whose the complex dielectric constant varies continuously between two limiting values, in a direction normal to the surface plane of the metal. A mean perturbation of the dielectric constant is defined by averaging its local change over the transition region and assuming that the part of dielectric constant due to the contribution of bound electrons is not altered by the applied low-frequency electric field. The McIntyre - Aspnes model is independent of the actual form and thickness of the surface charge distribution induced by a low-frequency electric field and quantitatively accounts for the electro-reflectance spectrum of silver and gold.

However, the perturbation of the complex dielectric constant has arbitrarily been defined as

$$\Delta\bar{\varepsilon}(z) = (\varepsilon_f - 1) \frac{\Delta N}{N}$$

This implies that ε_L, i.e. the lattice dielectric constant of the metal is 1; but this is generally not valid.

Thus,it may be argued that quantitative and qualitative discrepancies observed by McIntyre (1970), between his experimental and calculated electroreflectance spectra of silver and gold can be mainly attributed to the fact that the lattice dielectric constant has arbitrarily been

taken equal to 1.

Kofman, Garrigos and Cheyssac (1974) developed a model based on the following assumption: When a constant electric field is applied in a direction normal to the surface of the metal the free electron concentration at the surface increases so that the total electric field "inside" the metal vanishes. If an electromagnetic wave falls upon the metal, the excess electrons are forced by the electric field of the wave to move, giving rise to a surface current density. This surface current density is taken into account in the boundary conditions for the magnetic field at the surface of the metal.
The main handicap of that model is that the thickness of the perturbed layer is used as a scaling factor to obtain the best agreement with the experimental results for gold, silver and cooper. However, their interpretation is consistent because the values of the perturbed-layer thickness required for a good fitting of the experimental results are in agreement with the values predicted by the Thomas - Fermi theory.

Anderson and Hansen (1973) proposed a model which takes into account contributions from bound electrons. They assumed that the low frequency electric field creates an exponential band bending but it does not affect the Fermi level, which remains unchanged. The excess charge distribution (ρ) at the surface of the metal is calculated as a function of the distance (r) from the surface of the metal, from Poisson's equation in the same manner as the electrostatic screening length; this gives

$$\nabla^2 \Phi(r) = 4 \pi e \left[n (r) - n (o) \right]$$

where $\Phi(r)$ is the electrostatic potential, and $n(r) - n(o)$ is the deviation from uniform electron concentration. The reflectance, finally, of a metallic film with band-bending at the surface is calculated by dividing the surface region into a series of thinner films, each with a different set of optical constants. Knowing the dielectric constant of the metallic film having no surface charge, the change of reflectance can be calculated by substracting the latter from the former.
It has recently been claimed by Bewick and Robinson (1975) that the published details of this model contain a number of errors in the equations.

Finally, Howson, Avaritsiotis and Fox (1975) have shown that film thickness and changes in structure of thin films can strongly affect the shape and magnitude of the electro - reflectance effect.

However all these models are supported by only a limited number of measurements in the visible and near ultra - violet (silver) regions of the electromagnetic spectrum; only three metals have been studied:gold, silver and cooper.

In investigating different materials for an effect in the near infrared it has become obvious that the electro - reflectance spectrum depends to a large extent on the properties of free carriers.
Consequently it becomes necessary to derive an expression for the electro-reflectance in terms of the properties of the free carriers, i.e. carrier density, effective mass, relaxation time and lattice dielectric constant.

2.2 A New Model

When a static or low - frequency electric field is applied onto the surface of a conducting material a distribution of excess free carriers is generated in the vicinity of the surface; the depth , ℓ , of the perturbation depending on the free carrier density of the material and the strength of the field.

If $\ell << \lambda$ (where λ is the wavelength of the electromagnetic wave used as a probe, detecting changes of the optical properties of the interface), the optical behavior of the perturbed metal may be described in terms of a three-phase system consisted of two semi - infinite phases, and an ultra - thin intermediate region of enhanced carrier density; fig.(2.1). This is a widely accepted approximation firstly adopted by Hansen and Prostak, (1967). As far as the validity of the inequality $\lambda \gg \ell$ is concerned, ℓ is always much less than the wavelength of the incident electromagnetic radiation in a wide spectral region around the plasma edge, where the optical properties of the material are dominated by intra-band transitions.

An expression for electro - reflectance in bulk materials will be obtained by introducing the concept of optical impedance. Consideration will be given to the normal incidence only.

Since the magnetic (H) and electric (E) vectors of the incident electromagnetic radiation are continuous , at the interfaces, the optical impedance Y may generally be defined as:

$$(2.1) \qquad Y = \frac{E}{H} = \left(\frac{\mu_r \mu_o}{\varepsilon_r \varepsilon_o} \right)^{\frac{1}{2}} = \frac{(\text{const.})}{n} \text{ ohms} .$$

Heavens (1965) or Ramo, Whinery, and Van Duzer, (1965) give the impedance

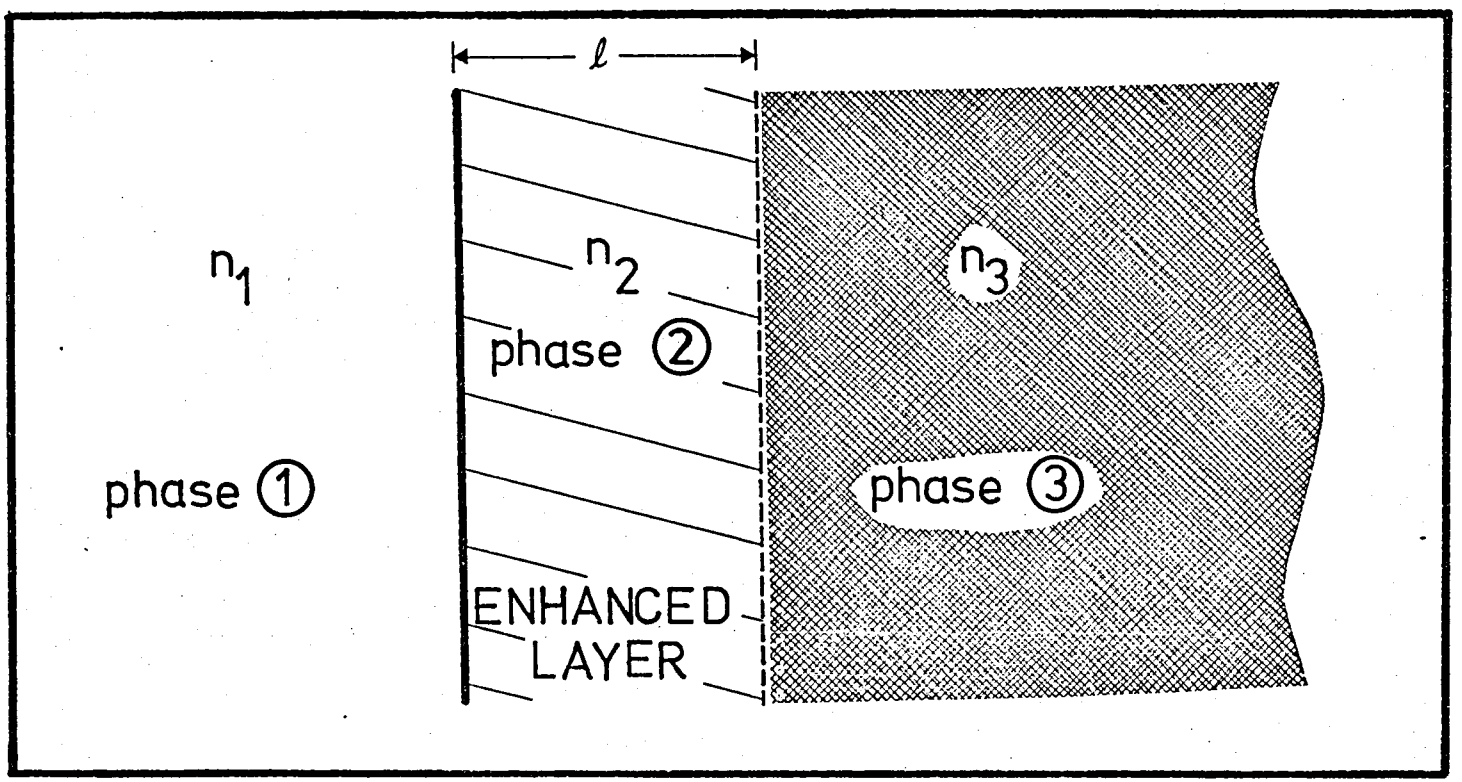

Fig.(2.1) Schematic illustration of the enhanced - layer configuration.

of the intermediate phase of a three phase system as

$$Y_i = \frac{Y_3 \cos K_2 \ell + j Y_2 \sin K_2 \ell}{Y_2 \cos K_2 \ell + j Y_3 \sin K_2 \ell} \tag{2.2}$$

where Y_2, Y_3 are the optical impedances of the enhanced layer and bulk material respectively, K_2 is the propagation constant in the enhanced layer and ℓ is its thickness. The propagation constant is generally given by

$$K_i = \frac{n_i \omega}{c} = \frac{2 \pi n_i}{\lambda} = K_i' + jK_i'' \tag{2.3}$$

where n_i is in general complex.
The refractive index of phase 1, however, is considered to be a real number. If $K_2' \ell \ll 1$, and $K_2'' \ell \ll 1$ eq.(2.2) may be written as

$$Y_i = Y_3 \left[1 + jK_2 \cdot \ell \left(\frac{Y_2}{Y_3} - \frac{Y_3}{Y_2} \right) \right] \tag{2.4}$$

In the case of weak perturbations the enhanced layer has a refractive index only slightly changed from that of the bulk material, such that

$$n_2 = n_3 + \Delta n_3 \tag{2.5}$$

Consequently, substituting eqs. (2.1) and (2.5) into eq. (2.3) gives

$$Y_i = Y_3 (1 - 2 j \omega \ell \Delta n_3 / c) \tag{2.6}$$

providing that n_2 / n_3 is $\ll 1$, i.e. that the real and / or imaginary part of n_3 are not close to zero.

The amplitude reflection coefficient, or in other words the Fresnel coefficient of the system is given by:

$$r = \frac{Y_i - Y_1}{Y_i + Y_1} \tag{2.7}$$

where Y_1 is the optical impedance of the electrolyte equal to (const.) / n_1 , ohms. Substituting eq.(2.6) into eq.(2.7) gives:

$$r = \frac{(n_1 - n_3) - 2j \frac{\omega}{c} n_1 \ell \Delta n_3}{(n_1 + n_3) - 2j \frac{\omega}{c} n_1 \ell \Delta n_3} \tag{2.8}$$

The coefficient of amplitude reflection for the unperturbed material, i.e. a two phase system, is given by:

$$r_o = \frac{n_1 - n_3}{n_1 + n_3} \tag{2.9}$$

Substituting eq.(2.9) into eq. (2.8) gives

$$r = r_o + 2j \frac{\omega}{c} n_1 \ell \Delta n_3 r_o \left(\frac{1}{n_1 + n_3} - \frac{1}{n_1 - n_3} \right) \tag{2.10}$$

or

$$\frac{r}{r_o} = 1 + 4j \frac{\omega}{c} \ell \Delta n_3 \frac{n_1 n_3}{n_3^2 - n_1^2} \tag{2.11}$$

For small perturbations we may write

$$r = r_o + \Delta r \tag{2.12}$$

Substituting eq.(2.12) into eq. (2.11) gives

$$(2.13) \qquad \frac{\Delta r}{r_o} = 4\, j \frac{\omega}{c}\, \ell \Delta n_3 \left(\frac{n_1 n_3}{n_3^2 - n_1^2} \right)$$

An expression for the change of refractive index will be found next. The complex dielectric constant of the free carrier material is in general given as

$$(2.14) \qquad \varepsilon_3 = n_3^2 = \varepsilon_{3F} + \varepsilon_{3B}$$

where ε_{3B} is the contribution from the bound electrons and ε_{3F} the contribution of the free carriers and is generally expected to be a function of frequency. The latter can be expressed according to Drude's model as

$$(2.15) \qquad \varepsilon_{3F} = \varepsilon_L \left(1 - \frac{\omega_p^2}{\omega^2 + j\omega\tau^{-1}} \right)$$

where ε_L is the lattice dielectric constant, τ is the relaxation time of the free carriers and ω_p is the plasma frequency given by

$$(2.16) \qquad \omega_p^2 = \frac{N e^2}{m_r^* m_e \varepsilon_o \varepsilon_L}$$

From eqs. (2.14), (2.15), and (2.16) an expression for Δn_3 can be obtained, given by

$$(2.17) \qquad 2 n_3 \Delta n_3 = (\varepsilon_{3F} - \varepsilon_L) \frac{\Delta N}{N}$$

Substituting in eq. (2.13) gives

$$(2.18) \qquad \frac{\Delta r}{r_o} = 2\, j \cdot \frac{n_1\, \omega\, \ell\, \Delta N}{c\, N} \left[\frac{\varepsilon_{3F} - \varepsilon_L}{\varepsilon_3 - \varepsilon_1} \right]$$

The quantity $\ell \cdot \Delta N$ represents the change of surface carrier density due to the application of a low frequency electric field on the surface of the conducting material. If we assume that the electric field is applied with the aid of a capacitive configuration, (and this is always the case in practice), the latter quantity can be expressed as

$$\ell \cdot \Delta N = \frac{C V}{q} \tag{2.19}$$

where C is the capacitance per unit area, V is the applied voltage, and q is the free carrier charge. Substituting eq.(2.19) into eq.(2.18) gives

$$\frac{\Delta r}{r_o} = 2 j \frac{n_1 \omega C V}{c N q} \cdot \frac{\varepsilon_{3F} - \varepsilon_L}{\varepsilon_3 - \varepsilon_1} \tag{2.20}$$

Finally the energy reflected by the unperturbed system is given from

$$R = r_o r_o^* \tag{2.21}$$

So,

$$\frac{\Delta R}{R} = \frac{\Delta r^*}{r_o^*} + \frac{\Delta r}{r_o} \tag{2.22}$$

where:

$$\frac{\Delta r^*}{r_o^*} = - 2 j \frac{n_1 \omega C V}{c N q} \cdot \frac{\varepsilon_{3F}^* - \varepsilon_L}{\varepsilon_3^* - \varepsilon_1} \tag{2.23}$$

Substituting eqs. (2.20) and (2.23) into eq.(2.22) we obtain:

$$\frac{\Delta R}{R} = \frac{4 \omega n_1}{N c q} \cdot Im \left[\frac{\varepsilon_{3F} - \varepsilon_L}{\varepsilon_3 - \varepsilon_1} \right] C V \tag{2.24}$$

Eq.(2.24) may finally be written as:

$$(2.25) \qquad \frac{\Delta R}{R} = \frac{4\, n_1\, q\, \tau}{c\, m_r^*\, m_e\, \varepsilon_o} \left[\frac{-\varepsilon_A + \varepsilon_1 + \varepsilon_B\, \omega\, \tau}{(\omega^2 \tau^2 + 1) \cdot \left[(\varepsilon_A - \varepsilon_1)^2 + \varepsilon_B^2 \right]} \right] C \cdot V$$

where:

$$(2.26) \qquad \varepsilon_3 = \varepsilon_A - j\, \varepsilon_B = (n^2 - k^2) - 2\, j\, n\, k$$

n and k being the refractive index and extinction coefficient of the bulk material. The expression in brackets determines the shape of the electro-reflectance spectrum. The magnitude of the effect is dominated by the terms outside the brackets: i.e. by the relaxation time, the relative optical mass, the capacitance , and the applied voltage.

Eq. (2.25) is applicable in the case of any real material because ε_A and ε_B , involve contributions from both intraband and interband transitions. In this model it is assumed implicitly that bound electron states are not affected by the applied electric field; only the plasma frequency of the free carrier gas in the enhanced layer is shifted. The influences of interband transitions appear only indirectly through their contribution to the bulk dielectric constant which is not modulated by the low - frequency electric field.

The mathematical result of our assumption is independent of the thickness of the enhanced layer and distribution of the excess free carrier density at the surface of the material. In other words, when $\ell \ll \lambda$ and to first order approximation, the magnitude of electro - reflectance is insensitive to the screening length and the actual charge - distribution profile.

The magnitude of the effect is linearly dependent on both the applied

voltage and the capacitance which is used in practice to generate the electric field responsible for the perturbation of the surface optical properties of the material under investigation.

In this treatment, no specific model has been assumed for the structure of phase 1 of fig.(2.1)at the neighbourhood of the enhanced layer. The optical modulation effects are assumed to be solely due to a perturbation of the free carrier density at the surface. Although idealized this assumption lays on a pragmatic basis: As a general rule phase 1 of fig.(2.1) is transparent in the range of optical measurements. Consequently since the frequency dispersion of its dielectric constant is small and monotonic, we can safely assume that the primary origin of the sharp peaks observed in the experimental ER spectra may be attributed to the pronounced structure of the optical constants of the metal,McIntyre(1973).

2.3 Implications of the Present Model

We are seeking a simplified version of eq. (2.24) in order to elucidate the role of the optical parameters (i.e. ε_L, m_r^* , τ , n ,) of our system, in the determination of magnitude and spectral response of the ER effect.

It is assumed that the peak of the ER effect occurs in the vicinity of the plasma frequency; this assumption will be verified later on theoretically and experimentally. If ω_{PEAK} is the frequency corresponding to the peak value of the ER spectrum, then

$$\omega_{PEAK} = \omega_p + \Delta\omega$$

where $\Delta\omega \ll \omega_p$; ω_p being the plasma frequency of the material under investigation. Moreover, if we assume that $(\omega_p \tau)^{-1} \ll 1$, eq.(2.15) can approximately be written as

$$\varepsilon_3 \simeq \varepsilon_L \left[\frac{2\Delta\omega}{\omega_p} + j\,(\omega_p \tau)^{-1} \right] \tag{2.27}$$

Consequently for Drude - type materials

$$\frac{\varepsilon_3 - \varepsilon_L}{\varepsilon_3 - \varepsilon_1} \simeq \frac{2\Delta\omega + j\tau^{-1} - \omega_p}{2\Delta\omega + j\tau^{-1} - \dfrac{\omega_p \varepsilon_1}{\varepsilon_L}} \tag{2.28}$$

The imaginary part of eq. (2.28) is

$$\mathrm{Im}\left(\frac{\varepsilon_3 - \varepsilon_L}{\varepsilon_3 - \varepsilon_1} \right) = \frac{\tau \omega_p \left(1 - \dfrac{\varepsilon_1}{\varepsilon_L} \right)}{\tau^2 \left(2\Delta\omega - \dfrac{\omega_p \varepsilon_1}{\varepsilon_L} \right)^2 + 1} \tag{2.29}$$

The right - hand side of the latter equation becomes maximum when

$$\Delta\omega = \Delta\omega_{MAX} = \frac{\omega_p \varepsilon_1}{2\varepsilon_L}, \tag{2.30}$$

giving the value at the maximum of

$$\mathrm{Im}\left(\frac{\varepsilon_3 - \varepsilon_L}{\varepsilon_3 - \varepsilon_1} \right)_{MAX} = \tau \omega_p \left(1 - \frac{\varepsilon_1}{\varepsilon_L} \right) \tag{2.31}$$

Substituting eq. (2.31) into eq. (2.24) we obtain , $[\omega \simeq \omega_p]$

$$\left[\frac{\Delta R}{R} \right]_{MAX} \simeq \frac{4 q n_1}{c \varepsilon_o} \cdot \frac{\tau}{m_r^* m_e \varepsilon_L} \left(1 - \frac{\varepsilon_1}{\varepsilon_L} \right) c V \tag{2.32}$$

A similar expression will be obtained when inter - band transitions are taken into account. In the presence of inter - band transitions eq. (2.16) is not valid any longer. The experimental plasma frequency in that case can be found from eq. (2.14) by putting the real part of ε_3 equal to zero. In this way we obtain the following expression for the experimental plasma frequency ω_x :

$$\omega_x^2 = \frac{\varepsilon_L}{R(\varepsilon'_L)} \cdot \omega_p^2 \tag{2.33}$$

where $R(\varepsilon'_L)$ is the real part of ε'_L which is defined as:

$$\varepsilon'_L = \varepsilon_L + \varepsilon_{3B} \tag{2.34}$$

By substituting ω_p by ω_x in eq. (2.27) and following the same procedure we obtain

$$\Delta\omega_{MAX} \simeq \frac{\omega_x \cdot \varepsilon_1}{2\, R(\varepsilon'_L)} \tag{2.35}$$

where $\Delta\omega_{MAX} \ll \omega_x$.

The maximum value of the effect is given by an equation similar to eq. (2.32) providing that the relaxation time τ is replaced by

$$\tau' = \left[\tau^{-1} + \omega_x \frac{\mathrm{Im}(\varepsilon_{3B})}{R(\varepsilon'_L)}\right]^{-1} \tag{2.36}$$

where $\mathrm{Im}(\varepsilon_{3B})$ represents the imaginary part of the dielectric constant due to inter - band transitions.

It is interesting to note that interband transitions affect strongly the effective relaxation time defined in Eq. (2.36). More specifically, the effective relaxation time may become very small if interband effects become pronounced. This will have as a result the degradation of the magnitude of the ER peak, according to Eq. (2.32).

2.3.1 Position of the ER Maximum

From eqs. (2.30) and (2.35) the following important points can be made: the position of the ER maximum depends upon the ratio of the dielectric constant of phase 1 of fig. (2.1) to the lattice dielectric constant and also on the spectral position of plasma frequency.

Table (2.1) contains the calculated spectral positions of ER maxima of various materials in comparison with reported experimental data. The values have been computed from optical measurements reported for gold and silver by Cheyssac et al (1972), for antimony by Fox et al (1974) and for gallium arsenide and germanium by Axe and Hammer (1967).

2.3.2 Magnitude of the ER Maximum

Eq. (2.32) can generally be written as

$$\left[\frac{\Delta R}{R}\right]_{MAX} \simeq \frac{4\, n_1 \mu}{c\, \varepsilon_o} \left[\frac{R(\varepsilon_L') - \varepsilon_1}{R(\varepsilon_L')^2}\right] c\, V \tag{2.37}$$

where μ is the so-called optical mobility and is defined as

$$\mu = \frac{q\, \tau'}{m^* m_e} \tag{2.38}$$

Table (2.1) Predicted ER data of various materials in comparison with reported experimental values.

	Au[1]	Ag[1]	Sb[2]	GaAs(Sn)[3]	Ge(Sn)[3]
ω_x ($\times 10^{15}$ sec^{-1})	3.43	6.08	0.126	0.0924	0.0773
$\lambda_{x\ observed}$ (μm)	0.55	0.40	15	20.4	24.4
$\lambda_{peak\ exp}$ (μm)	0.50	0.32	—	20	24
$\left\|\frac{\Delta R}{RV}\right\|_{max\ exp}$ (V^{-1})	3×10^{-3}	10×10^{-3}	REPORTED AS SMALL	KNOWN TO BE HIGH	KNOWN TO BE HIGH BUT LESS THAN GaAs
ω_p ($\times 10^{15}$ sec^{-1})	3.14	12.9	0.126	0.0924	0.0773
m_r^*	1.0	1.07	0.5	0.0675	0.23
τ ($\times 10^{-14}$ sec)	1.5(0.33)	2(0.94)	3.1	8.9	4.8
μ (m sec^{-1} V^{-1})	6×10^{-4}	1.6×10^{-3}	1×10^{-2}	2.3×10^{-1}	3.7×10^{-2}
N_L	20	6	90	10.9	16.0
$\mathrm{Re}(\varepsilon_L')$ at ω_x	23	18	90	10.9	16.0
$\mathrm{Im}(\varepsilon_B)$ at ω_x	1.7	2.5	0	0	0
ω_x ($\times 10^{15}$ sec^{-1})	0.154	0.405	0.001	0.007	0.004
$\lambda_{peak\ CALC}$ (μm)	0.51	0.29	15	19	24
$\left\|\frac{\Delta R}{RV}\right\|_{max\ CALC}$ (V^{-1})	1.7×10^{-3}	5×10^{-3}	3×10^{-2}	7×10^{-1}	1×10^{-1}

(1) Cheyssac et al (1972).
(2) Fox et al (1974).
(3) Axe and Hammer (1967).

where τ' is the apparent value of τ .

Equation (2.37) demonstrates that for a material to give a large electroreflectance effect for a given amount of induced charge it should have a high optical mobility and a value of $R(\varepsilon_L')$ such that the function in brackets is maximised i.e. $R(\varepsilon_L') = 2\varepsilon_1$.
Given that ε_1 is usually rather small,[«3»] materials with small values of $R(\varepsilon_L')$ are likely to exhibit large electroreflectance peaks.

An approximate expression for the magnitude of the ER maximum, when $\varepsilon_L = 2\varepsilon_1$, is

$$\left[\frac{\Delta R}{R}\right]_{MAX} \simeq \frac{\mu}{c\,\varepsilon_o n_1} \cdot C\,V \qquad (2.39)$$

The latter expression has been used to calculate the magnitudes of the ER maxima of various materials shown in Table (2.1). Although, eq. (2.39) is an approximate one, the results obtained using it are comparable to experimental data for gold and silver.

It is worth noting that the latter equation predicts considerably large ER maxima for values of optical mobility which several materials exhibit at room temperature, (for example GaAs , InSb,SiC).

Speaking in terms of the plasma edge morphology, a large value for optical mobility implies a sharp plasma edge. The sharpness of the plasma edge is the principal criterion for relatively large ER signals.

Moreover, the value of lattice dielectric constant affects the value of reflectance minimum; for small values of lattice dielectric constant

the reflectance minimum shifts towards zero reflectance.

The conclusion is that according to the present theory materials exhibiting a sharp plasma edge accompanied by a deep reflectance minimum are the most suitable for giving relatively large magnitudes of ER effect.

It is interesting to note that the value of ER effect may become zero, in the spectral region of an expected maximum, for both 'real' and 'ideal' materials. This will happen when the quantity $R(\varepsilon'_L) - \varepsilon_1$ of eq. (2.37) will become zero, i.e.

$$R(\varepsilon'_L) = \varepsilon_1 \qquad (2.40)$$

In the case of ideal materials, i.e. $\varepsilon'_L = \varepsilon_L$, the magnitude of the ER effect will become zero when the lattice dielectric constant of the material becomes equal to the dielectric constant of ambient. Thus, a Drude - type material will not exhibit an ER effect if its lattice dielectric constant becomes equal to the ambient dielectric constant, and not if the ambient dielectric constant takes the value 1 as it is predicted by McIntyre's model.

2.3.3 Polarity of the ER Effect

This is a controversial subject; Hansen and Prostak assign a positive sign for the ER effect and are justified by their experimental results. McIntyre and Aspnes deduce a negative sign for the ER effect and are justified by their experimental results. Koffman, Garrigos and Cheyssac give it a negative polarity, thanks to a negative sign emerging from their calculations, (Garrigos PhD Thesis 1974, Université de Nice).

McIntyre and Aspnes manipulation is unacceptable since the final answer to the question of the ER polarity is that for pure free - electron metals the effect is very small and positive whereas for metals with interband transitions the effect is predicted to be considerably larger and negative, by making various assumptions concerning the values of the free electron and bound electron parts of the dielectric constant. According to the present interpretation the polarity of the ER spectrum depends upon the polarity of the free carriers of the materials under investigation, the relative direction of the low - frequency electric field which generates the perturbation on the surface of the sample, and the value of $R(\varepsilon_L')$.

We assume that the specific capacitance C (in F / m^2) of eq. (2.37) is in general the one of a system consisted of two parallel plates, one of which is the surface of the material under investigation, separated by a dielectric of thickness d_D and dielectric constant ε_1. This assumption is a widely accepted approximation for the double layer capacitance when electrolytic techniques are employed, and there is no question of being invalid in cases where solid state configurations are used, i.e. schottky diode etc. Consequently, when d_D is small compared with the geometrical dimensions of the electrodes, so that edge effects become negligible:

$$C \cdot V \propto (\text{const.})\, E_{DC} \tag{2.41}$$

where E_{DC} is the low frequency electric field applied onto the surface of the material under investigation. Substituting eq. (2.41) into eq. (2.37) gives

$$\left[\frac{\Delta R}{R}\right]_{MAX} \propto \frac{4 n_1 \tau q}{m_r^* m_e c \varepsilon_o} \left[\frac{R(\varepsilon_L') - \varepsilon_1}{R^2(\varepsilon_L')}\right] E_{DC} \tag{2.42}$$

The prefactor on the right-hand side of the latter equation is always positive and the quantity into brackets is positive for most of the materials in the spectral region under consideration. So, the polarity of ER effect is a matter of defining the positive direction of the low - frequency electric field vector and knowing the polarity of the free carriers of the material under investigation.

Thus, if we define E_{DC} to be negative when its unit vector is directed onto the surface of the material and assume the existence of positively charged free carriers,(i.e. $q = +e$) , the polarity of the ER effect turns out to be positive . This definition is consistent with eq.(2.24 because an excess of holes causes a shift of the plasma frequency and consequently the reflectivity spectrum, towards larger photon energies which is generally expected to give positive differences.

However in frequency regions where $R(\varepsilon_L') < \varepsilon_1$, the term into brackets eq. (2.42) , becomes negative thus, changing the sign of the ER effect, determined by the polarity of free carrier and direction of the low frequency perturbing electric field. So, the polarity of the effect is governed by the polarity of free carriers, the relative direction of the low - frequency electric field, and the sign of the term in brackets of eq. (2.42).

2.3.4 A Detailed Manipulation of the Effect of the Optical Parameters of the ER Spectrum.

It is interesting to examine in detail how, for an ideal material, the various parameters affect the shape of the electro - reflectance spectrum, using the complete mathematical expression of our model.

2.3.4.1 Lattice Dielectric Constant Dependence

Assuming materials obeying Drude's model the quantity

$$F = \left[\frac{-\varepsilon_A + \varepsilon_1 + \omega\tau . \varepsilon_B}{(\omega^2\tau^2 + 1)\left[(\varepsilon_A - \varepsilon_1)^2 + \varepsilon_B^2\right]} \right] \tag{2.43}$$

has been plotted as a function of $\omega\tau$ for a large number of values of $(\omega_p\tau)$, and ε_L, as it is shown in figs (2.2 - 2.12). The effect of ε_L on the magnitude of F and eventually on $\Delta R / R$ is dramatic, specially for values of ε_L less than about 30 (See Figs. (2.2), (2.3) and (2.4); the lower the value of ε_L the higher the magnitude of electro-reflectance for given τ and m*.
If τ is frozen Fig.(2.13) shows that the electro - reflectance peak occurs in the vicinity of the plasma edge. The latter figure shows again $F = f(\omega\tau, \omega_p\tau, \varepsilon_L)$ but contains 8 curves only (instead of 200), for clarity. Figs.(2.2 - 2.12) show that there is a single peak for each value of $(\omega_p\tau)$, over $(\omega\tau)$ and for 200 values of $(\omega_p\tau)$.
The maximum values of F have been plotted against $(\omega_p\tau)$ in fig.(2.14). It is interesting to note, that, according to the present model and for ideal materials, the maximum value of F is not the same for all the values of $(\omega_p\tau)$. It seems that ε_L introduces a "ripple" in the function $F_{MAX} = f(\omega_p\tau, \varepsilon_L)$, the "amplitude" and "frequency" of which are inversely proportional to the value of ε_L.

Quantity F, as we have already pointed out, determines the spectral distribution of the ER effect; in order to find the actual value of ER effect we must multiply F by

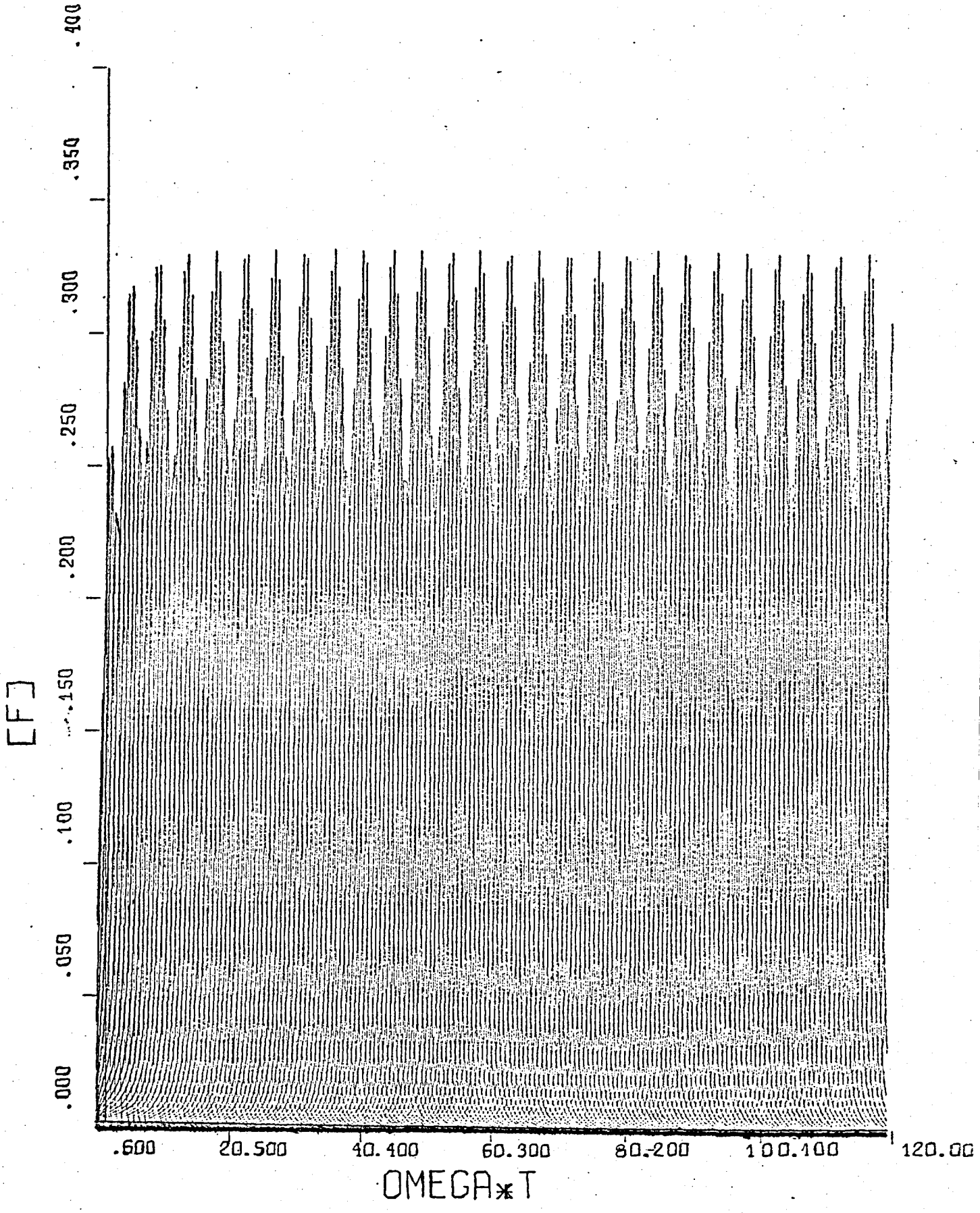

Fig.(2.2) Spectral distribution of function F for various values of $\omega_p \cdot \tau$ and materials obeying Drude's model, with $\varepsilon_L = 4$.

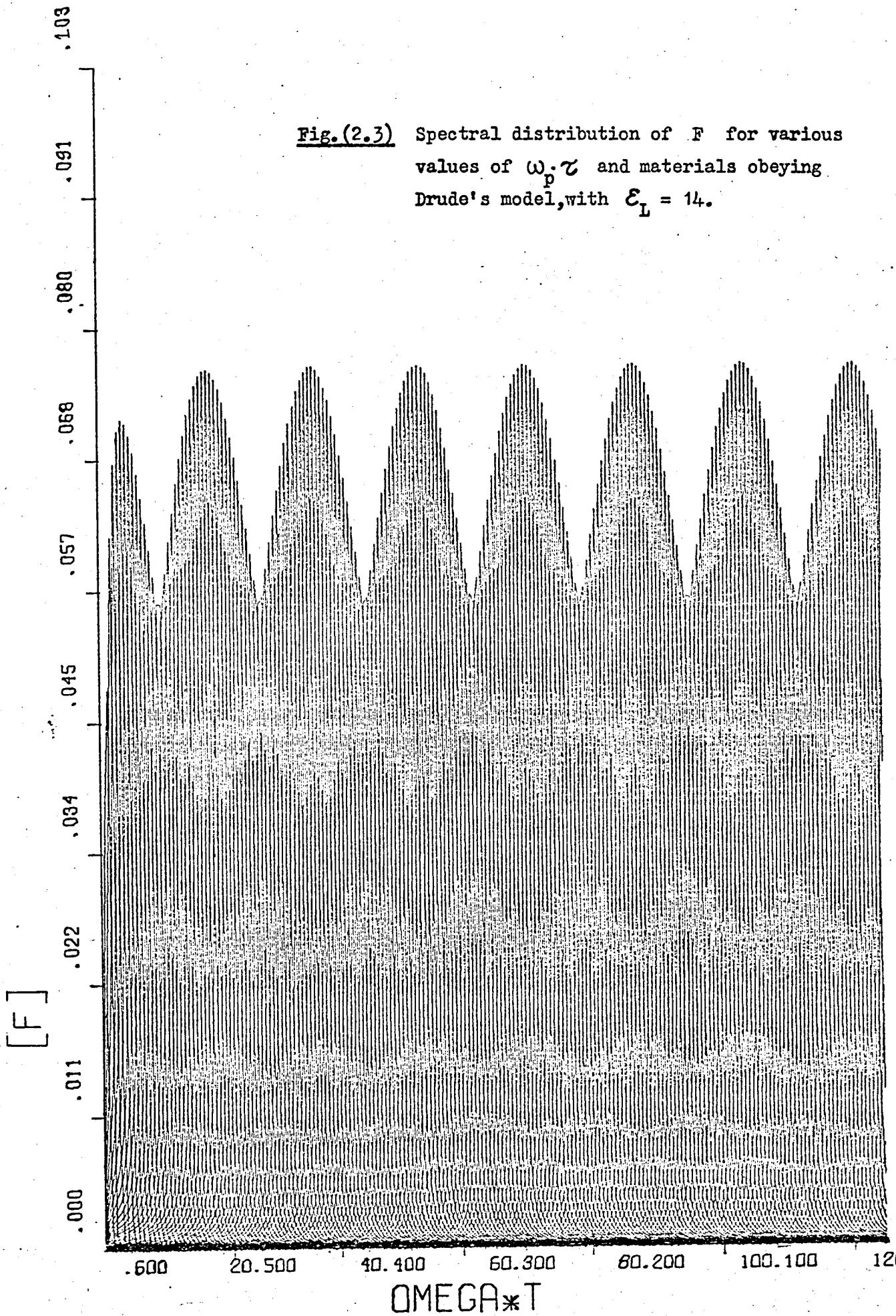

Fig.(2.3) Spectral distribution of F for various values of $\omega_p \cdot \tau$ and materials obeying Drude's model, with $\varepsilon_L = 14$.

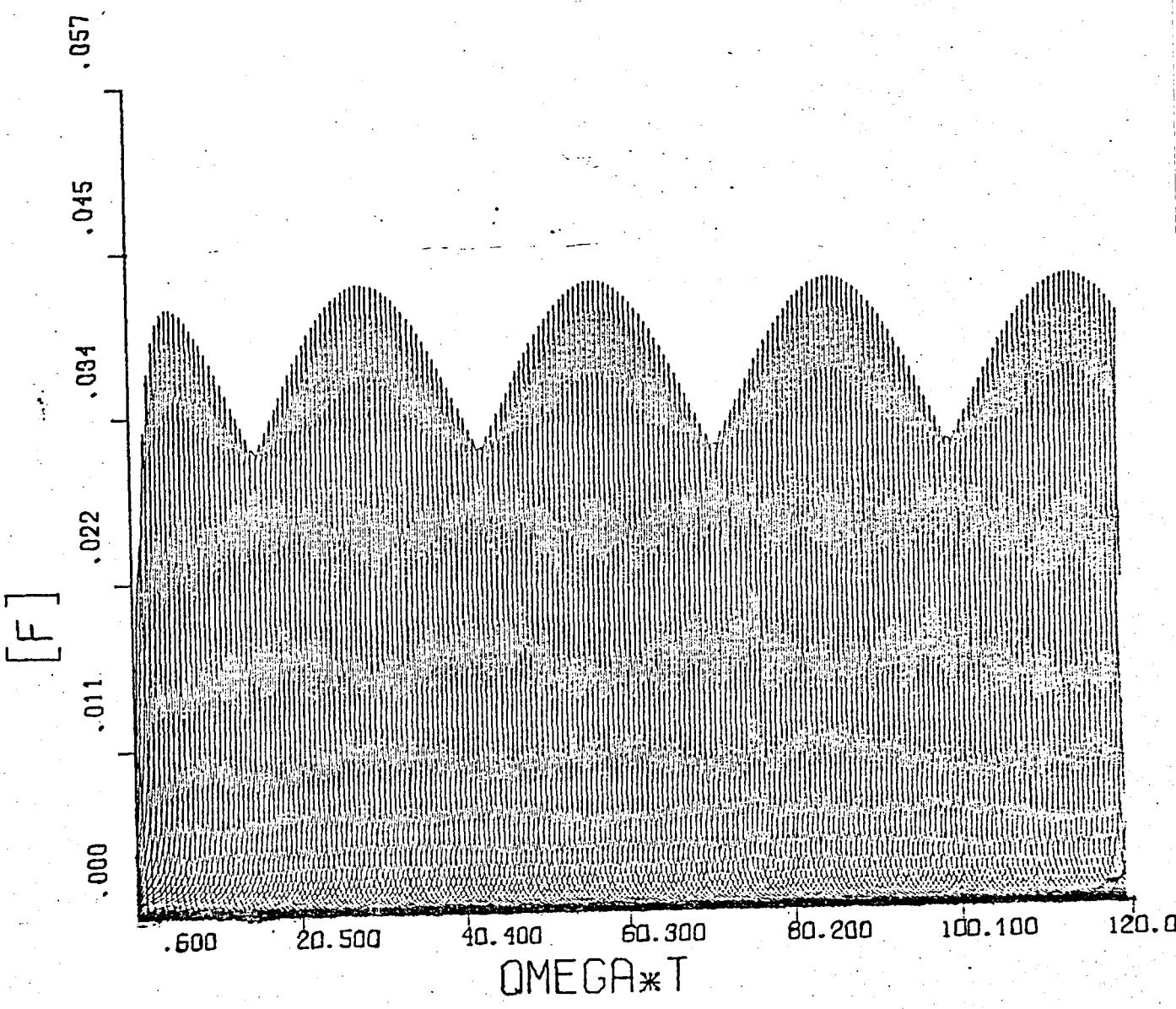

Fig.(2.4) Spectral distribution of F for various values of $\omega_p \cdot \tau$ and $\varepsilon_L = 24$.

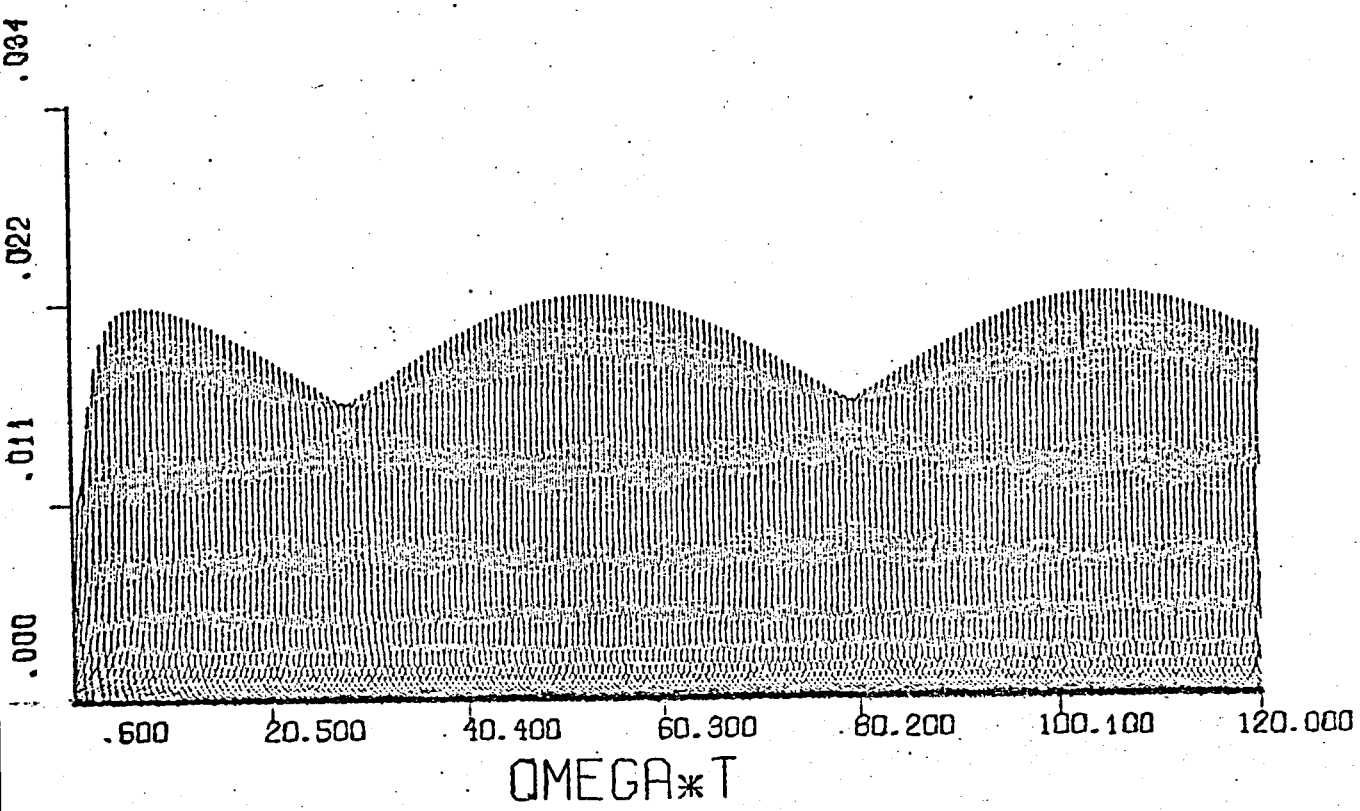

Fig.(2.6) Spectral distribution of F for various values of $\omega_p \cdot \tau$ and $\varepsilon_L = 44$.

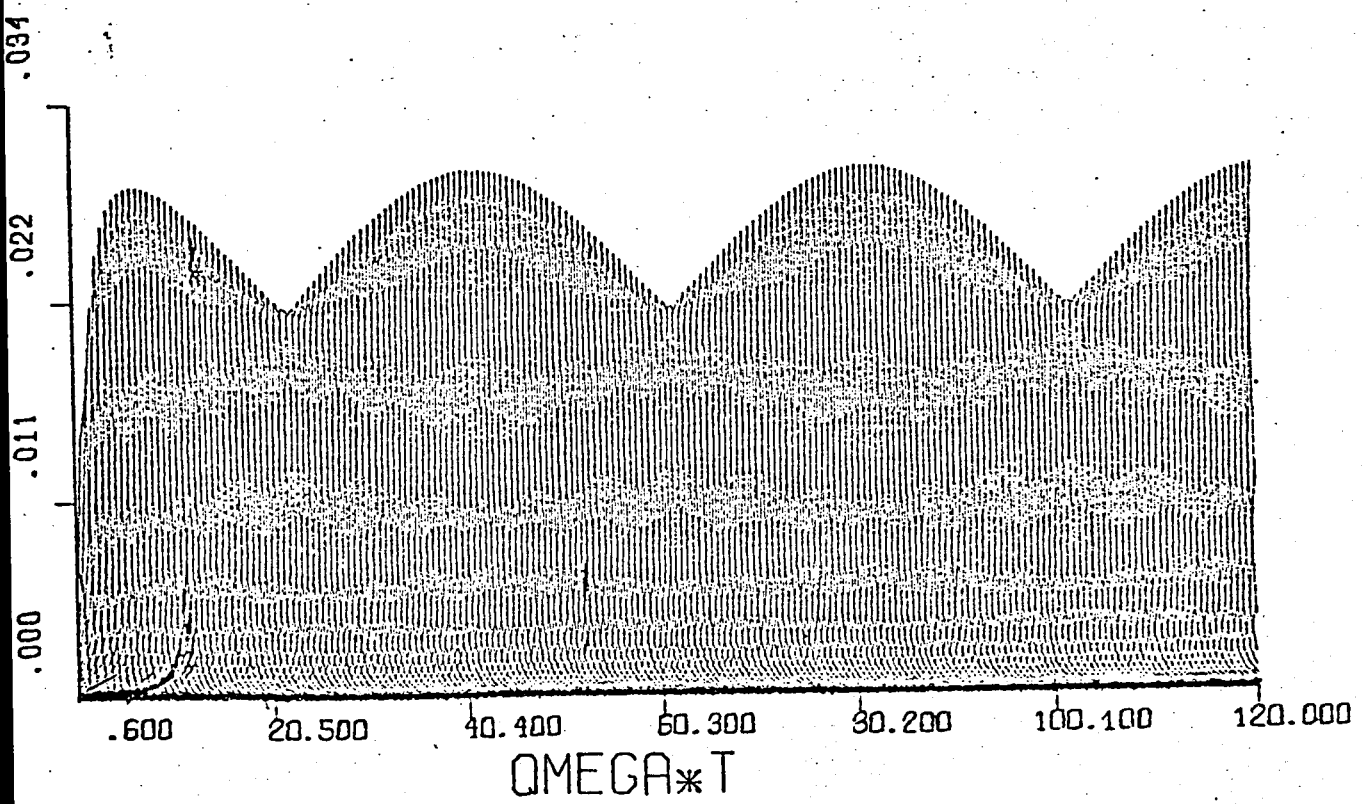

Fig.(2.5) Spectral distribution of F for various values of $\omega_p \cdot \tau$ and $\varepsilon_L = 34$.

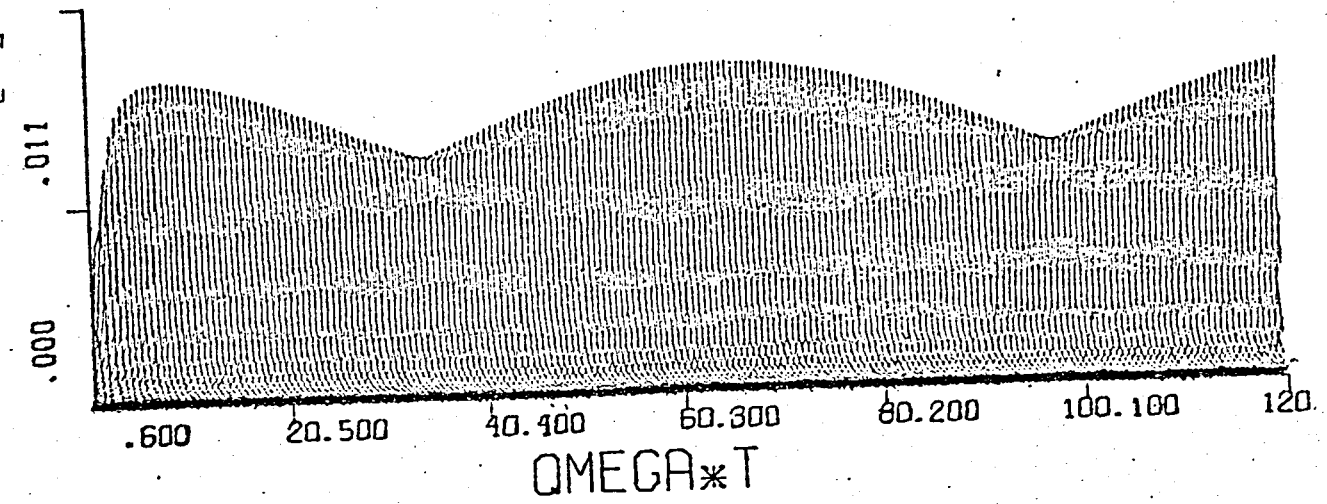

Fig.(2.7) Spectral distribution of F for various values of $\omega_p \cdot \tau$ and $\varepsilon_L = 54.$

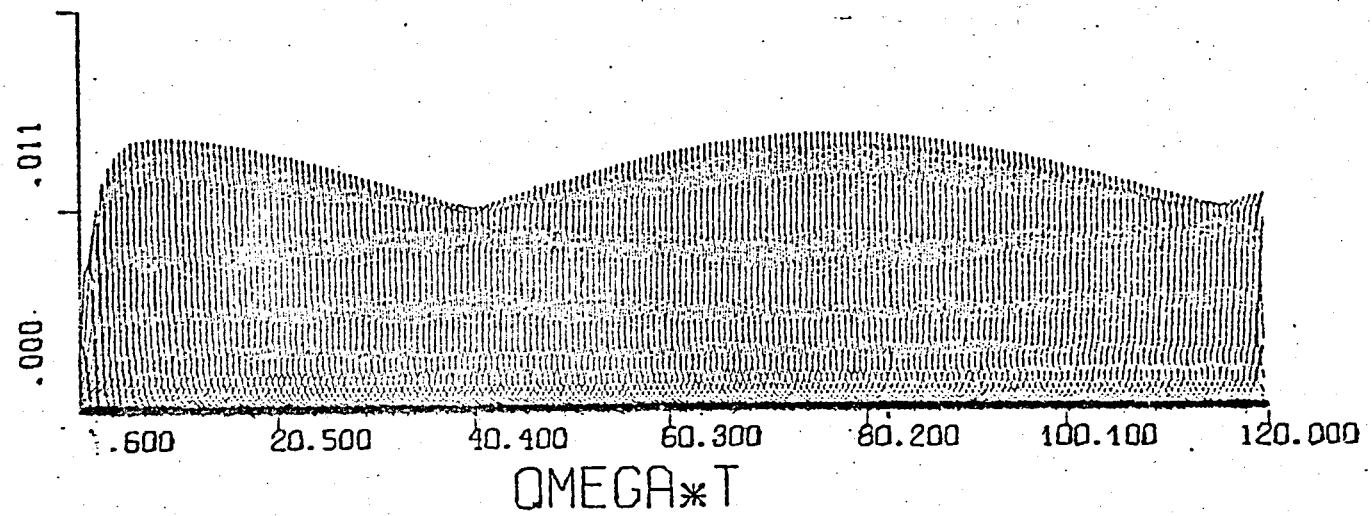

Fig.(2.8) Spectral distribution of F for various values of $\omega_p \cdot \tau$ and $\varepsilon_L = 64.$

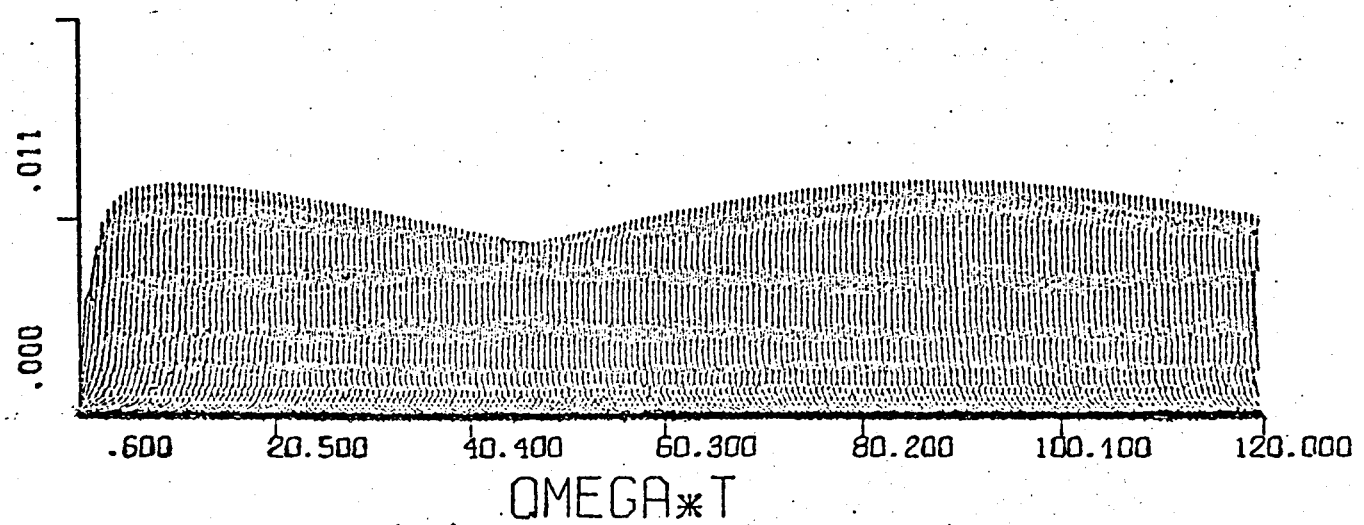

Fig.(2.9) Spectral distribution of F for various values of $\omega_p \cdot \tau$ and $\varepsilon_L = 74.$

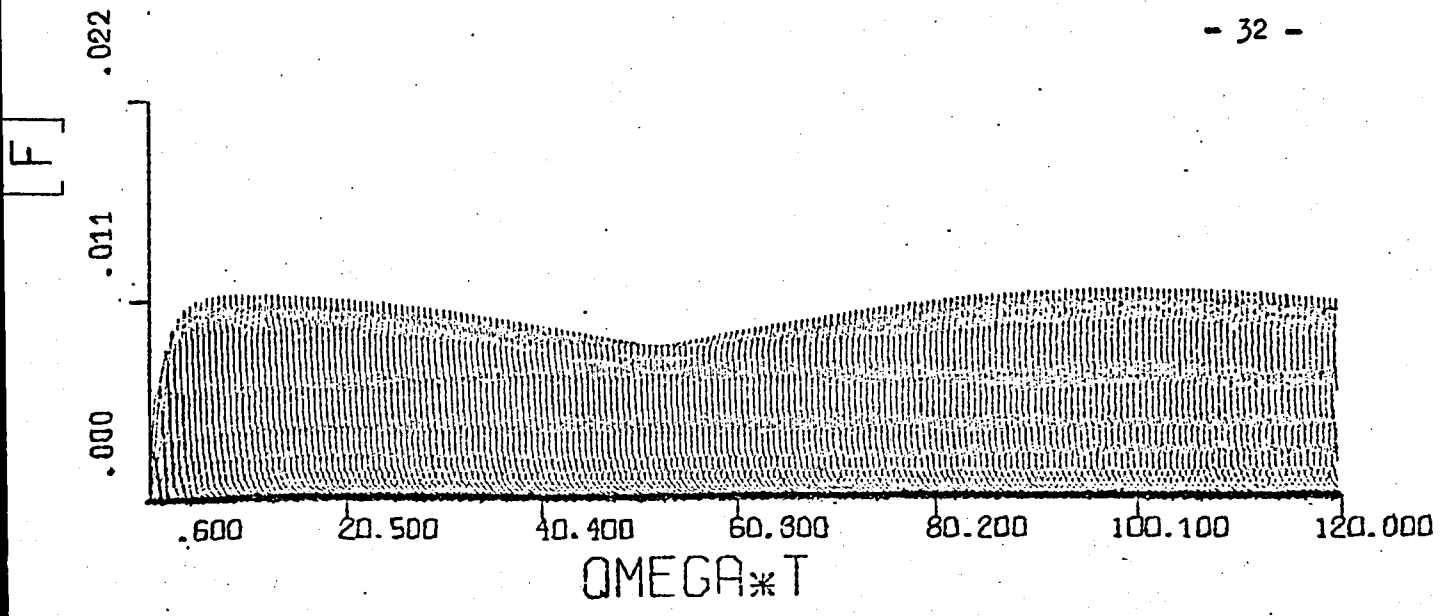

Fig.(2.10) Spectral distribution of F for various values of $\omega_p \cdot \tau$ and $\varepsilon_L = 84$.

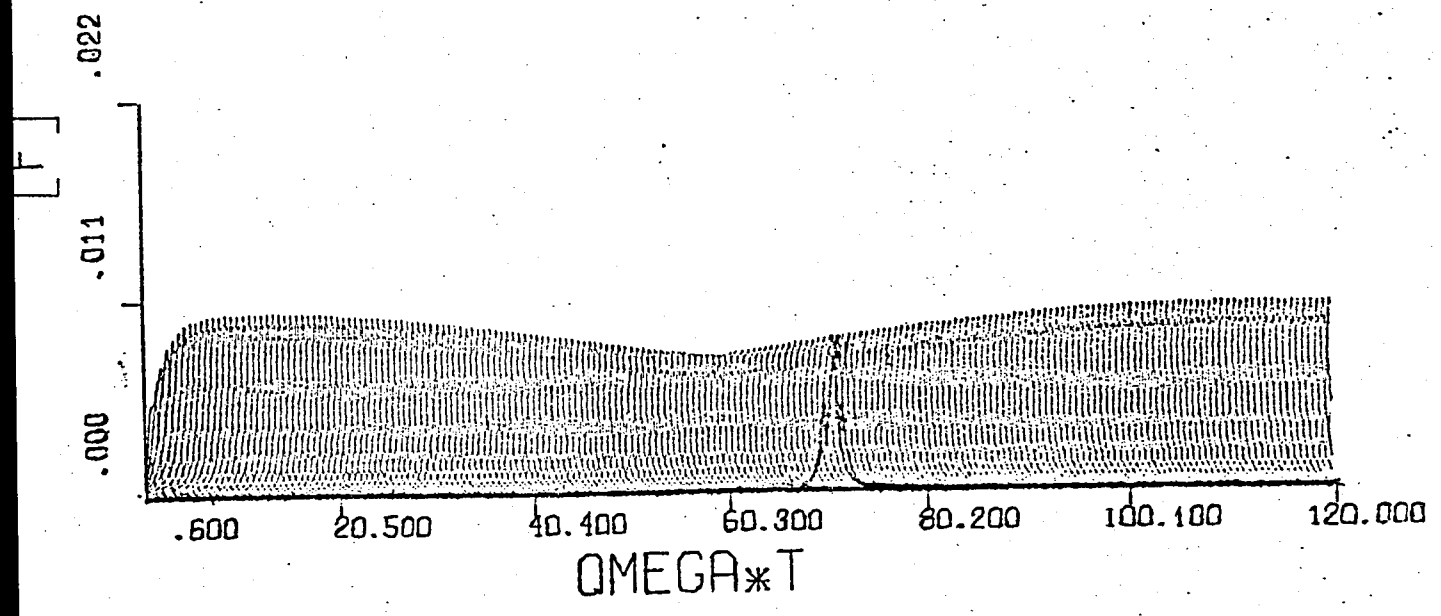

Fig.(2.11) Spectral distribution of F for various values of $\omega_p \cdot \tau$ and $\varepsilon_L = 94$.

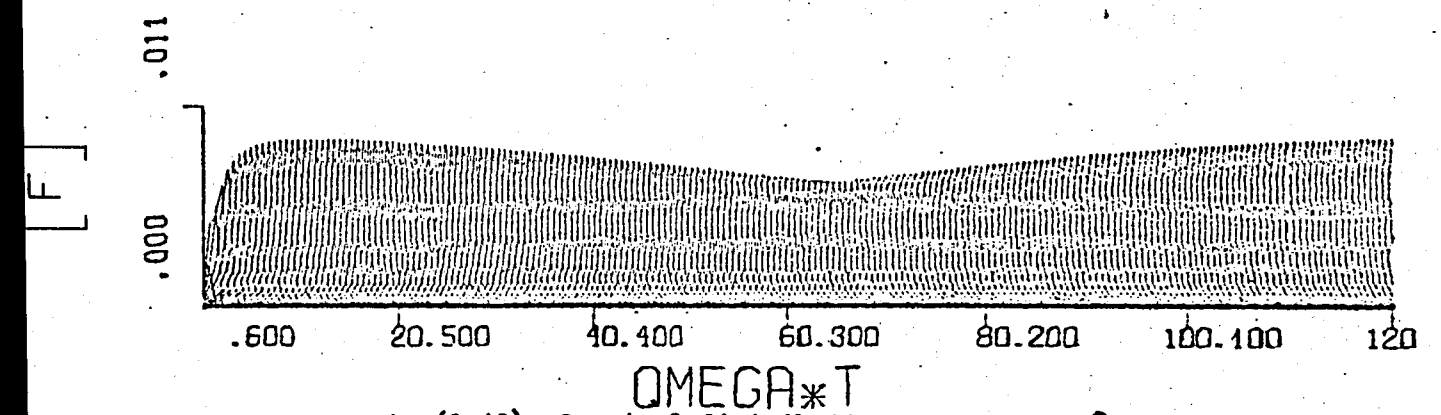

Fig.(2.12) Spectral distribution of F for $\varepsilon_L = 104$.

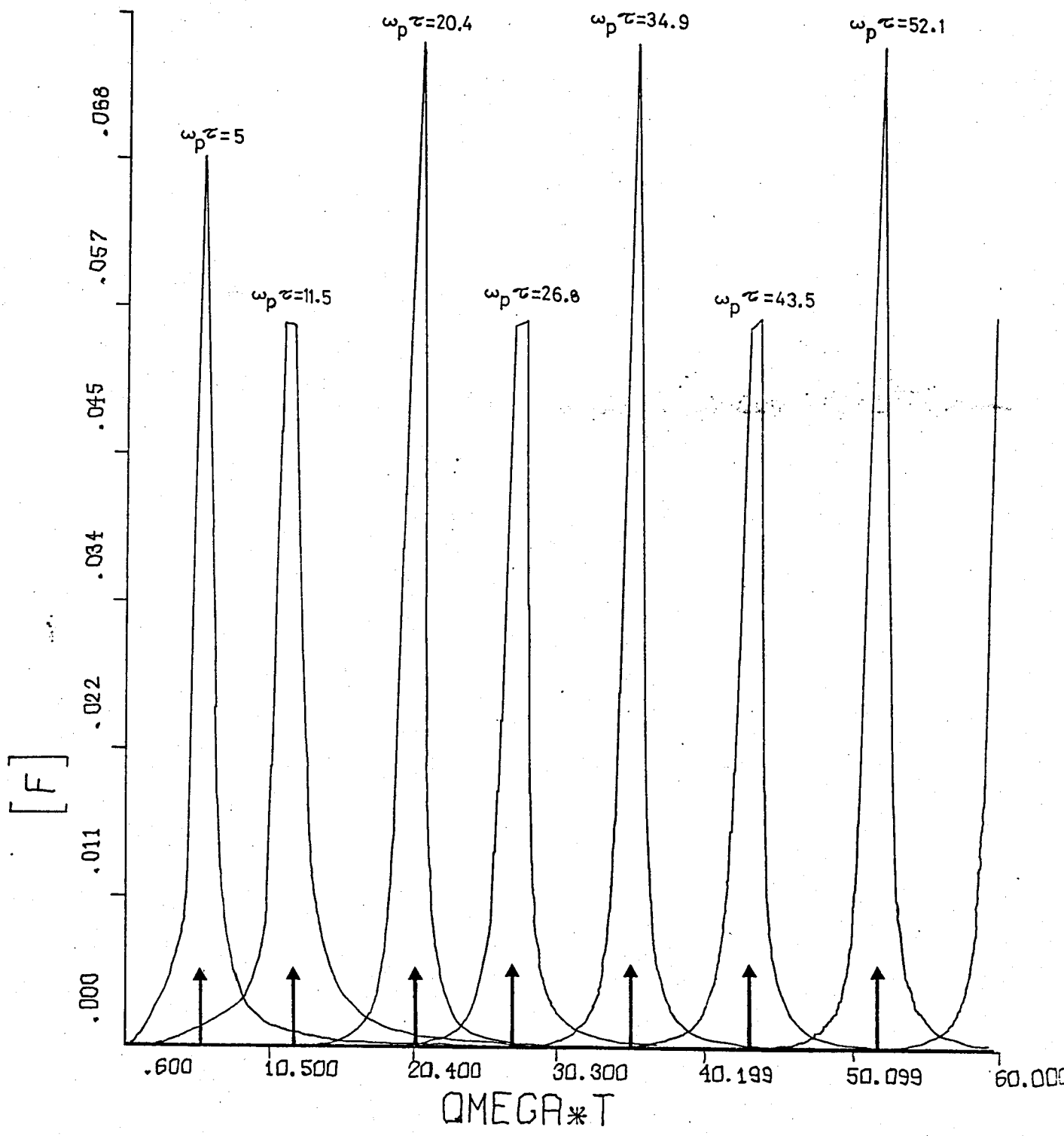

Fig.(2.13) Calculated qualitative spectral distribution of the ER effect for 'ideal', conducting materials; the ER peak occurs in the vicinity of the plasma frequency, (ε_L = 14).

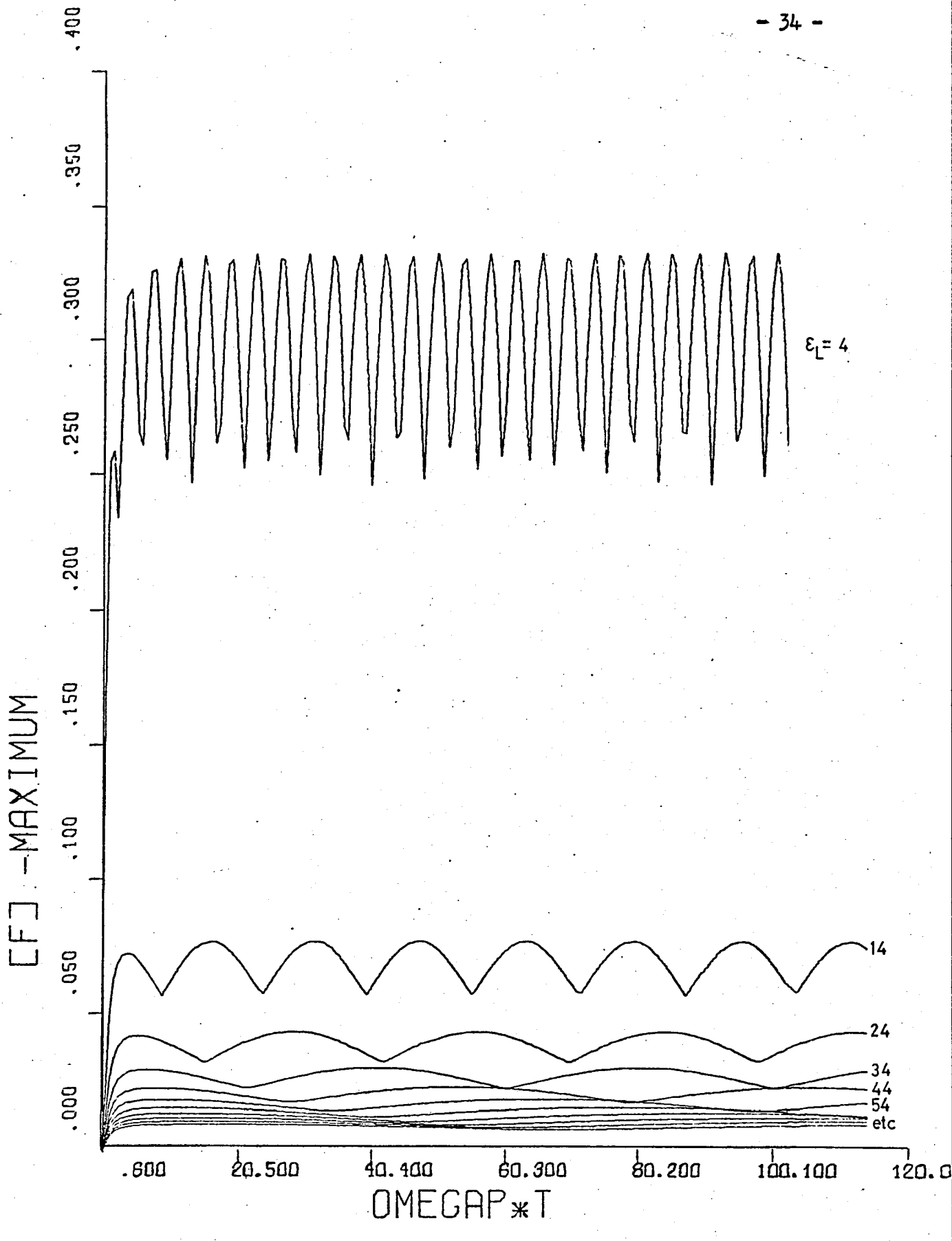

Fig.(2.14) F_{max} against $\omega_p \cdot \tau$ for various values of the lattice dielectric constant.

$$(2.44) \qquad T = \frac{4\, q\, n_1\, C\, V}{c\, \epsilon_o\, m_e} \quad \frac{\tau}{m_r^*\, \epsilon_L}$$

where τ , m_r^* , ϵ_L, N are the optical parameters of a material.

2.3.4.2 Relaxation Time Dependence

The relaxation time is contained in both the later constant term, T , and quantity F. So, its changes should affect the ER spectrum both in shape and magnitude. The effect of relaxation time on the ER spectrum is shown in fig.(2.15). As far as the reflectance is concerned, the effect of the relaxation time on it, is shown in fig.(2.16). In this case the optical constants of GaAs from Axe and Hammer (1967) have been picked up to demonstrate the effect of degradation of the relaxation time from 8.9 to 1.9 x 10^{-14}sec on the shape of the plasma reflection edge and the calculated ER spectrum.

It is interesting to note the brodening of the ER peaks, with degrading free carrier relaxation time. This effect has been attributed to a number of surface scattering mechanisms, located surface charges scattering by lattice vibrations, and scattering from surface roughness, [see McIntyre (1973) and Cahan et al (1970)], but no quantitative explanation has been given.

The proposed model , however, gives (for the first time), a quantitative explanation of that effect; the effect is explained independently of the nature of the scattering mechanism.

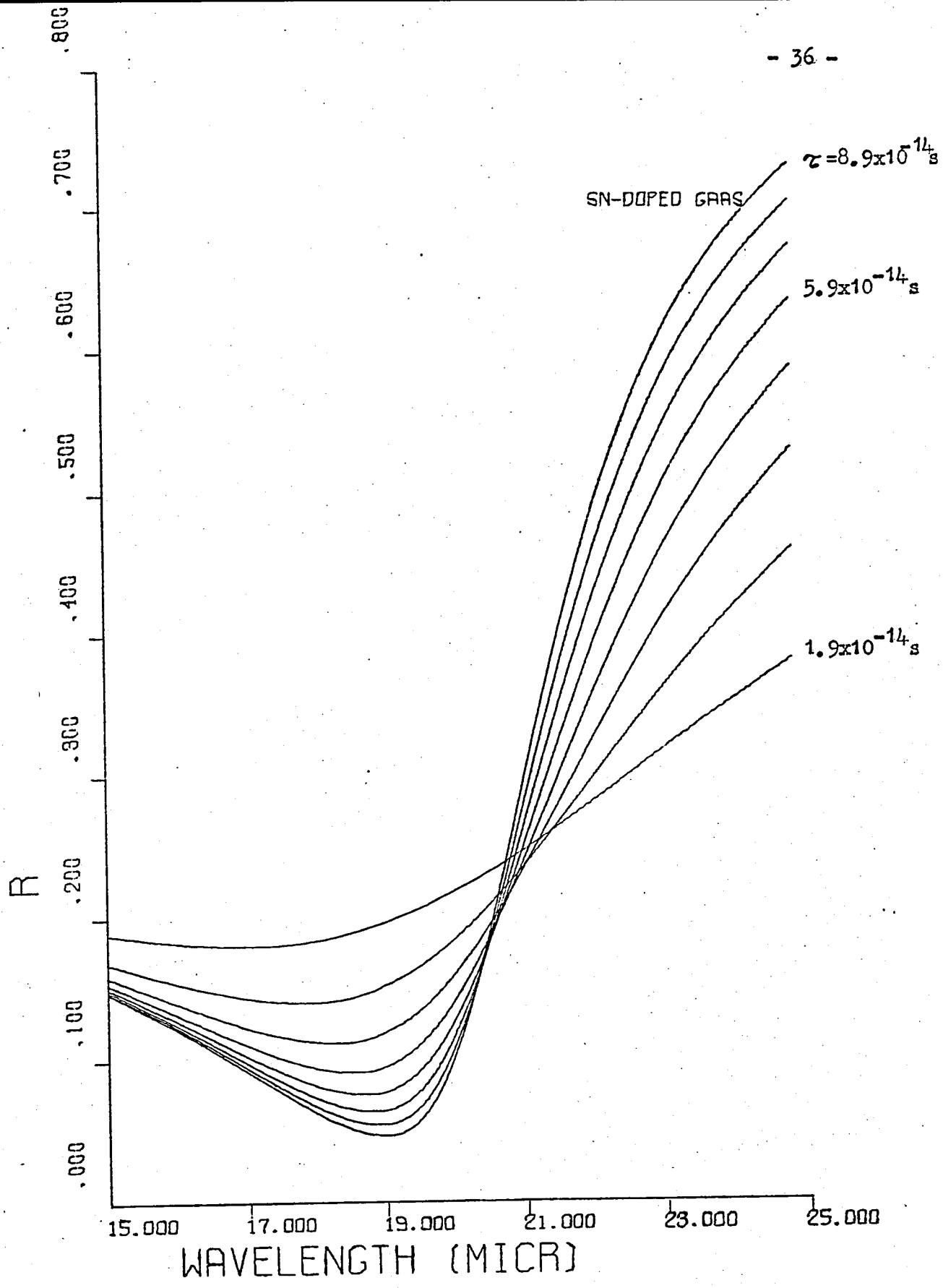

Fig.(2.15) The effect of degradation of the relaxation time from 8.9×10^{-14}sec to 1.9×10^{-14}sec on the shape of the plasma edge;free carrier paramaters were calculated from data taken from Axe and Hammer (1967).

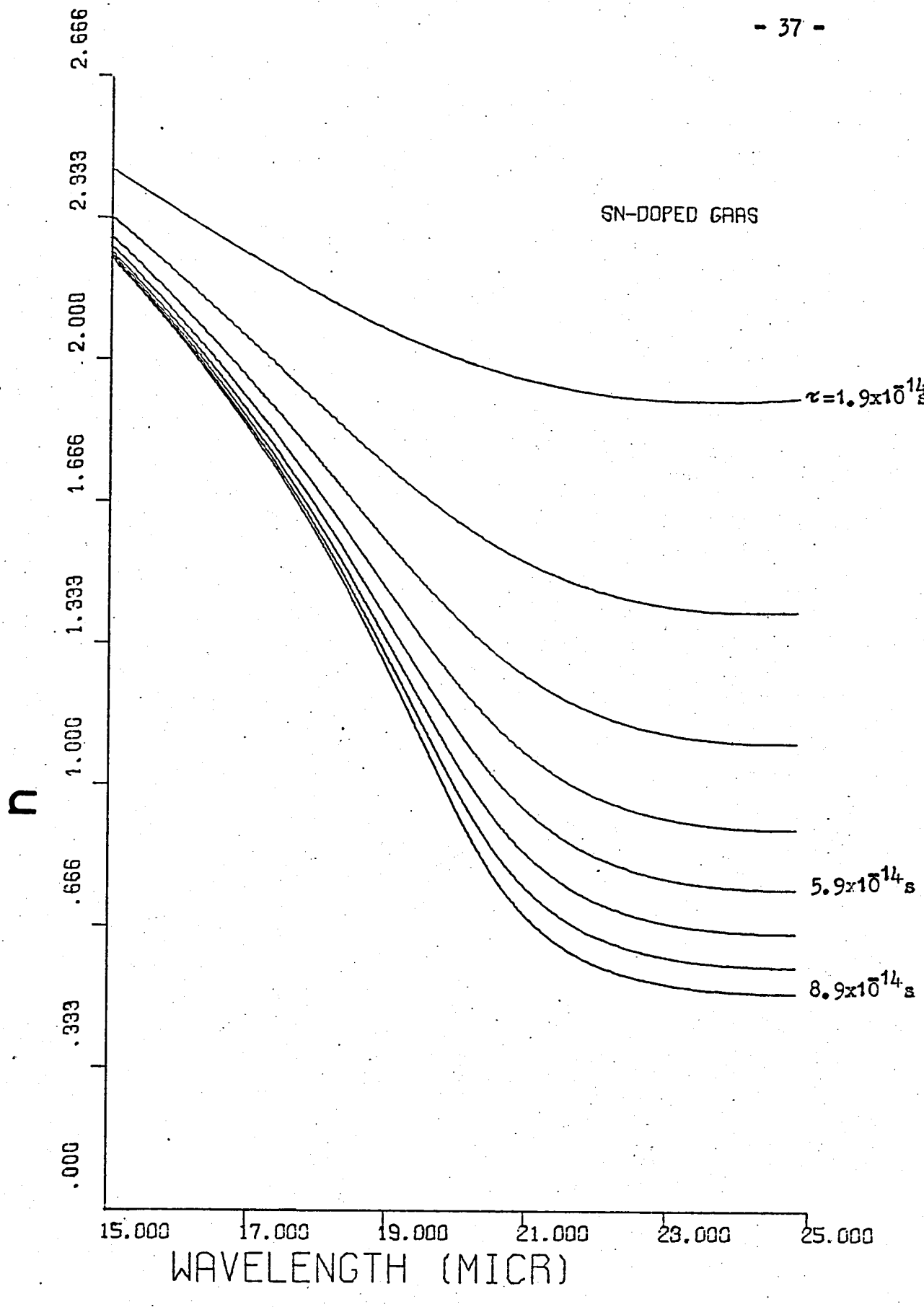

Fig.(2.15a) The effect of degradation of the relaxation time from 8.9×10^{-14}s to 1.9×10^{-14}s in GaAs on the shape of the spectrum of the refractive index, n.

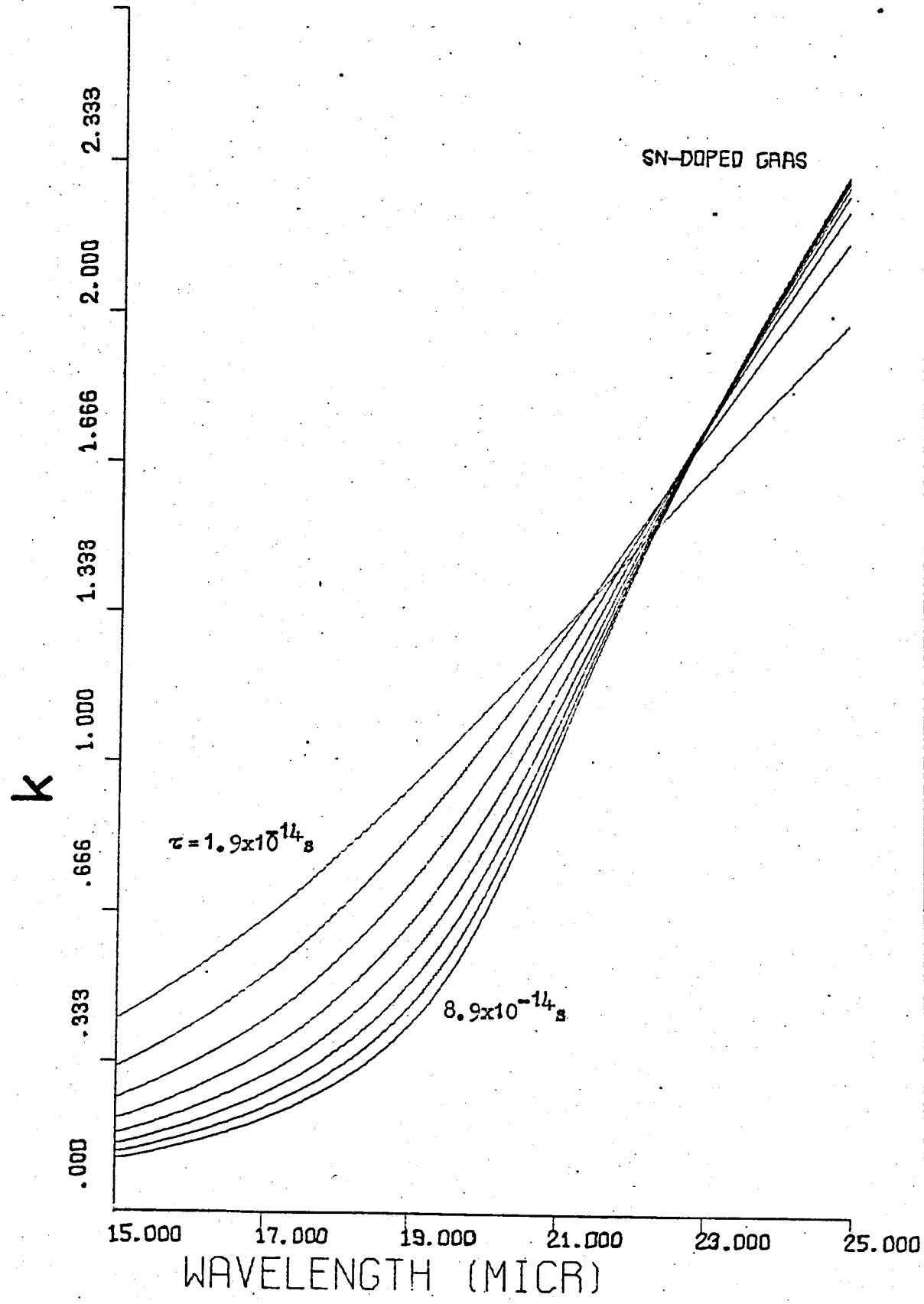

Fig.(2.15b) The effect of degradation of the relaxation time from 8.9 to 1.9 x 10^{-14}s in GaAs on the shape of the spectrum of the extinction coefficient, k.

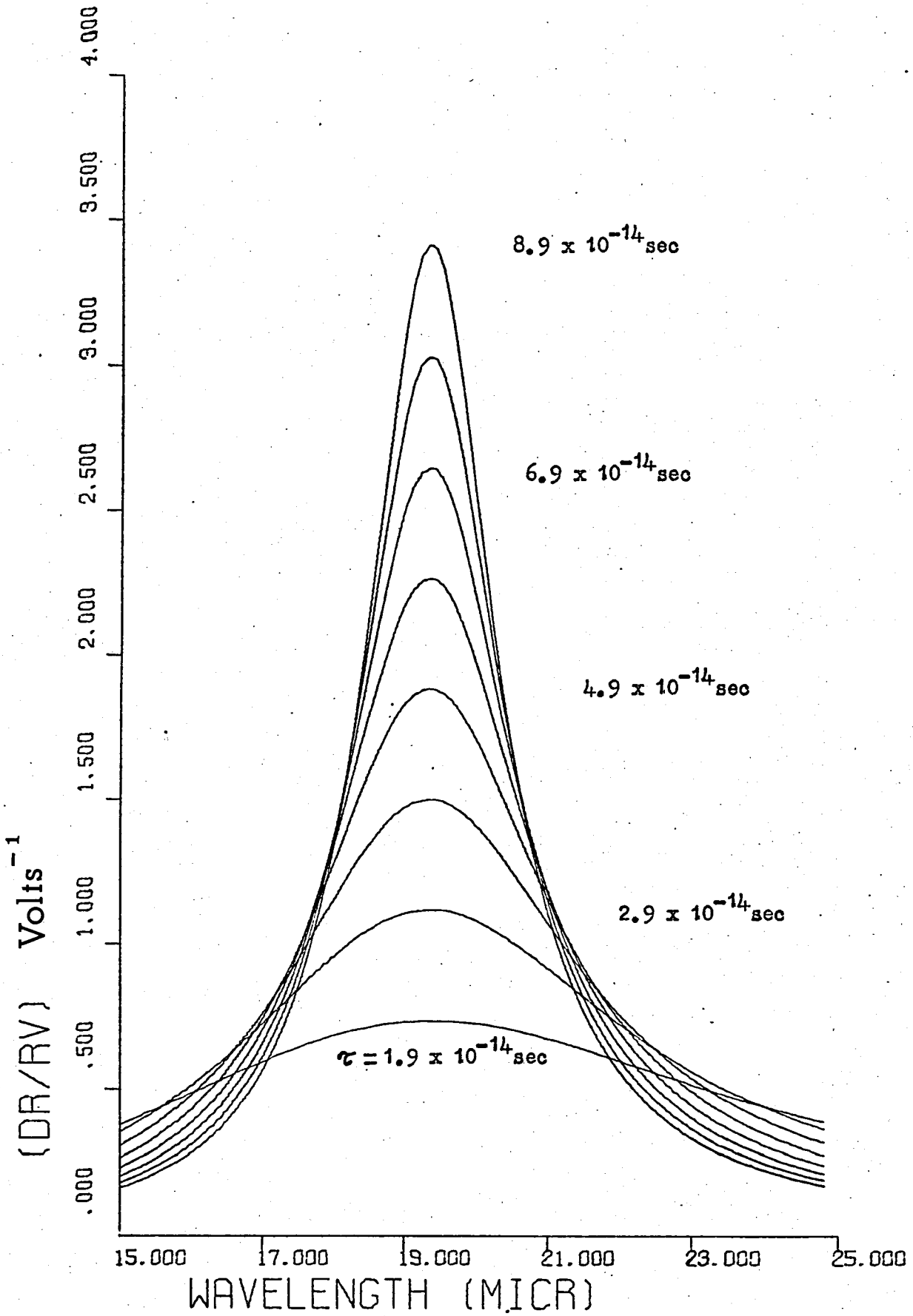

Fig.(2.16) The effect of degradation of the relaxation time from 8.9 to 1.9×10^{-14}s on the shape of the calculated ER spectrum of tin-doped GaAs.

2.3.4.3 Optical Effective Mass Dependence

Information concerning the effect of changing the effective mass, m_r^*, on the ER spectrum can be obtained from figs.(2.2)-(2.12). Careful examination shows that when $\omega_p \tau$ becomes small, i.e. ~ 0.6, the quantity F becomes very small, independently of ε_L. This implies that for a given value of relaxation time, F is small when $\omega_p \tau$ becomes small ($\omega_p \tau \rightarrow 0.6$). Since ε_L is constant each time, it can be argued that, when the free carrier density is constant, F becomes small when m_r^* becomes large.

The final effect is further affected by the presence of m_r^* in the denominator of the constant term , Eq.(2.44) .

Finally, in the case that $\omega_p \tau$ is small, for τ : constant, m_r^* : constant, and ε_L: constant, or in other words for materials with low-free carrier density F becomes relatively small.

It is worth noting that for very low free carrier concentrations and in spectral regions far enough from the reflectance plasma edge, towards short wavelengths, the basic assumptions of the present model become invalid, because the perturbation depth becomes large in comparison with the wavelength. The effect is still called electro - reflectance, although a Franz - Keldysh - type theory is used for its explanation, Cardona, Shaklee and Pollak (1967). Naturally the present model is valid in spectral regions covering the plasma edge and longer wavelengths.

The search has been carried out by varying ($\omega\tau$) and ($\omega_p \tau$) between 0.6 and 120.0; it was considered that this range covers most of

the cases met or to be met in practice, and the most important that the computer time needed was already considerable.

2.4 Application of the Model in Thin Films

Expressions for the electro-reflectance in thin films will be derived. Consideration will be given to two experimental configurations used in practice: a) the External Reflection Spectroscopy (ERS) and b) the Internal Reflection Spectroscopy (IRS), Howson, Avaritsiotis and Fox (1975), Avaritsiotis MSc Thesis (1974). In the first case the electromagnetic radiation falling onto the film comes from phase 1, meets the perturbed interface and immerses into the film, as it is shown in Fig.(2.17). In the second case the electromagnetic waves come from phase 3 and immerse into the film to meet the perturbed interface between phase 2 and phase 3 as it is shown in Fig.(2.17).

The reflectance of the film in both cases is given by Fox, Howson and Emmony(1974) :

(2.45) $$R = r_f \cdot r_f^*$$

where:

(2.46) $$r_f = \frac{r_1 + r_2 \exp(-j B)}{1 + r_1 r_2 \exp(-jB)}$$

(2.47) $$r_f^* = \frac{r_1^* + r_2^* \exp(+j B^*)}{1 + r_1^* r_2^* \exp(+jB^*)}$$

(2.48) $$B = \left[\frac{2\omega d}{c}\right] \bar{n}_2$$

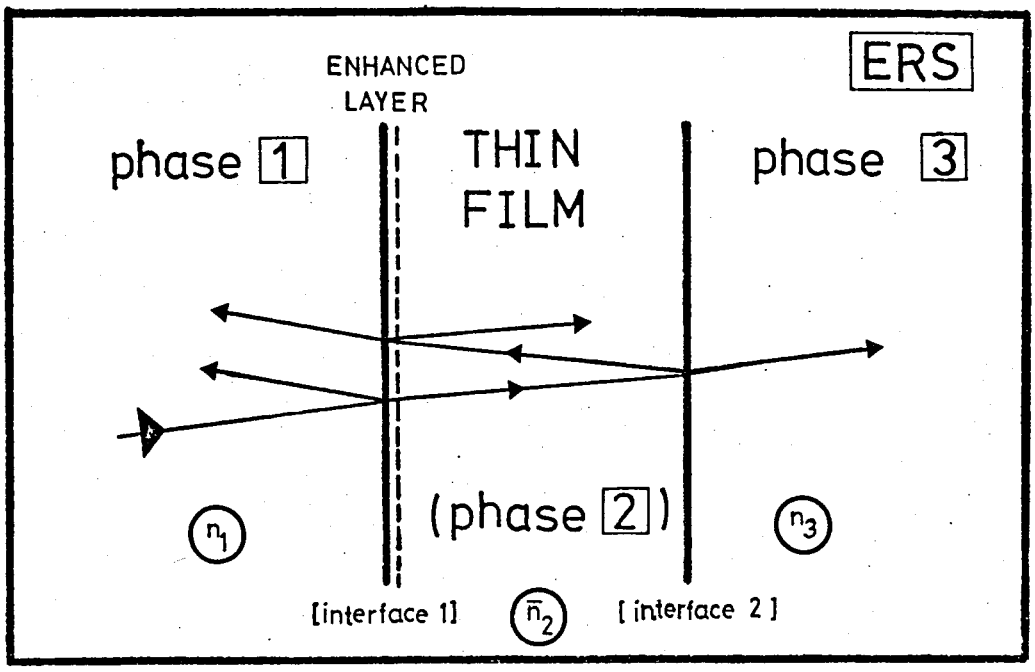

Fig.(2.17) External Reflection Spectroscopy (ERS).

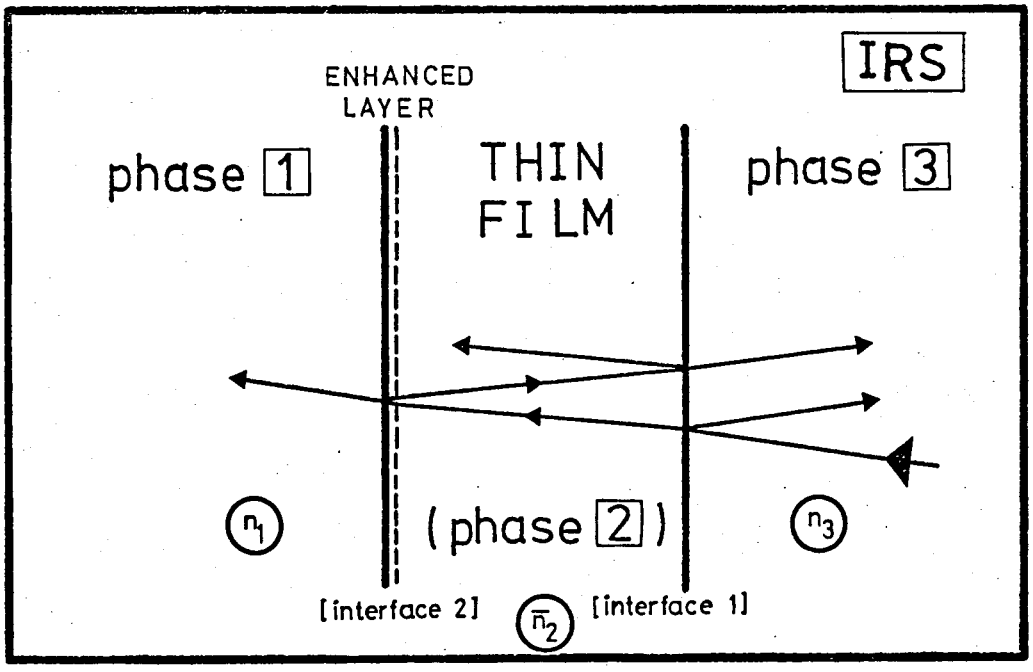

Fig.(2.18) Internal Reflection Spectroscopy (IRS).

and

(2.49) $$\bar{n}_2 = n_2 - j\,k_2$$

The case of normal incidence will be considered.

2.4.1 External Reflection Spectroscopy (ERS)

The Fresnel coefficients for the two interfaces of Fig.(2.17) are given in this case by (Heavens 1965).

(2.50) $$r_1 = \frac{n_1 - \bar{n}_2}{n_1 + \bar{n}_2}$$

(2.51) $$r_2 = \frac{\bar{n}_2 - n_3}{\bar{n}_2 + n_3}$$

Our aim is to express the normalized change in reflectance $(\Delta R/R)$ of a film in terms of normalized optical changes occuring at the interface between phase 1 and phase 2, i.e. in terms of $\Delta R_1 / R_1$ which has already been calculated for bulk materials eq.(2.25) and is given by

(2.52) $$\frac{\Delta R_1}{R_1} = \frac{\Delta r_1}{r_1} + \frac{\Delta r_1^*}{r_1^*}$$

From eq. (2.28) we obtain

(2.53) $$\frac{\Delta R}{R} = \frac{\Delta r_f}{r_f} + \frac{\Delta r_f^*}{r_f^*}$$

The quantities of the right hand side of the latter equation can be expressed in terms of $\Delta R_1 / R_1$ as it will be shown next.

From eqs.(2.46) and (2.47) we obtain respectively:

$$(2.54)\qquad \frac{\Delta r_f}{r_f} = \frac{\Delta r_1}{r_1 + r_2\,\exp(-jB)} - \frac{r_2 \cdot \exp(-jB)}{1 + r_1 r_2 \exp(-jB)} \cdot \Delta r_1$$

$$(2.55)\qquad \frac{\Delta r_f^*}{r_f^*} = \frac{\Delta r_1^*}{r_1^* + r_2^*\,\exp(+j\,B^*)} - \frac{r_2^* \cdot \exp(+j\,B^*)}{1 + r_1^*\, r_2^*\,\exp(+j\,B^*)} \cdot \Delta r_1^*$$

The latter equations may be written as

$$(2.56)\qquad \frac{\Delta r_f}{r_f} = \frac{A}{1 + \frac{r_2}{r_1} \cdot \exp(-jB)} - \frac{r_1\, r_2\, \exp(-j\,B)}{1 + r_1\, r_2\, \exp(-j\,B)} \cdot A$$

$$(2.57)\qquad \frac{\Delta r_f^*}{r_f^*} = \frac{A^*}{1 + \frac{r_2^*}{r_1^*} \cdot \exp(+jB^*)} - \frac{r_1^*\, r_2^*\, \exp(+j\,B^*)}{1 + r_1^*\, r_2^*\, \exp(+j\,B^*)} \cdot A^*$$

Where

$$(2.58)\qquad A = \frac{\Delta r_1}{r_1} \quad \text{and} \quad A^* = \frac{\Delta r_1^*}{r_1^*}$$

Substituting eqs. (2.56) and (2.57) into eq.(2.53) we finally obtain, (see Appendix B),

$$(2.59)\qquad \left[\frac{\Delta R}{R}\right]_{ERS} = (W1 - W2) \cdot \left[\frac{\Delta R_1}{R_1}\right]_{ERS}$$

where

$$(2.60)\qquad W1 = \frac{1 + \frac{|r_2|}{|r_1|} \cdot \exp(-\beta)\cos\Phi + 2H\frac{|r_2|}{|r_1|} \cdot \exp(-\beta)\cdot\sin\Phi}{1 + \frac{R_2}{R_1}\exp(-2\beta) + 2\frac{|r_2|}{|r_1|} \cdot \exp(-\beta)\cdot\cos\Phi}$$

$$W2 = \frac{R_1 R_2 \exp(-2\beta) + |r_1||r_2| \exp(-\beta)\cos\Theta + 2H|r_1||r_2|\exp(-\beta)\sin\Theta}{1 + R_1 R_2 \exp(-2\beta) + 2|r_1||r_2| \exp(-\beta)\cos\Theta} \tag{2.61}$$

$$H = \frac{\omega\tau(n_2^2 - k_2^2 - n_1^2) + 2n_2 k_2}{(n_2^2 - k_2^2 - n_1^2) + 2n_2 k_2 \omega\tau} \tag{2.62}$$

$$\beta = \frac{2\omega d}{c} k_2 \tag{2.63}$$

$$\Phi = \delta_2 - \delta_1 - \delta + \pi \tag{2.64}$$

$$\Theta = \delta_2 + \delta_1 - \delta + \pi \tag{2.65}$$

$$\delta = \frac{2\omega d}{c} n_2 \tag{2.66}$$

$$\tan(\delta_1) = \frac{2n_1 k_2}{(n_1^2 - n_2^2) - k_2^2} \tag{2.67}$$

$$\tan(\delta_2) = \frac{2n_1 k_2}{(n_3^2 - n_2^2) - k_2^2} \tag{2.68}$$

$$R_1 = |r_1|^2 \quad \text{and} \quad R_2 = |r_2|^2 \tag{2.69}$$

Expression (2.59) is a general equation for the electro-reflectance of thin films, in the case of ERS. It is valid for any thickness and as can be seen from eqs. (2.60) and (2.61) when $d = 0$, i.e. $\beta = 0$ the expression for one interface is obtained.

The right hand part of Eq.(2.59) consists of two main parts:the one in

the parentheses which regulates the magnitude of the electro-reflectance effect, being a function of film properties and thickness, and the one outside the parentheses which generates the spectral distribution of the effect and its initial magnitude, being a function of the perturbed optical properties of the interface.

Eq. (2.59) has been used to calculate ER spectra of a great variety of materials and film thicknesses. For the materials used in these calculations and the range of film thicknesses employed (i.e. 200 - 20,000 Å) it was found that $(W_1 - W_2)$ is always positive in the spectral region of the plasma edge. Thus, the polarity of the effect in the vicinity of the plasma edge is solely determined by the second term existing in the right-hand side of Eq. (2.59).

2.4.2 Internal Reflection Spectroscopy (IRS)

The Fresnel coefficients for the two interfaces of Fig.(2.18) are given by (Heavens 1965).

$$r_1 = \frac{n_3 - \bar{n}_2}{n_3 + \bar{n}_2} \tag{2.70}$$

$$r_2 = \frac{\bar{n}_2 - n_1}{\bar{n}_2 + n_1} \tag{2.71}$$

We are seeking an expression for the normalized change in reflectance of a film in terms of normalized optical changes occuring at the interface 2 with reference to fig.(2.18).

From eqs.(2.46) and (2.47) we respectively obtain

$$\frac{\Delta r_f}{r_f} = \frac{\Delta r_2 \exp(-j B)}{r_1 + r_2 \exp(-j B)} - \frac{r_1 \exp(-jB).\Delta r_2}{1 + r_1 r_2 \exp(-j B)} \tag{2.72}$$

$$\frac{\Delta r_f^*}{r_f^*} = \frac{\Delta r_2^* \exp(+j B)}{r_1^* + r_2^* \exp(+jB)} - \frac{r_1^* \exp(+j B^*).\Delta r_2^*}{1 + r_1^* r_2^* \exp(+j B^*)} \tag{2.73}$$

The latter equations may be rewritten as

$$\frac{\Delta r_f}{r_f} = \frac{G \exp(-j B)}{\frac{r_1}{r_2} + \exp(-j B)} - \frac{r_1 r_2 \exp(-j B).G}{1 + r_1 r_2 \exp(-j B)} \tag{2.74}$$

$$\frac{\Delta r_f^*}{r_f^*} = \frac{G^* \exp(+j B^*)}{\frac{r_1^*}{r_2^*} + \exp(+j B^*)} - \frac{r_1^* r_2^* \exp(+j B).G^*}{1 + r_1^* r_2^* \exp(+jB^*)} \tag{2.75}$$

where

$$(2.76) \qquad G = \frac{\Delta r_2}{r_2} \qquad \text{and} \qquad G^* = \frac{\Delta r_2^*}{r_2^*}$$

Substituting eqs.(2.74), (2.75) and (2.76) into eq.(2.53) we finally obtain, (See Appendix C),

$$(2.77) \qquad \left[\frac{\Delta R}{R}\right]_{IRS} = (Q1 - Q2) \cdot \left[\frac{\Delta R_2}{R_2}\right]_{IRS} \exp(-\beta)$$

where

$$(2.78) \qquad Q1 = \frac{\exp(-\beta) + \frac{|r_1|}{|r_2|}\cos\Phi + 2\frac{|r_1|}{|r_2|} H \sin\Phi}{\frac{R_1}{R_2} + \exp(-2\beta) + 2\frac{|r_1|}{|r_2|}\exp(-\beta)\cos\Phi}$$

$$(2.79) \qquad Q2 = \frac{R_1 R_2 \exp(-\beta) + |r_1||r_2|\cos\Theta + 2|r_1||r_2| H \sin\Theta}{1 + R_1 R_2 \exp(-2\beta) + 2|r_1||r_2|\exp(-\beta)\cos\Theta}$$

All the parameters of eqs.(2.78) and (2.79) have been defined previously. In the case of IRS the magnitude of the electro-reflectance signal is expected to be much more lower than in the case of bulk or ERS because of the expotential term present in the right hand side of eq. (2.77).

Expression (2.77) is valid for any film - thickness. When d=0, i.e. $\beta = 0$, Eq.(2.77) becomes similar to eq.(2.25) which determines the ER effect in a two-phase system.

Finally, calculations according to Eq.(2.77) showed that the quantity $(Q_1 - Q_2)$ of the right-hand side is always positive in the spectral region of the plasma edge and for film thicknesses from 200 to 20,000 Å.

REFERENCES

1. Anderson W.J., and Hansen W.N., J.Electroanal.Chem. 47, 229 (1973).
2. Avaritsiotis J.N.,MSc.Thesis, Loughborough 1974.
3. Axe J.D.,and Hammer R.,Phys.Rev. 162, 700 (1967).
4. Bewick A.,and Robinson J.,J.Electroanal.Chem.60, 163 (1975).
5. Cahan B.D.,Horkans J. and Yeager E. Symp.Faraday Soc.4, 36 (1970).
6. Cardona M.,Shaklee K.L. and Pollak F.H. Phys.Rev.,154, 696 (1967).
7. Cheyssac D.,Garrigos R.,Kofman R.,Penavaire L.,Richard J.,and Saissy A.,Thin Solid Films 13 275 (1972).
8. Fox T.,Howson R.P.and Emmony D.,J.Phys.D.:Appl.Phys., 7, 1864 (1974).
9. Garrigos R. PhD Thesis 1974 Universite de Nice, France.
10. Hansen W. and Prostak A.Phys. Rev.160, 600 (1967).
11. ———————— ———— 174, 500 (1968).
12. Heavens O.S.,"Optical Properties of Thin Solid Films" Dover 1965.
13. Howson R.P. ,Avaritsiotis J.,and Fox T.,Thin Solid Films 30 ,297 (1975).
14. Kofman R.,Garrigos R.,and Cheyssac P.,Surf. Sci., 44, 170 (1974).
15. McIntyre J.D.E.,Symp.Faraday Soc. 4 ,50,55,61 (1970).
16. ————————,Adv.Electrochem. Eng. 9,61 (1973).
17. McIntyre J.D.E. and Aspnes.D.E. Surf.Sci.,24, 417 (1971).
18. Ramo S.,Whinery J.and Van Duzer T.,"Fields and Waves in Communication Electronics" Wiley 1965,p.350.

CHAPTER 3

EXPERIMENTAL TECHNIQUES

3.1 Introduction

A technique using alternating signal processing of the incident radiation was used. The optical modulation was created and recorded using the following components:

a) Light source,

b) Monochromator,

c) Detector,

d) Phase sensitive detector and amplifier,

e) Modulation oscillator, recorder, attenuator, and chopper,

f) Modulating unit.

The block diagram of the setup is shown in Fig. (3.1). In the present chapter, the characteristics and the limitations of the individual components are discussed.

3.2 Light Source

The source choosen was a Nernst glower which consists of a mixture of rare earth oxides in the form of a rod about 2.5 cm long by 3mm diameter. It has a negative resistance rise with temperature and requires pre-heating to reach its operating conditions. The filament was mounted in a specially designed asbestos-jacket which reduced the effects of draughts and served as a holder for the heater. The operating temperature was about 1900^{o}C. At this temperature the distribution of energy in the infrared spectrum is shown in Fig. (3.2). From this figure it is evident that whithin the regions 1-2 and 3-12 microns the intensity of the radiation drops by three orders of magnitude.

Fig.(3.1) SCHEMATIC DIAGRAM OF THE APPARATUS

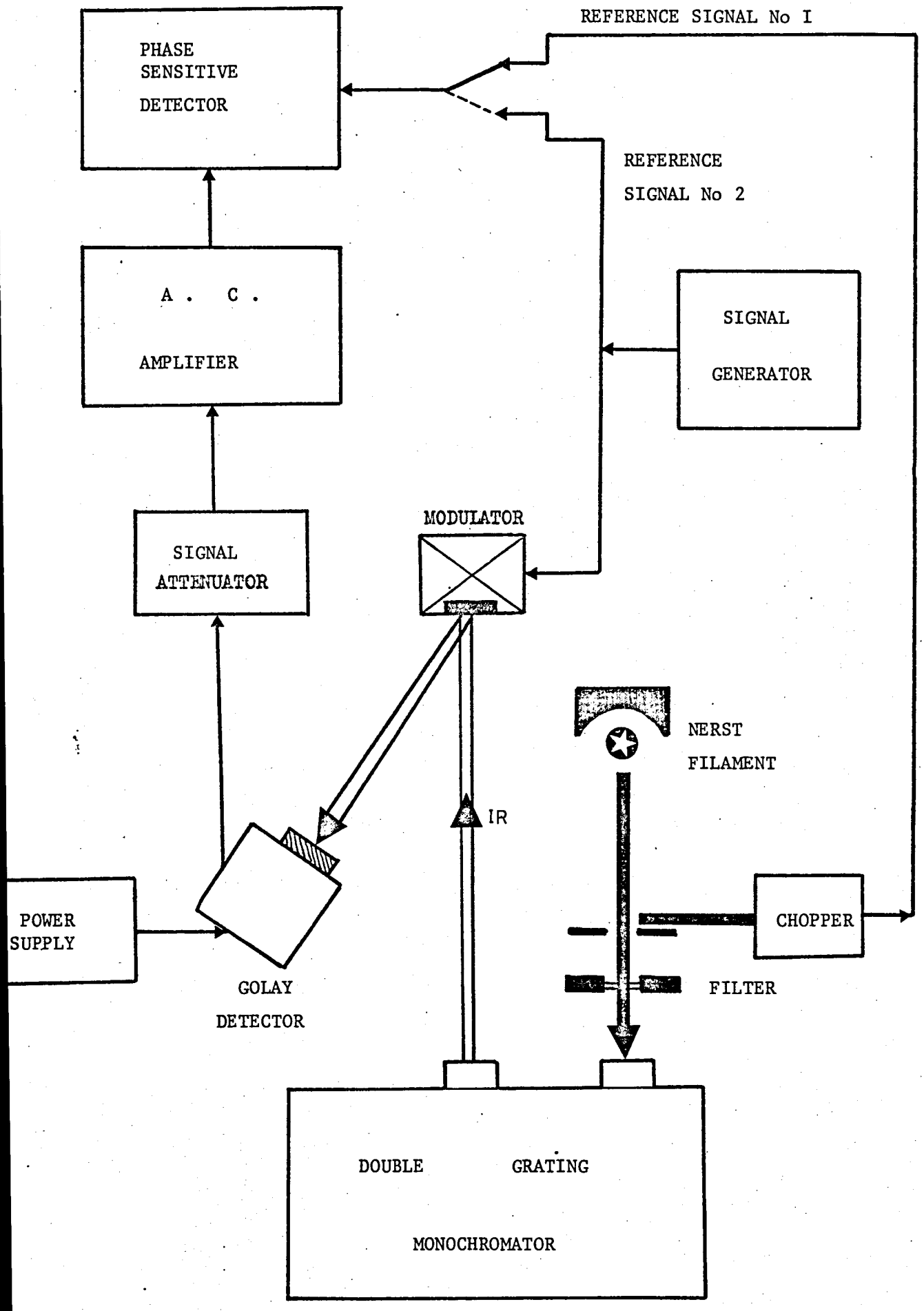

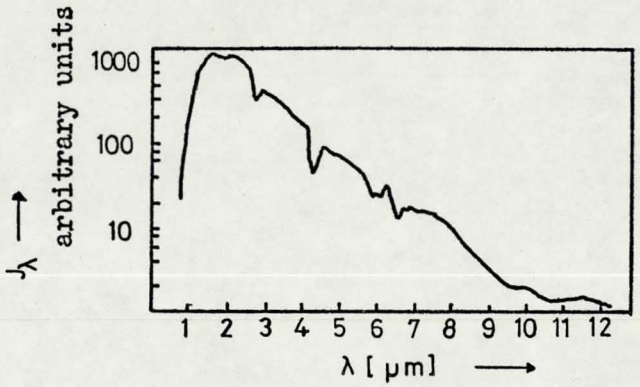

Fig. (3.2) Spectral distribution of the emission from a Nernst glower, at about 1900°C and upon dispersion by a rock salt prism according to A.Vaško (1968). Dents on the curve are due to the atmospheric absorption of the radiation.

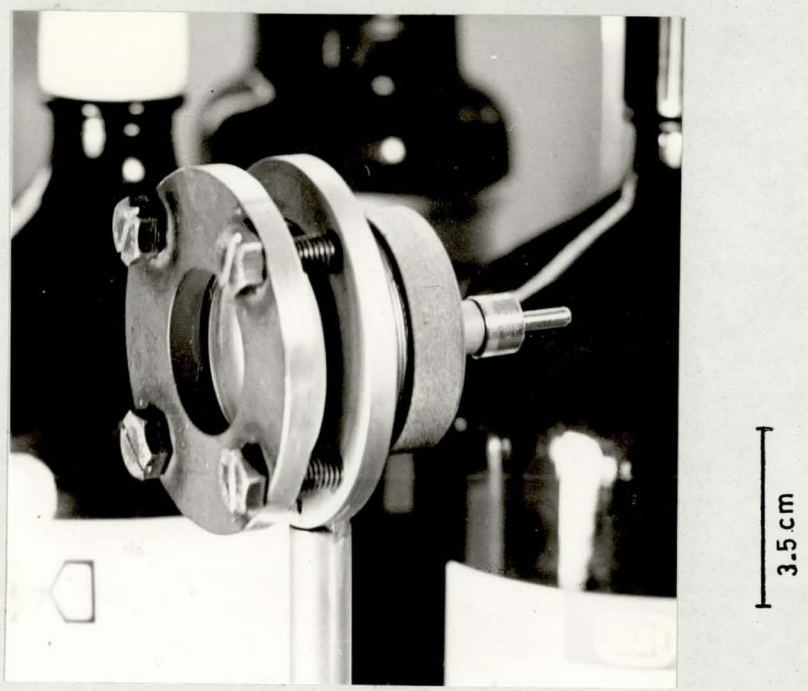

Fig. (3.3) Photograph of the electrolytic modulator used in the course of ER measurements.

Power to the filament is supplied from a Hilger and Watts Nernst Filament Power Supply Unit FL 111, designed to provide a 240 V a.c. voltage.

3.3 Monochromator

A Hilger and Watts D330-331 double monochromator was used; this is a plane grating , symmetrical Czerny - Turner instrument. The required wavelength at the exit slit is obtained either manually by rotating the grating table with a calibrated wavelength micrometer, or by motor-drive for spectral scanning purposes. Both entrance and exit slits were provided with a) calibrated width variation over a large range (0-3mm), and b) filter holders.

The luminosity (or the output factor) of the monochromator is in general proportional to the area of the disperser and the slit-height to focal length ratio. Moreover, it increases as the square of the slit width, (Stweart 1970,p.226), provided that entrance and exit slit widths are the same. The diffraction gratings used have a ruled area 52 x 52 mm^2. The focal length of the monochromator is 300mm and the maximum height of the slits is 18 mm.

Three diffraction gratings were available and used in the course of the measurements, covering the spectral regions from 0.67 to 2.0 microns and 2.7 to 16.0 microns, and having blaze wavelengths 1 micron (600 lines/mm), 4 microns (150 lines/mm) and 8 microns (75lines /mm).

Filters were used for selective attenuation in order to assist the mono - chromator in the purification of radiation. An indium - arsenide infrared

filter was used for the spectral region 3.8 to 7 microns in order to reject short wavelength radiation entering the monochromator. A silicon filter was used for the spectral region between 1.3 and 5 microns. Finally an indium antimonide filter was used for the spectral region between 7.5 and 16 microns.

A simple and inexpensive attachment to the monochromator was constructed for accurate recording of wavelengths and is described in Appendix E. The use of this attachment offers the possibility of remote wavelength monitoring and simultaneous recording of marks superimposed on the recorded spectrum, and corresponding to predetermined positions of the wavelength micrometer drum. Also, it facilitates the use of the monochromator when work is carried out in a poorly illuminated room. Its main features are: a) stable high accuracy in determining the position of the wavelength drum and b) no modification of any part of the monochromator is required.

The calibration of the wavelength drum was set using the known positions of absorption - line maxima of tetrachloroethylene (C_2Cl_4), acetonitrile (C_2H_3N), carbon disulphide (CS_2), and chloroform ($CHCl_3$). Table (3.1) summarizes the absorption - line maxima used in our calibration scheme. Moreover atmospheric absorption provided a sufficient check on the accuracy of the calibration of the wavelength drum. Wavelengths for water vapor absorption were taken from Burch et al (1963), and for carbon dioxide absorption from Burch, Gryvnak and Williams (1962) and Gebbie et al (1951). The carbon dioxide absorption band at 4.27 microns, being particularily intense, was suitable for quick checks of the correctness of the calibration of the monochromator during its use. Checks were also made, at frequent intervals, using a polystyrene sheet

exhibiting pronounced absorption peaks in the spectral region between 3 - 4 microns and 6 - 7 microns.

TABLE (3.1) Calibration Scheme (+)

WAVELENGTH Nos.	ACETO-NITRILE C_2H_3N	TETRACHLORO-ETHYLENE C_2Cl_4	CARBON DISULPHIDE CS_2	CHLOROFORM $CHCl_3$	POLYSTYRENE $(C_8H_4)_n$
1	2.28	4.02	3.56	1.74	3.303
2	3.34	5.38	4.36	2.39	3.42
3	4.36	7.39	4.63	3.32	3.51
4	4.44	-	6.61	4.17	6.69
5	6.67	-	-	6.58	6.88
6	-	-	-	6.77	7.39

(*) For the conversion into wave numbers from wavelengths quoted, the following relation holds good: $\nu[cm^{-1}] = \frac{10000}{\lambda[\mu m]}$,Vasko (1968).

(+) Values quoted have been obtained from: Mecke R.,and Langenbucher F., INFRARED SPECTRA of Selected chemical compounds,1964.

All calibration runs were performed at a scanning speed of 0.2 microns/min (for a 150 L / mm grating) in the direction of increasing wavelength, and a filter-period of 3 sec was used. The slit - widths were adjusted each time so that a compromise between high signal - to - noise ratio and adequate resolution was obtained. The reproducibility of the instrumental setting was checked by repeated running of the same sharp - lined spectrum at high signal - to - noise ratio and slow scanning rate and observing the magnitude of apparent changes (less than 0.05) in positions of the line maxima. The rate of recording was slow enough (30 cm / min) so that the entire detecting amplifying and recording system had time to reach a

high fraction (say 99%) of the recorded response which would be reached in an indefinitely long time (say 50 times the filter period).

3.4 Detector

Two types of I.R. detectors were used: a pyro - electric detector and a pneumatic detector.

The most commonly used figures of merit to describe the characteristics of the detector are the Noise Equivalent Power (NEP) and the detectivity (D*); see Nudelman (1962).

The NEP is defined as the rms value of the sinusoidally modulated radiant power falling upon a detector which will give an rms signal voltage equal to the rms noise voltage from the detector. The black body temperature of the source, the chopping frequency and the electrical bandwidth are specified. It is worth noting that the detector performance increases as the NEP decreases.

$$\text{NEP} = H.A \frac{V_N}{V_S} \cdot \frac{1}{(\Delta f)^{\frac{1}{2}}} \qquad (3.1)$$

where H is the rms value of the irradiance falling onto the detector of area A, and V_N / V_S is the ratio of the rms noise voltage in the bandwidth Δf of the rms signal voltage.

Neglecting surface effects most detectors exhibit a NEP which is directly proportional to the square root of the detector area.

The detectivity D* is defined as:

$$D^* = \frac{A^{\frac{1}{2}}}{\text{NEP}} \qquad (3.2)$$

The units of D^* are : cm . $Hz^{\frac{1}{2}}$. W^{-1}.

In the case of thermal detectors (pyroelectric, Golay, bolometers) the radiation absorbed causes their temperature to rise and this produces a change in some physical property of the detector. They do not require cooling and their response is theoretically independent of wavelength, but in practice the detector window and limitations of available blackening materials modify this assumption.

A pyroelectric detector consists of a ferroelectric crystal which exhibits a spontaneous electric polarization which is temperature dependent. The usual method of construction is to apply electrodes onto opposite faces of a thin slice of pyroelectric material which will then behave as a capacitor. If the absorbed radiation incident on one face is varied then the temperature and hence the polarisation will also fluctuate. This will induce charge on the electrodes which will appear as a voltage when measured by high impedance voltmeters; Holeman (1972), Blackburn and Wright (1970), Chynoweth (1956).

The Golay cell consists of a small cavity containing a gas such as xenon or helium at low pressure. Radiation is absorbed by a specially designed membrane and heats the gas. Part of the cavity wall is a flexible diaphragm, silvered on the outside, which is distorted when the gas pressure changes and deflects a beam of light shining on a photocell. A small change in incident radiation causes a large change in photocell output; Golay (1947), (1947) and (1949).

3.4.1 Pyro - electric Detector

A triglycine sulphate (T.G.S.) pyroelectric IR detector type No PSC222 was used at the early stages of our series of experimental studies. The PSC222 is made by Plessey Co Ltd and the complete unit consists of a sensitive element with a low noise preamplifier and a standard 709 operational amplifier output stage.

However the relatively low detectivity, D* , (500K,10,1) 5×10^{8} cm Hz$^{\frac{1}{2}}$ W^{-1} a N.E.P. (4×10^{-10} Watt Hz$^{-\frac{1}{2}}$) dictated the use of a more sensitive and low noise infrared detector having a broadband spectral response.

3.4.2 Golay Detector (IR50)

This unit contains the pneumatic head, the optical amplifier and a solid state amplifier. It is made by PYE UNICAM Ltd and is provided with a potassium bromide window 6mm thick which limits its wavelength range between 0.4 and approximately 25 microns. The sensitivity with KBr window is 3×10^{6} Volts / Watt and the NEP at a black body temperature of 500°K , chopping frequency of 11 Hz and bandwidth of 1 Hz is 7×10^{-11} Watts. Its maximum overload input is 2×10^{-3} Watts approximately, corresponding to an output of 7 Volts approximately. It is worth noting that the detector was never saturated in the course of our experimental studies.

The main handicap of the detector was its limited low frequency response and its sensitivity to a) vibrations in the range of 0.1 to 100 Hz through microphony, and b) draughts.

The optical modulation system between the pneumatic head and the photo - detector provides an initial gain and relatively high signal level which is further amplified by a succeeding electronic amplifier which is contained in the detector housing.

A power unit supplies two outputs, one being 24V/5mA supply to the signal amplifier. The L.E.D. supply (2-3V 0.25 A) has a high degree of current stabilization and a preset current control, which is initially adjusted at a standard detector unit temperature. Thereafter the supply eliminates mains variations and L.E.D. impedance changes. A thermistor in the detector unit conpensates for light output changes with temperature.

3.5 Amplifier and Phase Sensitive Detector

The amplifier used was a Brookdeal ORTEC precision A.C. amplifier, model 452. This model is a general purpose A.C. instrumentation amplifier incorporating a low - noise preamplifier, buffered high and low pass filters, and line reject filter. Its 100 dB gain is obtained by five 20dB gain blocks one of which is an active filter. The amplifier proved unstable at high gain positions ($\sim$ 50 dB) when the ΔR signal was measured.

The phase sensitive detector used was made by Brookdeal ORTEC, model 9412. The use of a phase sensitive detector was necessary because the signal due to reflectivity changes was buried in noise.

3.6 Modulation Oscillator, Recorder, Attenuator and Chopper

A SERVOMEX waveform generator, type L.F.141, supplied the modulating voltage to the modulating unit and the reference input of the phase

sensitive detector.

The output signal of the phase sensitive detector was recorded with the aid of a GOERZ - ELECTRO (SERVOSCRIBE) pen recorder. A Brookdeal (ORTEC) light chopper, type 9479 was used for the measurements of the reflectivity of the samples. The chopping frequency was selected to be 13Hz. A signal attenuator also used in the course of reflectivity measurements, when the detector output was too high for the phase sensitive detector (max. input signal 3V p-p).

3.7 Operating Parameters

It is generally difficult and time consuming to record IR spectra at low signal levels. Additional noise - problems, however, arise in the case of ER measurements because the A.C. signal due to reflectivity changes, generally is superimposed on a considerably larger D.C. signal which is the unmodulated percentage ($\sim 99\%$) of the radiation intensity falling onto the detector.

The Golay pneumatic detector is photon-noise limited. The rms fluctuations, $\bar{W}$, in the electrical bandwidth, Δf, and a detector area, A , is given [Limperis (1965)]:

$$\bar{W} \propto \sqrt{2A \cdot \overline{\Delta n^2} \cdot [\Delta f]} \qquad (3.3)$$

where $\overline{\Delta n^2}$, the mean square fluctuation (in photons) of wavelength falling onto the detector area, is proportional to the average number of photons.

Consequently, although the unmodulated component of the radiation falling

onto the detector is not "seen" , generates considerable noise which depends on the mean number of photons falling onto the detector per unit time and area. In other words the amount of noise depends on the unmodulated radiation intensity falling onto the detector area.

Since the A.C. signal is proportional to the radiation intensity, the signal - to - noise ratio is proportional to the square root of the light intensity. Thus, an increase of the radiation intensity (by increasing the source temperature and / or widening the slits of the monochromator) does not induce considerable improvement of the signal - to - noise ratio, (S/N), and thus an additional way of improving S/N must be sought.

It is worth noting that Johnson noise is present in the apparatus, caused by the random movement of electrons in the detector and associated circuitry. Johnson noise is determined from the formula (Jamieson et al 1963):

$$\bar{e}_J^2 = 4kTR\cdot[\Delta f] \qquad (3.4)$$

where e_J is the Johnson noise voltage of the output of the detecting system, T is the temperature of operation, R is the output resistance of the detecting system, k is Boltzmann's constant and Δf is the frequency bandwidth of the noise spectrum.

Inspection of relations (3.3) and (3.4) shows that both photon and Johnson noise can be potentially decreased by narrowing the bandwidth of the noise spectrum.

Phase sensitive detection is a method of implementing the latter way of improving S/N. A phase sensitive detector extracts a signal from noise by multiplying the signal input voltage with a reference and then filtering

the product with a filter of time constant To. The overall filter characteristic given by the system is that of a filter centered on the reference frequency whose noise - equivalent bandwidth is

(3.5) $$[\Delta f] \propto \frac{1}{To}$$

So, S/N can be improved employing relatively large time constants for the phase sensitive detector. The time constant of the model 9412 is variable from 10ns to 100s and therefor the bandwidth can be varied between 25Hz and 0.0025 Hz according to its specifications.

It is interesting to note that although an initial amplification of the input signal does not improve the S/N , it is required in our case to make the recovery of the ER signal more sensitive. In other words the magnitude of the ER signal, which is buried in noise, must be increased by amplification in order to make it greater than the "minimum detectable" (by phase sensitive detector) input voltage, which is taken as the signal level which gives rise to a psd output voltage equal to the maximum D.C. errors due to out - of - phase rejection or temperature changes.

However, the use of large To is limited by the scanning speed of the monochromator which eventually is determined by the r.p.m. of the motor which rotates the wavelength drum. So, having: a motor with 1 r.p.m. and gratings with characteristics given in previous paragraphs, as well as the intention to record an ER spectrum in a logical period of time, it was decided to employ a signal averaging technique instead of increasing the p.s.d.'s time constant by adding external capacitances.

According to the latter technique the same signal is recorded repetitively by scanning and rescanning the same spectral region. S is added arithmetically and is proportional to the number of scans, m, whereas the noise, N, tends to cancel itself and is proportional to $m^{\frac{1}{2}}$. Thus, S/N is proportional to $m^{\frac{1}{2}}$ and the quality of ER spectrum is improved specially in the spectral regions where the radiation intensity is relatively low.

The ideal solution in this case is to use an on-line mini-computer. In our case,however, the average values of a large number of sets of experimental points were obtained by averaging a large number of ER spectra from the same sample under similar conditions, point - by point ! Fortunately, this technique was employed for the lower ER values and in the case of Internal reflection Spectroscopy only. A number of 25 successive scans was employed for each sample.

The S/N can be further improved by increasing the modulating electric field applied on the surface of the sample. The electric field, however, can not be increased over certain values (depending on the nature of the configuration used) because the modulating unit may be damaged.

Finally, background - radiation noise, depending on the temperatures, emissivities, and geometry of the items "seeing" by the detector, was present.

3.8 Modulating Unit

This part is the "heart" of experimental setup since it is the unit where the changes of reflectivity are induced by the application of a high

electric field on the surface of the sample.

3.8.1 Introduction

The high values of electric fields ($\sim 10^5$ - 10^6 Volts /cm), required to induce the optical properties of the surface of the samples are usually obtained by creating a surface potential barrier , the electric field of which is directed normallyto the reflecting surface.
A periodic change of a voltage across the terminals of the modulating unit generates a periodically changing electric field which finally modulates the reflectivity of the sample-surface. The exact fraction of the potential drop accross the surface barrier generally is a complicated function of various parameters. A measurement, however, of the surface - barrier capacitance establishes the relationship between the external voltage and generated electric field.

The methods which have been used ,in the course of our studies, to create a surface potential barrier are discussed in the following sections.

3.8.2 Dry - sandwich Modulator

According to this technique an electric field is applied on the surface of the sample by means of a semitransparent electrode opposite the sample; the space between can be filled with a transparent material of high dielectric constant.

This technique was unsuccessfully employed during the first stages of our experiments. The film under investigation was covered with a film of ZnS (~ 3000Å) and a film of Al - mesh was evaporated on the top. This dry

sandwich needed a rather high voltage (~ 50 Volts) in order to create an adequate electric field on the sample surface, because of its low capacitance, (less than 100 p F).

In the case of antimony films the dry sandwich was fabricated in a different way. The methods of creating anodic oxide films on antimony are rather well established. Oxide film growth occurs in 0.1 M solution of H_2SO_4, for example, when the anode potential rises above ~ 60 V [see Stock and Purdy (1957), Norakidze et al (1969), Solov'eva et al (1970), Styrkas (1969), Ammar and Saad (1971),(1972), and finally Girginov and Ikonopisov (1974)].

So, antimony films evaporated on glass substrates held at 280°C were anodically oxidized so that a surface oxide film (~ 500 Å thick) was created. Unfortunately most of the sandwiches were short - circuited after the deposition of the top semitransparent electrode (Al - mesh).

The same type of dry sandwiches was constructed for various films deposited onto NaCl substrates, for internal reflection spectroscopy. Due to the inability of the experimental setup to detect the reflectivity changes induced by the previously described modulating units, a more powerful way of modulation was sought.

3.8.3 Electrolytic Modulator

At the early stages of these experiments aqueous electrolytes were used in electrolytic cells described by Fox (1974), and Avaritsiotis (1975). It was discovered, however, that antimony films evaporated onto glass and silicon substrates held at approximately 280°C were dissolved into the electrolyte even without the application of a voltage between the

Sb film (working electrode) and Pt wire (counter electrode).
Systematic study of the cause of the effect showed that atmospheric oxygen dissolved in the distilled water used for the preparation of the aqueous electrolytes (with Na_2SO_4) was responsible for the dissolution of Sb thin films.

It is interesting to note that no one, to the best of our knowledge, has reported the observation of a similar effect possibly because everybody is dealing with bulk samples of antimony.
The method adopted for the purification of the electrolyte from dissolved oxygen was typically: The electrolyte was purified in a specially designed bubbler, where oxygen was helped to diffuse into an oxygen - free nitrogen atmosphere and was subsequently driven out of the device in a stream of nitrogen. Purification periods of two weeks were necessary in order to prevent Sb films from dissolving into the electrolyte.

Unfortunately, the use of aqueous electrolytes was abadoned although cell capacitances of the order of 25 $\mu F/cm^2$ were measured, because the continuous application of more than 0.2 Volts caused dissolution of the Sb films.

3.8.3.1 Non - aqueous Electrolytes

A feasibility study showed that our requirements, i.e. a) high conductivity, b) high (more than 80%) transmittivity in the spectral region of interest (0.5 - 15 microns), c) high limiting anodic and cathodic potentials and, d) medium dielectric constant (2-30), were met by the following nonaqueous electrolytes:

1) Acetonitrile (ALDRICH CHEMICAL Co Ltd),

2) Carbon tetrachloride (FISONS SCIENTIFIC APPARATUS Ltd),

3) Carbon disulphide (BDH CHEMICALS Ltd).

Acetonitrile may be used alone although serves as an excellent solvent for some inorganic salts (Mann, 1969, Billon 1960). Both anodic and cathodic limiting currents apparently are caused by discharge of the supporting electrolytes. Supporting electrolytes used with carbon tetrachloride and carbon disulphide to reduce the electrolytes resistance; $NaClO_4$ (sodium perchlorate) bought from HOPKIN AND WILLIAMS LTD, and KNO_3 (potassium nitrate) bought from FISONS SCIENTIFIC APPARATUS LTD. Both the latter absorb strongly at approximately 9 microns only;[Mecke 1965].

However, acetonitrile's transmittivity at long wavelengths is reduced by the appearence of absorption bands. So, acetonitrile was used in the spectral region of 1-3 microns, and Carbon tetrachloride was mainly used for the ER measurements in the spectral region 2-10 microns. Carbon disulphide was used a few times only because of its high toxicity, although its transmittivity is extremely high (95%) in the spectral regions between 1-4.3 4.8 - 6.2, and 7.4 - 11 microns;[Mecke and Langenbucher 1965].

3.8.3.2 Solid Electrolytes

Our criteria for the nature of the electrolyte were met by the so-called solid electrolytes. Solids like $Ag_6I_4WO_4$ (Takahashi et al 1973), $Ag_2X - AgI - HgI_2$ (Takahashi et al 1973), LaF_3 (Lilly et al, 1973), Ag_2HgI_4 (Weil and Lawson 1964), $RbAg_4I_5$ (Rossi et al 1969, Scrosati 1973, Scrosati et al 1971, Kennedy et al 1973), Silver - Halide (Raleigh 1974, Foley 1969), AgBr (Kennedy and Chen 1968 and 1969, Hull and Pilla 1971) ,

show ionic conductivities up to 10^{-1} ohm^{-1}. cm^{-1} and have very high concentrations of mobile species (more than 10 mol/l).

Armstrong et al (1970,1973,1974) have reported large double layer capacitances for AgBr and Ag at room temperature ($\sim 5\ \mu F/cm^2$). Also, their transmittance is about 74% over the spectral region 0.45 - 35μm. The melting point of silver bromide (AgBr) in particular is 432°C although it starts becoming fairly soft when its temperature exceeds 100°C, (BDH Crystran, crystal products data sheet). Two polished AgBr crystal windows $\frac{1}{2}$ "Dia x 2 mm thick grown by BDH Chemicals Ltd, were used in the course of our experiments. Film deposition on their optically polished faces was excluded because of their low melting point. Thus, polished bulk Sb and GeTe were brought in direct mechanical contact on both sides of each AgBr window. Unfortunately the overall capacitances measured were (10pF), smaller than the ones published by Armstrong and Mason (1973) mainly because of the nature of the metal - electrolyte interface of our configuration. Additionally, silver migration was observed after one week, having as a result the complete damage of the unit.

Finally, the catholic use of non-aqueous electrolytes was decided, for their advantages which have been already discussed, and a special electrolytic cell was built.

3.8.3.3 Cell - configuration

A redistribution of charge carriers occurs at the interface of a solid in contact with an electrolyte. On the solution side, the depths of the redistribution from the surface depends on the nature and the concentration of the electrolyte, and it extends up to 1 micron into the solution. This

redistribution of charge carriers behaves like an electrical capacitor (Bockris and Reddy 1970), and is divided, for descriptive purposes, into the Helmholz layer, which is the locus of the electrical center of adsorbed ions on the surface, and the diffuse or Gouy - Chapman layer which extends into the solution, (MacArthur 1974, Reeves 1974).

On the solid side, the extent of the redistribution depends on the concentration of the free charges.

A wide range of techniques has been employed to measure the capacitance of the solid - electrolyte interface. The simplest uses A.C. bridge methods employing Weatstone bridges; in our case the Marconi TF2700 bridge was used. The electrolytic cell used is shown in Fig.(3.3). The same cell was used for both internal and external reflection spectroscopy. Fig.(3.4) shows a schematic of the cell in the case of IRS and Fig.(3.5) shows a schematic of the cell in the case of ERS.

The potential - sweep method has been used to determine the presence of electroactive contaminants. In this method the potential of the working electrode is changed linearly as a function of time. The current flowing in the electrode is monitorned. At low sweep speeds (less than 10 mV/sec) a steady - state condition is approached and the current is determined by reactions at the electrode occuring at the immediate potential; current peaks in the I-V curve manifest the presence of reacting species, (Kuta 1972). Fig.(3.6) shows a typical I-V curve which shows that no reaction was taken place on the working electrode (thin film).

Typical values for the electrolytic cell capacitance are 0.1 - 0.3 F/m^2 depending on the nature of the electrolyte and the cell configuration.

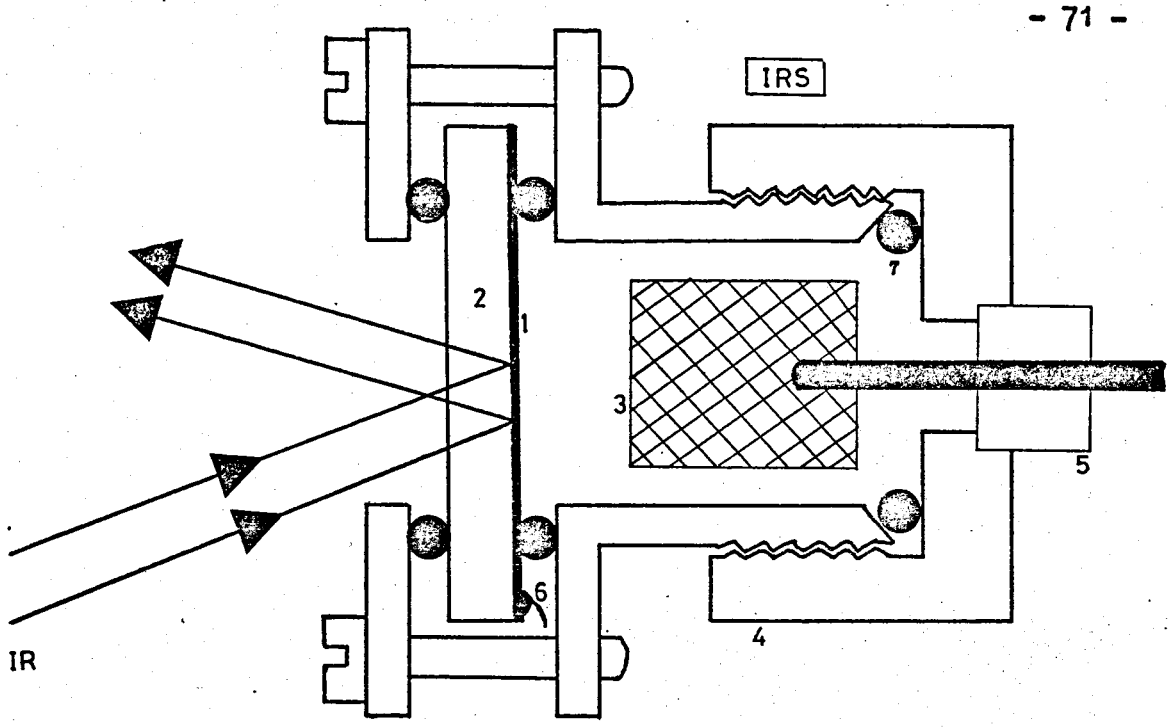

Fig.(3.4) ELECTROLYTIC CELL :1.Thin film, 2.NaCl substrate, 3.Pt counter electrode, 4.Stainless steel, 5.Ceramic Insulator, and 6. Electrical contact to thin film., 7.Neoprene o - ring.

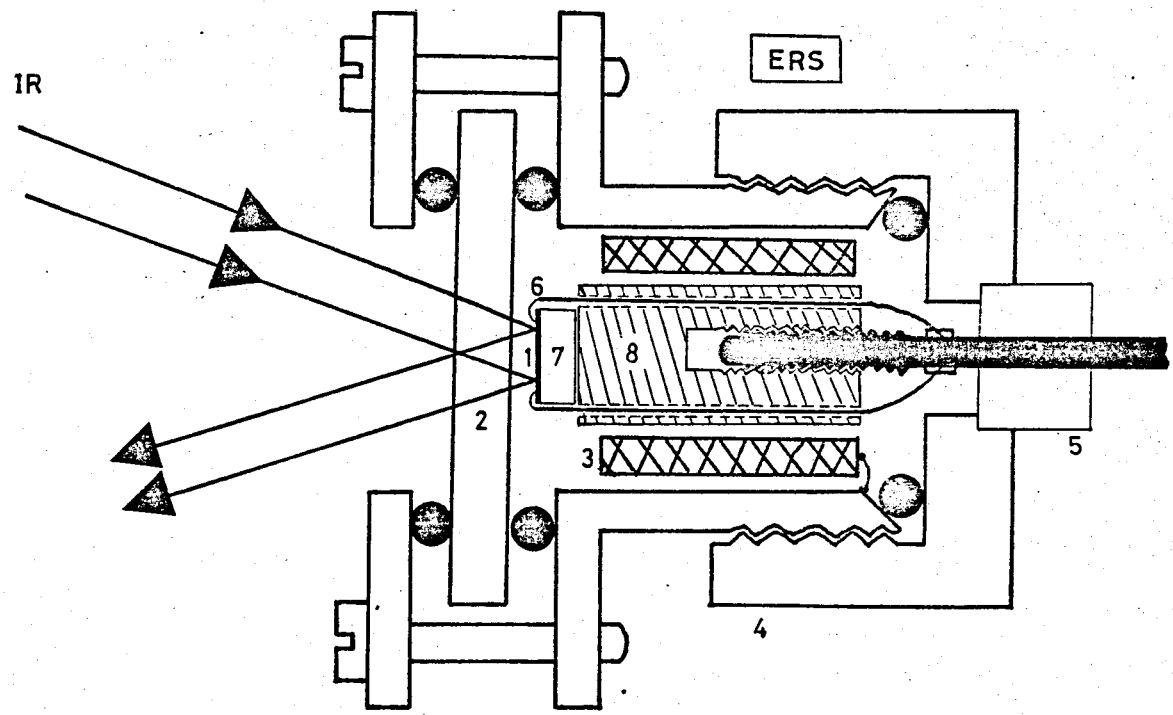

Fig.(3.5) ERS. 1.Sample, 2.NaCl window, 3.Pt electrode, 4.Stainless steel 5.Ceramic insulator, 6.Au - contact, 7.Glass substrate, and 8.Teflon cylinder.The distance between NaCl window and sample was variable (0.4mm - 5mm).

3.9 ER - measurement Procedures

Two measurements were obtained at each wavelength:one corresponding to the change of reflectance due to the application of electric field on the surface of the sample,and a second one corresponding to the near normal ($\sim 10^{o}$) reflectivity of the sample.

The first measurement was obtained using a reference signal from the signal generator, whereas the second measurement was obtained using the reference signal from the chopper. It is worth noting that the chopper was out of operation during the first measurement in order not to introduce additional (considerable) noise.

Measurements of relative reflectance were also performed in the spectral region around the reflectance plasma edge. The reflectivity spectrum of each sample was recorded before the ER measurements using the UNICAM SP 200 IR spectrophotometer, so that a quick check of the spectral position of the plasma edge was performed. The relative reflectance of the same sample was measured, after the course of ER measurements, by comparing the reflectivity of the sample to the reflectivity of the freshly deposited Al-film approximately 6000 Å thick, (Burtin 1964). The agreement between the results obtained using the UNICAM IR spectrophotometer and our experimental setup was very good.

3.10 Thin Film Fabrication Techniques

Various methods have been employed to fabricate thin films suitable for the study of ER effects. Thermal evaporation from asymetric oven - type point source was used for the evaporation of GeTe films. A similar

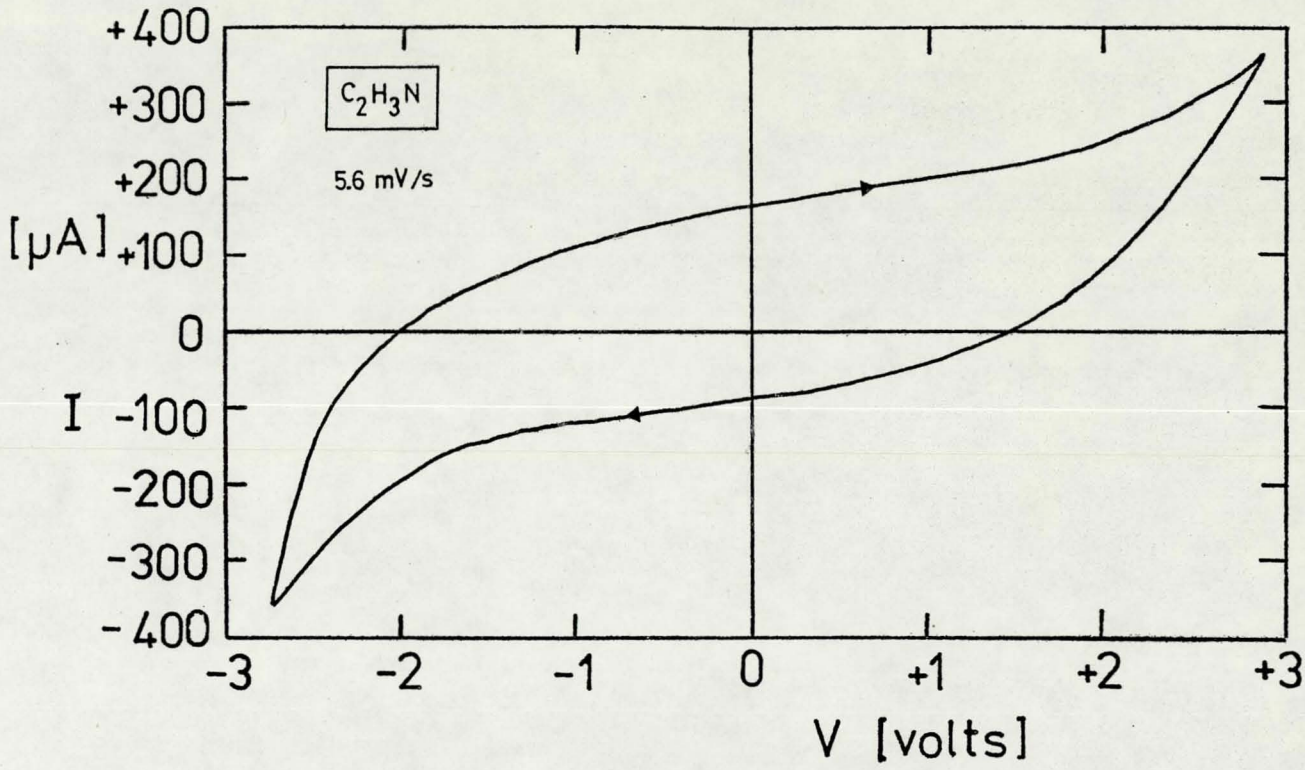

Fig.(3.6) Typical I-V curve for acetonitrile. Similar curves were obtained for carbon tetrachloride and carbon disulphide.

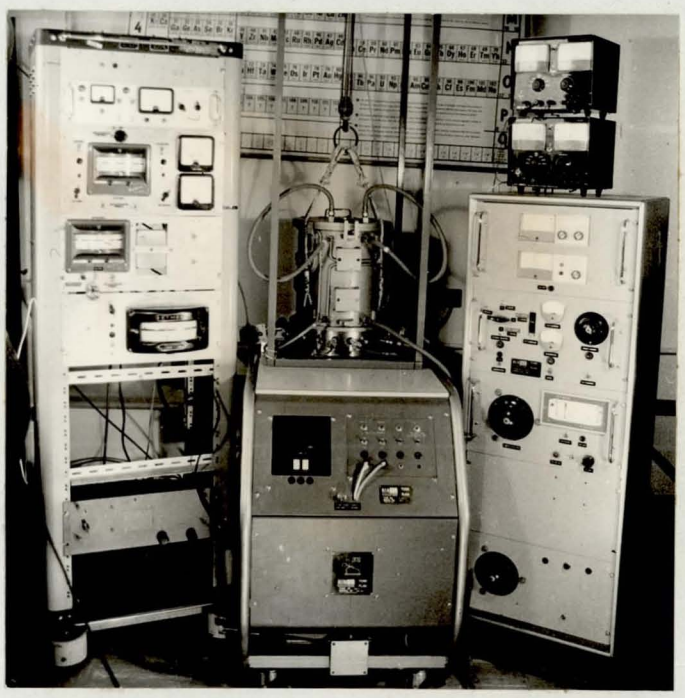

Fig.(3.7) Photograph of the vacuum plant used for the fabrication of Sb and GeTe films. It has been modified in order to fabricate Sn - doped In_2O_3 films by activated reactive sputtering.

technique was used for the fabrication of SnTe films. Fig.(3.7) is a photograph of the apparatus used to evaporate GeTe. This unit was later modified in an attempt to fabricate tin-doped indium oxide films by reactive sputtering. SnTe films were fabricated in a different vacuum plant which was previously used for the coating of substrates with Au islands, with the aid of an electron gun (Avaritsiotis 1974).

3.10.1 Antireflection Coatings

A third coating unit was used, in the initial stages, for the fabrication of antireflection coatings on silicon substrates. Zinc sulfide single coatings were evaporated from V-shaped tantalum heaters (Rood 1951), onto Si substrates held at room temperature and suspended 25 cm above the tantalum heater. The approximate value of the coating thickness was monitored by a simple optical system incorporating a tungsten light source and a Schottky - barrier photodiode.

A single - layer antireflection coating is the simplest both theoretically and experimentally. If light is incident at normal incidence onto a transparent massive medium coated with a single transparent layer, the reflected amplitude is given by

$$r = \frac{r_1 + r_2\, e^{-2j\Phi_1}}{1 + r_1\, r_2\, e^{-2j\Phi_1}} \qquad (3.6)$$

where $\Phi_1 = 2\pi n_1 d_1 / \lambda$. The thickness of the layer is d_1 and λ is the wavelength in the same units as d_1. If the reflectance is to be zero, eq.(3.6) yields (Cox and Hass 1964):

(3.7) $$r_1 + r_2 \cos[2 \cdot \Phi_1] = 0$$

(3.8) $$r_2 \sin[2 \cdot \Phi_1] = 0$$

These simultaneous equations yield two solutions. If $2 \cdot \Phi_1$ equals an even multiple of π , then $n_o = n_s$,(where n_o and n_s are the refractive indices of the surrounding medium and substrate respectively). This is a trivial case . The more important solution is that for which $2 \cdot \Phi_1$ equals an odd multiple of π and $n_1^2 = n_o \cdot n_s$. Thus, if $n_o \neq n_s$ the necessary and sufficient conditions for zero reflectance are:

(3.9) $$n_1^2 = n_o \cdot n_s$$

(3.10) $$\Phi_1 = (2m - 1) \frac{\pi}{2} , \quad m = 1,2,3,...$$

m was choosen to be one (one quarter wavelength thick layer).

Zinc sulphide ($n \simeq 2$) was used in our case because its refractive index was very close to the value indicated by eq.(3.9) for $n_o = 1$ and n_s=3.46(Si). Finally, the required thickness,in order to obtain minimum reflectance in the spectral region of 12 microns can be calculated from eq. (3.10) for $m = 1$.

3.10.2 Antimony Films

Polycrystalline antimony films were prepared in the apparatus shown in Fig. (3.7). They exhibit optical properties similar to the ones reported by Howson et al (1974). Figs.(3.8) and (3.9) show S.E.M. photographs

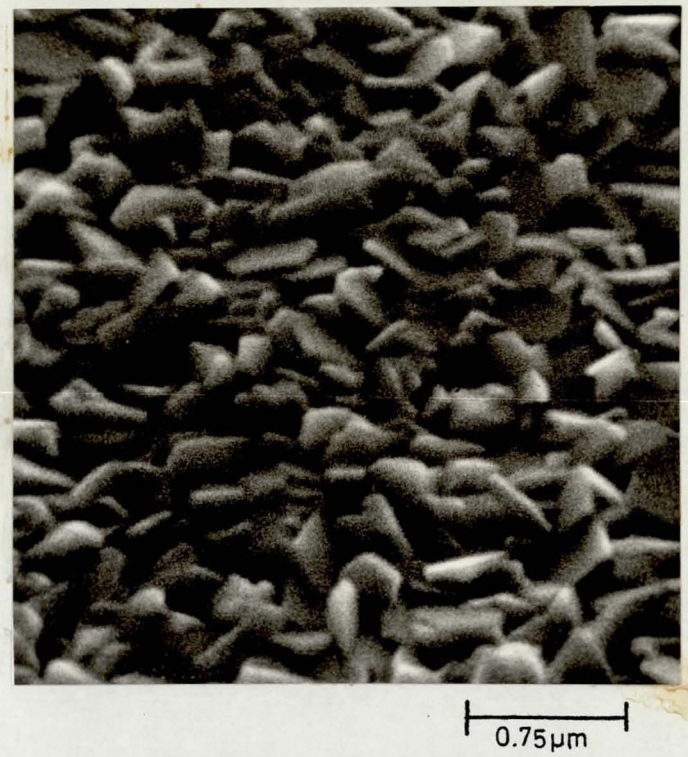

Fig.(3.8) SEM photograph of a thermally evaporated Sb film, 5500 Å thick, deposited onto glass substrate at 270°C.

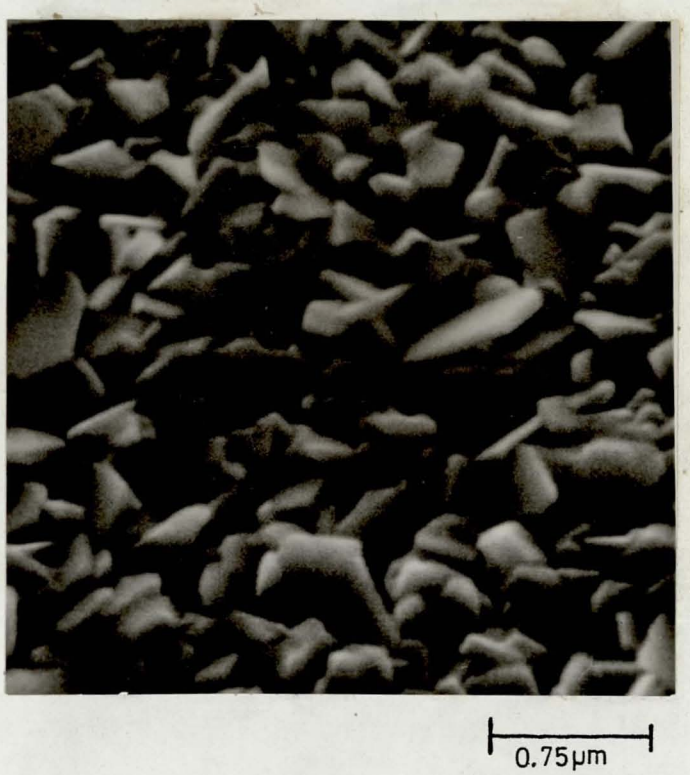

Fig.(3.9) SEM photograph of a thermally evaporated Sb film, 6000 Å thick, deposited onto glass substrate held at 280°C.

of two Sb films prepared at different substrate temperatures.

Attempts to measure ER effects in antimony films in the spectral region between 12-15 microns (where the reflectance plasma edge occurs) were unsuccessful because of the very low ER signal expected and the very low radiation intensity available in the spectral region of 10-15 microns.

3.10.3 Activated Reactive Sputtering

The synthesis of Sn - doped In_2O_3 was sought by activated reactive sputtering, (Grossklaus and Bunshan 1975). The process involves the introduction of a plasma between the evaporant source and the substrate. It enhances the probability of a reaction taking place by activating or ionizing the evaporant atoms and / or the gas. The vacuum plant shown in Fig.(3.7) was used for that purpose. Similar techniques have been recently used by various researchers to synthesize Ta oxide films (Westwood et al, 1975) and Tungsten films (Tisone and Bindell 1974). The idea is to create a high - plasma current density ($\sim$ 0.2 A/cm^2) by confining the plasma with an electrically floating physical enclosure and maintain it independently of the target and substrate, by maintaining a current between a thermionic cathode and anode. Ions are extracted from the plasma through openings by applying a negative bias to the target (Sn:In) supersimposed on a R.F. signal applied between target and substrate. In that way ions (O^+) are accelerated onto the target and sputter target atoms and / or oxidized target atoms towards the substrate located opposite the target. The sputtered atoms pass through the plasma and are likely to react with (O^+) present.

However there was not time to complete this project, although it seems to be very promising.

REFERENCES

1. Ammar I.A., and Saad A.,J.Electroanal. Chem. 30 , 395 (1971).
2. ——————— , ——————— 34 , 159 (1972).
3. Armstrong R.D.,and Mason R.,Electroanal. Chem.and Interf.Electrochem., 41, 231 (1973).
4. Armstrong R.D.,Electroanal.Chem. and Interf. Electroch.,52,413 (1974).
5. Armstrong R.D.,Dickinson T.,Race W.P. and Whitfield R., Electroanal. Chem. Interf.Electrochem.,27,158 (1970).
6. Avaritsiotis J.N.,M.Sc. Thesis,Loughborough,1974.
7. Billon J.P., J.Electroanal. Chem. 1,486 (1960).
8. Blackburn H. and Wright H.C.,Infrared Physics 10,191 (1970).
9. Bockris J.O'M.,and Reddy A.K.N.,Modern Electrochemistry, 2 ,Plenum Press, N.Y. (1970).
10. Burch D.E.,France W.L.,and Williams D.Appl.Optics 2 ,585(1962).
11. Burch D.E.,Gryvnak A.D.,and Dudley W. Appl.Optics 2,759(1962).
12. Burtin R.,Rev.Opt. 43,463 (1964).
13. ————,————, 43,619 (1964).
14. Chynoweth A.G.,J.Appl.Physics 27, 78 (1956).
15. Cox J.T.,and Hass G.,Physics of Thin Films Vol. 2,1964,Acad.Press.
16. Foley R.T.,J.Electroch. Soc. 116,13 C (1969).
17. Fox T.J.,PhD.Thesis, Loughborough, 1974.
18. Gebbie H.A.,Harding W.R.,Hilsum C.,Pryce A.W.,and Roberts V.,Proc. Roy.Soc. 206,87 (1951).
19. Girginov A.A.,and Ikonopisov S.M.,Electrochemiya 10,638 (1974).
20. Golay M.J.E. Review Sc.Instr. 18 ,347 (1947)
21. ———————— ,———————— 18 ,357 (1947)
22. ———————— ,———————— 20 ,816 (1950)
23. Grossklaus W.,and Bunshah R.F. J.Vac.Sci.Technol.,12, 593 (1975)

24. Holeman B.R., Infrared Physics 12, 125 (1972).

25. Howson R.P., Fox T., and Emmony D.J. Appl. Phys. D.

26. Hull M.N., and Pilla A.A. J. Electroch. Soc., 118 72 (1971)

27. Jamieson J.A., McFee R.H., PlassG.N., Grube R.H., and Richards R.G., Infrared Physics and Engineering McGraw Hill Inc. 1963, Chapter 10.

28. Kennedy J.H., Chen F. and Clifton A., J. Electroch. Soc. 115, 918 (1968)

29. Kennedy J.H., and Chen F. J. Electroch. Soc., 116, 207 (1969).

30. Kennedy J.H., Chen F., and Hunter J. J. Electroch. Soc. Solid State Sc. Techn. 120, 454 (1973).

31. Kuta J., Overpotential measurements in Techniques of Electrochemistry, Vol. 1 p. 141, edited by Yeager E. and Salkind A.J. Wiley N.Y. 1972.

32. Lilly A.C., LaRoy B.C., Tiller C.O. and Whiting B., J. Electroch. Soc.: Electroch. Sc. Techn. 120, 1673 (1973).

33. Limperis T., Handbook of Military Infrared Technology, Chapter 11, 1965.

34. MacArthure D.M. Electrochemical techniques Chapter 8, of Characterization of Solid Surfaces Edited by Kane P.F. and Larrabee G.B. Plenum Press N.Y. 1974.

35. Mann C.K., Non aqueous Solvents for Electrochemical Use, in Electroanalytical Chemistry Vol. 3, edited by Bard A.J., Marcel Dekker, Inc. N.Y. 1969.

36. Mecke R., and Langenbucher F. Infrared Spectra of Selected chemical compounds, Heyden and Son Ltd., London 1965.

37. Norakidze I.G., Kazakov V.A., and Vagramyan A.T., Elektrokhimiya 5, 970 (1969).

38. Nudelman S. Applied Optics 1, 627 (1962).

39. Plessey Co Ltd, Infrared Products, Data sheet.

40. Pye Unicam, Low noise Infrared Detector, Type IR50, Data sheet.

41. Raleigh D.O., J. Electroch. Soc. 121, 632 (1974).

42. Reeves R.M. The electrical Double layer: The current status of data and models, with particular emphasis on the solvent. Chapter 4 of Modern Aspects of Electrochemistry, No 9, edited by Conway B.E., and J.O'M. Bockris Plenum Press N.Y. 1974.

43. Rossi M., Pistoia G., and Scrosati B., J. Electroch. Soc. Electroch. Sc., 116, 1642 (1969).

44. Rood J.L. J. Opt. Soc. Am. 41, 201 (1951).

45. Scrosati B., J. Electroch. Soc. Electrochem. Sc. Techn. 120, 78 (1973).

46. ———————————————————— 118, 86 (1971).

47. Solov'eva Z.A., Solodkova L.N., and Bagramyan A.T., Elektrokhimiya 6, 579 (1970).

48. Stock J.T., and Purdy W.C., Chem. Revs. 57, 1159 (1957).

49. Styrkas A.D., Elektrokhimiya 5, 1414 (1969).

50. Takahashi T., Ikeda S., and Yamamoto O., J. Electroch. Soc. 120, 647 (1973).

51. Takahashi T., Kuwabara K., and Yamamoto O., J. Electroch. Soc. 120, 1607 (1973).

52. Tisone T.C., and Bindell J.B., J. Vac. Sci. Techn. 11, 519 (1974).

53. Vaško A., Infrared Radiation, Iliffe Books Ltd, London (1968), p.29.

54. Weil R., and Lawson A.W. J. Chem. Phys., 41, 832 (1964).

55. Westwood W.D., Waterhouse N., and Wilcox P.S., "Tantalum Thin Films" Academic Press 1975, p.43.

56. Stewart j.e., Infrared Spectroscopy - Experimental Methods and Techniques, Dekker, N.Y. 1970, p.226.

C H A P T E R 4

ELECTRO - REFLECTANCE IN POLYCRYSTALLINE GeTe FILMS

4.1 Introduction

Poly-crystalline GeTe films exhibit p-type metallic conductivity (Tsu , Howard, and Esaki, 1968). The conductivity is due to high carrier (hole) concentration ($\sim 10^{20}$ $\sim 10^{21}$ cm^{-3}) and is considered to be the result of Ge vacancies in the GeTe lattice (Mazelsky and Lubell, 1963, Wooley and Nicolic, 1965). It has been shown by Tsu et al (1968) that the optical effective mass, m_r , shows a pronounced dependence upon carrier concentration. Bahl and Chopra (1969) showed that the observed high free carrier concentration in poly-crystalline GeTe films can be changed by varying the substrate temperature.
Finally, the reflectivity spectrum of the poly-crystalline films exhibit a well defined edge at the plasma resonance frequency corresponding to a wavelength of about 3 to 5 μm.

All these properties make GeTe suitable for the present ER measurements. The sharpness of its plasma edge due to relatively high optical mobility (about 100 $cm^2/V.sec$) promises large electroreflectance signals. Moreover, the possibility of shifting the plasma edge by changing the concentration of Ge vacancies, during the fabrication process, offers the possibility of studying the ER effect, in the vicinity of the reflectance plasma edge, over a rather wide spectral region.

4.2 Film Fabrication

Germanium telluride films of thickness ranging between 200 Å and 3 microns were prepared by thermal evaporation of prefabricated germanium telluride, from an asymmetric oven-type point source. The films were deposited onto the substrates at deposition rates varying from about 100 Å/sec to 300Å/sec

as was calculated from film thickness and deposition time. The deposition rate was controlled by the current passing through the evaporant source. Typically, the source was brought up to a temperature of approximately 750°C, (GeTe melts at about 725°C, HcHugh and Tiller 1960), and material was evaporated for more than thirty seconds with the shutter closed, in order to allow for the melting of the material in the oven - type source. The shutter was then opened for periods of time varying from a few seconds to several minutes. In the mean time the evaporation chamber was continuously pumped to maintain a pressure of less than 1×10^{-5} torr.

The films were deposited on properly cleaned glass substrates and freshly polished NaCl crystals. The substrates were maintained at temperatures ranging from room temperature to 280°C by means of a feedback controlled heating source. At the end of a deposition period the shutter was closed and the substrates were allowed to cool to room temperature before to be taken out of the vacuum chamber.

The material used for the fabrication of the films was prepared by vacuum melting of various proportions of the elements of high purity. Germanium ingots 99.999% from KOCH-LIGHT LABORATORIES LTD and tellurium lump 99.9% from the BRITISH DRUG HOUSES LTD were used. The proportions of the constituents were varied (5-10%) around the 50.61 a/o Te and 49.39 a/o Ge, of stoichiometric GeTe , Hansen (1958), Elliot (1965), and Shunk (1969).

4.3 Film Structure

When the substrate temperature was held below 150°C the evaporated films exhibited an amorphous structure and behaved optically like dielectrics. It was also found that the deposition temperature below of which the amorphous phase was obtained was independent of the substrate nature

(e.g. glass,NaCl); this is in agreement with Bahl's (1969) results.

An amorphous GeTe film can be transformed to a poly-crystalline one if it will be annealed to temperatures above the so-called transformation temperature, which in this case and for films thicker than 300 Å is approximately 150°C. Bahl and Chopra (1969) found that the transformation temperature significantly depends on film thickness for films thinner than about 300 Å, increasing linearly with decreasing film thickness. It is worth noting the absence of ageing effects after the transformation. This implies that GeTe films crystallize homogeneously throughout the film.

Crystalline films were, however, obtained when the substrate temperature was kept above 150° C. With increasing substrate temperature partially oriented structure was obtained. Fig. (4.1) shows the electron diffraction pattern of a 200Å thick poly-crystalline GeTe film deposited on a glass substrate at 280°C. The nature of the pattern gives evidence (Heavens 1970, p.27) that partial orientation occured at that deposition temperature. Fig. (4.2) is an electron transmission photograph of the same film showing that at that thickness the film was continuous with an average grain size of about 0.1 microns.

A good deal of trouble was encountered in the early experiments because the use of medium substrate temperatures (about 200°C), although yielding high carrier concentrations, did not give high optical mobilities, and consequently films exhibiting sharp plasma edges, when the films were deposited on glass substrates.

Also at temperatures above 280°C germanium telluride films did not deposit

Fig.(4.1) Electron diffraction pattern of a 200 Å polycrystalline GeTe film.

Fig.(4.2) Electron transmission photograph (50K) of the GeTe film shown in Fig.(4.1).

on the substrates due to thermal re-evaporation of the material. In order to improve the film grain size by increasing the deposition temperature above 280°C the glass substrates were precoated with gold islands. This technique was first introduced by Dutton and Muller in (1971) and was subsequently employed by Okuyama et al in (1974), in order to fabricate large grain tellurium films on glass substrates. They found that the presence of Au islands prevents tellurium from re-evaporation at high substrate temperatures.

The process of coating glass with gold islands was as follows:Gold was evaporated onto glass substrates held at room temperature from an electron-gun source. The very thin films of gold (40-50Å) obtained in that way were subsequently annealed at 260°C in order to create completely isolated Au islands, Avaritsiotis (1974). The film thickness was estimated from the colour of the film in reflected light; the yellow-green colours observed when white light was incident on the gold films from the glass substrate side, correspond to film thicknesses between 40 - 50 Å ,[Heavens (1954), p. 169].Germanium telluride films 1000 Å - 3000 Å thick were subsequently deposited on the precoated substrates at about 300°C with a deposition rate of about 100 Å/sec. The obtained films had a grain size similar to the one presented in Fig. (4.2), but showed a much sharper reflection plasma edge ($dR/d\lambda = 20\%/\mu m$) in the vicinity of 3 microns.

4.4 Optical Properties of Poly-crystalline GeTe Films

The optical properties of poly-crystalline germanium telluride films were the same whether the films were obtained initially by depositing on a substate held above 150°C or subsequently by the transformation of

the amorphous film by heat treatment.

All the films exhibiting plasma edges in the spectral region of 3.5-5 microns were prepared from pre-fabricated ingots of GeTe, containing 49.39 a/o Ge and 50.61 Te, by changing the deposition temperature each time. It was found that by varying the substrate temperature between 200°C and 280°C, films were obtained exhibiting plasma edges lying at 3.5 and 4.8 microns respectively, as shown in Table (4.1).

TABLE (4.1) Optical Properties of Poly-crystalline GeTe Films Evaporated onto Glass Substrates.

Substrate temperature (°C)	Plasma wavelength (microns)	Relaxation Time ($\times 10^{-14}$ sec)
200	3.5	0.3
220	3.8	0.4
240	4.1	0.6
260	4.5	0.7
270	4.7	0.8
280	4.8	0.9

The data presented in Table (4.1) were obtained employing the computer program analysed in Appendix D and using reflectance data of germanium telluride films about 3000 Å thick, deposited onto glass substrates. The values obtained and presented in Table(4.1) are in good agreement with the experimental results of Bahl and Chopra (1969).

Also, Table (4.1) shows that the free carrier relaxation time decreases with substrate temperature , as it is naturally expected, due to the dependence of film grain size on deposition temperature; smaller grain sizes are generally obtained with decreasing substrate temperature; because of a decrease in surface mobility of adatoms and because the substrate does not provide the activation energy required for the adatoms to take up a suitable position.

Moreover the gradual decrease in the plasma frequency $\omega_p = 2\pi c / \lambda_p$ with increasing substrate temperature implies a decrease of the effective free carrier (hole) concentration. This suggests a reduction in Ge vacancies, which act as acceptors, with decreasing substrate temperature, or in other words an increase of the number of tellurium atoms in the GeTe film.

When the substrate temperature increases, the deposition of Te is generally difficult because of the high vapor pressure of the material. So, the method of adjusting the value of the free carrier density by varying the substrate temperature was not suitable for the fabrication of poly-crystalline GeTe films exhibiting sharp reflection plasma edges in the vicinity of 3 microns, because the obtained films exhibit relatively low optical mobilities (about 10 cm^2 / V.sec), resulting from the low substrate temperature.

It was found that when a glass substrate is predeposited with Au islands, it is possible to deposit poly-crystalline GeTe films at elevated substrate temperatures, thus obtaining films which exhibit relatively sharp plasma edges in the vicinity of 3 microns (low concentration of Ge vacancies).

This can be attributed to the fact that Au islands prevent re-evaporation of Te at elevated substrate temperatures (about 290°C) as has been shown by Okuyama et al (1974) and (1975).

Several poly-crystalline germanium telluride films of about the same thickness (3000 Å) exhibiting plasma edges at the vicinity of 3.5 μm, prepared according to the previously mentioned techniques; germanium telluride films evaporated onto Au-predeposited glass substrates held at 270°C exhibit both comparatively high carrier relaxation times ($\sim 0.6 \times 10^{-14}$sec) and high free carrier concentrations ($\sim 10^{21}$cm^{-3}), whereas germanium telluride films evaporated onto uncoated glass substrates held at 200°C exhibit relatively low free carrier relaxation times ($\sim 0.3 \times 10^{-14}$sec).

Fig. (4.19) shows a typical example of the difference between the reflectance of two films prepared on Au predeposited glass (270°C) and uncoated glass at 200°C.

Poly-crystalline GeTe films evaporated onto heated NaCl substrates, however, exhibited different optical behaviour with changing substrate temperature, in comparison with the data of Table (4.1). The free carrier relaxation time was comparatively larger at medium substrate temperatures (around 200°C).

Table (4.2) summarizes the optical properties of a series of germanium telluride films prepared on heated NaCl substrates and having thicknesses which varied between 1500 and 2000 Å.

TABLE (4.2) Optical Properties of Poly-crystalline GeTe Films Evaporated onto NaCl Substrates.

Substrate temperature (^{o}C)	Plasma wavelength (microns)	Relaxation Time (x 10^{-14} sec)
190	3.1	0.6
220	3.8	0.6
240	4.0	0.7
260	4.5	0.8
280	5.3	0.9

GeTe films prepared on heated NaCl substrates were used for the study of ER effect in the case of internal reflection spectroscopy (IRS). Typical reflectance and transmittance spectra of a poly-crystalline film 0.15 microns thick grown on a NaCl substrate at 250^{o}C are shown in Fig. (4.3). The reflectance minimum due to free carriers is located at about 4.5 microns whereas the reflectance minimum at 4 microns and the reduction of reflectance below 3 microns are indications of interference effect due to film thickness. It should be noted that the transmission spectrum does not exhibit any interference. This is probably due to the considerable loss of light by absorption and scattering in the film.

Thickness dependence studies of the reflectance spectra in the vicinity of plasma edge showed no detectable dependence on film thickness for similarly prepared poly-crystalline GeTe films of any thickness greater than 300 Å . This is in very good agreement with the results of Bahl and Chopra (1969), obtained from systematic thickness dependence studies of

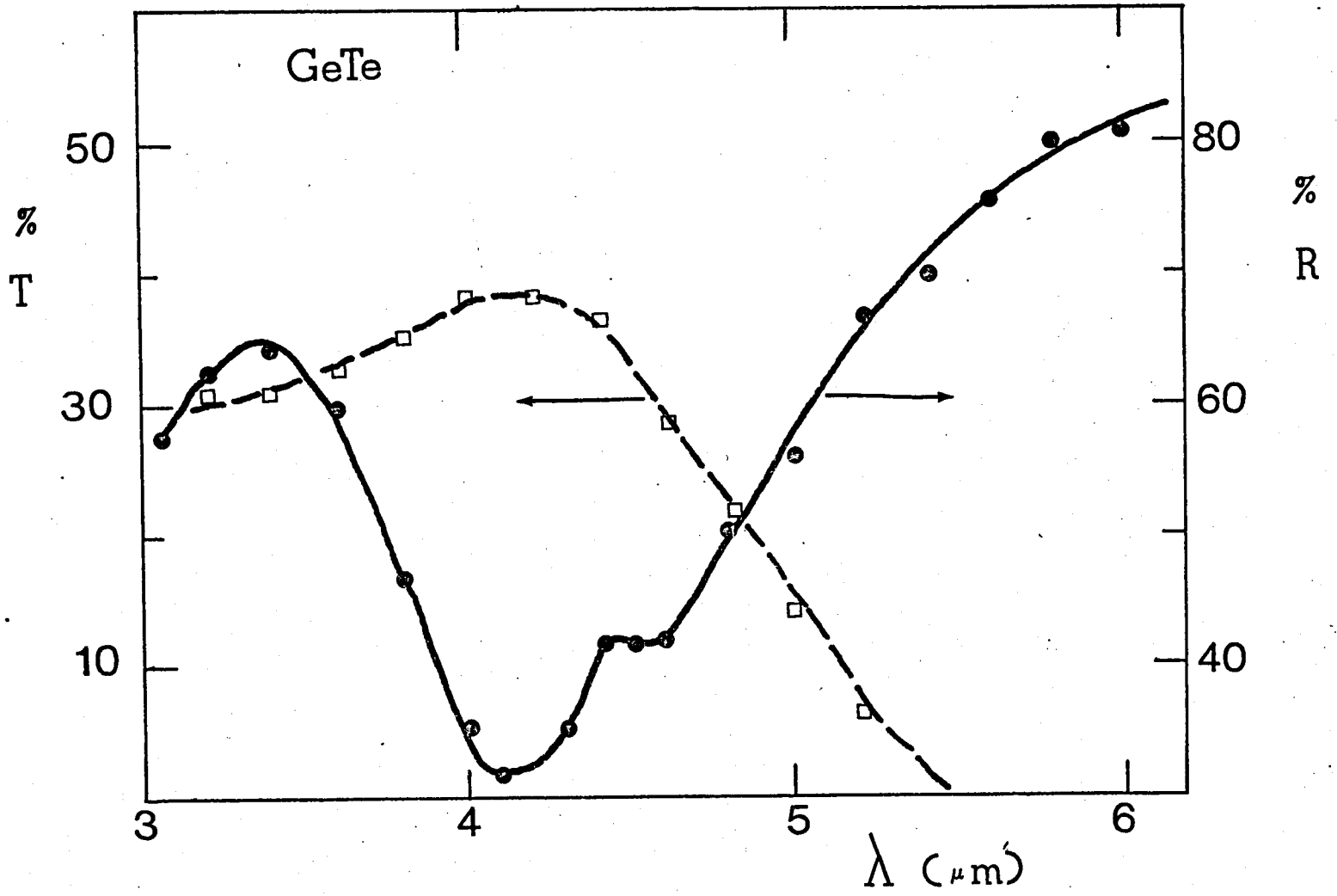

Fig.(4.3) Reflectance and transmittance spectra of a GeTe poly-crystalline film 1500 Å thick, evaporated onto a NaCl substrate.

the optical constants of similarily prepared GeTe films.

Finally, the homogeneity of the films deposited on NaCl substrates was checked by measuring the reflectance of different areas of the films on both the front and back surfaces. Variations were less than $\pm$ 3% for all of the samples studied.

4.5 Deduction of Optical Constants of GeTe Films.

The near normal incidence ($\sim 10^{o}$) experimental reflectivity spectra of a large number of poly-crystalline GeTe films were used as data for the deduction of their optical constants as a function of wavelength. The method employed is discussed in detail in Appendix D. Assuming that the reflectivity spectrum of a poly-crystalline GeTe film in the vicinity of its plasma edge is dominated by interband transitions, the parameters ϵ_L , τ , and ω_p can be calculated. So, the spectral dependence of the refractive index, n , and extinction coefficient, k , can be calculated from Drude's model formulae. Fig. (4.4) shows that an average value of 36.5 is expected for the lattice dielectric constant of poly-crystalline GeTe films.

However, an additional parameter is required for the evaluation of our electro-reflectance model, i.e. the optical effective mass of the free carriers (holes), which has to be deduced from a method different than optical, (usually from Hall measurements).
Fortunately, the relationship between optical effective mass, m_r , and free carrier concentration N , and also plasma frequency is well established. Consequently an approximate value for m_r and N can be obtained for each one of our samples from other investigator's experimental results.

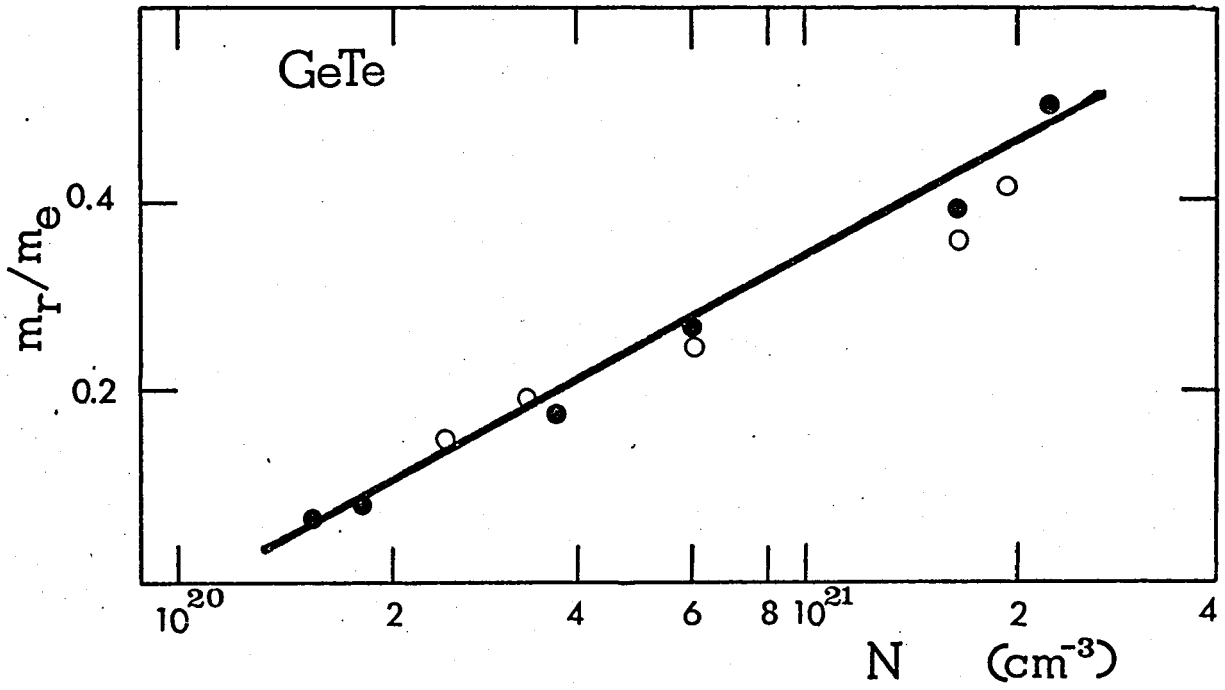

Fig. (4.5) Calculated carrier concentration dependence of the susceptibility hole mass at 295°K

- ● by Tsu et al (1968)
- ○ by Bahl and Chopra (1969)

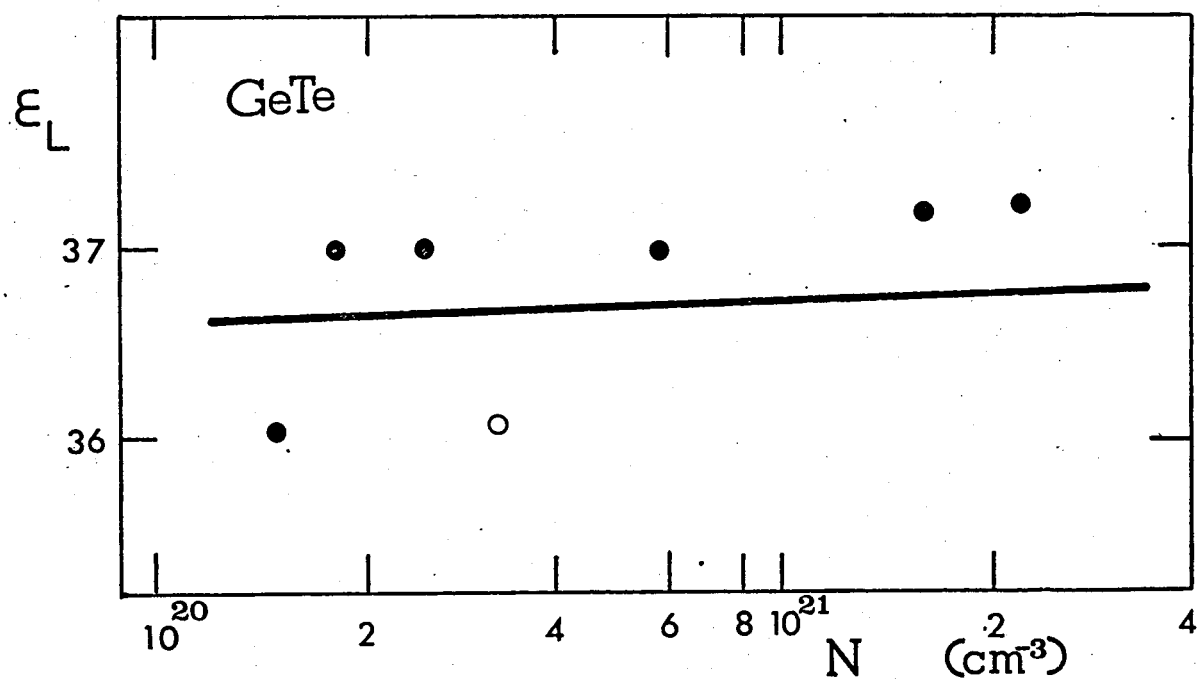

Fig. (4.4) Calculated carrier concentration dependence of the lattice dielectric constant at 295°K. The data obtained from the references of the previous figure.

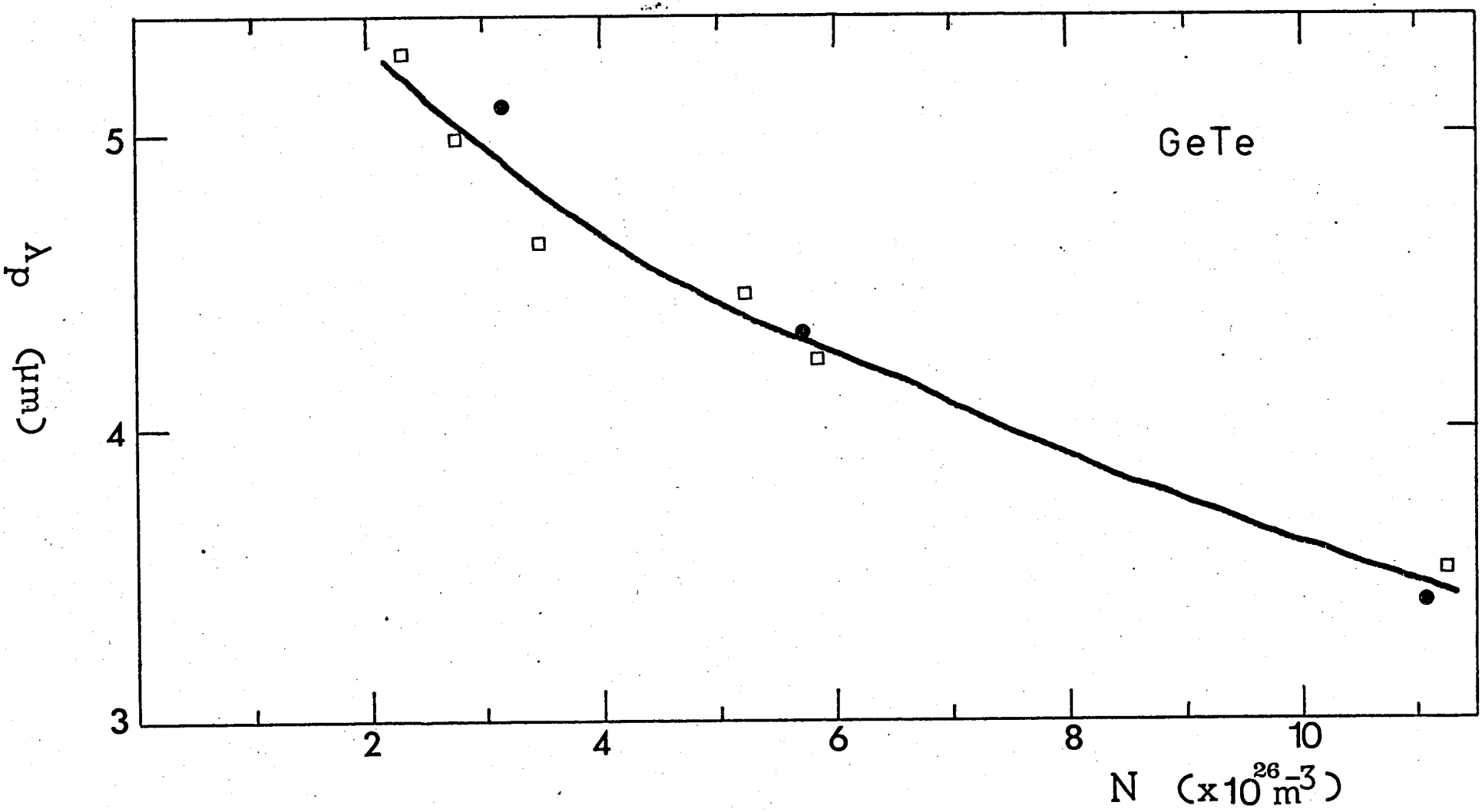

Fig. (4.6) Plasma wavelength ($2\pi c/\omega_p$) against free carrier (hole) concentration of poly-crystalline and crystalline GeTe films.

● by Bahl and Chopra (1969)

□ by Tsu et al (1968)

Fig.(4.5) shows that the ratio of the free carrier optical effective mass to the electron mass increases rather linearly from approximately 0.1 to 0.5 when the free carrier concentration increases from 1.5×10^{20} to 2.5×10^{21} cm^{-3} respectively.

Assuming that the nature of the substrate does not affect the value of the optical effective mass, a relationship between plasma wavelength and free carrier concentration may be deduced by comparing our experimental results, presented in Tables (4.1) and (4.2), by those published by Bahl and Chopra in 1969, and Tsu et al in 1968.

As far as the validity of the latter assumption is concerned we found that the nature of the substrate affects the free carrier relaxation time only, since deposition of poly-crystalline GeTe films under similar conditions (vacuum, substrate temperature, and deposition rate) onto glass and NaCl substrates yields films exhibiting diferent relaxation times but similar plasma frequencies, i.e. similar N/m_r^*, where $m_r = m_r^* \cdot m_e$. Fig. (4.6) shows an approximate relationship between plasma wavelength and free carrier concentration for films deposited onto glass and NaCl substrates. So, an approximate value for the optical effective mass of our GeTe samples can be calculated from Figs.(4.5) and (4.6).

Some of the results obtained according to the previously described method are presented in Table (4.3). Each set of optical parameters corresponds to two films: the first one being evaporated onto glass and the second one being evaporated onto NaCl substrate. These films have been selected from a plethora of poly-crystalline GeTe fabricated onto glass and NaCl substrates, for comparative electro-

reflectance studies.

It is worth noting that the values for the lattice dielectric constant tabulated in Table (4.3) are in good agreement, within the error quoted in Appendix D, with the experimental results of various research workers. As far as the values for the free carrier relaxation time are concerned the observed discrepancy between our and other's results is due to the fact that our films are poly-crystalline whereas values for the relaxation time quoted in the literature vary around 2×10^{-14} sec because they refer to single-crystal films.

The spectral variation of the refractive index and extinction coefficient of the films in Table (4.3) have been calculated according to Drude's model. Average values for each set (i.e. a and b) of optical parameters are presented in Figs. (4.7), (4.8), (4.9), and (4.10). The use of Drude's model for the calculation of the optical constants of poly-crystalline GeTe films, in the spectral region of the reflectance plasma edge, is consistent because the optical absorption edge according to Bahl and Chopra's (1969) experimental results is approximately 0.8 eV (or 1.55 μm) for both crystalline and amorphous GeTe films. This implies that bound electron optical effects become pronounced at wavelengths shorter than 1.55 μm.

4.6 Electro - reflectance Measurements

The electro - reflectance effect has been measured in a large number of GeTe films of various free carrier (hole) concentrations and relaxation times employing the experimental techniques discussed in a previous chapter. Some typical examples will be presented in the following paragraphs.

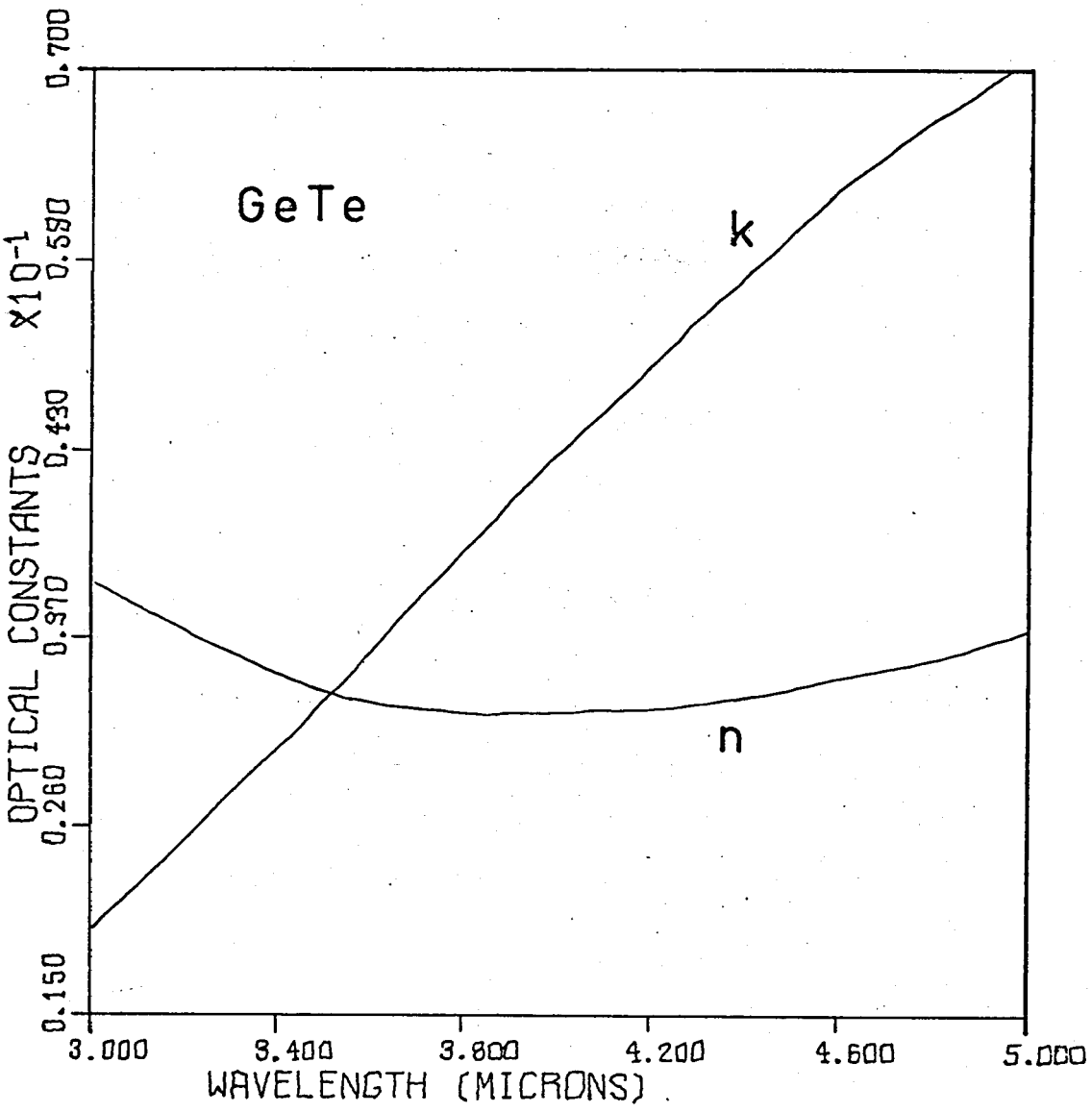

Fig. (4.7) Calculated refractive index and extinction coefficient for the films 1a and 1b of Table(4.3).

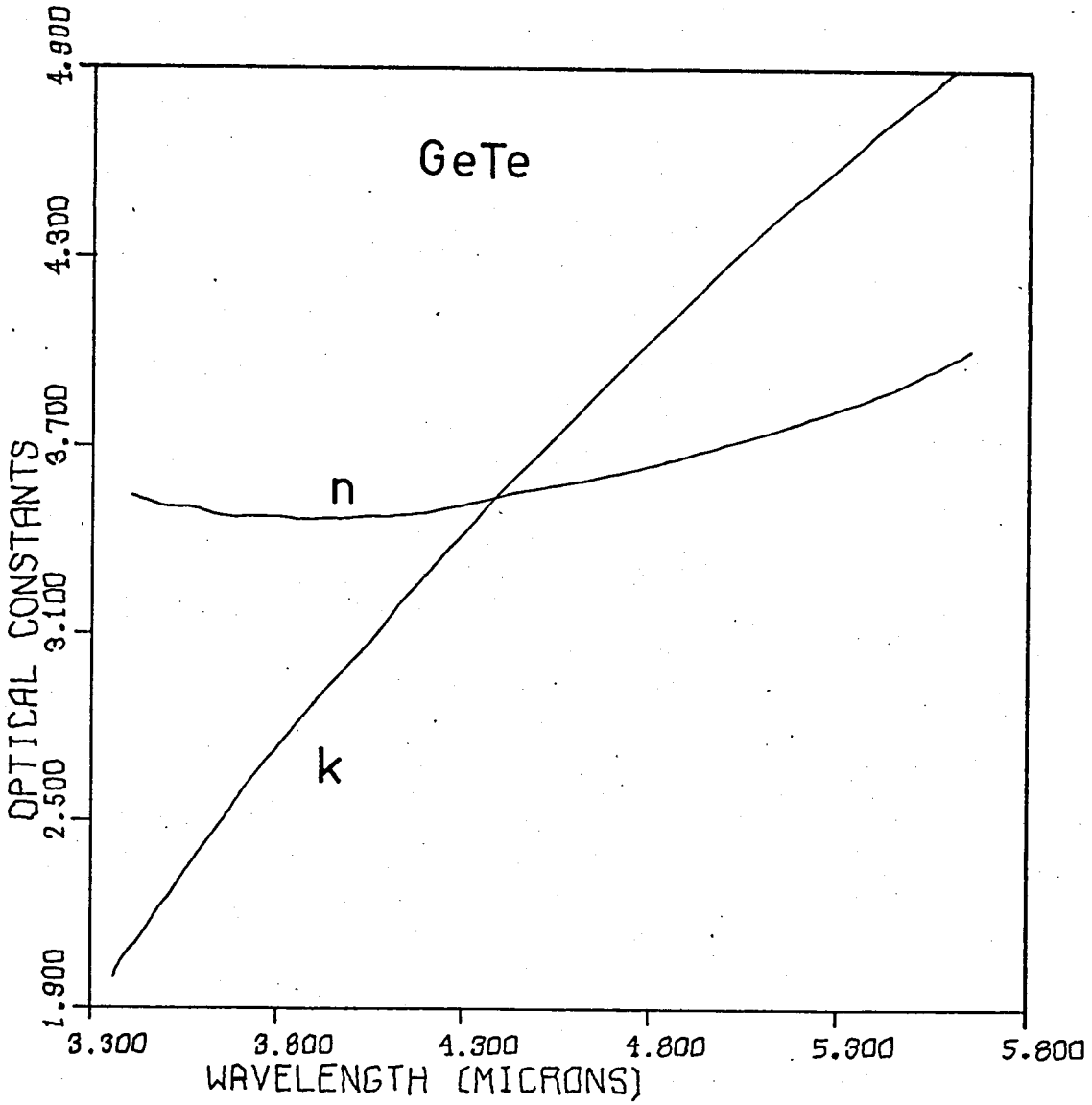

Fig.(4.8) Calculated refractive index and extinction coefficient for the films 2a and 2b of Table (4.3).

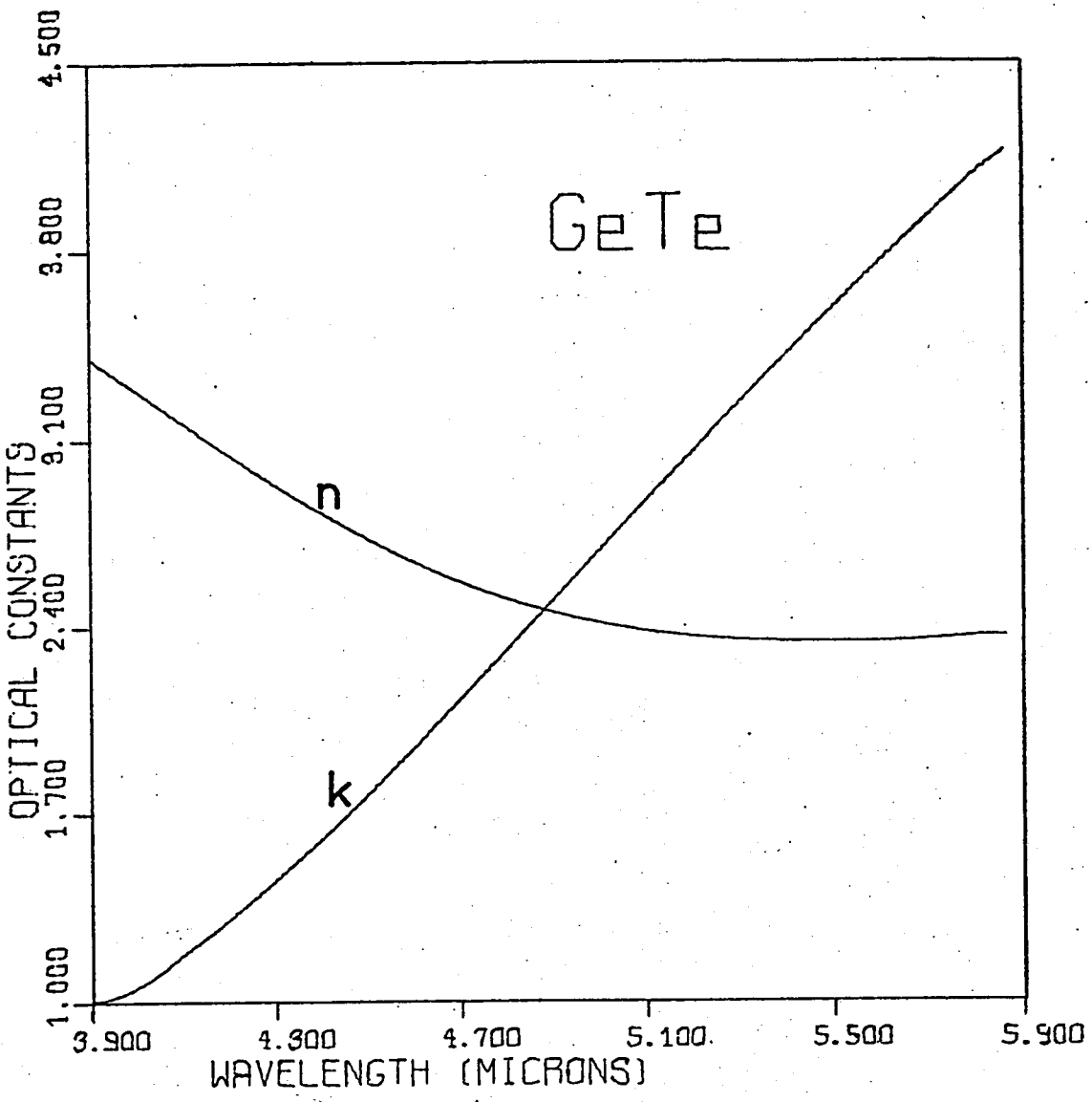

Fig.(4.9) Calculated refractive index and extinction coefficient for the films 3a and 3b of Table (4.3).

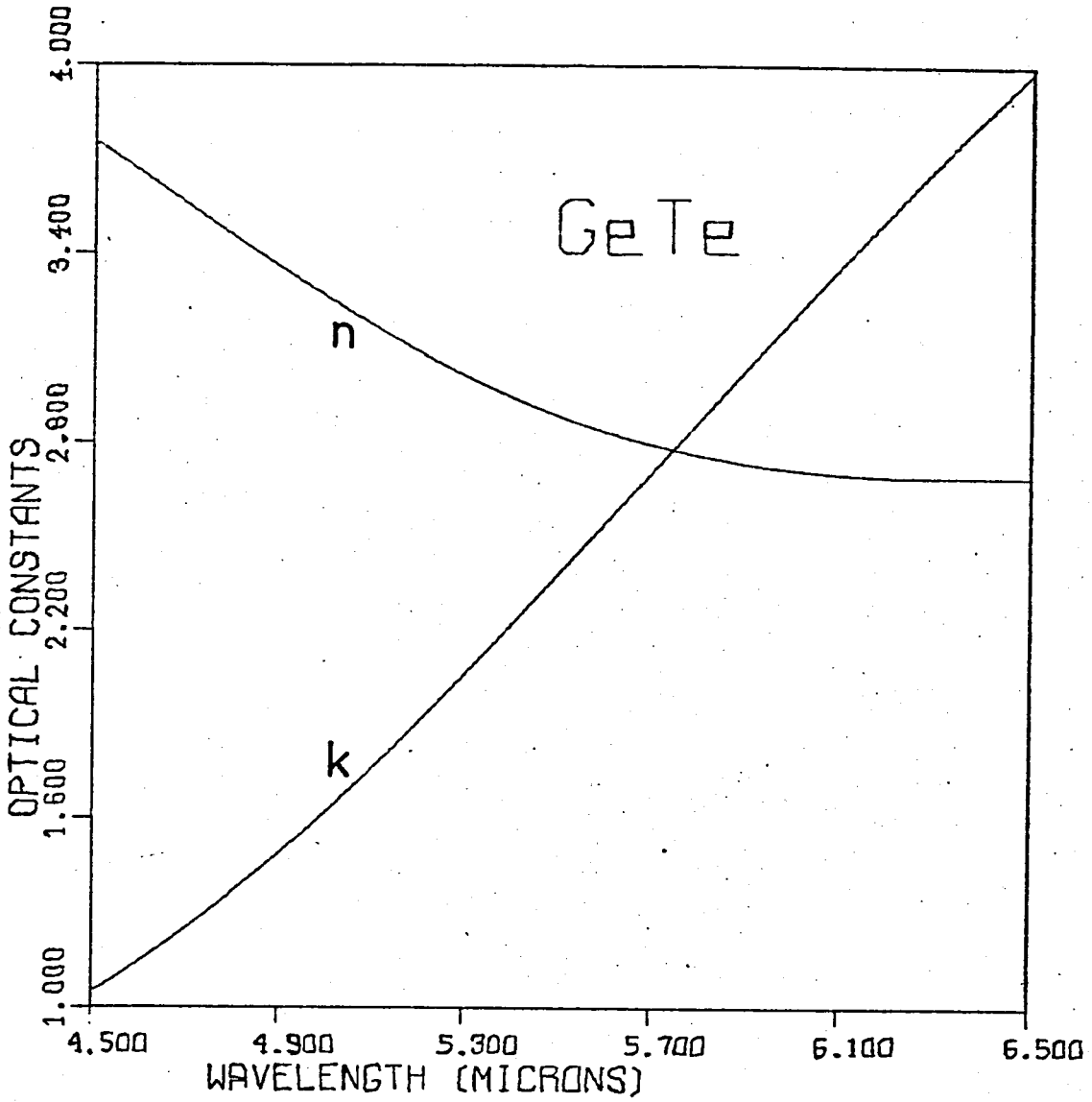

Fig.(4.10) Calculated refractive index and extinction coefficient for the film 4a of Table (4.3).

Both Internal Reflection Spectroscopy (IRS) and External Reflection Spectroscopy (ERS) modes were employed. The latter technique, however, gave relatively more accurate results both in terms of ER magnitude ($\pm$ 20%) and wavelength resolution (wavelength band-width: 0.06 μm). The main problem encountered with the IRS technique was inaccuracy in both ER magnitude (sometimes $\pm$40%) and wavelength resolution (0.08 μm) due to the low radiation intensity available.

4.6.1 I.R.S.

Typical examples of ER spectra of polycrystalline GeTe films evaporated onto NaCl substrates are presented in Figs. (4.11), (4.12), (4.13), and (4.14). These ER spectra were recorded using the IRS technique.

The accuracy of the values of the ER effect presented in Figs.(4.13), and (4.14) is approximately $\pm$ 40%, whereas ER values of Figs (4.11) and (4.12) have an accuracy of about $\pm$25 and $\pm$30 percent respectively.

The following important features of the ER effect are apparent in Figs. (4.11), (4.12), (4.13) and (4.14):

a) The ER peak occurs in the vicinity of the plasma frequency as can be seen by comparing the spectral positions of the ER peaks with the corresponding plasma frequencies (or plasma wavelengths). The plasma frequency corresponds to the wavelength for which $n = k$,(See Table (4.4)).

b) The magnitude of the ER effect strongly depends on the thickness of the film, decreasing with increasing thickness. The magnitudes of the ER peaks obtained from the ER spectra of Figs.(4.11),(4.12),(4.13) and (4.14) together with the corresponding plasma wavelengths deduced

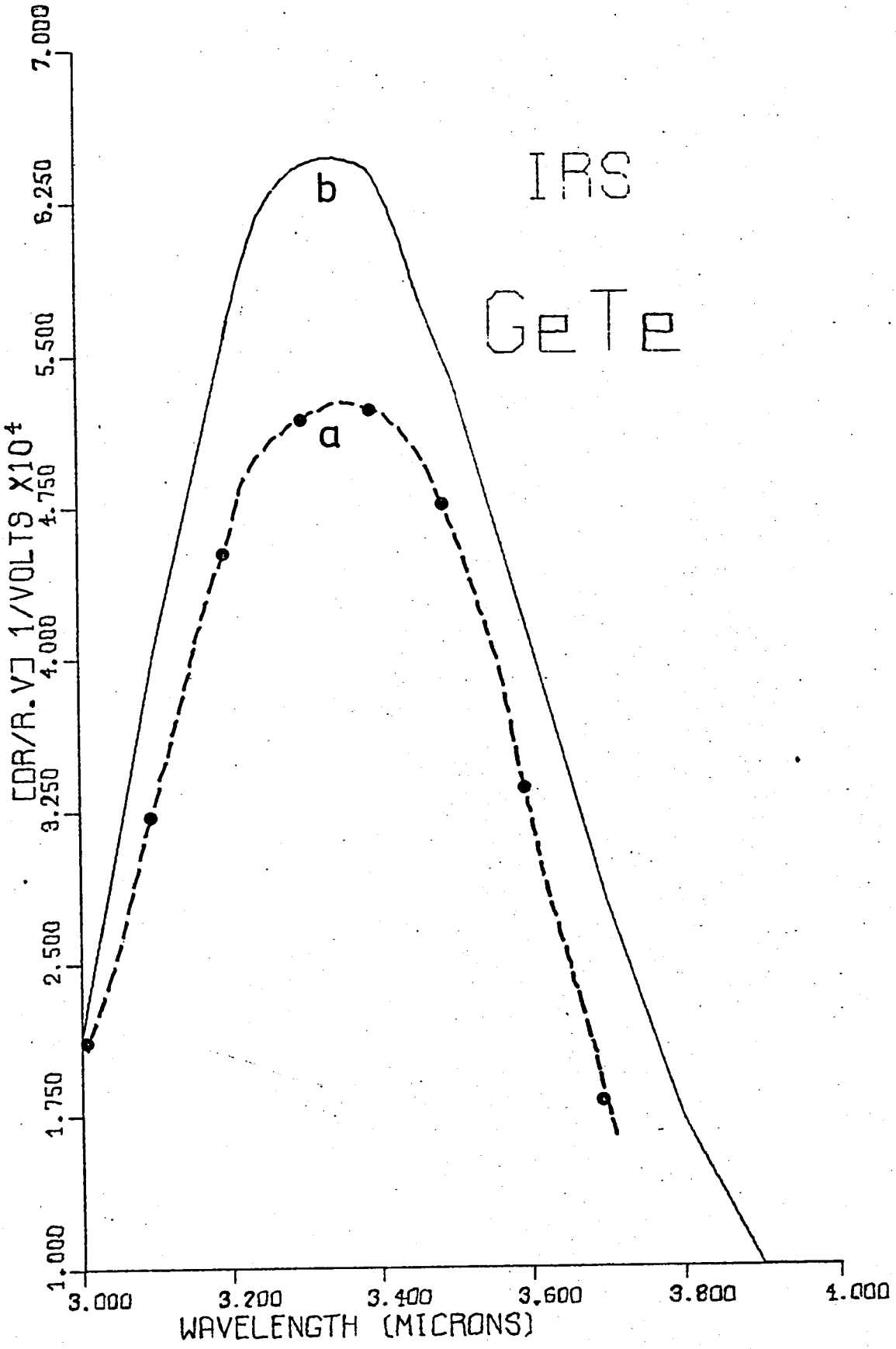

Fig.(4.11) a. Experimental ER spectrum and

b. Calculated ER spectrum of a poly-crystalline GeTe film 1800 Å thick grown on NaCl substrate at 200°C.

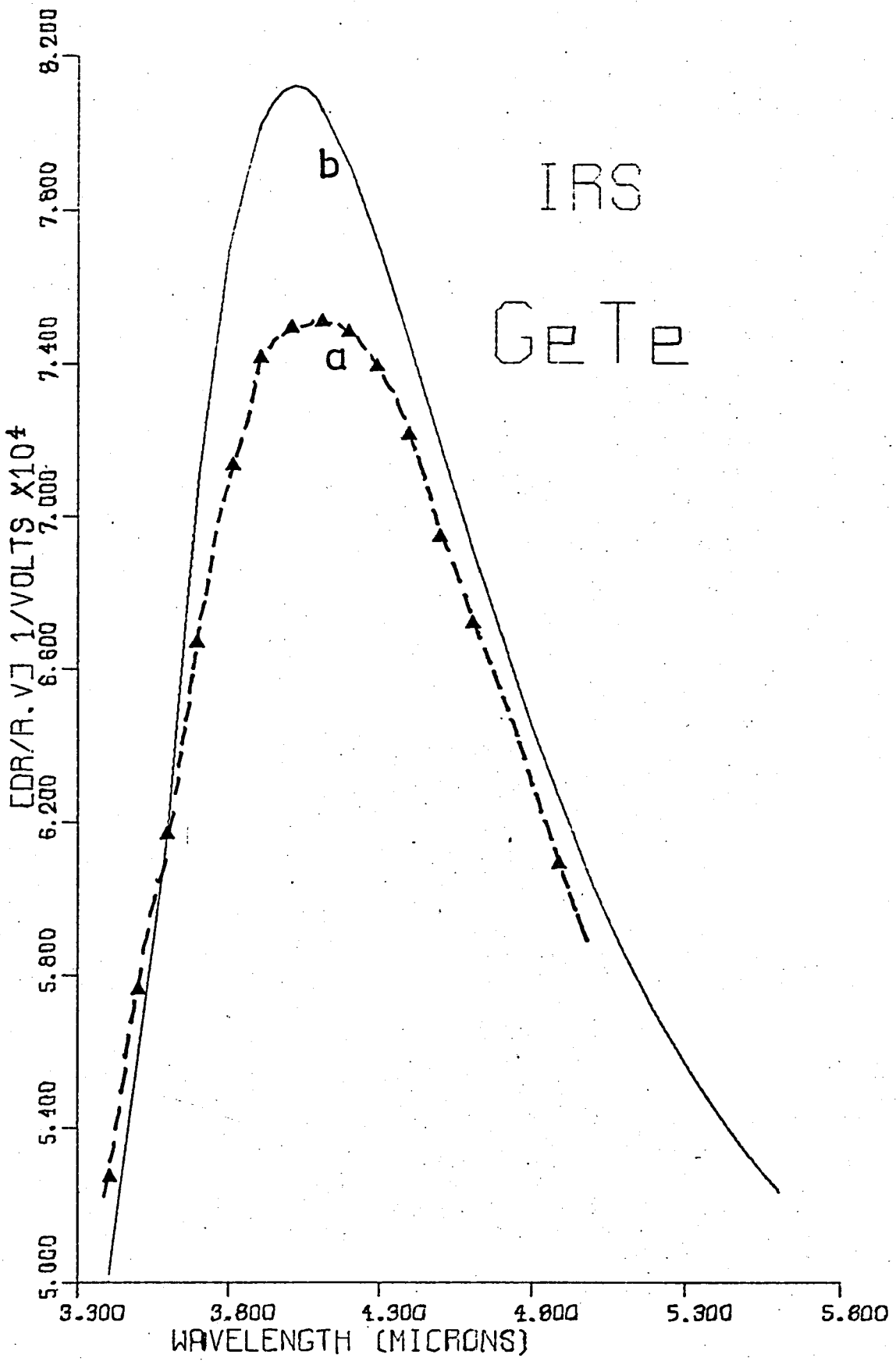

Fig.(4.12) a. Experimental and

b. Calculated ER spectrum of a poly-crystalline GeTe film 1500 Å thick grown on NaCl substrate at 250°C.

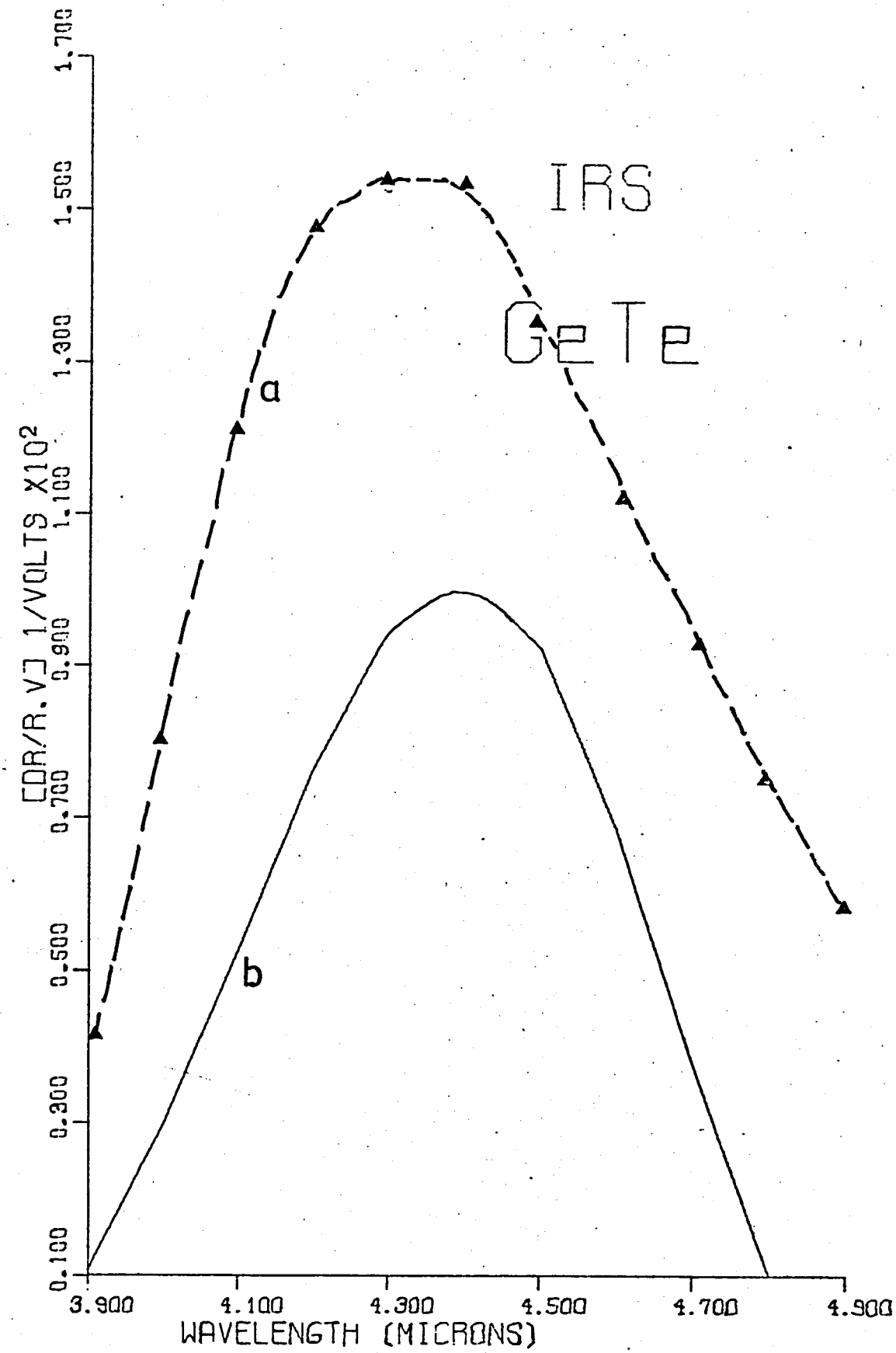

Fig.(4.13) a. Experimental and

b. Calculated ER spectrum of a poly-crystalline GeTe film 500 Å thick grown on a NaCl substrate at 270°C.

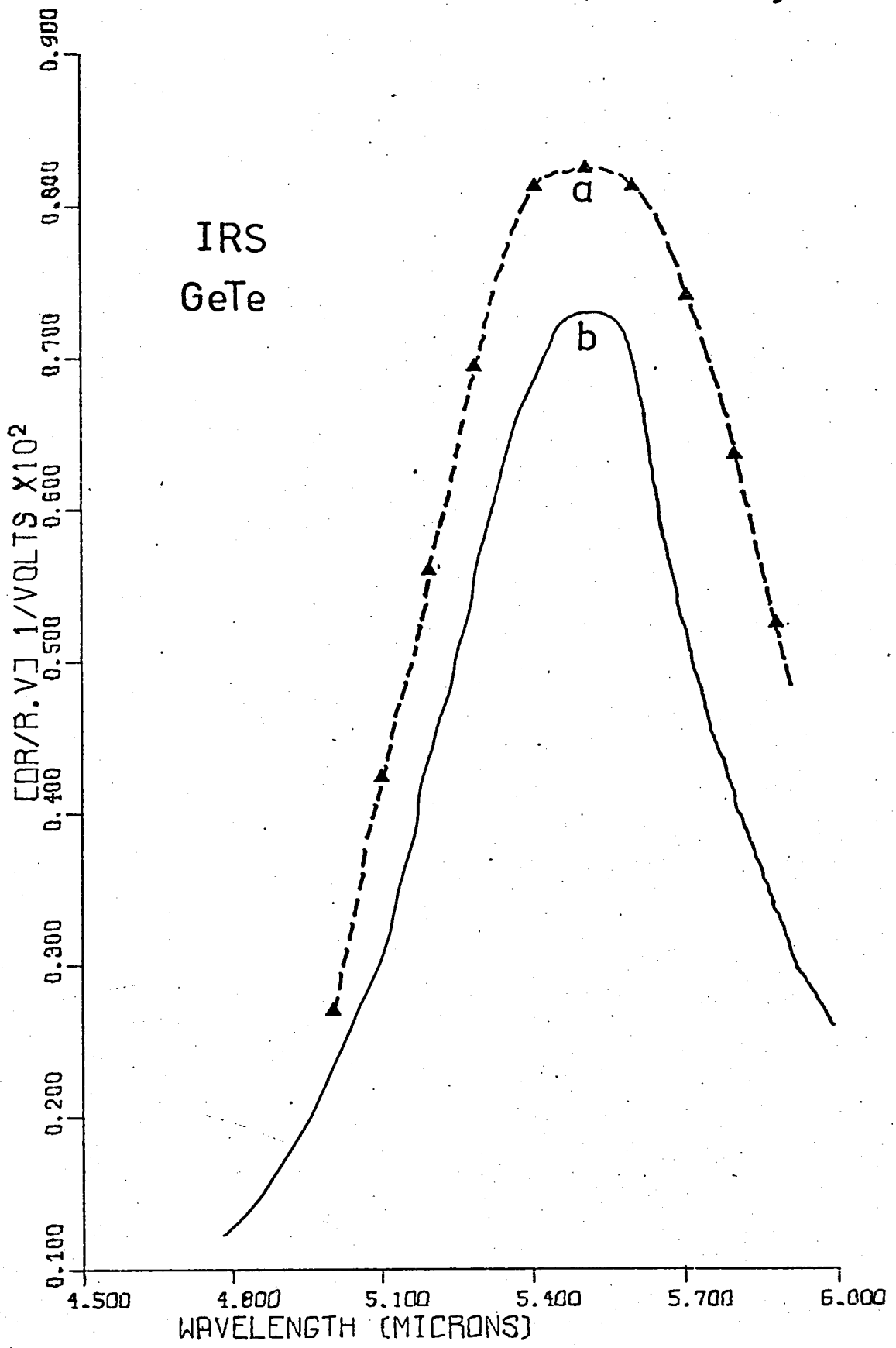

Fig.(4.14) a. Experimental and

b. Calculated ER spectrum of a poly-crystalline GeTe film 800 Å thick grown on a NaCl substrate at 280°C.

TABLE (4.3) Optical Parameters of Poly - crystalline GeTe Films

	DEDUCED BY OUR METHOD				OBTAINED FROM FIGS. (4.4) and (4.5)	
SAMPLE No	ε_L	τ 10^{-15} sec	ω_p 10^{14} sec^{-1}	λ_p μm	N 10^{26} m^{-3}	m_r/m_e
1a	39	6	5.40	3.49	10.7	0.3
1b	38	6	5.43	3.47		
2a	35	8	4.32	4.36	5.2	0.2
2b	36	8	4.30	4.38		
3a	34	8	3.85	4.90	3.2	0.2
3b	34	8	3.89	4.85		
4a	37	9	3.28	5.75	2.1	0.2

a refers to poly - crystalline GeTe films on NaCl substrates.

b refers to poly - crystalline GeTe films on glass substrates.

from Figs. (4.7), (4.8), (4.9) and (4.10) are tabulated versus film thickness in Table (4.4). The differences in ER peak values are not solely due to film thickness but part of the differences can be attributed to differences in the film optical parameters tabulated in Table (4.3).

TABLE (4.4) Magnitude and Position of ER peak (in IRS) Versus Film Thickness and Plasma Wavelength.

λ_p μm	λ_{peak} μm	$\Delta R/R.V$ (EXPERIM.) $(Volts)^{-1}$	d Å	$\Delta R/R.V$ (CALCUL.) $(Volts)^{-1}$
3.5	3.4	5.2×10^{-4} (±25%)	1 800	6.4×10^{-4}
4.4	4.2	7.5×10^{-4} (±30%)	1 500	8.1×10^{-4}
4.9(*)	4.4	1.5×10^{-2} (±40%)	500	1.0×10^{-2}
5.8(*)	5.2	8.4×10^{-3} (±40%)	800	7.5×10^{-3}

(*) The discrepancy between the position of ER peak and the plasma frequency can be attributed to experimental errors occured during the deduction of the Drude model parameters by fitting the experimental reflectivity spectrum of the film.

The ER spectra of the same films were calculated according to our model; the following parameters were used in each case, in addition to the ones in Table (4.3), for these calculations.

Film No	Double layer specific capacitance (F/m^2)
1a	0.15
2a	0.25
3a	0.22
4a	0.15

These values have been measured with a Marconi bridge and represent the total capacitance of the electrolytic cell. Moreover a constant value of 1.5 was assumed for the refractive index of the NaCl in the spectral region of our experiments.

Table (4.4) shows that the agreement between theory and experiment in the case of IRS is good within the limits of the experimental errors. It was thought that, because of the rather large experimental error, in the ER values it is meaningless to adjust the value of specific capacitance within the limits of the experimental error in order to bring the calculated ER spectra almost in coincidence.

However, the good agreement between theoretical and experimental ER spectra gives us evidence that the formulae employed for the calculation of the ER spectra in the case of IRS , are the right ones.

Four thin poly-crystalline GeTe films were prepared under similar conditions on NaCl substrates held at 210°C. The optical parameters of all four films, deduced from their reflectivity spectra were approximately ($\pm$10%) the same, giving us the possibility of studying the effect of film thickness on the shape and magnitude of the electro-reflectance spectra obtained according to the IRS technique. The following parameters (in Table(4.5)) were used for the calculation of the ER spectrum as a function of film thickness according to our model:

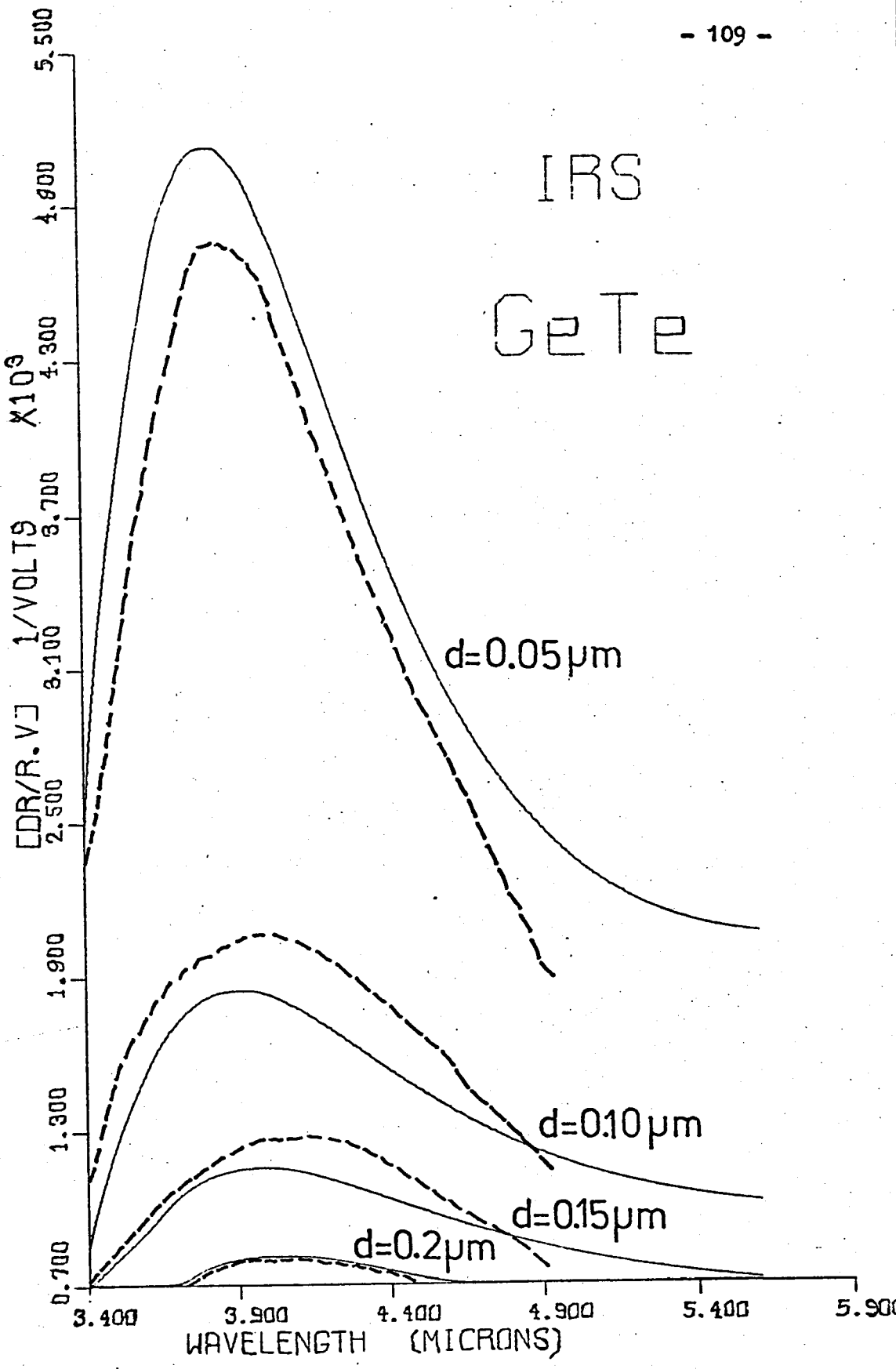

Fig.(4.15) Dependence of experimental ER spectrum on film thickness. Bulk lines are calculated ER spectra corresponding to films of thicknesses and optical properties similar to the ones used for the ER measurements.

TABLE (4.5) Parameters Refering to the Films of Fig. (4.15).

d Å	ε_L	τ ($\times 10^{-15}$ sec)	ω_p ($\times 10^{14}$ sec^{-1})	λ_p μm	m_r^*	C F/m^2
500	29.0	5.1	5.2	3.62	0.22	0.11
1000	28.5	4.9	5.3	3.56	0.22	0.13
1500	28.7	5.0	5.2	3.62	0.22	0.12
2000	28.9	5.2	5.3	3.56	0.23	0.14

The experimental and calculated ER spectra for these four films are shown in Fig.(4.15). The agreement of the calculated with the experimental results is quite good. Discrepancies in the ER values between calculated and experimental results is believed to be the result of inaccuracies in the a) calculation of the optical constants of the films and b) film thickness measurements.

4.6.2 E.R.S.

The ER spectra of poly-crystalline thin GeTe films evaporated onto glass substrates at various temperatures, and thus having various free carrier (hole) concentrations, are shown as typical examples of the external reflection spectroscopy in Figs.(4.16),(4.17) and (4.18). The optical parameters of the films are summarised in Table (4.3). The reflectivity spectra in the vicinity of the plasma edge have also been superimposed on the ER spectra, in order to show the relative position of the ER peak. Again, as in the case of Internal Reflection Spectroscopy, the ER peak occurs in the vicinity of the plasma frequency, as is

(*) cnd.

The uncertainty of the experimental values of parameters like double layer capacitance and film thickness,as well as the inaccuracy of the values for m_r^* and N which were obtained from other researchers' results constitute the stimulus for the decision taken to quote the largest possible error as an absolute error over the entire ER spectrum.
The comparative error,however,is relatively smaller,thus permitting us to draw a smooth curve,representing the spectral distribution of the effect,through the experimental points which represent the mean values of the ER effect at various wavelengths.The comparative error kept small by averaging the values of ΔR,shown on the output of the p.s.d.,over a number of 20 values of ΔR at each wavelength.This technique,which is discussed in detail in paragraph (3.7),yields a fairly small comparative error (<1%) by increasing the reproducibility of the values of ΔR.

expected from our theory and shown in the previous figures.

Computer calculations yielded the ER spectra predicted by our model in the case of ERS, are shown with bulk lines in Figs. (4.16),(4.17) and (4.18). The optical parameters of Table (4.3) were used for the calcula - tion of the spectral variation of the refractive index and extinction coefficient of each one of the films.
Moreover an average value of 0.1 F/m^2 was measured for the electrolytic cell specific capacitance and was assumed to be an approximate value for the double layer specific capacitance. Also, the refractive index of the glass substrates was taken to be 1.5 over the spectral region of our measurements.

The very good approximation of the ER experimental results with the calculated ones gives us evidence that the proposed model for the ER effect, in the case of ERS, is valid.

The generally better agreement between theoretical and experimental results in the case of ERS can be attributed to the more accurate experimental ER spectra available and possibly to the fact that film thickness is not a significant determinant of the ER magnitude as in the case of IRS. It seems that significant experimental errors ($\pm$ 10%) associated with film thickness measurements do not affect the calculated ER spectra as much as in the case of IRS.

The accuracy of the ER values of Figs. (4.16), (4.17) and (4.18) is approximately $\pm$ 20 %. (*) cnd.

A series of ten poly - crystalline GeTe films of various thicknesses were deposited under similar conditions onto glass substrates held at

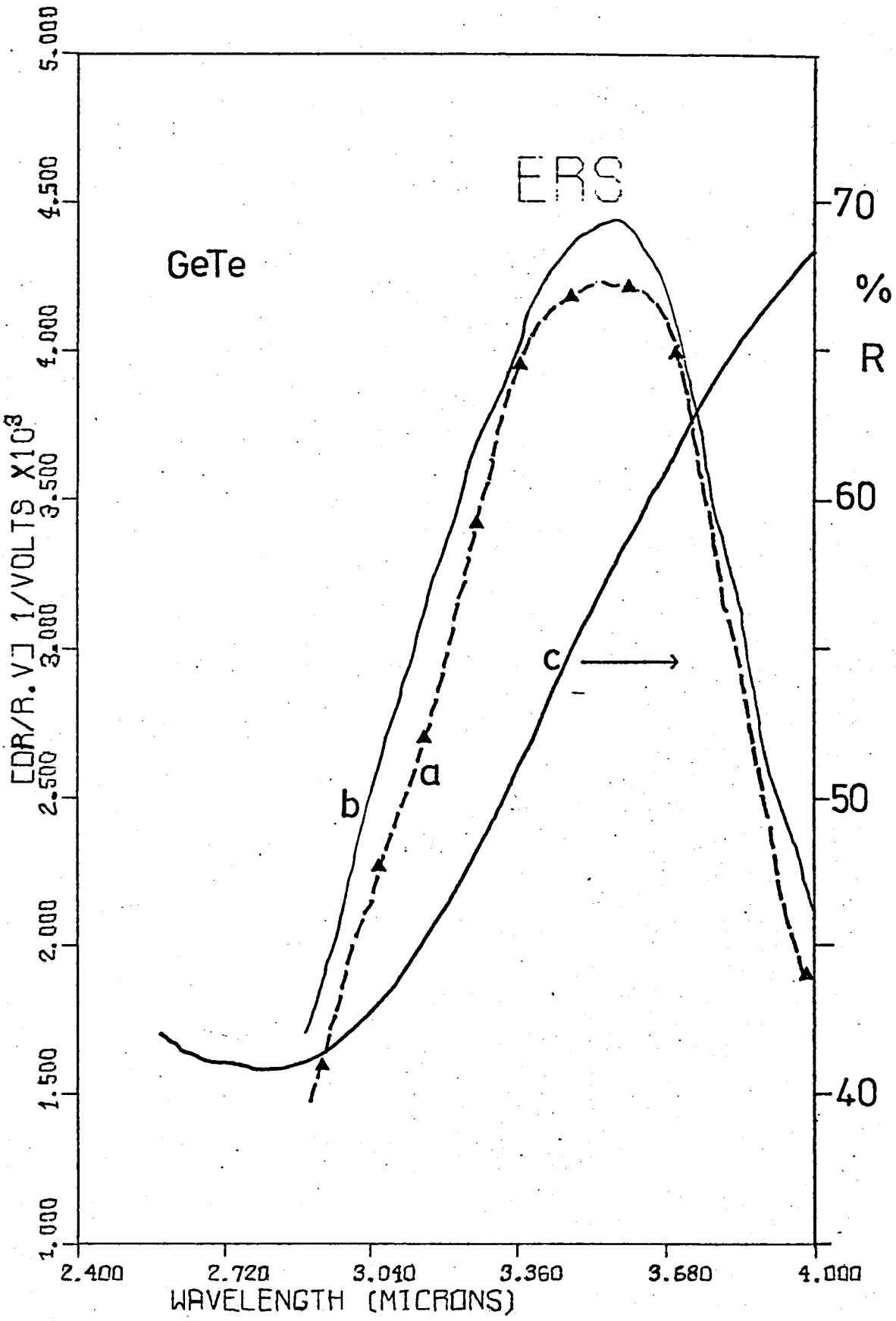

Fig.(4.16) a. Experimental and

b. Calculated ER spectrum of a poly-crystalline GeTe film 1500 Å thick deposited onto a glass substrate precoated with Au islands and held at 200°C.

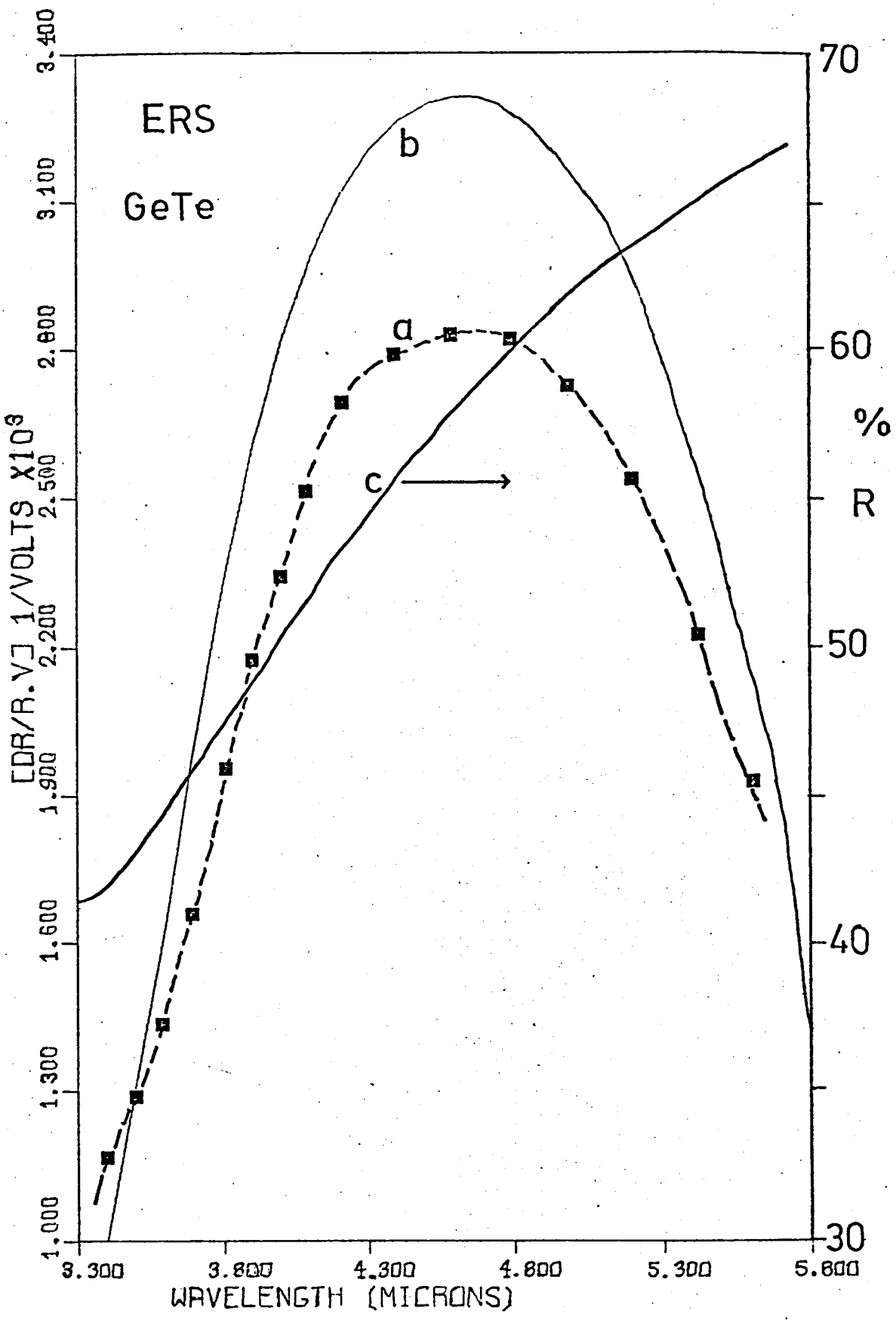

Fig.(4.17) a. Experimental and

b. Calculated ER spectrum of a poly-crystalline GeTe film 2500 Å thick grown on glass substrate at 250°C.

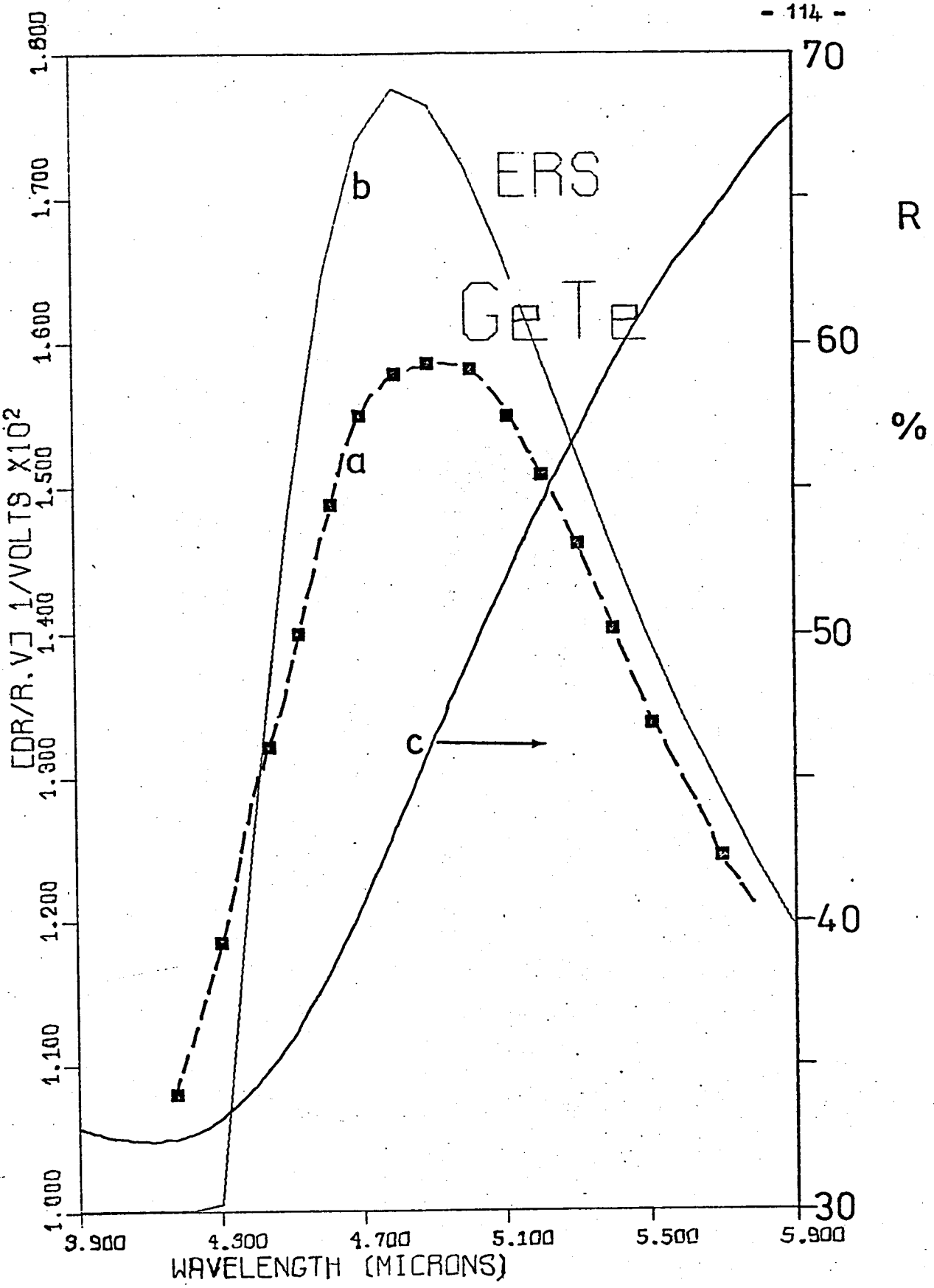

Fig.(4.18) a. Experimental and

b. Calculated ER spectrum of a poly-crystalline GeTe film 2000 Å thick deposited onto glass at 260°C.

270°C in an attempt to study the dependence of the ER spectrum on film thickness. The films exhibited similar optical properties and their reflectivity spectra in the vicinity of the plasma edge were almost coinciding. The result, however, was that there was no detectable quantitative and /or qualitative change in their ER spectra, within the limits of experimental errors of course. This is in very good agreement with the values predicted by our model; according to computer calculations the magnitude of the ER spectrum of the latter films in the ERS mode, is expected to remain the same independently of the value for film thickness.

The relatively high accuracy associated with ER measurements, in the ERS case, gave us the opportunity to study the effect of the free carrier relaxation time on the magnitude and shape of the ER spectrum.
A good deal of troubles was encountered trying to fabricate two poly - crystalline GeTe films exhibiting similar free carrier concentrations but different relaxation times. Two films of approximately the same thickness (3000 Å) and the desired optical properties were eventually fabricated by evaporating prefabricated GeTe onto a) a glass substrate at 250°C with an evaporation rate of about 100 Å/ sec and b) a glass substrate precoated with Au islands and held at 270°C, with an evaporation rate of 10Å/ sec.

Fig. (4.19) shows the experimental reflectivity spectra of the latter films. Our fitting procedure gave the following optical parameters for the films.

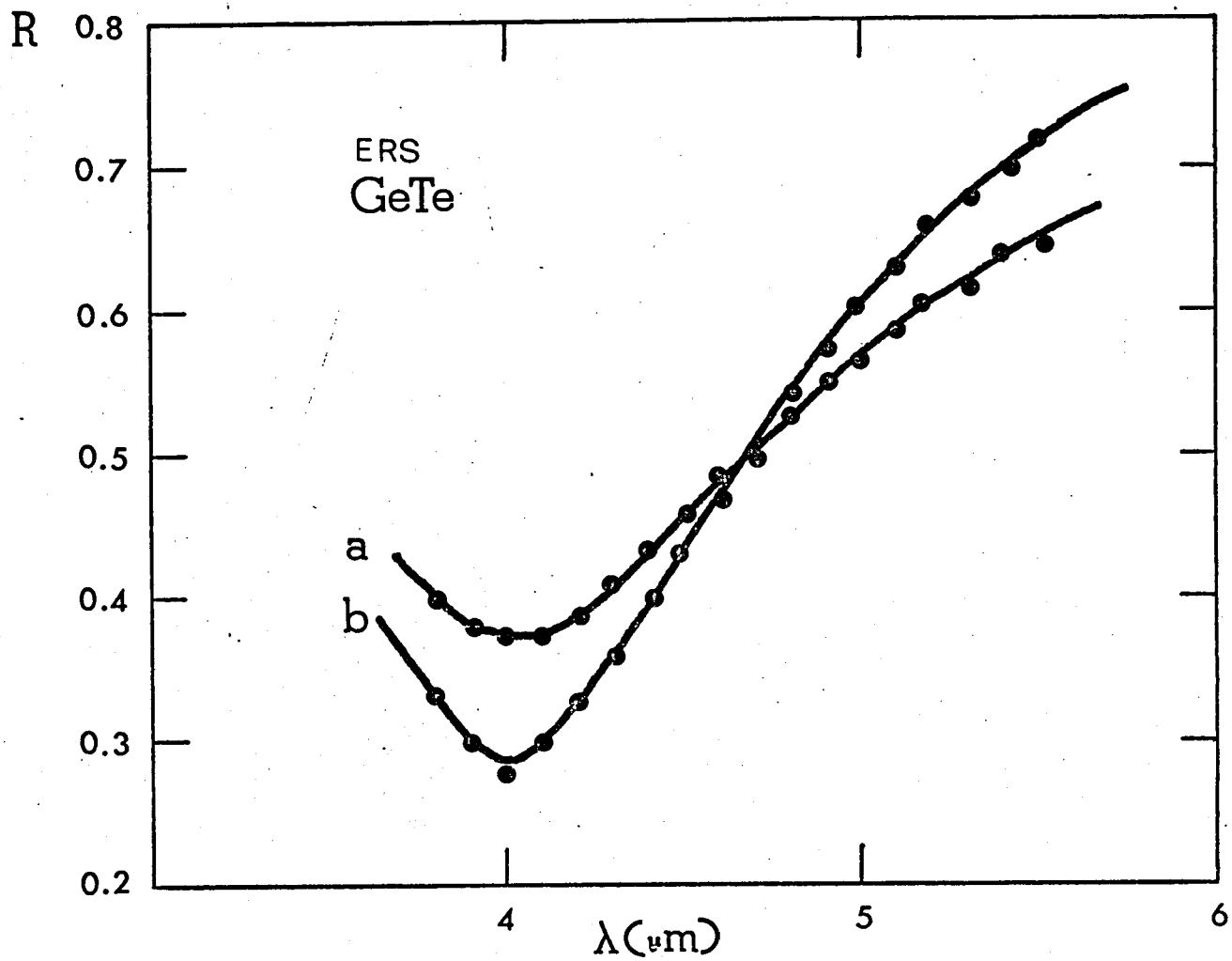

Fig. (4.19) Experimental reflectivity spectra of two poly-crystalline GeTe films, exhibiting relaxation times a) 5.5×10^{-15} sec and b) 8×10^{-15} sec respectively.

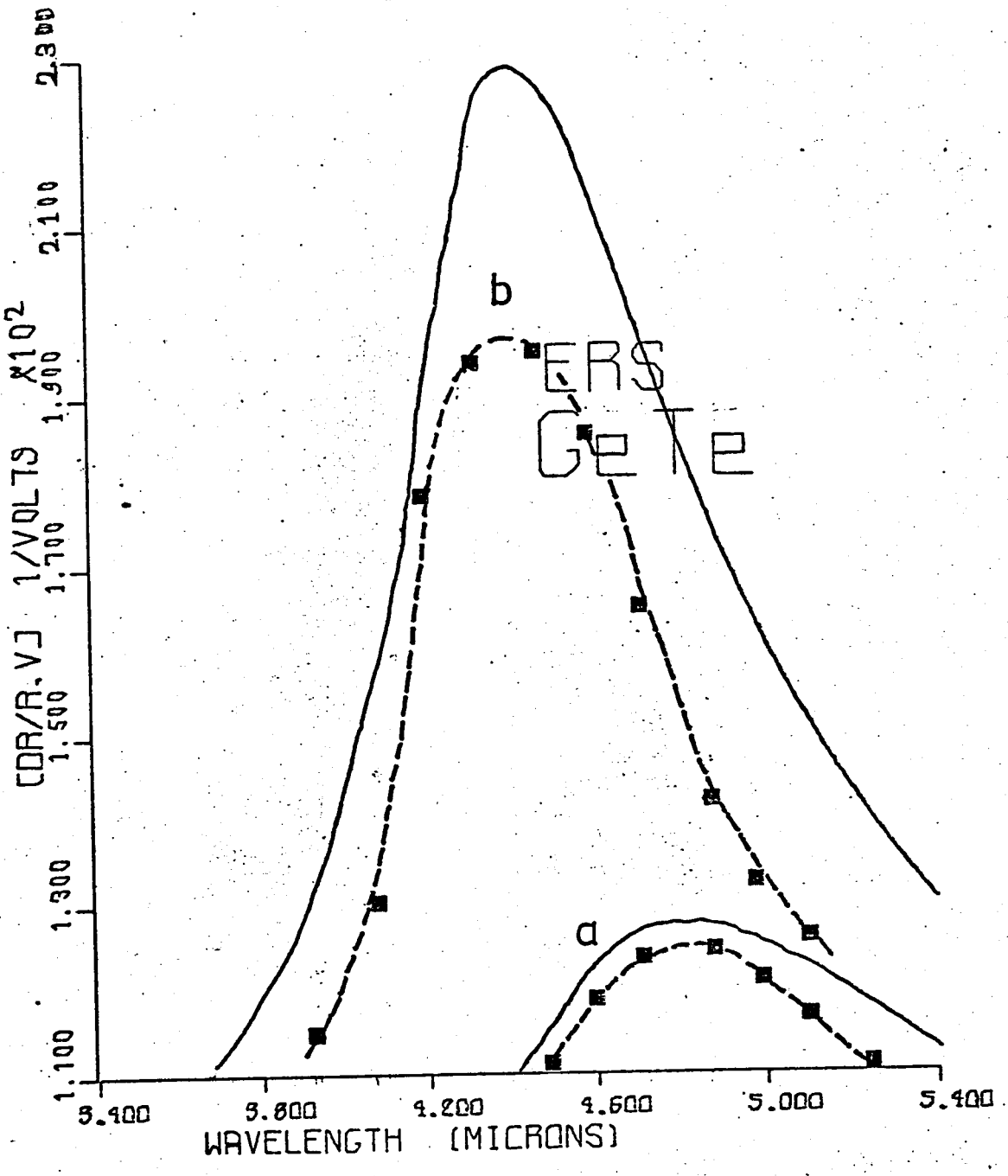

Fig.(4.20) Experimental (dashed lines) and calculated (bulk lines) ER spectra of two poly-crystalline GeTe films exhibiting relaxation times a) 5.5×10^{-15} sec and b) 8×10^{-15} sec respectively.

Film a	Film b
$\varepsilon_L = 37$	$\varepsilon_L = 36$
$\tau = 5.5 \times 10^{-15}$ sec	$\tau = 8 \times 10^{-15}$ sec
$\omega_p = 4.35 \times 10^{14} sec^{-1}$	$\omega_p = 4.38 \times 10^{14}$ sec^{-1}
($\lambda_p = 4.33$ μm)	($\lambda_p = 4.30$ μm)

Moreover, the value of 0.14 was assumed for the optical effective mass of both films and a value of 0.1 F/m^2 was given to the double layer capacitance. The experimental and calculated ER spectra of these poly - crystalline GeTe films are shown in Fig. (4.20). Film a, which exhibits a large free carrier relaxation time, also exhibits a large ER effect.

Also, the ER peak of the film with lower free carrier relaxation time occurs at a longer wavelength comparatively to the position of the ER peak exhibited by the poly-crystalline GeTe film with higher relaxation time.

It is worth noting that the same effect was observed in the case of thin gold films (100 Å thick), [Howson, Avaritsiotis, Fox (1974)].

4.7 Polarity of ER Effect

The polarity of ER effect in the case of GeTe poly-crystalline films is positive, as has been shown in the previous examples. This is in agreement with our initial statement on the polarity of ER effect. As has been discussed, GeTe is a p - type material exhibiting a lattice dielectric constant of approximately 36. When a positive bias is applied

on the GeTe film, produces an increase of the number of holes at the surface of the film. Consequently an increase on reflectivity is expected at a fixed wavelength in the special region of the plasma edge. The result is that a positive sign for the ER effect is expected according to the definitions made in previous chapter. The fact that the experimentally recorded polarity for the ER effect in GeTe films is in exact agreement with the theoretically predicted one gives us evidence concerning the validity of our model.

4.8 IRS Versus ERS

Comparison of the ER spectra, obtained according to the IRS technique, with the ER spectra obtained according to ERS shows that the positions of the ER peaks are not the same for optically similar films, (as the films of Table (4.3)).

Table (4.6) contains the spectral positions of the ER peaks (of the films tabulated in Table (4.3)) obtained from Figs. [(4.11) and (4.16)], [(4.12) and (4.17)], [(4.13) and (4.18)].

TABLE (4.6) IRS Versus ERS

Sample No	d (Å)	λ_p (microns)	λ_{peak} IRS (microns)	λ_{peak} ERS (microns)
1a	1800	3.49	3.4	-
1b	1500	3.47	-	3.5
2a	1500	4.36	4.2	-
2b	2500	4.38	-	4.4
3a	500	4.90	4.4	-
3b	2000	4.85	-	4.9

It has already been stated that film thickness is irrelevant, as far as the optical constants are concerned, when it is greater than 300 Å. Consequently the occurrence of ER peaks at relatively short wavelengths when the IRS is employed, as is shown in Table (4.6), can be attributed to free carrier (hole) absorption.

The proposed model takes indeed free carrier absorption into account; the term $\exp(-\beta)$ of our formula for IRS accounts for that effect.

4.9 Film - thickness Measurements

The thickness of germanium telluride films used in the course of electro-reflectance measurements was measured before and after the ER measurements using a RANK - TAYLOR - HOBSON "Tallystep".

The same instrument was used to measure the film-thickness in the case of antimony and tin telluride films.

An error of approximately $\pm 10\%$ should in general be quoted to the film-thickness values mentioned or to be mentioned.

REFERENCES

1. Avaritsiotis J.N., MSc Thesis, Loughborough, 1974.
2. Bahl S.K., and Chopra K.L., J.Appl. Phys. 40, 4940 (1969).
3. ———————— J.Vac.Sc.and Techn. 6 , 558 (1969).
4. Dutton R.W, and Müller R.S., Proc. IEEE 59 , 1511 (1971).
5. Elliot R.P., Constitution of Binary Alloys, First Suppl. McGraw-Hill Inc. (1965), p.491.
6. Hansen M., Constitution of Binary Alloys, McGraw-Hill Inc. 1958, p.776.
7. McHugh J., and Tiller W., Trans.Met.Soc.AIME 218 , 187 (1960).
8. Heavens O.S., Optical Properties of Thin Solid Films, Dover 1965, p.169.
9. ———————— Thin Film Physics, Methuen 1970, p.27.
10. Howson R.P., Avaritsiotis J.N., and Fox T., 3d International Conference on Thin Films, Budapest, 25-29 August 1975.
11. Mazelsky R., and Lubell M.S., Advan.Chem. 39 , 210 (1963).
12. Okuyama K., Yamamoto H., and Kumagai Y., Appl.Phys. 46 , 105 (1964).
13. ———————— J.Appl.Phys. 46 , 1473 (1974).
14. ———————— Thin Solid Films 33 , 165 (1976).
15. Shunk F., Constitution of Binary Alloys Second Supplement, McGraw - Hill Inc. 1969, p.396.
16. Tsu R., Howard W.E., and Esaki L., Phys. Rev. 172 , 779 (1968).
17. ———————— Solid Stat. Comm. 5 , 167 (1967).
18. Wooley J., and Nicolic P., J.Electrochem.Soc. 112 , 82 (1965).

CHAPTER 5

ELECTRO - REFLECTANCE IN POLYCRYSTALLINE SnTe FILMS

5.1 Introduction

Tin telluride is a IV - VI compound. Single - phase SnTe exists over a wide range of compositions (Schoolar, and Dixon, 1968) and always exhibits p-type conduction as has been found from the plethora of Hall effect measurements, on bulk and thin film material, carried out by a large number of investigators (see for example Shunk 1969 p.688, and Connoly 1972). Brebrick (1963) first pointed out that tin telluride can only be prepared as a p-type material with free carrier concentrations ranging from 4×10^{21} cm^{-3}. Riedl et al (1967),and Bis and Dixon (1969) have shown that the compound is characterized by large deviations from stoichiometry.

Kalafas et al (1964), Houston et al (1964) and Rogers (1968) showed that the high free carrier (hole) concentration is due to a high concentration of Sn vacancies, always present in SnTe, which act as acceptors.

Some particularly appealing characteristics of this material are :

a) its carrier concentration can be easily controlled over a wide range by well established heat treatment procedures (Riedl et al.,1966),

b) the electric susceptibility effective mass is relatively small ($m_r^* = 0.06 - 0.2$) and decreases with decreasing hole concentration (Riedl, Dixon and Schoolar 1967), and

c) reflectivity measurements carried out on SnTe films by Schoolar and Dixon (1968), Burke and Riedl (1969), Bis and Dixon (1970), Otta and Zemel (1969), and Otta and Rabii (1974) showed the existence of a well defined reflectivity plasma edge in the near infra - red, and a negligible bound electron contribution to the dispersive dielectric constant, in the

spectral region of the plasma edge.

5.2 Film Fabrication

Tin telluride poly-crystalline films were deposited in vacuum onto heated glass and NaCl substrates by thermal evaporation from an asymmetric oven - type source. The source material was pre - fabricated as in the case of GeTe, by vacuum melting of the proper quantities of the constituents i.e. Sn : 48.38% wt and Te : 51.62% wt, in evacuated sealed quartz ampules. The source temperature was maintained between 550°C and 800°C throughout the series; change of the source temperature by changing the current passing through it implied a change of evaporation rate. The evaporation procedure was typically as follows: the source was brought up to temperature (about 550°C) and material was evaporated for about 15 seconds with the shutter closed, in order to allow for the melting of the evaporant. The source temperature was then increased and the shutter was subsequently opened for periods of time from 10 seconds to 3 minutes.

The free carrier (hole) concentration of the deposited films was affected by the substrate temperature; the higher the substrate temperature that was employed, the lower free carrier concentration obtained. Also, the optical mobility and consequently the sharpness of the reflectance plasma edge was increased with increasing substrate temperature. The combination, however, of medium substrate temperatures (about 240°C) and high evapora - tion rates (i.e. 100 - 300 Å / sec) yielded poly-crystalline tin telluride films on glass and NaCl substrates, exhibiting well defined plasma edges in the spectral region between 3.5 - 4.5 microns. The problem of obtaining SnTe films exhibiting well defined plasma edges in the spectral regions

of 3.0 to 3.5 microns, and 4.5 to 6.0 microns was initially solved with the application of the following well established technique.

Riedl, Schoolar and Houston (1966) developed a technique for the adjustment of free carrier (hole) concentration in SnTe films. According to their technique, free carrier concentration of prefabricated films are changed by annealing at 400°C or below in evacuated sealed ampules and in the presence of SnTe ingots containing approximately 60 atomic percent Sn (when the free carrier concentration is to be increased), or about 60 atomic percent Te (when the free carrier concentration is to be decreased). Typically, a film on its substrate (17 x 25 x 1) mm^3 together with an ingot (3 - 5) mm^3 were sealed off in a silica ampule (about 100 mm long, having a diameter of 18 mm) at a pressure of about 10^{-5} torr and placed in a pre - heated furnace (GRIFFIN ELECTRIC FURNACE) the temperature of which was kept constant automatically with the aid of an ETHER DIGI controller. The ampule was removed from the furnace after the end of the annealing time period, which varied between 14 and 100 hours, and allowed to cool in room temperature. Room temperature was reached within 5-10 minutes.

This procedure adjusts the Sn vacancies by driving the film from the Te - rich to the Te - richer limit of the deviation from the SnTe stoichiometry, i.e. 50.2 atomic percent Te and 49.8 atomic percent Sn, (Shunk, 1969, p. 688).

However this technique has several disadvantages. Firstly, a free carrier concentration gradient is expected according to Riedl, Schoolar and Houston (1966). The carrier concentration gradient is expected to become more pronounced with increasing film thickness and decreasing time of annealing.

Secondly, it is an expensive technique in the context that requires a large number of silica tubes and a large amound of energy for the annealings.

Several films were prepared on glass substrates by this method. The following table summarizes the heat treatment parameters and approximate carrier concentration of the films.

TABLE (5.1) Heat Treatment Parameters

Film No	INGOT	TIME (hours)	TEMPERATURE (^{o}C)	N(x $10^{26}m^{-3}$)
1	Sn-rich	96	400	2.5
2	Sn-rich	68	400	3.0
3	Sn-rich	14	400	3.3

It is worth noting that the heat - treated films retained their original thickness to within the limit of our ability to determine it ($\pm$ 10%).

Most of the films used as samples in our ER studies, however, were fabricated by evaporation of SnTe evaporants of various concentrations onto glass and NaCl substrates held at various temperatures, and without subsequent heat treatment.

Table (5.2) contains information concerning the evaporant (SnTe ingots), substrate temperature, evaporation rate and plasma wavelength of the films. As in the case of GeTe, SnTe films on glass and NaCl substrates having similar optical constants have been selected and are presented in Table (5.2).

TABLE (5.2) Preparatory Conditions for some SnTe Films

Film No	INGOT Sn in % wt	Substrate temperature (°C)	λ_p (μm)	Evaporation rate (Å /sec)
1a	48.38	240	3.6	300
1b	48.38	240		
2a	48.38	250	3.7	250
2b	48.38	250		
3a	48.67	260	4.3	100
3b	48.67	260		

a refers to SnTe films deposited onto glass substrates.

b refers to SnTe films deposited onto NaCl substrates.

Inspection of the films with the aid of a scanning electron microscope showed that the film grain size was similar to that observed for GeTe films (less than 0.1 microns). It may be argued that although the employment of relatively high evaporation rates, does create comparatively small film grain size, it is also responsible for the comparatively high carrier (hole) concentration exhibited by the SnTe films which have been deposited onto glass and NaCl substrates held at temperatures ranging from 240 to 260°C. This is the case because high deposition rate (for example 300 Å/ sec) implies high supersaturation rate of SnTe vapor and hence an increase of the condensation rate of SnTe molecules for the same substrate temperature. It is worth noting that SnTe vaporizes predominantly as the molecular species because of its high dissociation energy, (Hirayama et al, 1963).

5.3 Optical Properties of Poly-crystalline SnTe Films.

The spectral position of the plasma edge of thin (100 - 350 nm) poly-crystalline films strongly depends on the preparation and / or subsequent heat treatment, as has already been discussed. The large changes of the plasma frequency with free carrier (hole) concentration are also attributed to the carrier concentration dependence of the lattice dielectric constant, ε_L , and optical effective mass, $m_r = m_r^* \cdot m_e$. Figs. (5.1) and (5.2) display the known dependence of m_r/m_e and lattice dielectric constant on free carrier concentration respectively. The optical effective mass increases rather linearly with increasing free carrier concentration, in the region from $3.5 \times 10^{20} cm^{-3}$ to $1 \times 10^{21} cm^{-3}$. On the contrary the lattice dielectric constant decreases from 48 to about 44 with free carrier concentration increasing from $3.5 \times 10^{20} cm^{-3}$ to $1 \times 10^{21} cm^{-3}$. The dependence of plasma wavelength on free carrier concentration has been calculated with the aid of Figs. (5.1) and (5.2) and is shown in Fig. (5.3).

It is interesting to note that at wavelengths less than about 3 microns the contribution from bound electrons into the dispersive dielectric constant becomes significant, thus influencing the reflectivity spectra of poly-crystalline SnTe films. The effects of bound carriers in this spectral region (strong bound carrier absorption) can be seen in the data of Bylander et al (1965), Finkenrath and Kohler (1966), Riedl et al (1967), Burke and Riedl (1969), and Otta and Rabii (1974).

Ageing effects of the films were determined by remeasuring the reflectance spectrum of a few SnTe films five to ten weeks after the original measurement; no change in reflectivity spectra was observed, a fact which

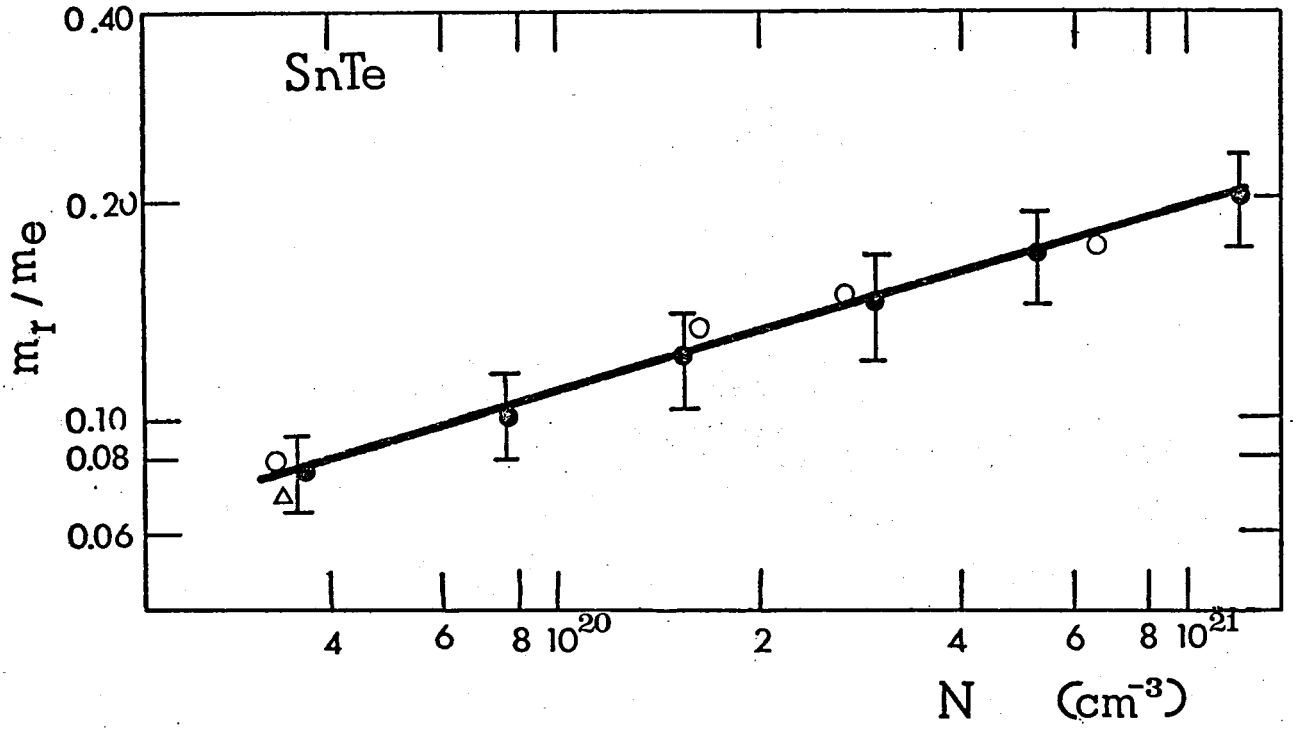

Fig.(5.1) Carrier concentration dependence of the electric susceptibility hole mass at 300°K by:

- ● Bis and Dixon (1970).
- ○ Riedl et al (1967), Schoolar and Dixon (1968)
- △ Burke and Riedl (1969)

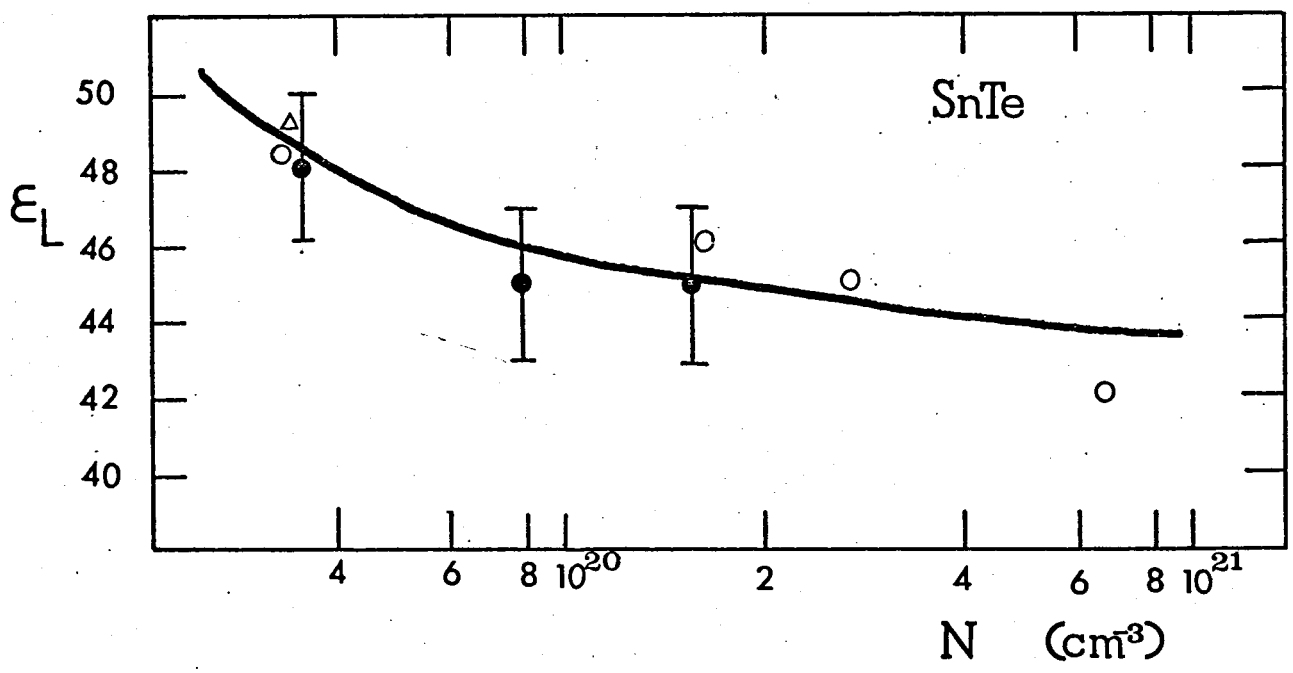

Fig.(5.2) Experimental values of the lattice dielectric constant at 300°K. The data were obtained from the previous references.

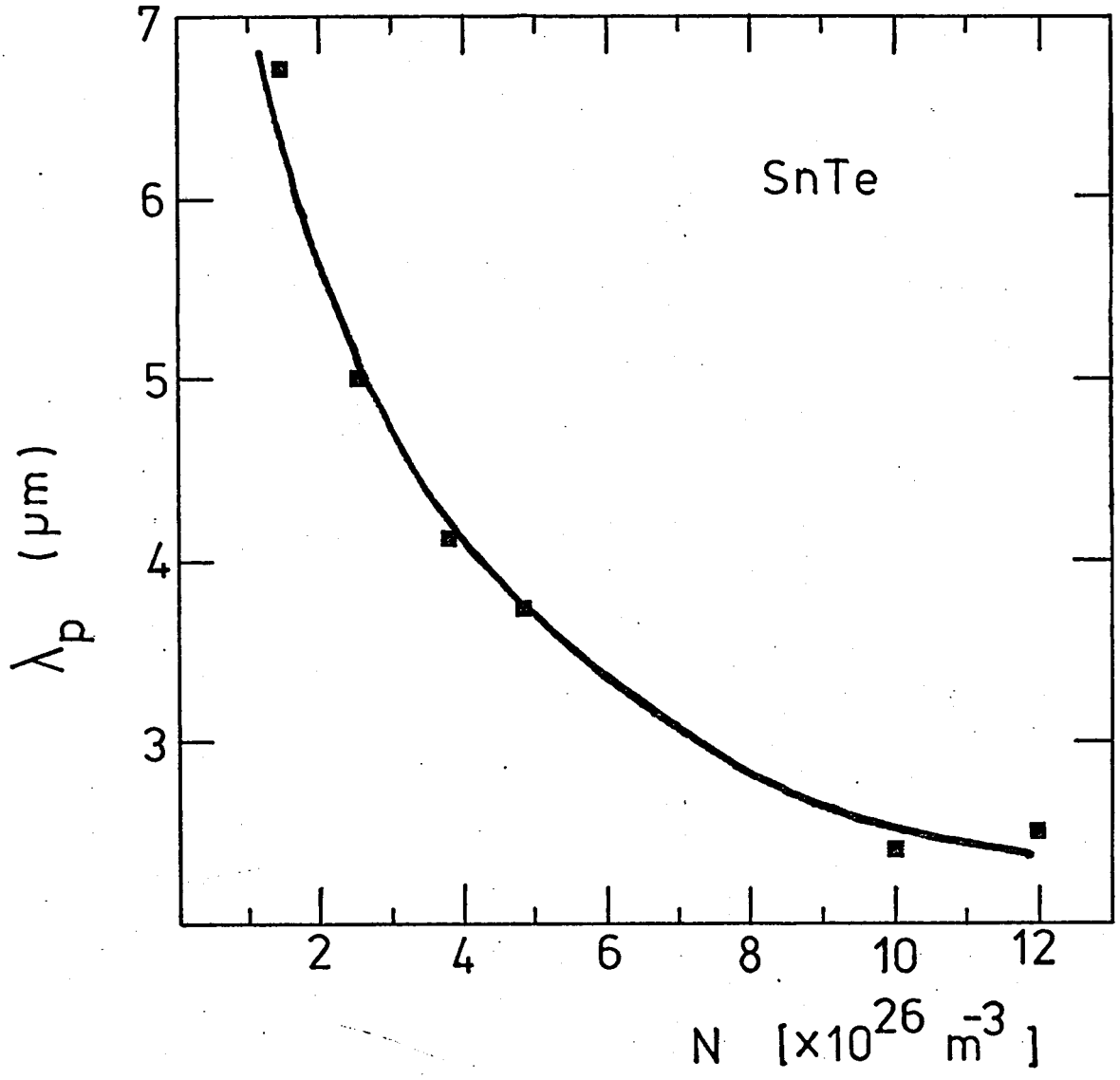

Fig. (5.3) Plasma wavelength against free carrier (hole) concentration calculated from Figs(5.1)and (5.2).

implies that no detectable change in the free carrier concentrations of the films occured.

5.4 Deduction of the Optical Constants of SnTe Films.

The same method was employed, as in the case of GeTe films, for the deduction of the optical constants of our SnTe films as a function of wavelength. The assumption that the reflectivity spectrum of a poly - crystalline SnTe film in the spectral region of the plasma edge is dominated by free carrier effects is again valid. So, the parameters of the Drude model can be calculated by fitting the experimental near normal incidence (10^{o}) reflectivity spectra of our SnTe films, according to the method discussed in Appendix D.

Some selected results obtained according to the previously described method are presented in Table (5.3). These films were selected from a large number of poly-crystalline SnTe films prepared for comparative electroreflectance studies.

Comparison between the values of the lattice dielectric constant tabulated in Table (5.3) and the ones given by various authors in Fig.(5.2) shows that our method gives values very close to the ones found by various investigators. The values of relaxation time, however, which has been deduced by our method are not in very good agreement with the ones given in the literature (about 1×10^{-14} sec). This attributed to the fact that the latter value refers to single crystal films whereas our values refer to poly-crystalline SnTe films.

TABLE (5.3) Optical Parameters of Poly-crystalline SnTe Films Prepared as has been explained in the Text.

	DEDUCED BY OUR METHOD				Taken from Figs.(5.1) and (5.3).	
SAMPLE No	ε_L	τ ($\times 10^{-15}$ sec)	ω_p ($\times 10^{14}$ sec^{-1})	λ_p μm	N ($\times 10^{26}$ m^{-3})	m_r / m_e
1a	43	8	5.19	3.63	5.2	0.140
1b	43	8	5.22	3.61		
2a	44	8	4.41	4.28	3.7	0.135
2b	45	8	4.45	4.23		
3b(*)	46	10	3.69	5.11	2.7	0.135
4b(*)	39	0.8	5.69	3.31	6.5	0.145

a refers to SnTe deposited onto NaCl substrates.

b refers to SnTe deposited onto glass substrates.

(*) the free carrier (hole) concentration has been adjusted by heat treatment.

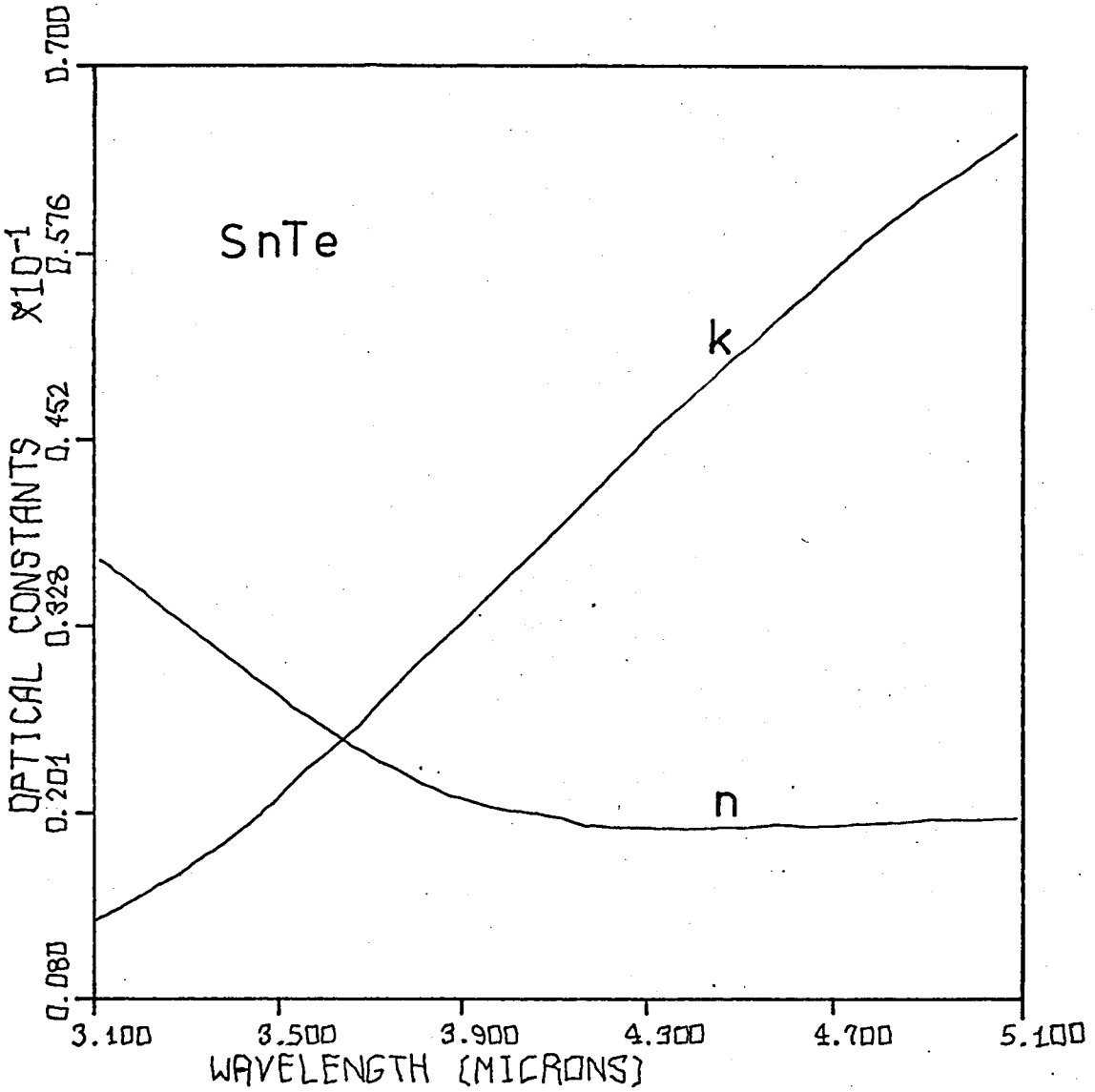

Fig.(5.4) Calculated refractive index and extinction coefficient of films 1a and 1b of Table (5.3).

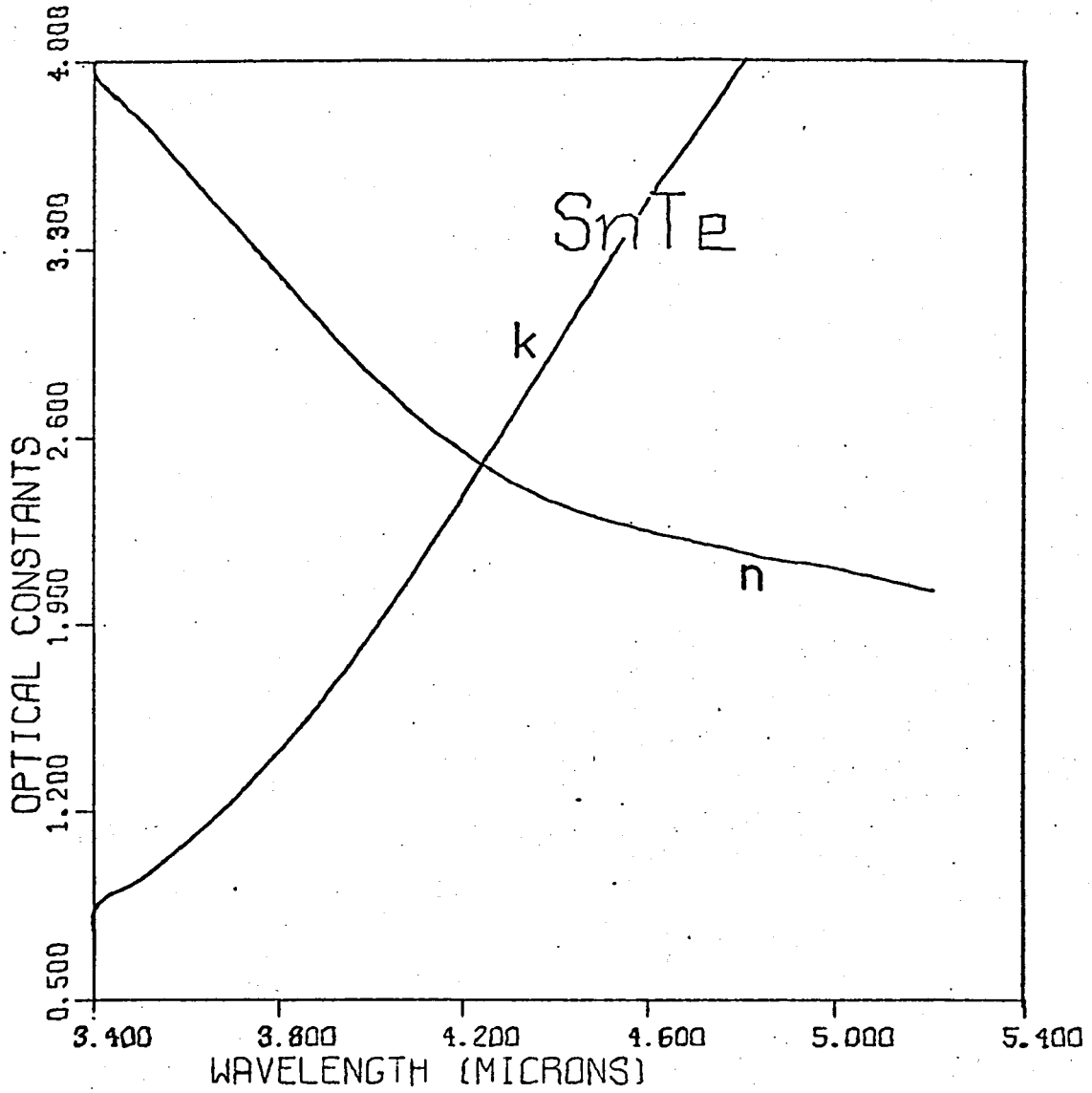

Fig.(5.5) Calculated refractive index and extinction coefficient of films 2a and 2b of Table (5.3).

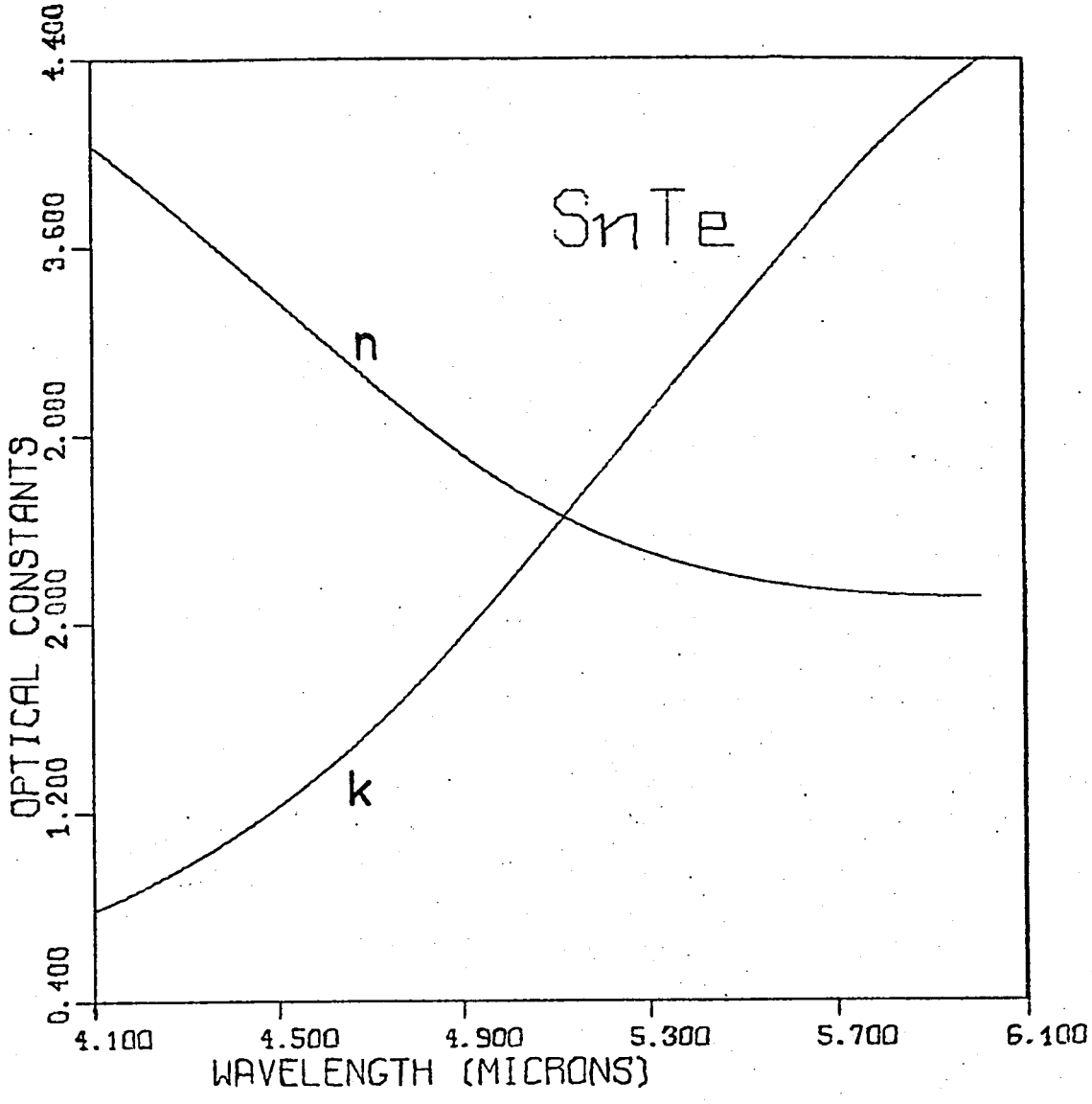

Fig.(5.6) Calculated refractive index and extinction coefficient of film 3b of table (5.3).

The average refractive index and extinction coefficient of each group of films in Table (5.3) have been calculated from Drude's model parameters and are presented in Figs.(5.4),(5.5) and (5.6), against wavelength and in the spectral region of the plasma edge.

5.5 Electro - reflectance Effect Measurements.

Some typical examples of ER spectra in thin poly-crystalline SnTe films are presented in this paragraph. As far as the accuracy of the ER values is concerned the figures quoted in the case of poly-crystalline GeTe films are generally repeated here. In other words ±20 % for ERS, ± 40 % for IRS measurements and a wavelength bandwidth of (0.06 to 0.08) microns. The thickness of the films investigated in the case of ERS varied around 2000 Å. In the contrary films with thicknesses less than 2000 Å were studied in the case of IRS.
The main problem encountered was inaccuracy in both ER magnitude and wavelength resolution in the case of IRS, due to the low radiation intensity available.

5.5.1 IRS

Typical examples of electro - reflectance spectra of thin poly-crystalline SnTe films evaporated onto heated and freshly polished NaCl substrates are shown in Figs.(5.7)and (5.8). The very good agreement between the experimental and calculated ER spectra of Fig.(5.7) is due to the relatively high accuracy (± 30%), whereas the rather poor fitting of the experimental with the theoretical ER spectrum in Fig. (5.8) is attributed to the high inaccuracy in experimental ER values (±45 %) and wavelength

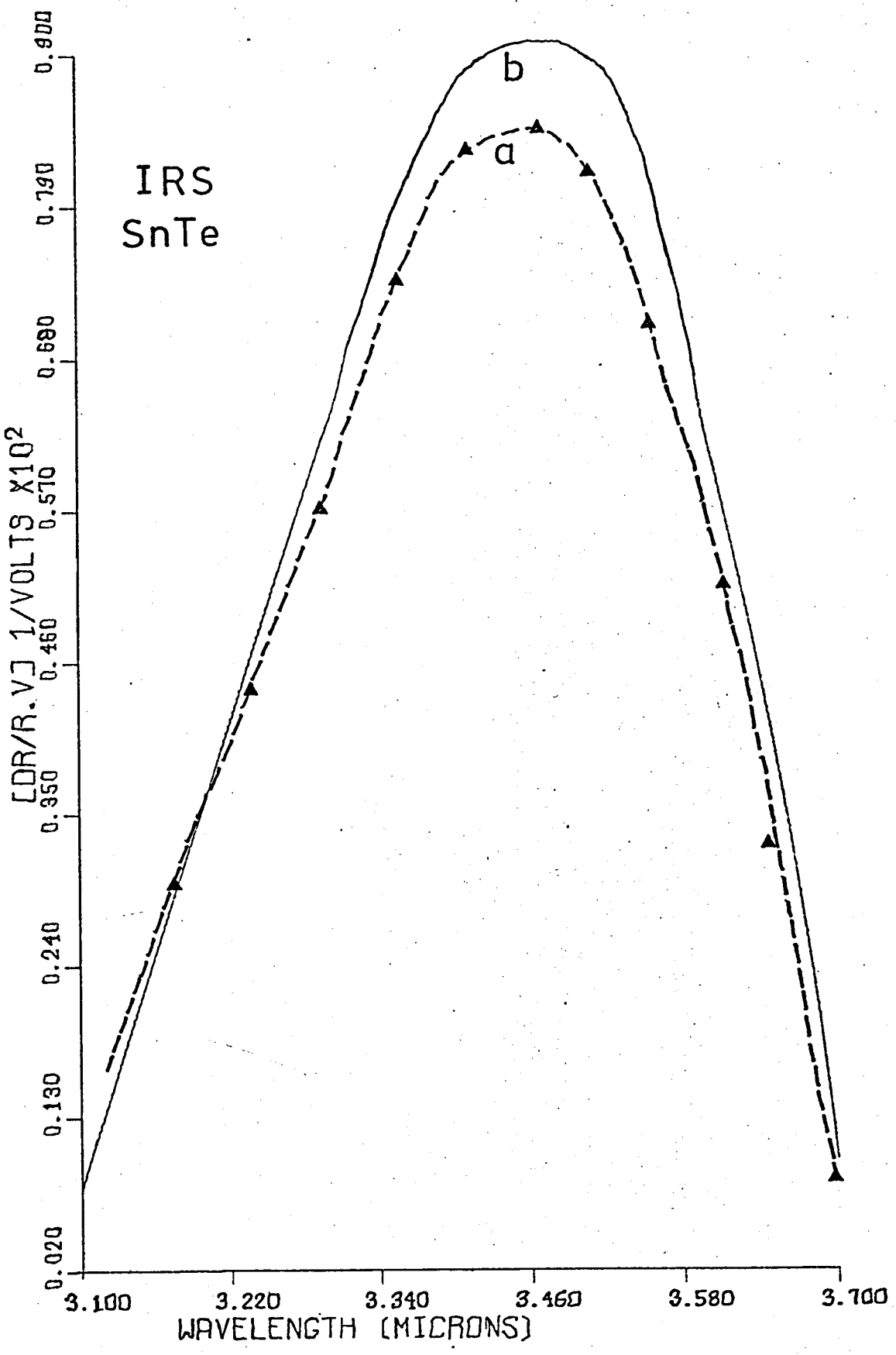

Fig.(5.7) a. Experimental and b. Calculated ER spectrum of a polycrystalline SnTe film 1350 Å thick grown on NaCl substrate at 240°C with a deposition rate of approximately 300 Å / sec.

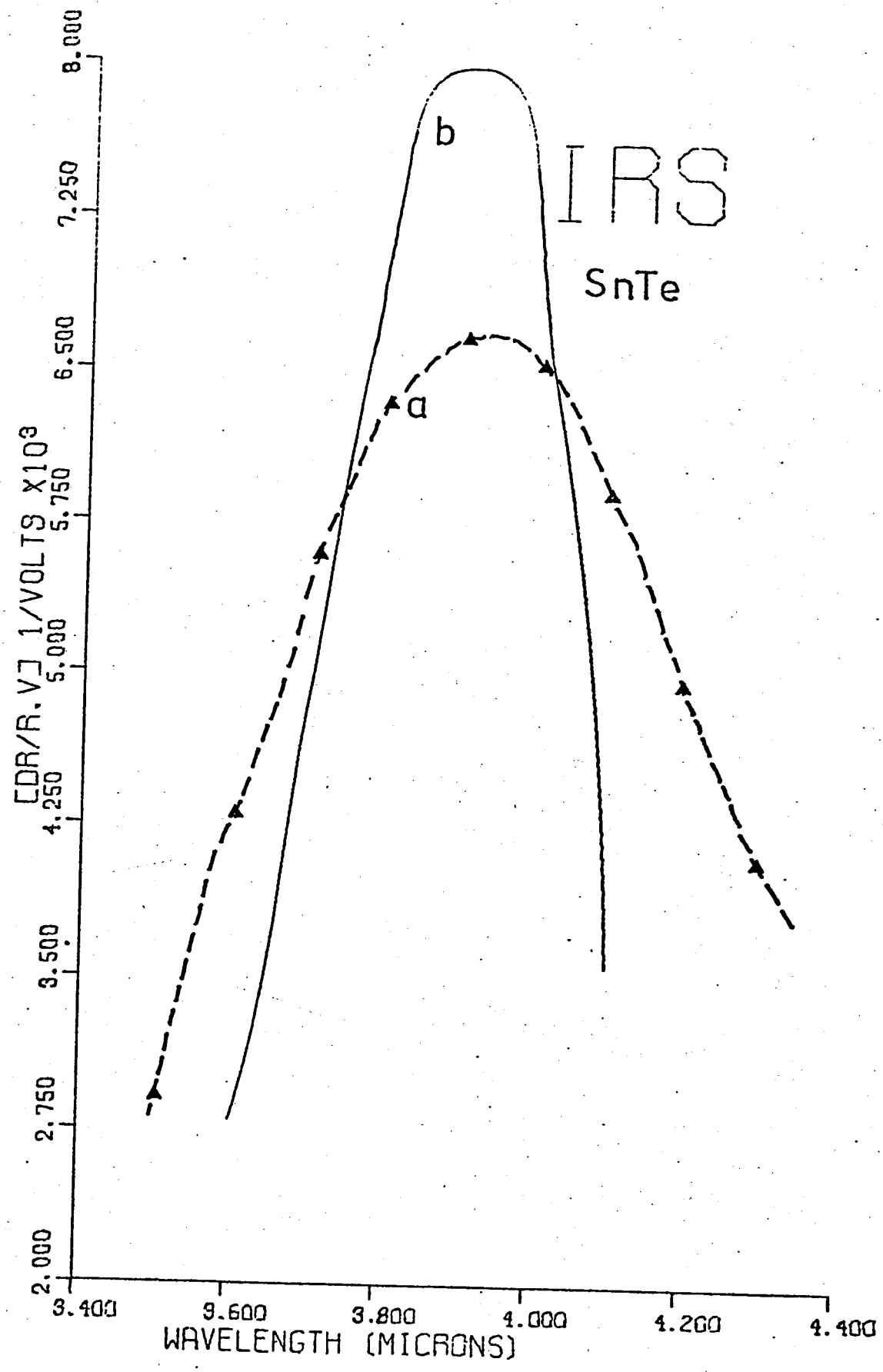

Fig.(5.8) a. Experimental and b. Calculated ER spectrum of a polycrystalline SnTe film 1130 Å thick grown on NaCl substrate at 260°C with a deposition rate at approximately 100 Å / sec.

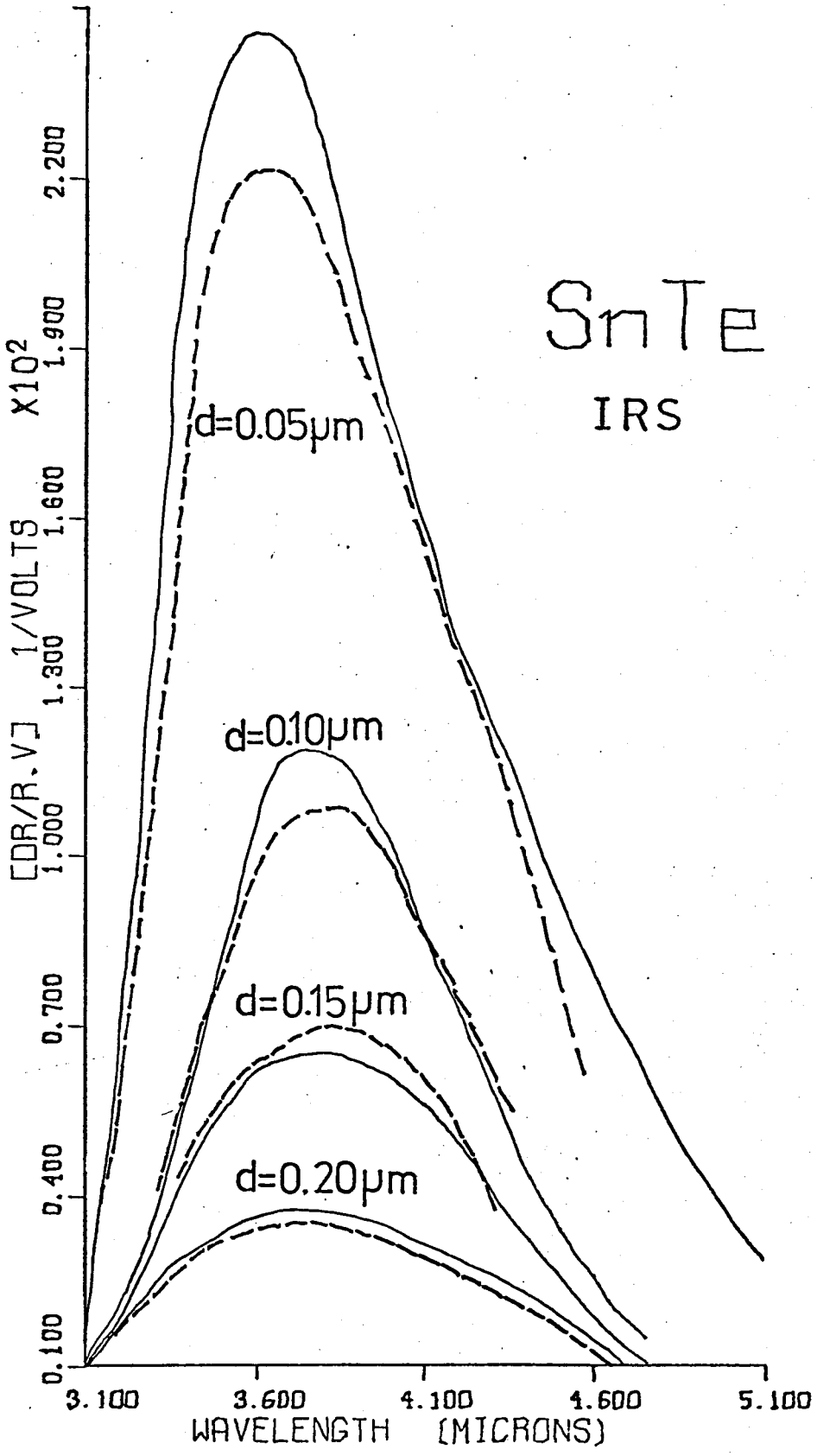

Fig.(5.9) Dependence of experimental ER spectrum on film thickness. Bulk lines represent calculated ER spectra corresponding to the same films.

determination (wavelength bandwidth 0.08 microns).

A series of four thin poly-crystalline SnTe films of various thicknesses was prepared on NaCl substrates held at 260°C with an evaporation rate of 100 Å / sec, under similar conditions, so that their reflectivity spectra were coinciding within ± 5 %. The optical parameters of the films were deduced in the usual way and the results are presented in Table (5.4).

TABLE (5.4) Parameters Refering to Films of Fig.(5.9)

d (± 10%) Å	ε_L	τ ($\times 10^{-15}$ sec)	ω_p ($\times 10^{14}$ sec^{-1})	λ_p μm	m_r^*	C F / m^2
500	43	8	5.09	3.70	0.14	0.11
1000	44	8	5.20	3.62	0.14	0.15
1500	43	8	5.16	3.65	0.14	0.13
2000	45	8	5.11	3.69	0.14	0.14

The experimental and calculated ER spectra for these four films are presented in Fig.(5.9). Discrepancies between calculated and experimental ER spectra can be attributed to errors associated with film thickness measurements, deduction of optical parameters, and experimental errors in reflectivity and ER measurements.

5.5.2. ERS

The ER spectra of several poly-crystalline SnTe films were studied in this case. The optical parameters of the films are summarized in Table (5.3).

Fig.(5.10) shows the calculated optical constants, n and k, the experimental reflectivity and the experimental and calculated ER spectra of a poly-crystalline SnTe film refered as 4b in Table (5.3). It is interesting to note that the experimental electro - reflectance peak occurs in the vicinity of the plasma frequency which corresponds to the wavelength where $n = k$. The agreement between theoretical and experimental ER spectra is very good.

Similarly, Fig.(5.11) shows the reflectance plasma edge, the experimental and calculated ER spectra of a poly-crystalline SnTe film, 3500 Å thick, deposited on to a glass substrate and exhibiting a comparatively low free carrier (hole) concentration adjusted by heat treatment. This is refered as film 3b in Table (5.3). The agreement between theoretical and experimental results is excellent.

Figs.(5.12) and (5.13) show the experimental and calculated ER spectra of two SnTe films 2450 Å and 2850 Å thick respectively, in the spectral region of the reflectance plasma edge. They refer as sample No 1b and 2b respectively in Table (5.3). The value of 0.1 F/m^2 was assumed for the double layer capacitance in the calculations for the derivation of the theoretical ER spectra of the films. The agreement between calculated and experimental ER spectra is very good.

5.6 Polarity of ER Effect

The polarity of ER effect in the case of poly-crystalline SnTe films is positive as has been shown in the previous examples, being in full agreement with our previous discussions concerning the polarity of ER effect in GeTe films.

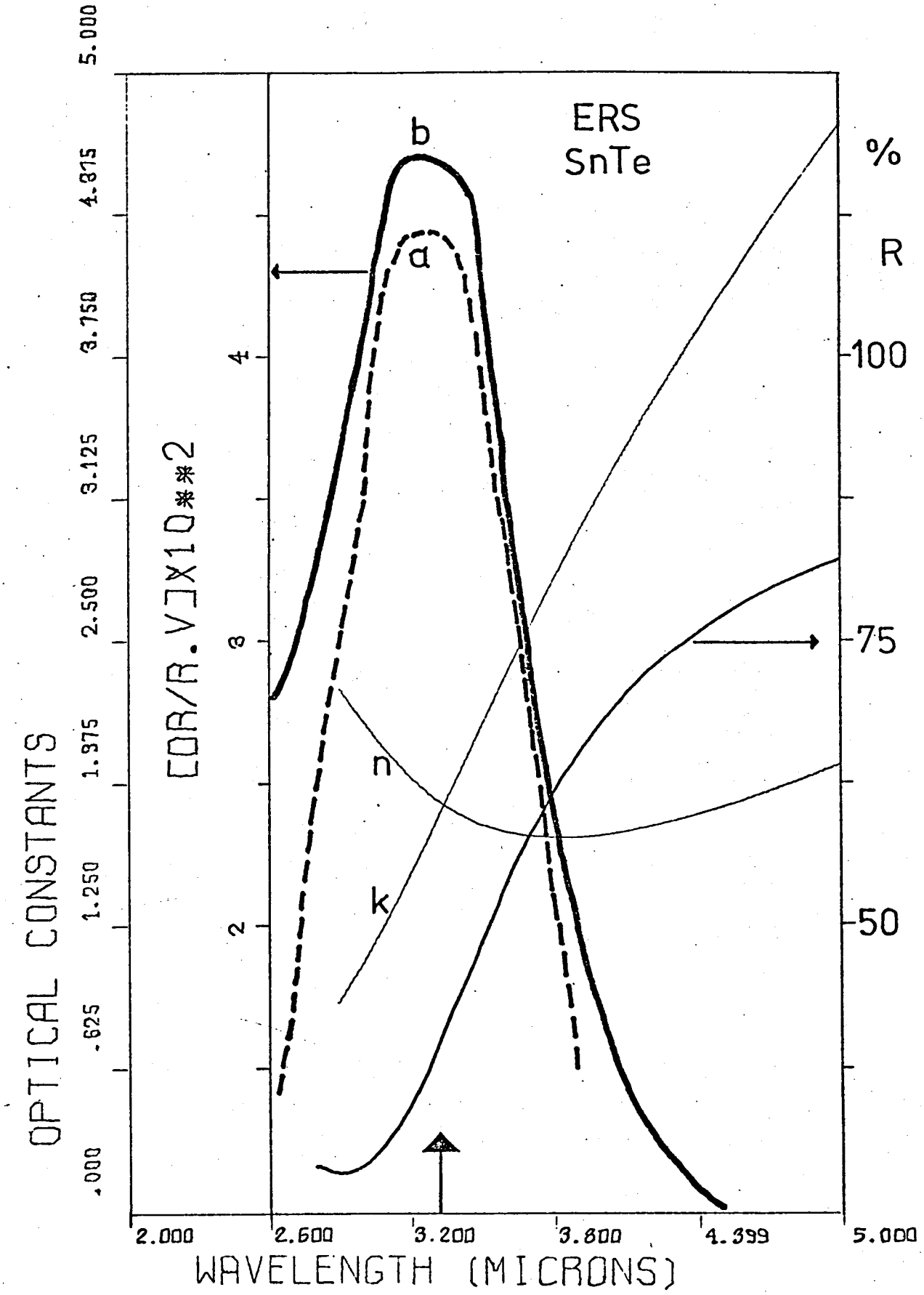

Fig.(5.10) Optical properties of the film 4b from table (5.3). The free carrier (hole) concentration ($N=6 \times 10^{26} m^{-3}$) has been adjusted by heat treatment in the presence of Te-rich ingot at 400°C for 2h. Film thickness: 1450 Å. Curve b is the calc. ER spectra; $C=0.1 F/m^2$.

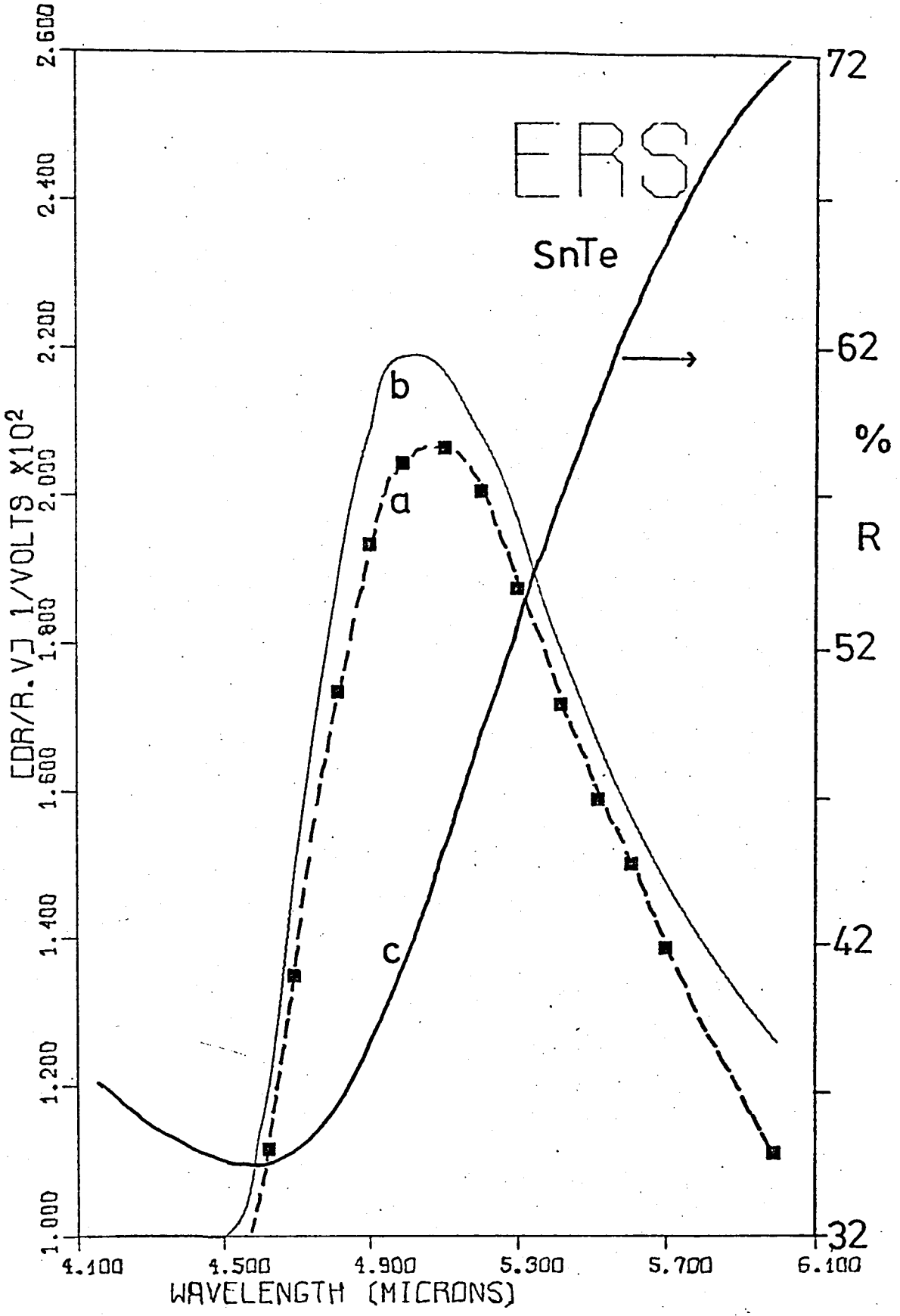

Fig.(5.11) a. Experimental and b. Calculated ER spectrum of the film 3b of Table (5.3). Film thickness: 3500 Å. Double layer capacitance $C = 0.1\ F/m^2$. The free carrier (hole) concentration has been adjusted by heat treatment.

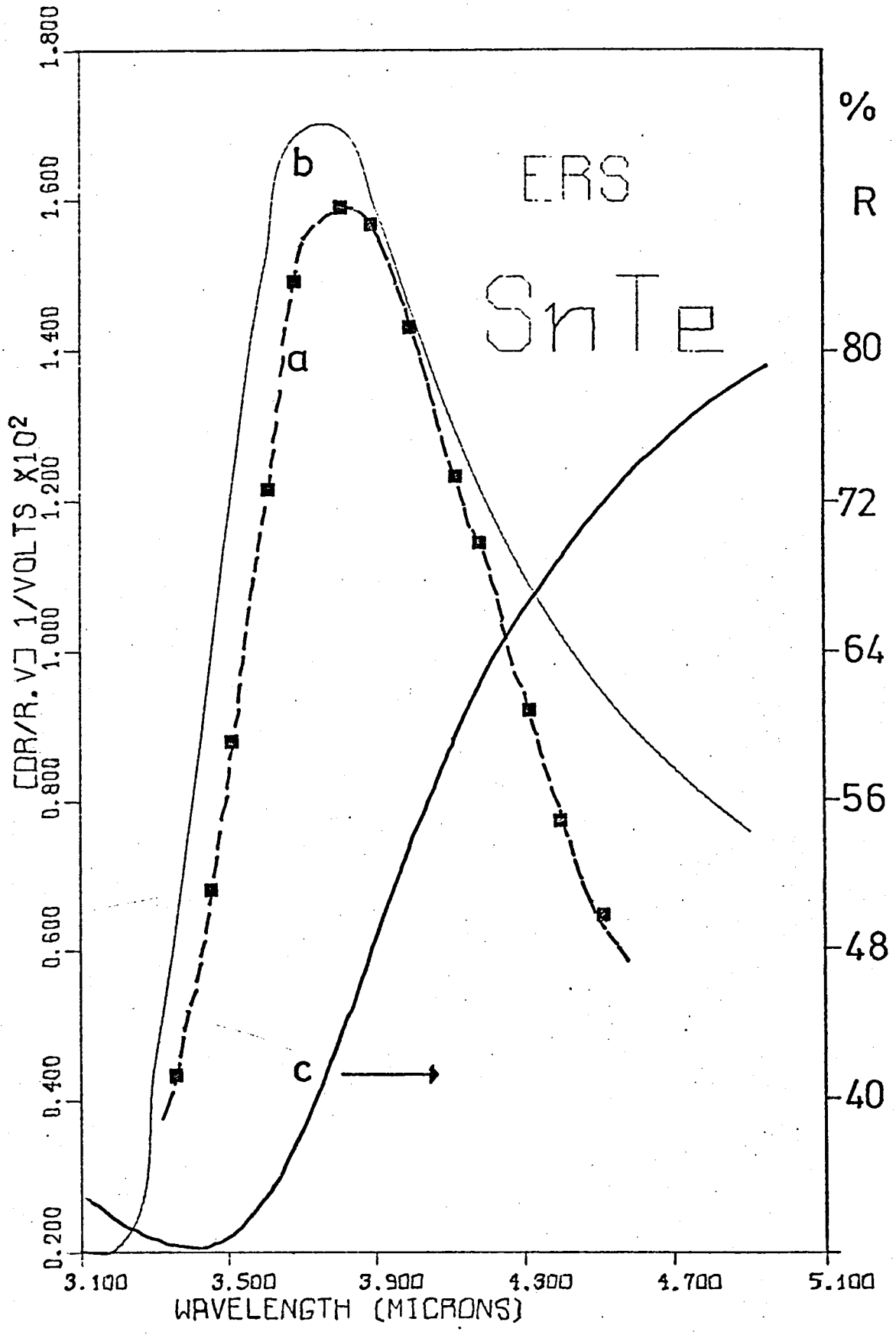

Fig.(5.12) a. Experimental and b. Calculated ER spectra of sample 1b of Table (5.3). Film thickness: 2450 Å.

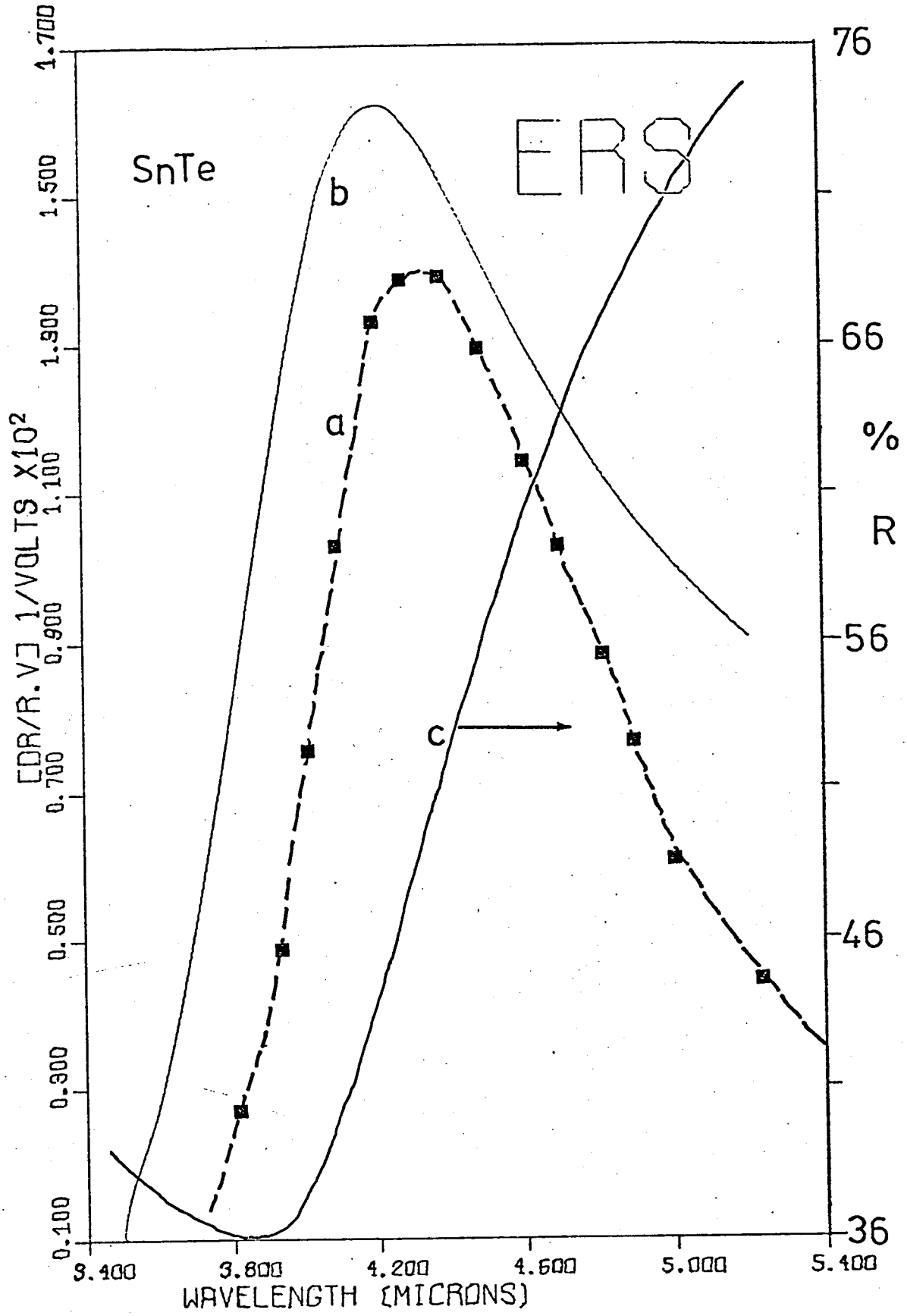

Fig.(5.13) a. Experimental and b. Calculated ER spectra of sample 2b of Table (5.3). Film thickness 2850 Å .

This gives us additional evidence for the validity of the proposed model.

5.7 IRS Versus ERS

The position of ER peaks depends on the technique which has been employed for the measurement of the ER spectrum. As in the case of GeTe poly-crystalline films the position of ER peaks obtained with IRS occur at shorter wavelengths in comparison with the ones obtained with the ERS technique. This effect is attributed to free carrier (hole) absorption and is taken into account in our model. Table (5,5) shows the positions of the ER peaks obtained from Figs.(5.7),(5.8),(5.12) and (5.13).

TABLE (5.5) IRS versus ERS

Sample No	d (Å)	λ_p (microns)	λ_{peak} IRS (microns)	λ_{peak} ERS (microns)
1a	1350	3.63	3.5	-
1b	2450	3.61	-	3.65
2a	1130	4.28	3.95	-
2b	2850	4.23	-	4.3

REFERENCES

1. Bis R.F., and Dixon J.R., Phys. Rev. B, 2 , 1004 (1970).
2. Brebrick R.F., J.Phys.Chem.Solids, 24 , 27 (1963).
3. Burke J.,and Riedl H.R. Phys.Rev., 184 , 830 (1969).
4. Bylander E.G., Dixon R.J.,Riedl H.R.,and Schoolar R.B.,Phys.Rev. 138 , A 864 (1965).
5. Connoly T.F., Solid State Physics Literature Guides, Vol.2, Semiconductors, IFI/PLENUM,1972,p.149.
6. Finkerath H.,and Kohler H.,Phys.Letters, 23 , 437 (1966).
7. Hirayama C.,Ichikawa Y.,and Deroo A, J.Phys.Chem.,67,1039(1963).
8. Houston B.B.,Allgaier R.S.,and Siebenman P.G.,Bull.Am.Phys.Soc.,9, 60 (1964).
9. Kafalas J.A.,Brebrick R.F., and Strauss A.J.,Appl.Phys.Letters, 4,93 (1964).
10. Otta Y.and Rabii S.,Physics of IV-VI Compounds and Alloys,p.113, Edited by J.Rabii, Gordon 1974 .
11. Otta Y.and Zemel J.N.,J.Vac.Sc.Techn.,6,558 (1969).
12. Riedl H.R.,Dixon J.R. and Schoolar R.B.,Phys.Rev.162,692 (1967).
13. Riedl H.R.,Schoolar R.B. and Houston B. Solid State Communications,4, 399 (1966).
14. Rogers L.M.,J.Phys.D. 1, 845 (1968).
15. Schoolar R.B.,and Dixon J.R. J.Optic.Soc.Am.,58,119 (1968).
16. Shunk F.,Constitution of Binary Alloys - Second Supplement, McGraw - Hill Inc. 1969.

CHAPTER 6

ELECTRO - REFLECTANCE IN Sn - DOPED In_2O_3 FILMS

6.1 Introduction

Although tin oxide is a well known material used for the fabrication of transparent conducting coatings and high stability resistors, little is known about the optical properties of doped tin oxide films. SnO_2 (stannic oxide) is used extensively , usually with Sb-doping to increase the electrical conductivity in transparent conducting layers (McMaster 1947 , Holland and Siddall 1953) for preventing the formation of ice on the windscreens of ships etc., in antistatic coatings on glass windows, and finally for the fabrication of the so-called "cold mirrors", i.e. heat shields as a protection against long wavelength IR radiation, (Boort and Groth 1968, Köstlin 1974).

Much interest has recently been aroused in using tin oxide doped with antimony a) in the exploitation of solar energy conversion (Redaelli, 1976), b) the fabrication of transparent highly conducting (less than 20 Ω / $\square$) films for modern electro - optic device applications (Lehmann and Widmer 1975), Fraser and Cook 1972), and thin - film optical waveguides (Molzen 1975).

The electrical conduction of stannic oxide is due to electrons produced by oxygen vacancies. SnO_2 has been found to be an n - type semi - conductor (Inagaki et al 1969). The SnO_2 conductivity can be adjusted by changing the concentration of anion vacancies. It has been found, however , that the previous technique is not controllable (Vossen 1971) and yields small changes of free carrier concentration around $10^{19} cm^{-3}$.

Sinclair et al (1965) suggested that In_2O_3 can be used as an acceptor dopant in SnO_2 films in order to obtain films of controllable free

carrier concentration (or SnO_2 can be used as a donor impurity in the In_2O_3 films). Today, Sb is used as a dopant in the case of SnO_2 and Sn is used as a dopant in the case of In_2O_3 . Doping with metals of higher valency leads to such a high free carrier (electron) density as 10^{21} cm^{-3} (Vainshtein and Fistul' 1970). There is still some controversy in the literature about the amount of doping which has to be introduced in the films to obtain minimum resistivity.

Sn - doped indium oxide films are prepared by either chemical vapor deposition (CVD) or sputtering, and the as deposited resistivity (3 - 300 $\Omega/\square$) depends on substrate temperature (Frazer and Cook 1972, Pankratz 1972, Kane and Schweizer 1975). The films if sprayed or sputtered are exclusively n-type. A well known technique has been recently introduced for the preparation of conductive (3 - 30 $\Omega/\square$,depending on thickness) coatings of tin - doped indium oxide: the so-called reactive sputtering (Holland and Campbell 1968). The new technique has the advantage of yielding indium - tin oxide films having smooth surfaces; a grain size of 300 Å is obtained compared to 80 Å obtained by other techniques. The technique therefore is suitable for the fabrication of photovoltaic cells (Thorton and Hedgcoth 1976).

A systematic study of the dependence of free carrier mobility of In_2O_3 films on the nature of the dopant by Growth (1966) showed that the free carrier (electron) mobility strongly depends on the particular impurity used (Sn, Ti, Sb, Zr). It is worth noting that the electron mobility reported varies by about 10 cm^2 / V.sec An unusually high value (~ 170 cm^2 / V. sec) was measured by Groth (1966) on Zr - doped In_2O_3 films.

6.2 Optical Properties

Reflectance and transmittance spectra of a large number of Sn - doped In_2O_3 films have been recorded and studied. The films were prepared on plain glass substrates, by both chemical vapor deposition (THORN LIGHTING LTD) and D.C. sputtering (PLESSEY COMPANY LTD). The films fabricated with CVD have been deposited onto the glass substrates with an average deposition rate of approximately 2000 Å / sec. The deposition rate and other preparatory conditions of the films prepared by sputtering were not given by the manufacturer.

Figs. (6.1) and (6.2) are S.E.M. photographs of two tin - doped indium oxide films having similar thicknesses (checked with the aid of the interference colors reflected by the films), but prepared by CVD and D.C. sputtering respectively. The film prepared by the latter technique shows a relatively smoother surface as shown in Fig. (6.2).
It is worth noting that, to the best of our knowledge, there has been no systematic study of the differences in optical properties between Sn - doped indium oxide films prepared by chemical vapor deposition and these prepared by D.C. sputtering.

It was decided to make a comparative study of the reflectivity spectra of the films available firstly to investigate the effect of the preparation method on the reflectivity spectrum and secondly to select the most suitable films (i.e. the ones having the sharpest reflectance plasma edges) for our electro - reflectance measurements.

Fig. (6.3) shows the reflectivity spectra of some of the films prepared by CVD in the plants of THORN LIGHTING LTD., Leics. The pronounced

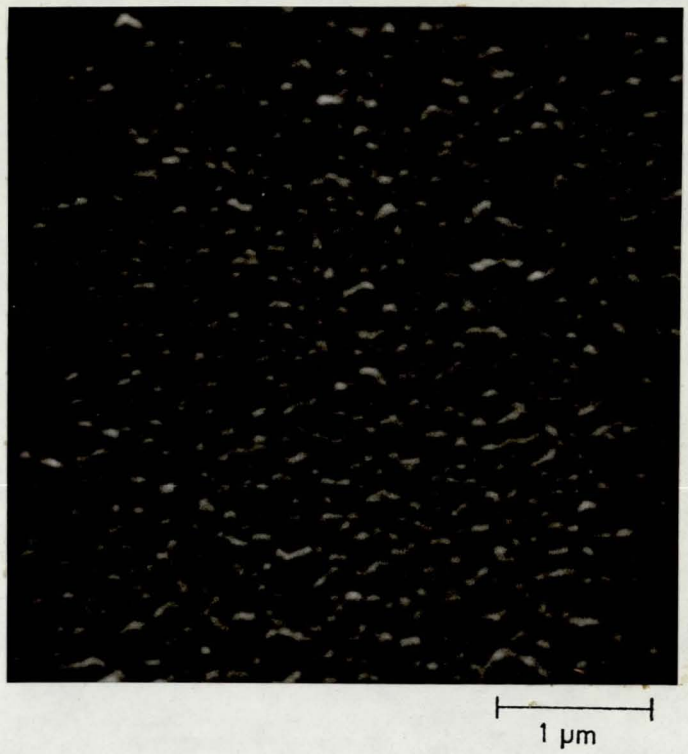

Fig.(6.1) S.E.M. photograph (20K,50°) of Sn-doped In_2O_3 film prepared by CVD.

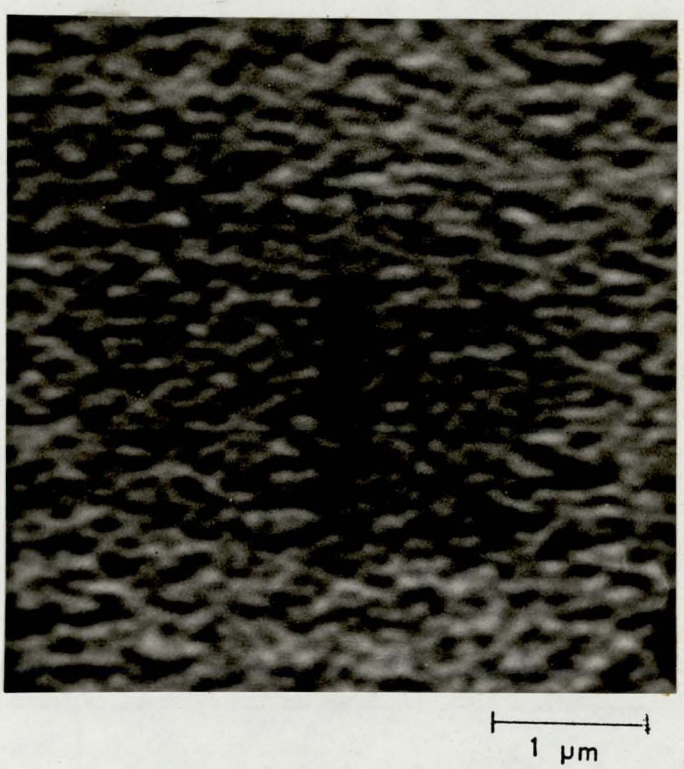

Fig.(6.2) S.E.M. photograph (20K,50°) of Sn-doped In_2O_3 film prepared by d.C. sputtering.

increase of reflectance is due to free carrier (electron) effects. The reflectivity spectra between 0.30 and 0.7 microns were recorded with the aid of a Unicam SP8000 ultraviolet Recording Spectrophotometer and two Perkin-Elmer attachments for near normal incidence ($\sim 10^{o}$) reflectivity measurements.

The reflectivity spectra of Fig. (6.3) correspond to films which have been prepared under similar conditions but having different thicknesses. So, Fig. (6.3) gives us evidence that the free carrier (electron) concentration depends on film thickness; a fact very important for various applications.

Fig. (6.4) shows the reflectivity spectra of two Sn - doped indium oxide films which exhibit a rather interesting feature; the dip in reflectance, at the spectral region of the plasma edge arises from surface plasmons excitation which has been made possible by surface roughness. Similar dip in reflectance was not observed in the reflectivity spectra of the rest of the films; this implies that the latter had comparatively smoother surfaces.

The frequency, ω_s of this additional mode, distinct from the bulk plasma oscillation (which corresponds to a frequency ω_p), is given by Stern and Ferrell (1960) as the one which satisfies the following relation;

$$\varepsilon_A(\omega_s) = -\varepsilon_B(\omega_s)$$

Where, ε_A and ε_B denote the dielectric constants of medium A (air), and B (Sn - doped indium oxide) respectively.

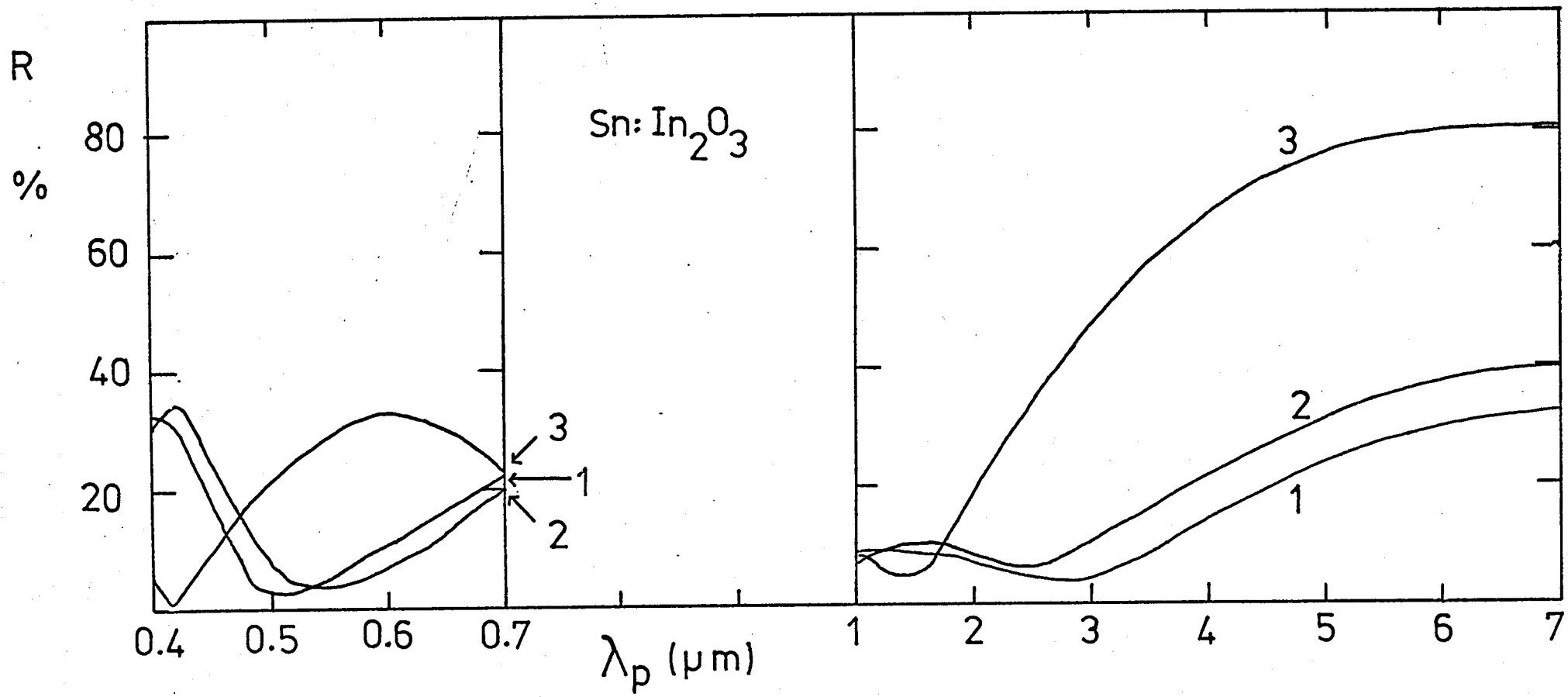

Fig. (6.3) Reflectivity spectra of Sn - doped In_2O_3 films prepared by CVD [See Table (6.2)].

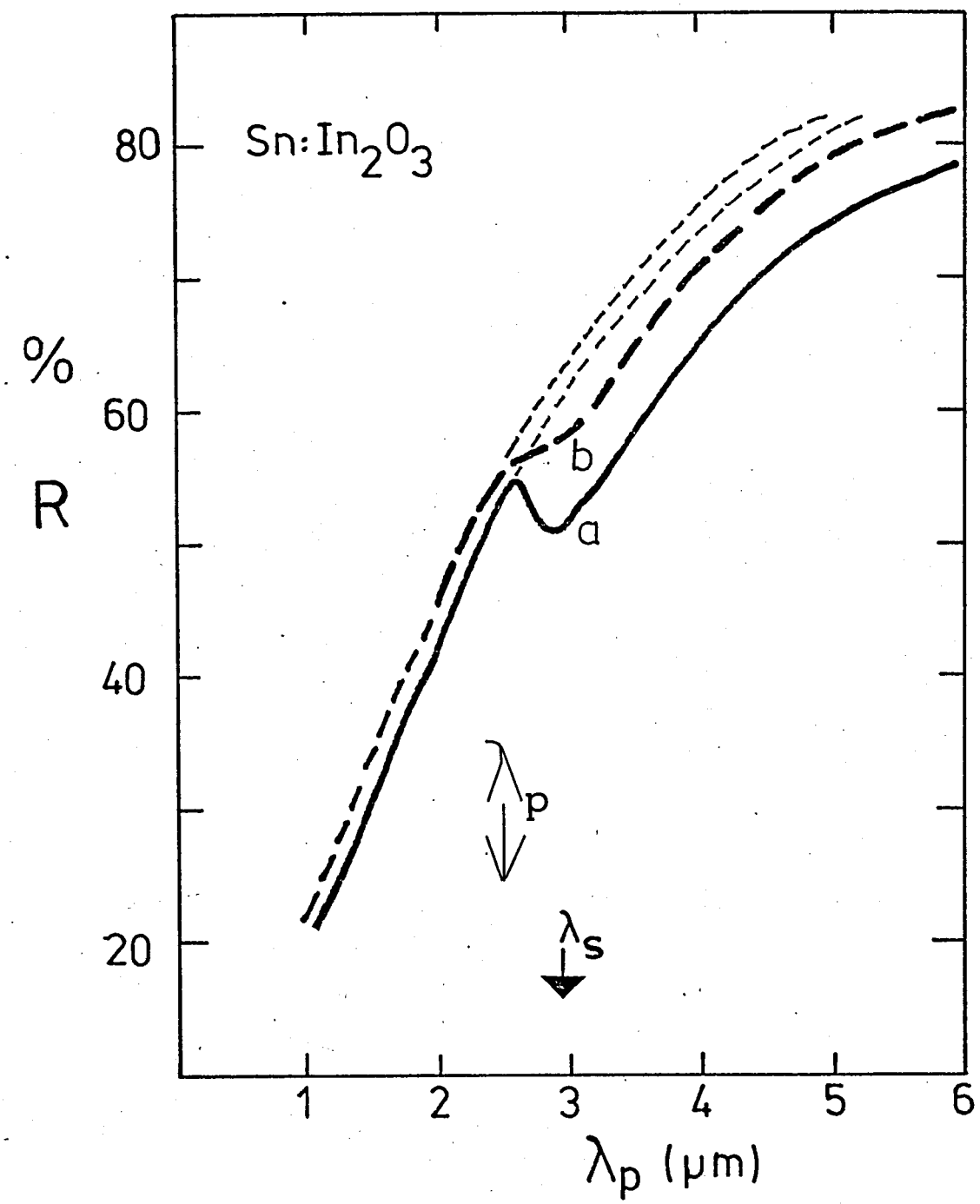

Fig. (6.4) Reglectivity spectra of two Sn - doped In_2O_3 films prepared by CVD. The wavelengths λ_p and λ_s indicate, according to the classical theory, the plasma wavelength and the surface-plasmons wavelength respectively; see Table (6.1).

In the case of

$$\varepsilon_A(\omega_s) = 1 , \quad \omega\tau \gg 1,$$

and for a free electron gas, Drude's model yields

$$\omega_s = \frac{\sqrt{\varepsilon_L} \cdot \omega_p}{\sqrt{\varepsilon_L + 1}}$$

This relation is approximately valid in our case as has been verified by comparing the calculated and experimental values of ω_s (or $\lambda_s = \frac{2 \cdot \pi \cdot c}{\omega_s}$).

TABLE (6.1) Calculated and Experimental Values of Surface Plasmon Frequencies (and Wavelengths)

	Film a of Fig. (6.4)	Film b of Fig. (6.4)
$\omega_{p_{CALC.}}$ (*)	$7.5 \times 10^{15} sec^{-1}$	$7.5 \times 10^{15} sec^{-1}$
$\omega_{s_{CALC}}$ (**)	$\sim 6 \times 10^{14} sec^{-1}$	$\sim 6 \times 10^{14} sec^{-1}$
$\lambda_{p_{CALC}}$	~ 2.5 μm	~ 2.5 μm
$\lambda_{s_{CALC}}$	3 μm	3 μm
$\lambda_{s_{EXP}}$	~ 2.9 μm	~ 2.9 μm

(*) The values for plasma frequency have been deduced from reflectivity spectra of Fig. (6.4) with the aid of the computer method discussed in Appendix D.

(**) A value of 4 assumed for the lattice dielectric constant. That

value was deduced from reflectivity data employing the computer method analyzed in Appendix D.

Fig. (6.5) shows the reflectivity spectra of tin-doped indium oxide films fabricated by D.C. sputtering in PLESSEY'S laboratories at Northants. There is no indication of surface plasmons effect; this can be attributed to the comparatively smoother film surface. Moreover the reflectance plasma edges are not sharper than the ones exhibited by the films prepared by chemical vapor deposition (as it was expected because of the deposition rate), this may be attributed to possible lower substrate temperatures that were employed.

Tin-doped indium oxide films prepared by CVD method were deposited on glass substrates held at around $500^{o}C$ whereas D.C. sputtered films are usually deposited onto substrates held at room temperature.

6.2.1. Film Thickness Deduction

The thickness of Sn - doped In_2O_3 was determined from the reflectance extrema due to thickness interference effects (multiple reflections), in the visible part of the spectrum.

The conditions for the occurence of minimum values for reflectance are given by Heavens (1965), p. 157,

$$n\,d = (2\,m + 2)\,\lambda / 4 \qquad (6.1)$$

where n is the refractive index of the tin - doped oxide film, which is assumed to be non - absorbing in the visible part of the electromagnetic spectrum, d is its thickness and λ are the wavelengths where the

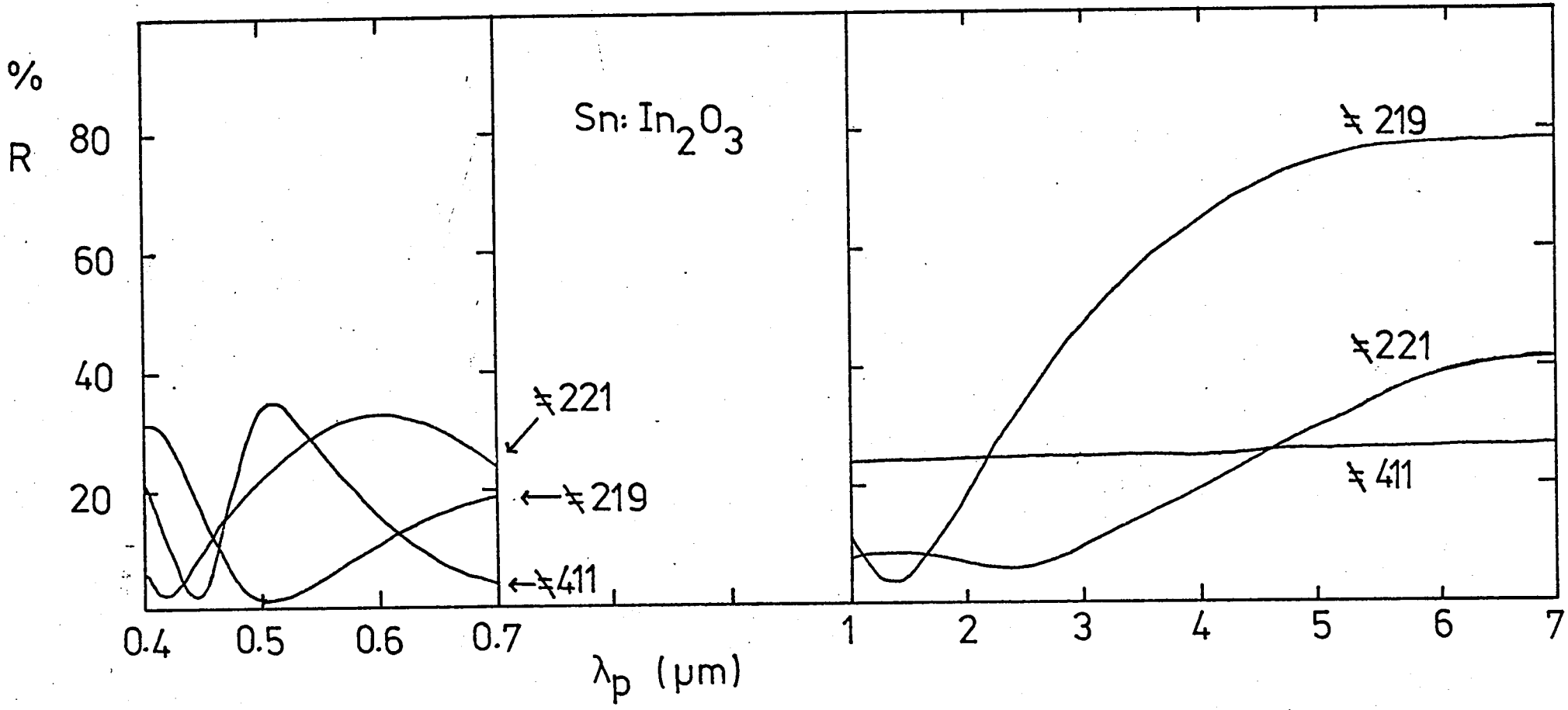

Fig. (6.5) Reflectivity spectra of Sn - doped In_2O_3 films prepared by D.C. sputtering [See Table (6.3)].

reflectance minima occur.

Similarily, the conditions for the occurrence of reflectance maxima are

(6.2) $$n\,d = (2\,m + 1) \cdot \lambda / 4.$$

These relations can be used to determine the parameter , m , present in Eqs. (6.1) and (6.2), provided that n is unambiguously known. A value of 2.0 is given by Fraser and Cook (1972) for the refractive index in the spectral region around 500 nm . Moreover refractive index values of 2.03 and 1.95 have been quoted for 480 and 620 n m respectively. If the value of n does not change very rapidly with wavelength, as in our case, then by assuming nd to be constant, we may substract the relations

(6.3) $$4\,n\,d = (2\,m + 2)\,\lambda_1$$

(condition for reflectance minimum at λ_1), and

(6.4) $$4\,n\,d = (2\,m + 1)\,\lambda_2$$

(condition for reflectance maximum at λ_2), for two successive interference extrema and obtain

(6.5) $$m = \frac{2\lambda_1 - \lambda_2}{2\,(\lambda_1 - \lambda_2)}$$

Consequently, m has been determined. Substituting the value of m , found in that way, into Eq.(6.1) yields a value for the thickness of the film:

$$d = \left[\frac{2 \cdot \lambda_1 - \lambda_2}{2(\lambda_1 - \lambda_2)} + 1\right] \frac{\lambda_1}{2n} \qquad (6.6)$$

Film thicknesses calculated according to the previously discussed method are presented in Tables (6.1) and (6.2), which are refering to Figs (6.3) and (6.5) respectively.

TABLE(6.2) Characteristics of Sn-doped In_2O_3 Films Fabricated by CVD on plain Glass.

Sample No	R (ohms/square) (*)	d (Å)
1	50	260
2	40	370
3	20	450

(*) Sheet resistance was measured between two strips of In-Ga amalgam; the distance between the strips was equal to their lengths, approximately 1cm.

TABLE (6.3) Characteristics of Sn - doped In_2O_3 Films Fabricated by sputtering onto Plain Glass Substrates.

Run No	R (ohms/square)(*)	d (Å)
221	40	450
219	26	270
411	147	590

(*) The sheet - resistance of the films fabricated by PLESSEY COMPANY LTD. were given by the manufacturer.

The extraordinary effect of having thicker Sn - doped In_2O_3 films exhibiting higher ohmic resistances can simply be attributed to the preparatory conditions and mainly to the sputtering gas mixture, (Fraser and Cook, 1972).

6.2.2 Deduction of Optical Constants

The spectral variation of the refractive index and extinction coefficient of two tin doped indium oxide films (No 3 and ≠ 219) have been deduced from reflectivity measurements employing the optimization strategy discussed in Appendix D. These particular films were selected for ER measurements because they were optically homogeneous and exhibited comparatively sharp plasma edges shown in Figs.(6.3) and (6.5).

The Drude's parameters, from which the dispersive real and imaginary parts of the complex dielectric constant have been calculated, are presented in Table (6.4).

TABLE (6.4) Drude model Parameters deduced by fitting the Reflectivity Spectrum.

	Film No 3 of Fig. (6.3)	Film ≠ 219 of Fig. (6.5)
τ	1.78×10^{-15} sec	1.73×10^{-15} sec
ε_L	5	8
ω_p	8.83×10^{14} sec^{-1}	8.84×10^{14} sec^{-1}
λ_p	2.1 μm	2.1 μm

It is worth noting that a lattice dielectric constant of 4.0 and an effective optical mass of $0.35\ m_e$ have been found by Köstlin et al (1974) by fitting a number of free electron concentrations N versus plasma wavelength, with the relation

$$\lambda_p = 2\pi c\left[\frac{4\pi N e^2}{\varepsilon_M \cdot m_c}\right]^{-\frac{1}{2}}$$

From their results is obvious that the fitting is adequate for low values of N only. This means that the term $\varepsilon_M \cdot m_c$ is not constant over all the values for free carrier (electron) concentration. Köstlin et al (1974) have also deduced a value of $30\ cm^2/V.\ sec$ for electrical mobility, which implies a value of approximately 6×10^{-15} sec for the free carrier relaxation time. They stated, however that the value for the free carrier relaxation time has always been found to be less than 6×10^{-15} sec .

Clanget (1973) gives a value of 4 for the lattice dielectric constant, independently of the carrier concentration, by extrapolating the real part of the dielectric constant to $\lambda = 0$ and assuming that
a) the relaxation time in the spectral region 3 - ∞ eV is negligible and
b) that interband effects are negligible.
Extrapolation of their experimental results for the imaginary part, ε_i, of the dielectric constant to $\lambda = 0$ under the same assumptions should give $\varepsilon_i = 0$, but it does not.

Vainshtein and Fistul' (1967) found that the energy gap of undoped indium oxide is 3.55 eV. This implies that the onset of interband transitions in Sn - doped In_2O_3 is expected at the vicinity of 360 nm. So, the assumption that interband effects are negligible in the photon region between 3 eV and higher photon energies is questionable.

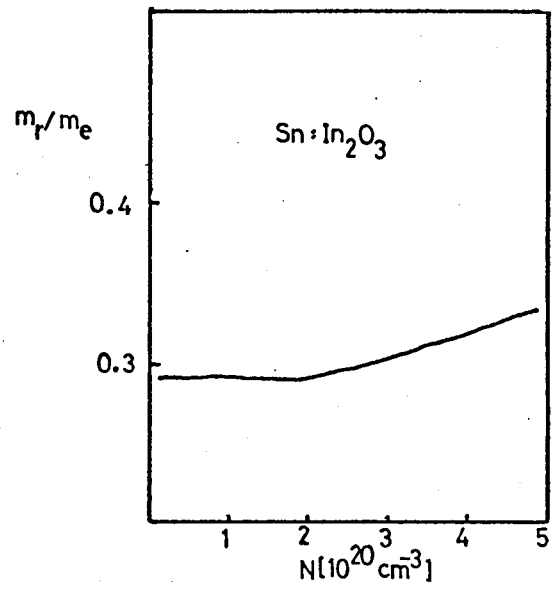

Fig.(6.6) Optical effective mass dependence on free electron concentration, after Clanget (1973).

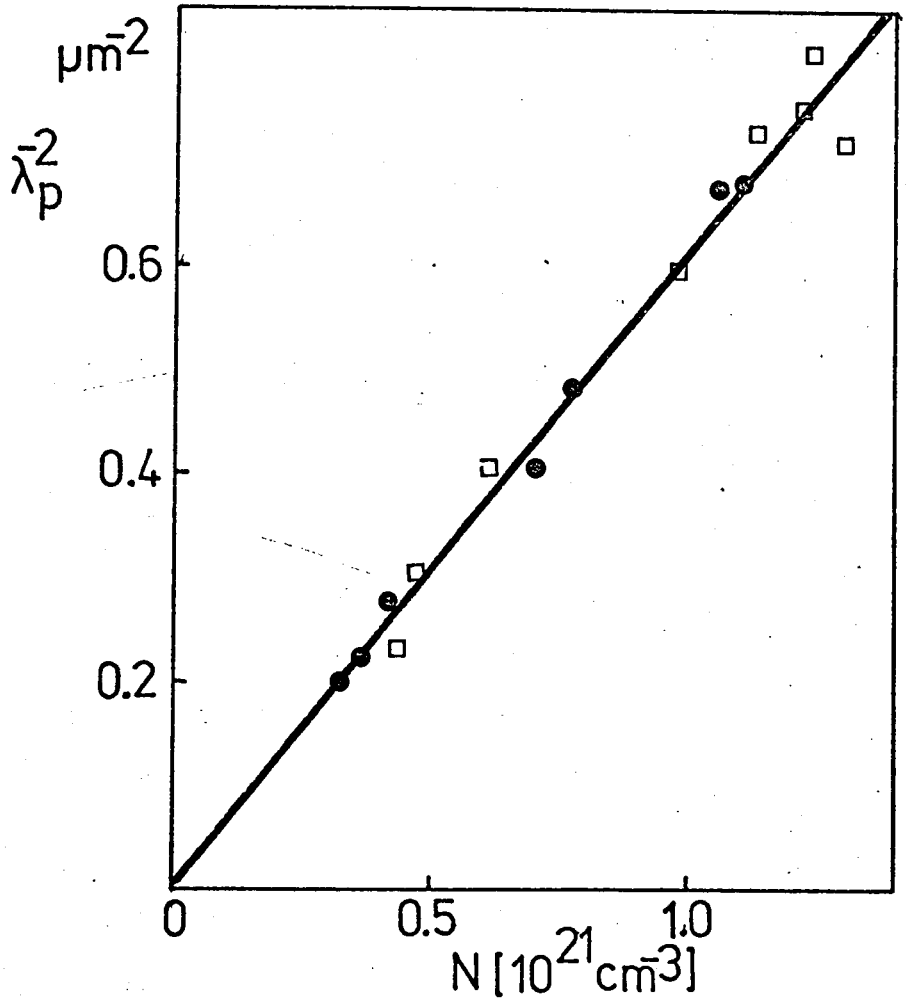

Fig. (6.7) Plasma wavelength dependence on free electron concentration of $Sn:In_2O_3$ films, after Clanget (1973), and Köstlin et al (1974).

It is obvious that there is a degree of uncertainty as far as the optical parameters of Sn - doped In_2O_3 is concerned.

As far as the optical effective mass is concerned various values have been found. Köstlin et al (1974) , found a constant value of 0.35 m_e, whereas Clanget (1973) found that the optical effective mass depends slightly on free carrier concentration as shown in Fig.(6.6). Additionally Vanshtein and Fistul' (1967) found that the optical effective mass of Sn - doped In_2O_3 is 0.28 m_e independently of free carrier concentration.

Finally, the dependence of plasma wavelength on free electron concentration is shown in Fig.(6.7) which has been drawn according to the results of Clanget (1973) and Köstlin et al (1974).

6.3 Electro - reflectance Measurements

The ER effect in tin - doped indium oxide films has been measured employing the ERS technique. An unexpected difficulty emerged in the course of our measurements; the use of carbon tetrachloride as an electrolyte gave small cell capacitances ($\sim$ 1000 pF). This had as a result the induction of very small changes in free carrier concentration and consequently the recording of comparatively small (less than $10^{-4} \times R$) signals for ΔR.

However, the use of acetonitrile solved the problem of low signals because it yielded cell capacitances of approximately 15 μF, although it introduced the problem of strong absorption bands shown on Figs.(6.8) and (6.9). The latter problem was solved by extrapolation.

6.3.1 E.R.S.

Curve, a, of Fig. (6.8) is the experimental ER spectrum of film No 3, the reflectivity spectrum of which is shown in Fig. (6.3). Deduction of Drude's optical parameters by fitting the experimental reflectivity spectrum yield the values presented in Table (6.4). The free carrier concentration and optical effective mass can be obtained from Figs. (6.7) and (6.6) respectively. A value of approximately $N = 4.3 \times 10^{26}\ m^{-3}$ is obtained for $\lambda_p = 2.1$ microns, and a value of approximately $0.33\ m_e$ for the optical effective mass.

The theoretical electro - reflectance spectrum for the same film has been calculated according to the proposed model and is shown as curve, b , in Fig. (6.8). The following values have been used in these calculations additionally to the ones tabulated in Table (6.4).

Film No 3 (THORN)

$C = 10\ \mu F / cm^2$

$m_r^* = 0.42$

$V = 1$ Volt

$d = 450$ Å

The value of $0.42\ m_e$ was used for the optical effective mass, instead of $0.33\ m_e$ deduced from Clanget's results since it gave a better approximation to the experimental results.

Curve, a , of Fig. (6.9) is the experimental ER spectrum of film ≈ 219 which has been fabricated by D.C. sputtering. Its reflectance plasma edge is shown in Fig. (6.5).

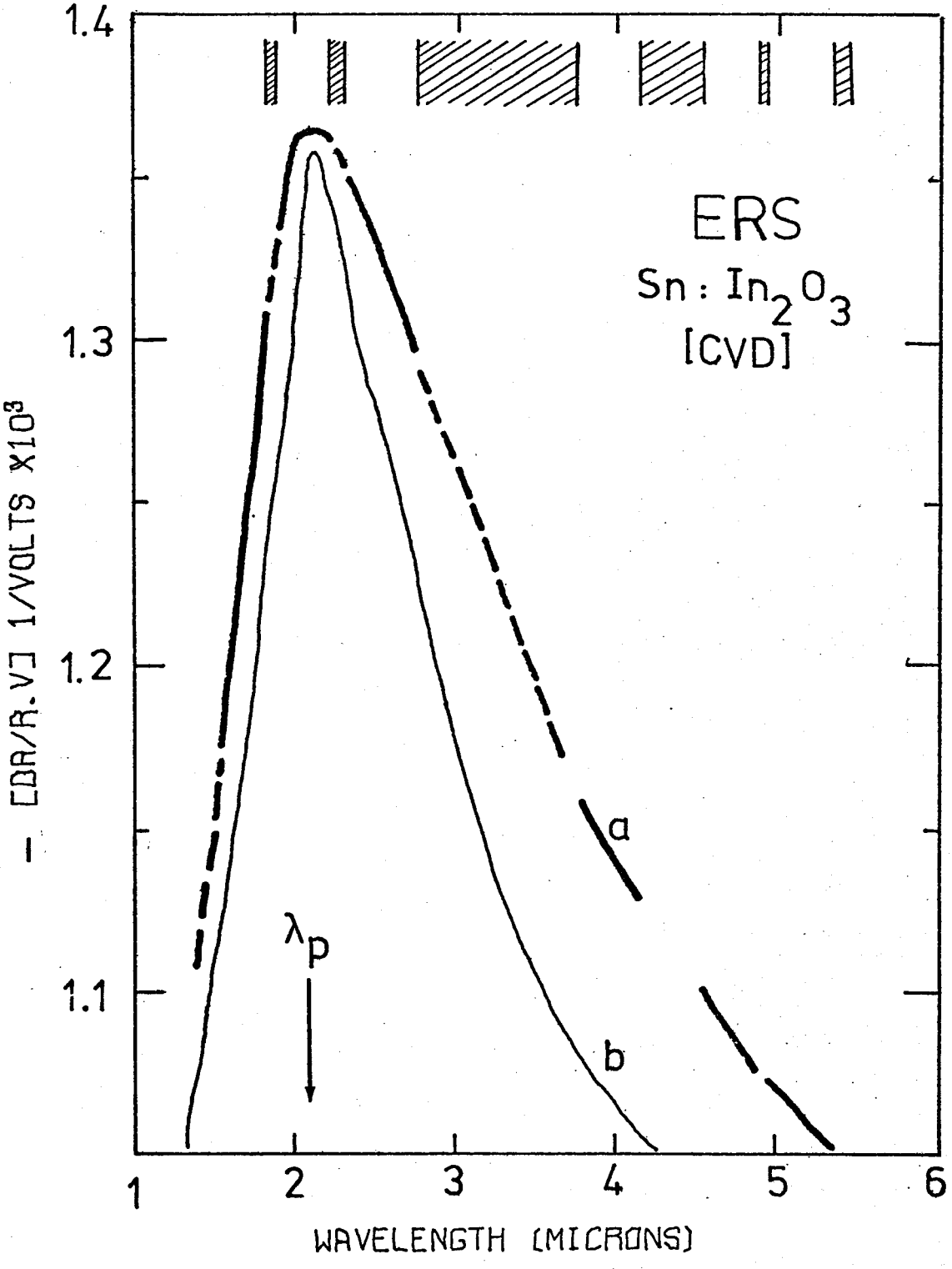

Fig.(6.8) a. Experimental and

b. Calculated ER spectrum of Film No 3 of Table (6.4). Shadowed areas on the top show the absorption bands of acetonitrile. The dashed parts of the experimental curve represent extrapolated values.

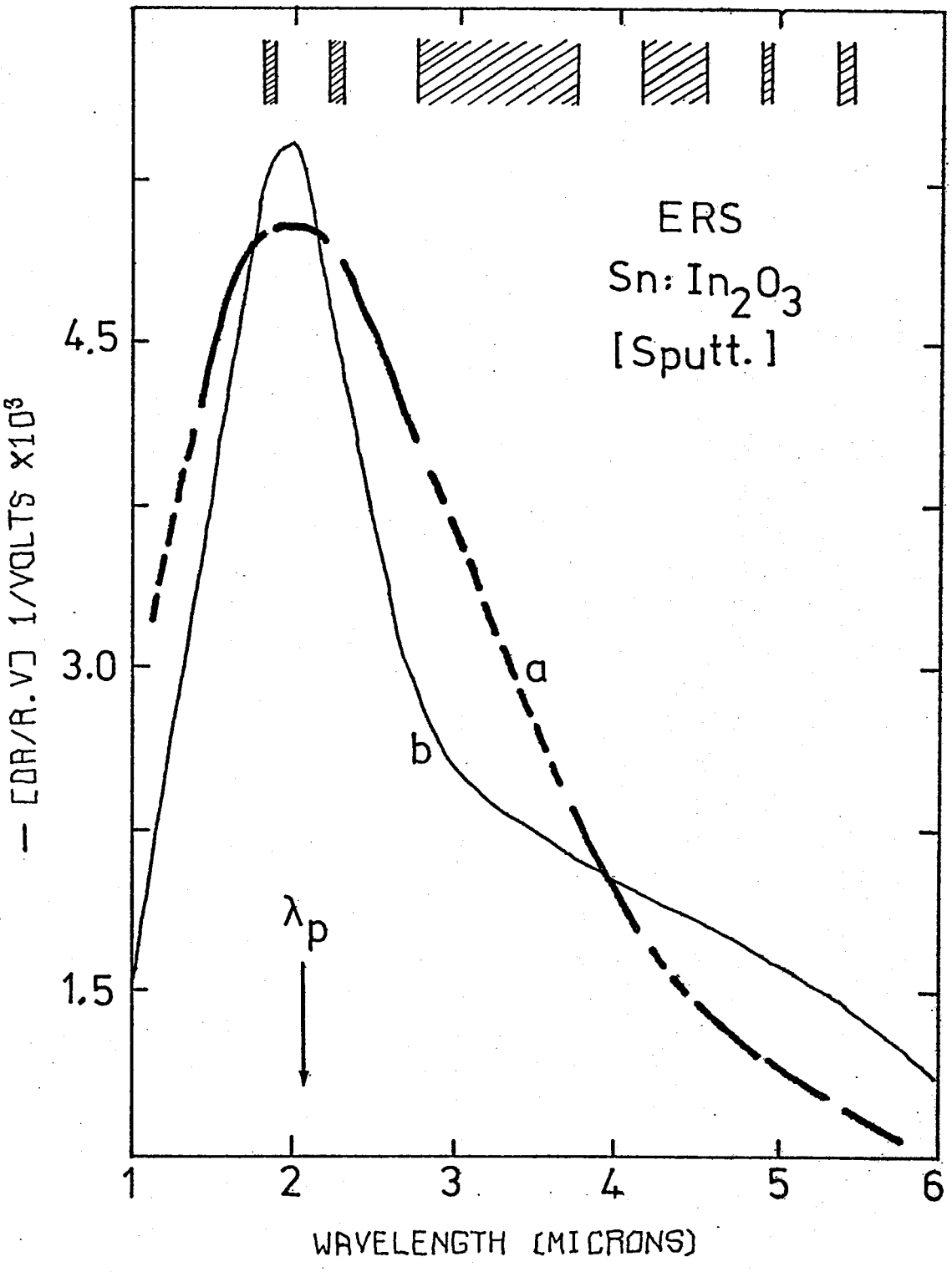

Fig.(6.9) a. Experimental and

b. Calculated ER spectra of film ≒ 219 from Table (6.4) .

The theoretical ER spectrum for the same film has been calculated according to the proposed microscopic model and is shown as curve, b, in Fig. (6.9). The Drude model parameters, tabulated in Table (6.4), have been used in these calculations. The following values have been also used in the course of these calculations:

Film ≯ 219 (PLESSEY)

$C = 16\ \mu F / cm^2$

$m_r^* = 0.42$

$V = 1$ Volt

$d \simeq 270$ Å

The agreement between experimental and theoretical ER spectra is very good, as can be seeing from Figs. (6.8) and (6.9).

An experimental error of approximately 15% is quoted for the experimental ER spectra of Figs. (6.8) and (6.9). As far as the wavelength bandwidth is concerned, an approximate value of 0.07 microns is quoted in these ER measurements.

The polarity of ER effect in the case of Sn-doped In_2O_3 films is negative. According to the assumptions made in Chapter 2, when a positive potential (i.e. E_{DC}= +ve) , is applied on a sample which has electrons as free carriers (q = -e), a negative change is expected. This is in agreement with eq.(2.24) since a positive E_{DC} decreases the number of electrons on the sample - surface, thus yielding a negative polarity for $\Delta R/R$.

REFERENCES

1. Boort H.J.J. and Groth R. Philips Thechnical Review 29, 17 (1968).
2. Clanget R., Appl. Phys. 2 , 247 (1973).
3. Fraser D.B., and Cook H.D., J. Electrochem. Soc. 119 , 1368 (1972).
4. Heavens O.S., Optical Properties of Thin Solid Films, Dover Publ. Inc. 1965, p. 157.
5. Hollands E., and Campbell D.S., J.Mater.Sci. 3 , 544 (1968).
6. Holland L., and Siddall G., Vacuum 3 , 375 (1953).
7. Inagaki T., Nakajima J., and Nishimura Y.,Fujitsu Sc. Techn. J. March 1969, p. 235.
8. Kane J., Schweizer H.P. and Kern W., Thin Solid Films 29 , 155 (1975)
9. Köstlin H., Philips tech. Rev. 34 , 242 (1974).
10. ———— Symposium on Incoherent Light sources, Loughborough, 8-10 April 1975.
11. Köstlin H., Jost R., and Lems W. Publication Nr. 20 / 74, 24.09.74 /Ko Philips Forschlings laboratorium , Aachen GmbH, Aachen W.Germany.
12. Lechmann H.W., and Widmer R., Thin Solid Films 27, 359 (1975).
13. McMaster H.A., U.S.A. Patent 2,429, 420, Oct. 21, 1947.
14. Molzen W.W., J. Vac. Sci. Technol., 12, 99 (1975).
15. Pankratz, J.M., J. Electronic Mater. 1 95 (1972).
16. Redaelli G. Applied Optics, 15, 1122 (1976).
17. Sinclair W.R., Peters F.G., Stillinger O.W.,and Koonce S.E. J. Electrochem.Soc.112 , 1096 (1965).
18. Stern E.A., and Ferrell R.A. Phys. Rev. 120 , 130 (1960).
19. Thornton J.A., Hedgcoth V.L., J.Vac.Sci. Technol. 13,117 (1976).
20. Vainshtein V.M. and Fistul' V.I., Sov. Phys. Semicond. 4, 1495 (1970).
21. ———— Sov. Phys. Semicond. 1, 104 (1976).
22. Vossen J.L., RCA Review, 32, 289 (1971).

CHAPTER 7

CONCLUSIONS AND PROPOSALS FOR FURTHER WORK

7.1 Introduction

It has been shown that the electro-reflectance spectrum in the vicinity of the reflectance plasma edge of thin conducting film and / or bulk materials can be predicted quantitatively.

The proposed microscopic model gives a good understanding of the qualitative and quantitative dependence of the ER spectrum on free carrier parameters (such as: free carrier concentration, free carrier relaxation time, optical effective mass, lattice dielectric constant and free carrier concentration) as well as bound electron effects.

The validity of the present model has been proved by the good agreement between the theoretical and experimental results .It is worth noting that comparison between the experimental ER spectra of IV-VI compounds and tin-doped indium oxide films shows that their ER-peak values are similar, despite the fact that the IV-VI compound films exhibit relatively higher optical mobilities. This is due to the fact that the IV-VI compounds - lattice dielectric constant is approxomately 9 times greater than the one of tin-doped indium oxide films.
Thus , it can be argued that the effect of the value of the lattice dielectric constant on the magnitude of the ER peak has been demonstrated experimentally as well as theoretically.

Due to the limit of the apparatus used, which was approximately $\Delta R/RV \simeq 10^{-4}(\text{Volts})^{-1}$ over the spectral region 1.5 - 5.5 microns it was impossible to verify calculated ER peak values tabulated in Table (2.1) for Sb and GaAs.
Antimony films were fabricated in our laboratory whereas a GaAs single

crystal (optically polished) wafer was provided by Plessey Co.Ltd (Towcester). Attempts to dope the latter with tin, in order to shift the plasma edge from 25 microns to 12 microns, were unsuccessful.

However, having established an essentially quantitative theory a search was made to find materials exhibiting sharp reflectance plasma edges (i.e. large optical mobility) and relatively small dielectric constants (not greater than 30) in order to obtain large ER signals ($> 1 \times 10^{-1}$).

Doped (n - type) indium antimonide [Spitzer and Fan (1957) , Fan (1967)] is a potential candidate exhibiting a very large optical mobility: 1.12 $m^2 . sec^{-1} . V^{-1}$ for $N=4 \times 10^{24}$ m^{-3} and $\lambda_p \simeq 13.1$ μm. A major problem is how one can dope it in order to shift the plasma edge wavelength to approximately 10.6 microns, and use the material for the modulation of CO_2 lasers.

Doped (n-type) gallium arsenide [Madelung (1964)] can also be employed yielding a considerable modulation shown in Table (2.1).

Finally a — Hexagonal silicon carbide seems to meet the requirements in order to yield a large ER signal, and additionaly exhibits excellent mechanical and thermal properties suitable to stand considerably high temperatures ($< 1800^{\circ}C$) without degradation of its optical properties [Marshall et al (1973)].
A value of approximately 0.8 has been reported for m_r^* whereas there is no value given for the electron relaxation time.

7.2 Large Values of Electro - reflectance Effect

With large changes of the optical properties of the surface layer, n_2 is no longer close to n_3. The approximation for Y_i from eq. (2.4) in that case gives

$$Y_i = Y_3 \left[1 + jk_2 \ell \left(\frac{n_3}{n_2} - \frac{n_2}{n_3} \right) \right] \tag{7.1}$$

where n_2 will be small ,i.e. on the creation of the enhanced layer on the surface of the sample the reflectance will rise to a value which is assumed to be unity. That assumption is expected to be valid in the case of materials with very sharp reflectance plasma edges like SiC, and InSb, and large modulating voltages.

So, the Fresnel coefficient of the perturbed system is given by

$$r = \frac{n_1 \left[1 + j \frac{n_2 \omega \ell}{c} \left(\frac{n_3}{n_2} - \frac{n_2}{n_3} \right) \right] - n_3}{n_1 \left[1 + j \frac{n_2 \omega \ell}{c} \left(\frac{n_3}{n_2} - \frac{n_2}{n_3} \right) \right] + n_3} \tag{7.2}$$

Considering "ideal" materials (i.e. $\tau^{-1} \ll \omega$) the refractive index is real between the reflectance minimum and the plasma frequency and goes from 0 to a constant value. Interband effects are assumed to be zero in this spectral region. Then, the energy reflected by the system can be expressed as

$$R_E = rr^* = \frac{(n_1 - n_3)^2 + b^2}{(n_1 + n_3)^2 + b^2} \tag{7.3}$$

where

$$b = \frac{n_1 n_2 \omega \ell}{c} \left(\frac{n_3}{n_2} - \frac{n_2}{n_3} \right) \tag{7.4}$$

$$= \frac{\omega \ell}{c} \cdot \frac{n_1}{n_3} \cdot \left[n_3^2 - n_2^2 \right]$$

Now

$$n_3^2 - n_2^2 = \varepsilon_L \left[\frac{\omega_{p_E}^2 - \omega_p^2}{\omega^2} \right] \tag{7.5}$$

$$= \frac{N_E - N}{m_r^* m_e m_0} \cdot \frac{1}{\omega^2}$$

where ω_{p_E} and N_E refer to the properties of the enhanced layer.

Using:

$$(N_E - N) \cdot \ell = CV/q \tag{7.6}$$

Equation (7.4) becomes

$$b = \frac{q}{c \varepsilon_o} \cdot \frac{1}{m_r^* m_e} \cdot \frac{n_1}{n_3} \cdot \frac{1}{\omega} \cdot CV \tag{7.7}$$

and consequently

$$R_E = \frac{(n_1 - n_3)^2 + \left[\frac{q n_1 C V}{\varepsilon_o c m_r^* m_e n_3 \omega} \right]^2}{(n_1 + n_3)^2 + \left[\frac{q n_1 C V}{\varepsilon_o c m_r^* m_e n_3 \omega} \right]^2} \tag{7.8}$$

Substracting

$$R = \frac{(n_1 - n_3)^2}{(n_1 + n_3)^2}, \tag{7.9}$$

from eq.(7.8) an estimate of large changes in reflectivity can be obtained when an electric field is applied normally on the surface of a material.

It is worth noting that from eq.(7.8) , R_E reaches unity asymptotically. When $n_3 \simeq n_1$, no modulation will take place.

Table (21) shows the large effect calculated according to the previous formulae for an applied voltage of 1 volt in the case of GaAs.

Additional calculations were performed for the case of InSb and SiC.

a) Indium Antimonide

The peak value of the ER effect was obtained from computer calculations using the following data

$$N = 4 \times 10^{24} \quad m^{-3}$$

$$\tau = 2.6 \times 10^{-13} \text{ sec.}$$

$$m_r^* = 0.041$$

$$\epsilon_L \simeq 15$$

$$\lambda_p = 13.1 \ \mu m$$

$$C = 0.1 \ F/m^2$$

yielding

$$\left[\frac{\Delta R}{R}\right]_{V = 1 \text{ Volt}} = 0.7$$

b) Silicon Carbide

In this case the following data were used in addition to the ones presented in Table (D-3)

$$C = 0.1 \ F \ / \ m^2$$

yielding

$$\left[\frac{\Delta R}{R}\right]_{V = 1 \text{ Volt}} = 0.3$$

This particular material may be suitable for the fabrication of IR modulator at 10.6 microns if a way of increasing its optical mobility will be employed.

After these encouraging theoretical results modulating units can be built employing either the electrolytic technique using CS_2 (90%) transmission at 10.6 microns for a layer 0.1 cm thick) or the Schottky - barrier technique (Avaritsiotis 1974).

The electrolytic technique in conjuction with the use of thin-layer cells (like the one used in the course of the present ERS -ER measurements) seems very promising. This is due to the fact that large double layer capacitances, and consequently high electric fields, can be achieved easily.

Moreover, incorporation of a magnetic field utilizing the magnetoplasma effect [Lax and Wright (1960), Elliot and Gibson (1974)] may yield a versatile modulating unit which may work over a relatively wide spectral range.

Finally, greater ER signals can be obtained by employing low temperatures in order to increase the optical mobility. For example, computer calculations showed that the ER- peak value for PbTe at room temperature is of the order of 10^{-3} for V = 1 Volt, whereas at $80^{o}K$ it becomes 6×10^{-1}.

It is believed that the proposals put forward here together with the basic experience gained in this project may possibly lead to the development of a simple, cheap, effective, and versatile method of modulating infra-red radiation.

REFERENCES

1. Avaritsiotis J.N., MSc.Thesis, Loughborough, 1974.

2. Elliot R.J. and Gibson A.F.,"An Introduction to Solid State Physics and its Applications" MacMillan,London, 1974,p.276.

3. Fan H.Y. "Semiconductors and Semimetals",Vol.3,Optical Properties of III - V Compounds,Edited by R.K.Willardson and A.C.Beer Acad. Press 1967, Chapter 9.

4. Lax B.,and Wright G.B.,Phys.Rev. 4 16 (1960).

5. Madelung O.,"Physics of III - V Compounds", 1964,(optical Properties).

6. Marshall R.C., Faust J.W. and Ryan C.E.,"SILICON CARBIDE - 1973", Proceedings of the 3rd International Conference on Silicon Carbide.

7. Spitzer W.G.,and Fan H.Y.,Phys.Rev.,106 , 882 (1957).

APPENDIX A

DERIVATION OF THE COMPLETE EXPRESSION FOR ER EFFECT IN BULK SAMPLES

Bearing in mind that

$$(A-1) \qquad \varepsilon_{3F} - \varepsilon_L = -\frac{1}{\varepsilon_3 - \varepsilon_1} \cdot \frac{\omega_p^2}{\omega^2 + j\omega\tau^{-1}}$$

the term

$$\left[\frac{\varepsilon_{3F} - \varepsilon_L}{\varepsilon_3 - \varepsilon_1}\right]$$

of Eq. (2.24) can be written as:

$$(A-2) \qquad \frac{\varepsilon_{3F} - \varepsilon_L}{\varepsilon_3 - \varepsilon_1} = -\frac{\left[(\varepsilon_A - \varepsilon_1)\omega\tau + \varepsilon_B\right]\omega_p^2}{\tau\omega(\omega^2 + \tau^{-2})\left[(\varepsilon_A - \varepsilon_1)^2 + \varepsilon_B^2\right]}$$

$$- j\frac{\left[\omega\tau\varepsilon_B - (\varepsilon_A - \varepsilon_1)\right]\omega_p^2}{\omega\tau(\omega^2 + \tau^{-2})\left[(\varepsilon_A - \varepsilon_1)^2 + \varepsilon_B^2\right]} \cdot$$

Substituting Eq. (A-2) into Eqs. (2.23) and (2.22) yields Eq. (2.25) which is the complete formula for the electro - reflectance effect in bulk materials. It is worth noting that the plasma frequency, ω_p, has been defined as

$$\omega_p = \left[\frac{Ne^2}{\varepsilon_L \varepsilon_o m_r^* m_e}\right]^{\frac{1}{2}}$$

APPENDIX B

DERIVATION OF THE EXPRESSION FOR E.R.S.

Substitution of eqs. (2.56) and (2.57) into eq. (2.53) yields:

$$(B\text{-}1)\quad \frac{\Delta R}{R} =$$

$$\frac{(A+A^*) + \frac{|r_2|}{|r_1|}\exp(-\beta)\cos\Phi\cdot(A+A) + \frac{|r_2|}{|r_1|}\exp(-\beta)\cdot\left[j\sin\Phi\,(A-A^*)\right]}{1 + \frac{R_2}{R_1}\cdot\exp(-2\beta) + 2\,\frac{|r_2|}{|r_1|}\exp(-\beta)\cos\Phi}$$

$$-\frac{(A+A^*)\,R_1R_2\exp(-2\beta) + |r_1||r_2|\cdot\exp(-\beta)\cdot(A+A^*) + |r_1||r_2|\left[j\sin\Theta\,(A-A^*)\right]}{1 + R_1R_2\cdot\exp(-2\beta) + 2\,|r_1||r_2|\exp(-\beta)\cos\Theta}$$

However $(A+A^*)$ and $(A-A^*)$ can be calculated from eqs. (A-2), (2.20) and (2.23); substituting these values into (B-1) yields eq. (2.59).

A P P E N D I X C

DERIVATION OF THE EXPRESSION FOR I.R.S.

The same procedure is used here as in the case of E.R.S.

However, it is worth noting that the Fresnel coefficient, r_1, defined in eq. (2.70) with referenc to fig. (2.17) has the same magnitude but an opposite sign in relation to, r_2, which has been defined in eq. (2.71) with reference to fig. (2.18).

Consequently A of eq.(2.58) is equal to G of eq. (2.76).
Thus from eqs. (2.20), (2.22) and (2.23) the validity of the following equality can be proved:

(C-1)
$$\left[\frac{\Delta R_1}{R_1}\right]_{ERS} = \left[\frac{\Delta R_2}{R_2}\right]_{IRS}$$

APPENDIX D

A METHOD FOR THE DEDUCTION OF OPTICAL CONSTANTS FROM REFLECTANCE MEASUREMENTS IN THE VICINITY OF THE PLASMA EDGE.

D.1 A Brief Review of the most Popular Methods

There are many ways to determine the optical constants of bulk or thin film materials. An extensive review of the various methods employed so far is given by Heavens (1964, 1965) and Wohlgemuth and Bradie (1975). Most of these methods require either lengthy computations or time consuming optical measurements taken over wide spectral regions.

A popular and rather accurate method for the calculation of the bulk optical constants of a solid consists of measuring the normal incidence reflectivity of an optically polished sample of that material over a wide range of frequencies, followed by a Kramers - Kroning analysis. This method follows from the fact that in order to determine the refractive index and extinction coefficient the modulus and phase of the Fresnel complex coefficient, r , for the air - material interface must be known. The value of $|r|$ can be determined from normal incidence reflectance measurements since $R = |r|^2$. Given that $|r|$ is known over the entire frequency spectrum, the phase, $\delta\ (\omega_o)$, at a single frequency, ω_o, can be calculated by means of the Kramers - Kroning dispersion relation,

$$\delta(\omega_o) = -\frac{2\omega_o}{\pi}\int_0^\infty \frac{\ln|r(\omega)|}{\omega_o^2-\omega^2}d\omega \qquad (D-1)$$

which is a consequence of the principle of causality i.e. that electromagnetic radiation can not be reflected or absorbed by a system before the arrival of the primary electromagnetic wave.
This method first introduced by Simon (1951) and Robinson (1952) was critically evaluated by Bowlden and Wilmshurst (1963).

In many cases, however, the reflection over a limited spectral range is readily available, so that it is not possible to obtain accurate results by using the Kramers - Kroning method. Although in practice extrapolation procedures are used to obtain R outside of range of measurements, experimental data from other investigators are necessary for accurate results specially in the high - energy regions where the reflectance, due to strong interband transitions, is characterized by structure. This, of course, implies that the materials examined by various investigators have exactly the same optical properties, which in fact is not always the case.

Also, if thin films are involved the expression for R in terms of n and k becomes complicated and can no longer be converted to yield corresponding equations for the refractive index and extinction coefficient. To obtain the optical constants in this case two quantities, such as reflectance and transmittance of the same film or the transmittance of two films of different thicknesses are measured at each frequency. An obvious disadvantage a) of the first case is that it is time consuming and b) of the second case is that the method assumes no variation of the optical properties with thickness, which unfortunately is not always the case specially when the optical thickness is small, Avaritsiotis (1975).

Moreover a classical oscillator fit to reflectance spectra in a trial - and - error basis always is a lengthy process, even if the spectra do not exhibit considerable structure and thus only three parameters are required for an adequate fit.

A most straight forward approach is to fit the experimental reflectance and/or transmittance point - by - point using an iteration procedure.

The main disadvantage of the latter technique is that there are cases where small errors in the measured reflectance and / or transmittance lead to large errors in n and k.

The use of a smooth curve fitting seems to be more promising. In order to eliminate the problems of the point - by - point technique a fit over the whole spectral region covering the experimental data has been attempted. All these attempts are based on the same principal idea : i.e. the simultaneous fitting of all the experimental points. But the computer techniques employed are different, depending on the accuracy required and the computer time to be consumed. The latter is not necessarily a function of the required accuracy but it mainly depends on the iteration procedure employed.

In the present method a general - purpose curve fitting subroutine has been used, which converts an initial guessed set of parameters to a final set which gives the best fit to the experimental reflectance spectrum of bulk and thin film materials.

The main features of the present method are:

a) Calculation of the parameters of a classical oscillator, i.e. ε_L, ω_p, and τ, from the knowledge of the reflectance spectrum only, in the vicinity of the plasma edge.
   The oscillator parameters themselves have physical significance in this region of the reflectance spectrum, which is dominated by intraband transitions. Also, the classical oscillator automatically satisfies the Kramers-Kronig dispersive relations.

b) Errors in n and k due to errors in experimental reflectance are reduced since a smooth curve fitting is employed. This makes

the present method superior to point - by - point fitting methods employed by Abelès and Thèye (1966), and Bennett and Booty (1966).

D.2 Optical Constants from Bulk Data

The presentation of the complex dielectric constant according to Drude's model has been shown to reproduce the reflectance spectrum of a solid in the spectral region of the plasma edge, and when interband transitions can be ignored.

According to Drude's model

$$\bar{\varepsilon}(\omega) = \varepsilon_1 + j\varepsilon_2 = \varepsilon_L - \frac{\omega_p^2}{\omega^2 + j\omega\tau^{-1}} \qquad (D-2)$$

where ε_L is the lattice dielectric constant, τ is the free carrier relaxation time and ω_p is the plasma frequency. The optical constants n and k are defined in terms of ε_1 and ε_2 by

$$n = \left[\frac{1}{2}\left[(\varepsilon_1^2 + \varepsilon_2^2)^{\frac{1}{2}} + \varepsilon_1\right]\right]^{\frac{1}{2}} \qquad (D-3)$$

and

$$k = \varepsilon_2 / 2n \qquad (D-4)$$

Finally, the reflectivity for normal incidence is given by

$$R = \frac{(n_o - n)^2 + k^2}{(n_o + n)^2 + k^2} \qquad (D-5)$$

where $n_o = 1$ for air.

The fitting procedure of the experimental reflectivity spectrum consists of an initial estimation of the parameters ε_L, τ, and ω_p, calculation of the reflectivity from the latter equation and subsequent adjustment of the parameters until the so - called objective function, defined as

$$X = \sum_{i=1}^{N} \left[R_{EXP}(\omega_i) - R_{CALC}(\omega_i) \right]^2 \qquad (D - 6)$$

N: Number of experimental points,

becomes smaller than a predetermined value, which eventually governs the accuracy with which the parameters are calculated.

Similar methods have been employed by several research workers, Verleur (1968), Rivory (1970); their iterative hill - climbing processes were specially developed for that purpose.

In the present method ,however, a general purpose FORTRAN IV subroutine E04FBF - N.A.G., was employed on the ICL 1900 computer.

The present method has been tested on several materials exhibiting a plasma edge and the results were quite satisfactory. Experimental data of various researchers have been used for comparison:

A] LEAD TELLURIDE , figs.(D-1) and (D-2)

TABLE (D - 1)

	EXPERIMENTAL (*)	ACCORDING TO THE PRESENT METHOD
τ	2×10^{-13} sec	4×10^{-13} sec
ε_L	32.6	32.6
ω_p	1.24×10^{14} sec^{-1}	1.22×10^{14} sec^{-1}
λ_p	15.2 μm	15.4 μm
m_r^*	0.095	—

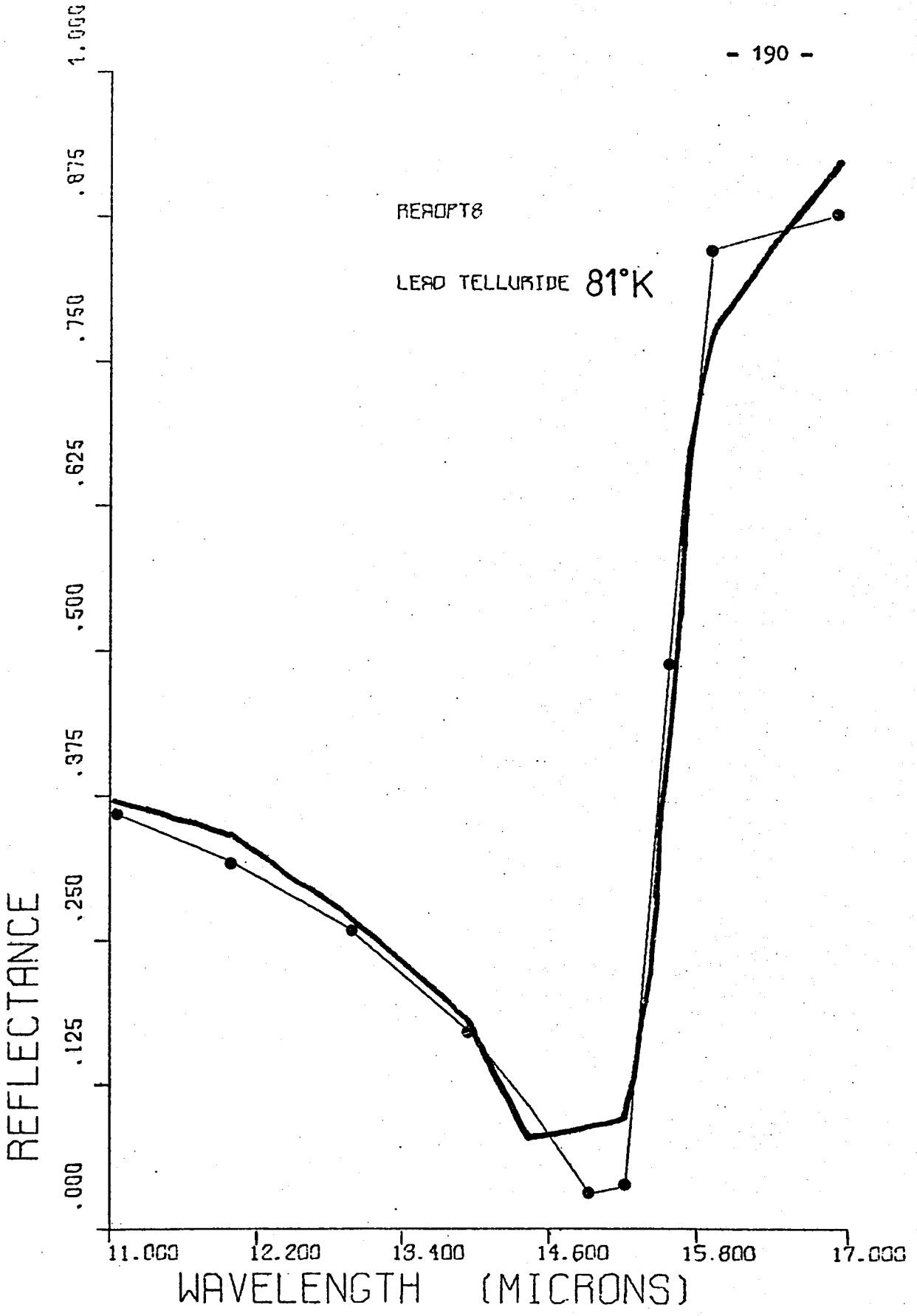

Fig. (D-1) The experimental data of Dixon and Riedl (1965) for the reflectivity of PbTe at 81°K are represented by dots. The heavy printed curve is the one obtained by our method.

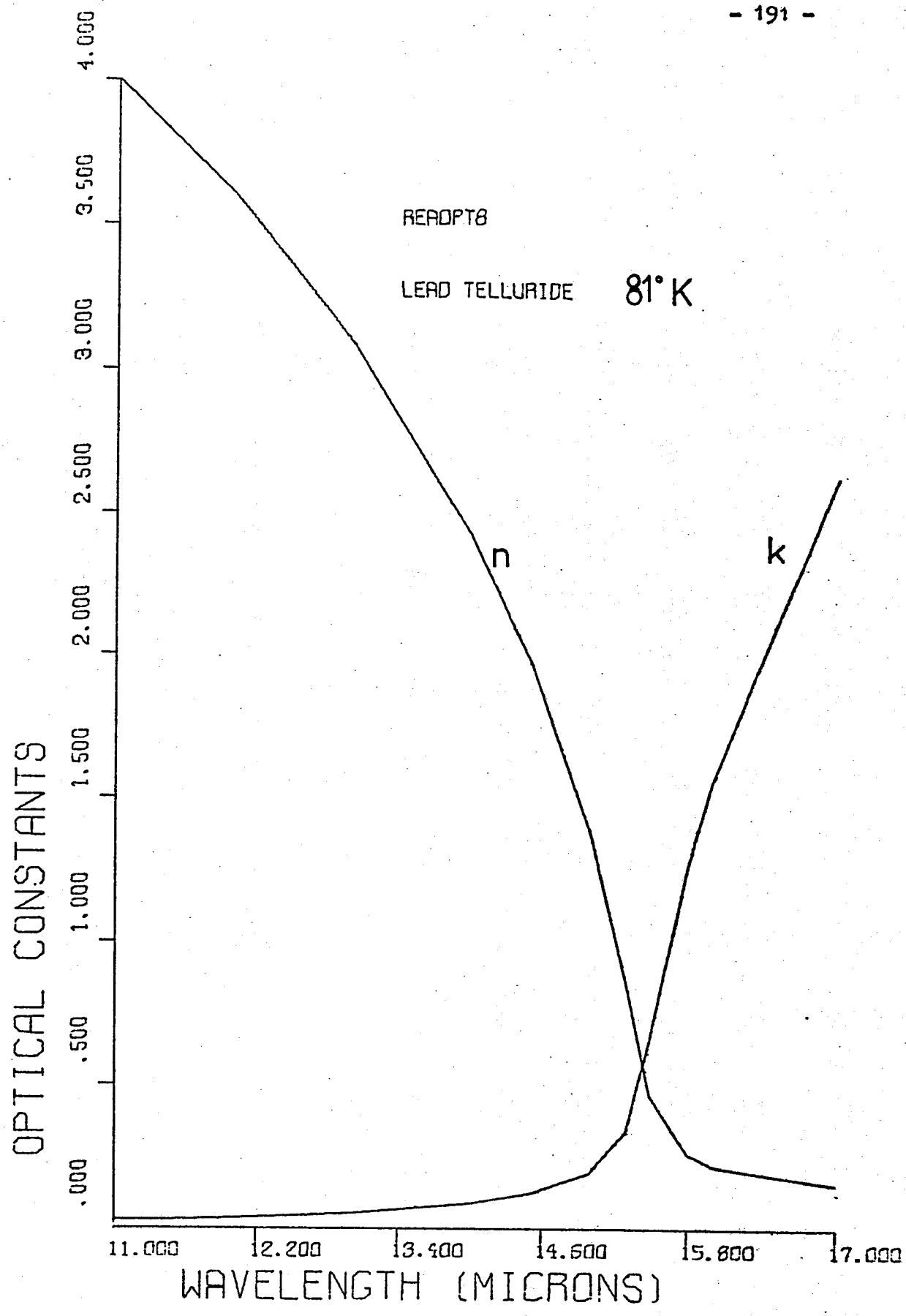

Fig. (D-2) Optical constants of PbTe at 81°K calculated from the optimum values of the classical oscillator parameters determined by the fitting of experimental data of fig. (D-1).

(*) The experimental reflectivity data of p-type PbTe at 81°K ($N = 1.5 \times 10^{25}\ m^{-3}$) were obtained from Dixon and Riedl (1965). The optimum values of the classical oscillator parameters were used to obtain the reflectivity spectrum and the optical properties against wavelength. Figs (D-1) and (D-2) show how they compare to the experimental values.

B] HEXAGONAL SILICON CARBIDE, figs (D - 3) and (D - 4).

TABLE (D - 2)

	EXPERIMENTAL	ACCORDING TO THE PRESENT METHOD
τ	—	4×10^{-13} sec
ε_L	6.7	3.2
ω_p	$1.82 \times 10^{14}\ sec^{-1}$	$1.83 \times 10^{14} sec^{-1}$
λ_p	10.3 μm	10.3 μm
m_r^*	0.25(*)	-

(*) This value of effective mass was obtained from Appendix B of the proceedings of the 3rd International Conference on Silicon Carbide, 1973 edited by R.C.Marshall, J.W.Faust, and C.E. Ryan, University of South Carolina Press, Columbia, South Carolina (I SBN 0 - 87249 - 315 - 6).
The rest of the experimental data have been taken from Spitzer et al 1959.

The optimum values of the classical oscillator defined by the present method were used to calculate the reflectivity spectrum and the optical properties of green alpha (hexagonal) SiC. Figs (D-3) and (D-4) show how they compare to the experimental values.

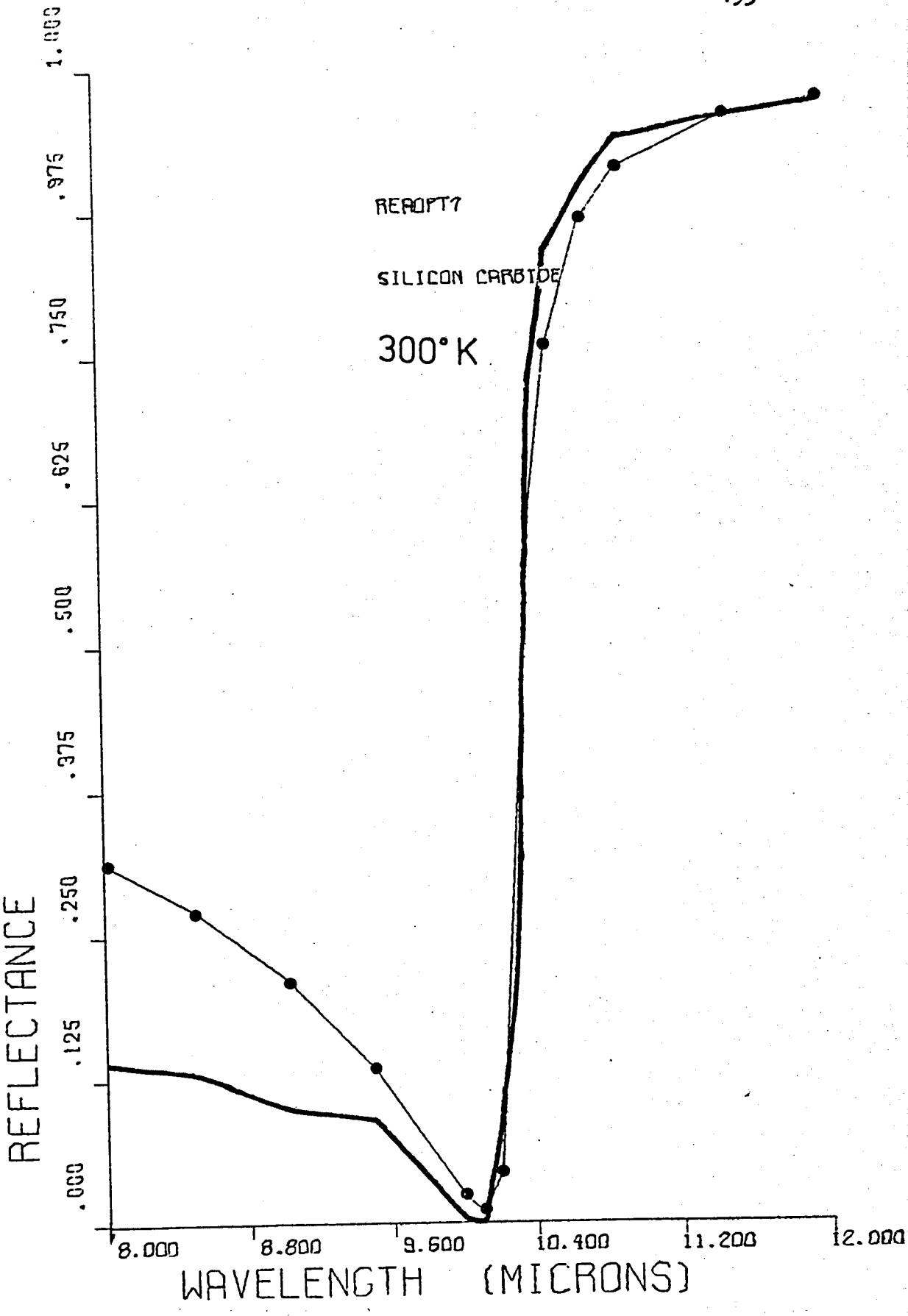

Fig.(D-3) Dots represent the experimental reflectance versus wavelength. The heavy printed curve has been obtained by our method.

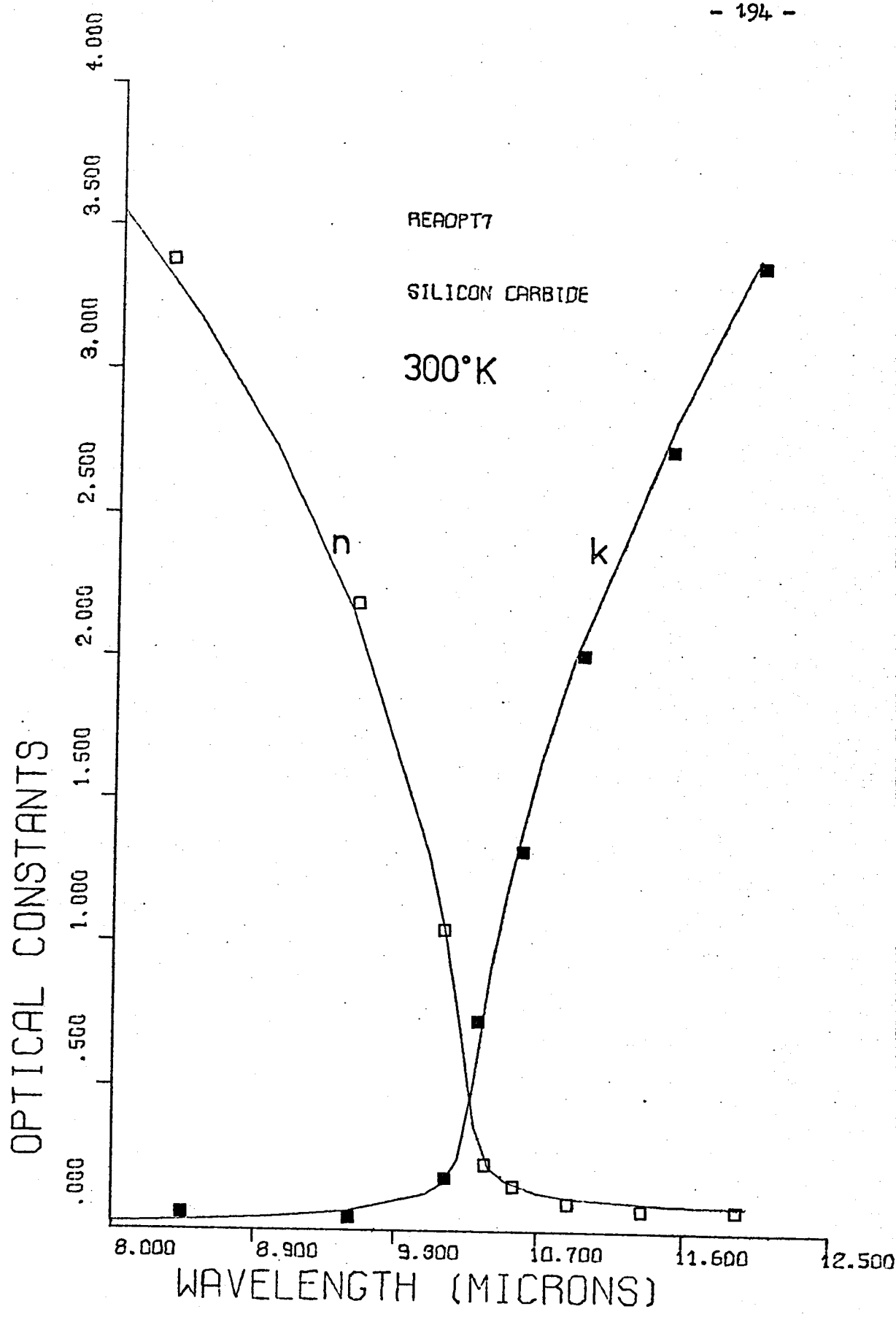

Fig.(D-4) Optical properties of hexagonal silicon carbide calculated according to our method are compared with the ones given by Spitzer et al (1959).

c] TIN - DOPED GALLIUM ARSENIDE , Figs (D-5) and (D-6).

TABLE (D-3)

	CALCULATED BY TRIAL AND ERRORS METHOD	ACCORDING TO THE PRESENT METHOD
τ	(**) 8.9×10^{-14} sec	8.93×10^{-14} sec
ε_L	(**) 10.9	10.9
ω_p	(**) 9.24×10^{13} sec^{-1}	9.23×10^{13} sec^{-1}
λ_p	20.4 μm	20.45 μm
m_r^*	0.067(*)	-

(*) The value of effective mass was obtained from Madelung (1964), Physics of III - V Compounds, p.97.

(**)According to Axe and Hammer (1967).

All these examples demonstrate that in the region of the plasma edge and for reflectance spectra dominated by intraband transitions the proposed method gives results comparable to the ones calculated by other researchers. The obtained solutions are unique and correspond to a global minimum of the objective function. The uniquity of the solutions has been numerically verified by using 10 different initial sets of the parameters ε_L, τ, and ω_p and obtaining the same minimum, i.e. the same optimum values for ε_L, ω_p and τ, every time.

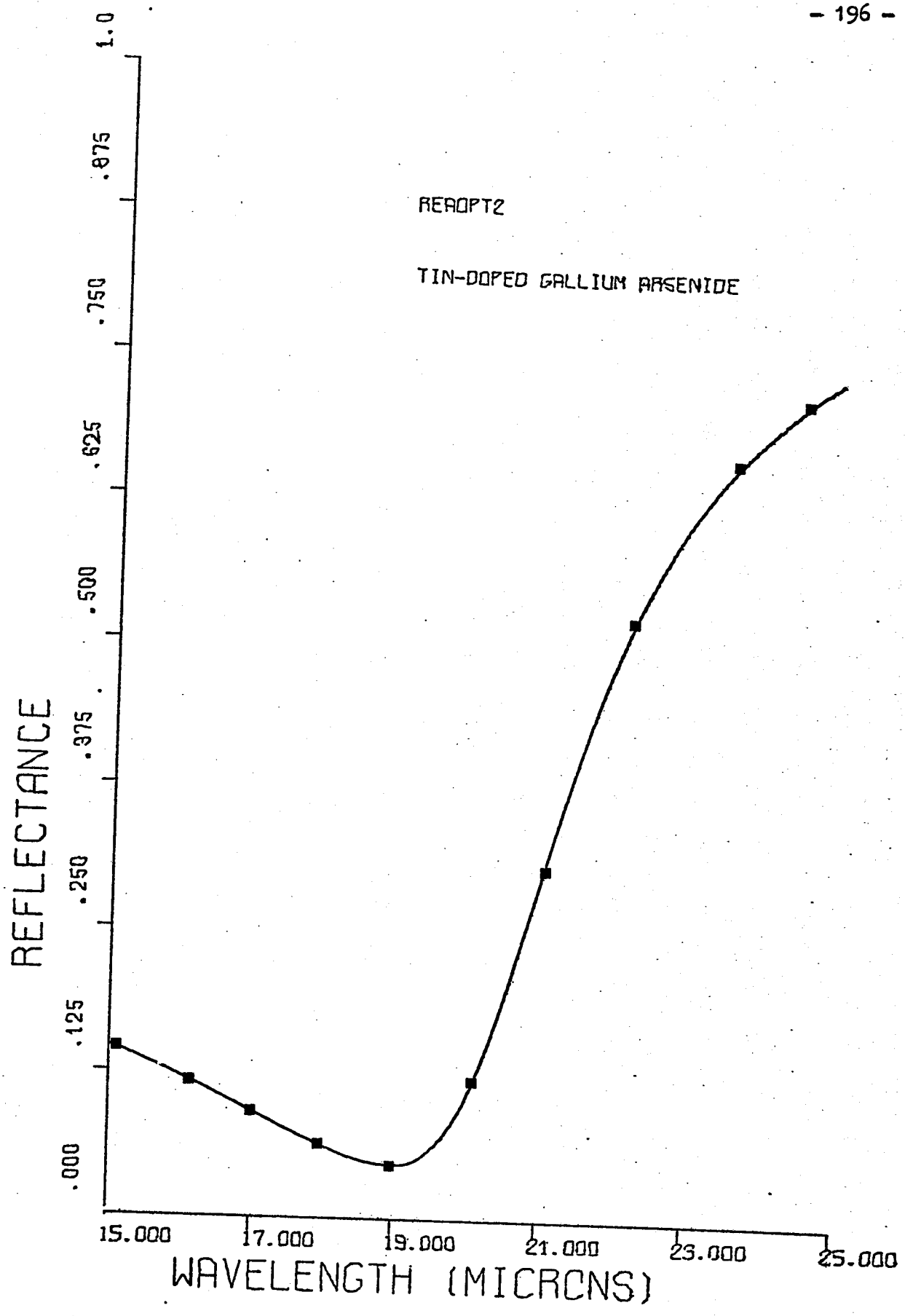

Fig.(D-5) Reflectance spectrum calculated by Axe and Hammer (1967) and the present method. The two curves coincide.

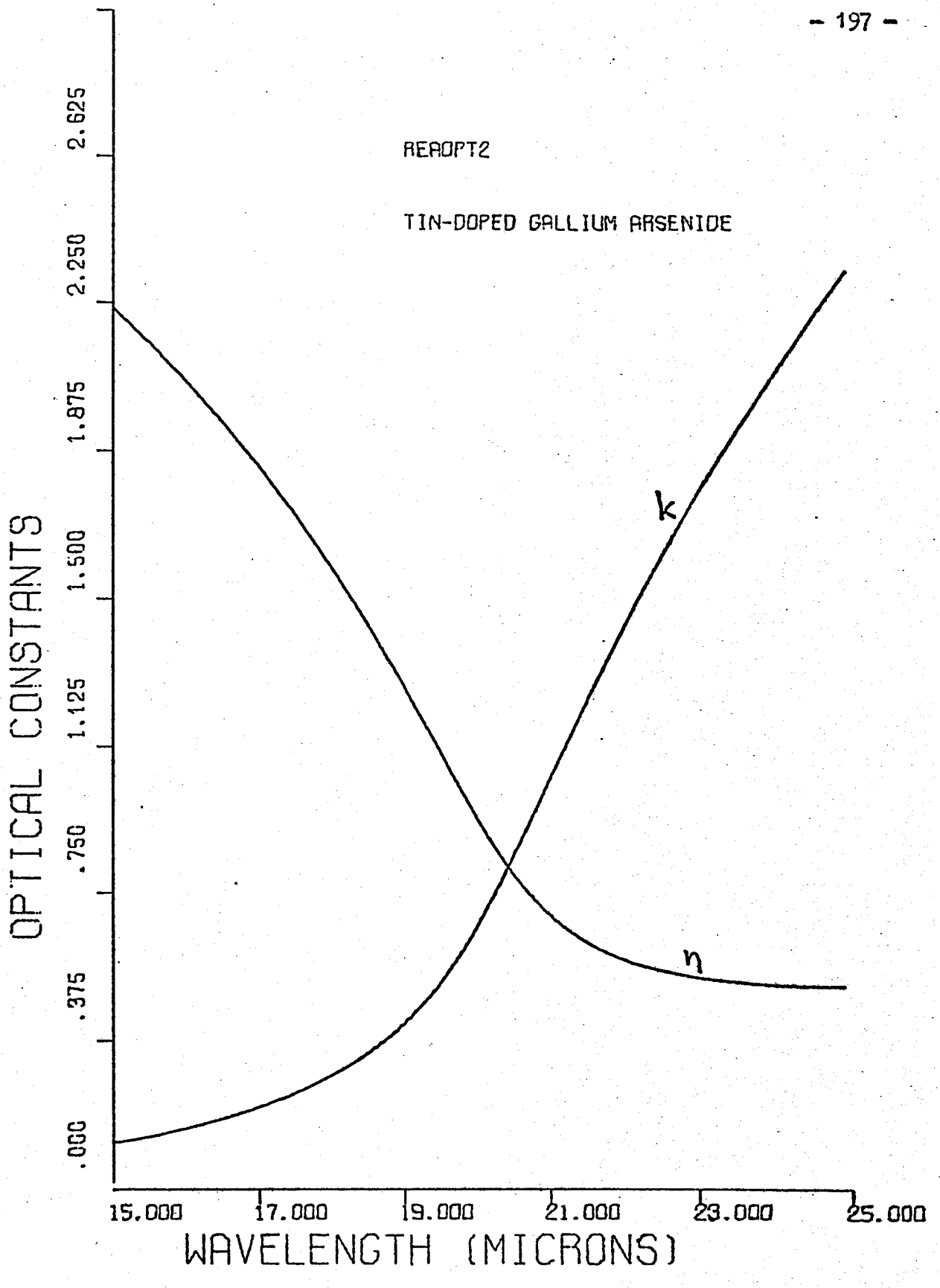

Fig.(D-6) Optical constants calculated using the two sets of classical oscilator parameters from Table (D-3).

D.3 Optical Constants from Thin-Film Data.

The same strategy has been employed for the calculation of classical oscilator parameters and thickness of thin films from their reflectance spectra in the vicinity of the plasma edge.

However, the introduction of thickness as a fourth parameter creates problems; local minima occur in physically unlikely regions (See Fig. (D.7). The same type of problems met by other investigators: Valeur (1968), Ward et al (1969), Rivory (1970).

A modification was introduced in an attempt to overcome the local minima problems; the experimental reflectance spectrum was divided into two parts, one including the plasma edge only and a second one including reflectance pattern due to film thickness in shorter wavelengths. Reflectance spectra of antimony films of various thicknesses were used obtained from Harris and Corrigan (1964,1965) and Fox, Howson and Emmony (1974). The first spectral portion was fitted using the thin film thickness, d , as a fourth parameter. The second spectral portion was subsequently fitted using the optimum value for d, obtained by the first fitting procedure as a starting point for the second fitting procedure; in the latter case d was the only parameter to be adjusted. Unfortunately, although such a modification gave a more accurate value for the film thickness, did not reduce the local minimum problem.

In a third attempt the film thickness was given to the subroutine as a constant and the optimum values of the classical oscillator were calculated. This method gave non-pragmatic values for the set of classical oscilator parameters mainly because of the inaccuracy in the values of d quoted in the literature.

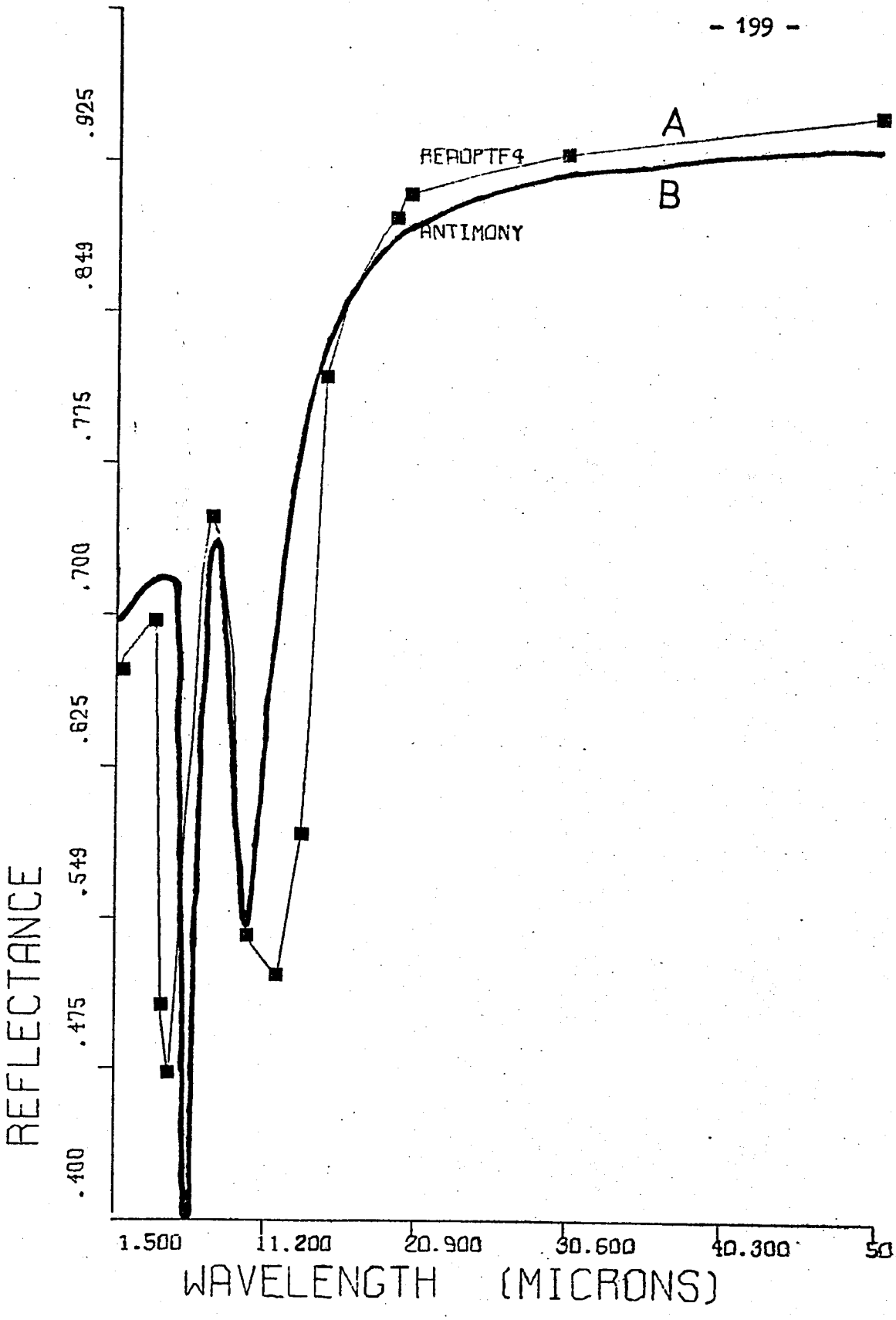

Fig.(D-7) A: Experimental reflectivity spectrum of Sb thin film from Harris (1964).

B: Calculated reflectance from classical oscilator parameters corresponding to a local minimum of the objective function.

Finally, it was decided to employ the same method used in the case of bulk materials. The results were adequate specially when $d \geq \lambda$. This was expected since it is known, Avaritsiotis (1974), that when $d \geq \lambda$ the reflectance of a film is qualitatively and quantitatively comparable to that of the bulk material. In the case of relatively thin films, i.e. when $d \ll \lambda$, the optimum values of the classical oscillator parameters obtained according to the latter technique were used as initial values in an iteration procedure where the film thickness was the fourth parameter to be adjusted. The latter stage was giving a fine adjustment in particular to the values of relaxation time and film thickness. Problems related with local minima were overcomed by using various starting points. Table (D-4) summurizes the results obtained for a SnTe film, using our experimental data, and compares them with others' results for bulk SnTe with similar optical properties. The thickness of the film measured with a Talystep and found to be 2500 Å ($\pm$ 15 %).

TABLE (D - 4), (SnTe film)

	THE PRESENT METHOD (STAGE I) *	THE PRESENT METHOD (STAGE II) **	DATA FROM THE LITERATURE***
τ	0.5×10^{-14} sec	0.96×10^{14} sec	0.8×10^{-14} sec
ε_L	19.3	22.7	40
ω_p	5.98×10^{14} sec^{-1}	6.01×10^{14} sec^{-1}	4.8×10^{14} sec^{-1}
λ_p	3.2 μm	3.13 μm	3.9 μm
d	0.29 μm	0.208 μm	(BULK)

* see fig.(D.8)

** see fig.(D.9)

*** for bulk material from Riedl et al. (1967).

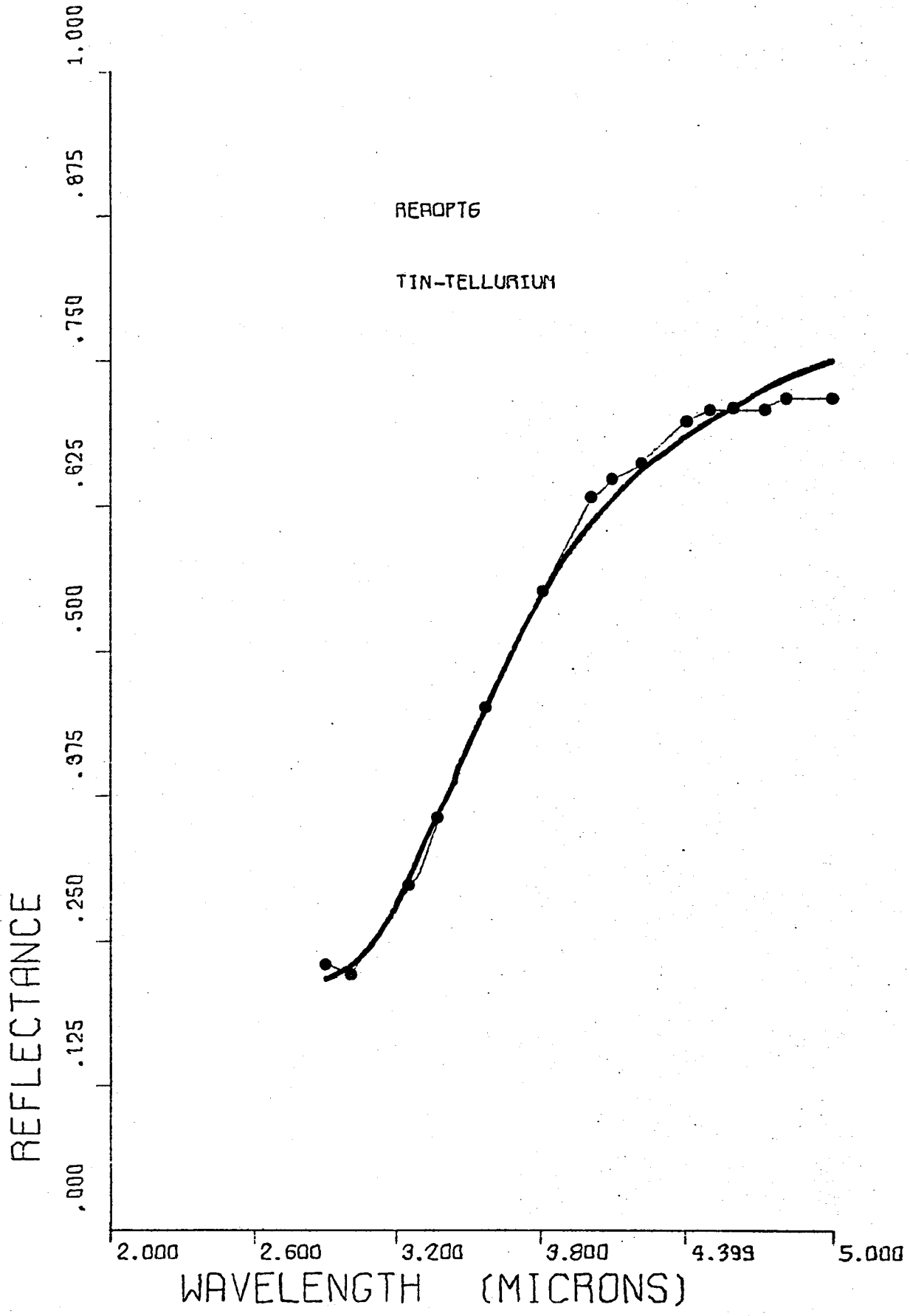

Fig.(D-8) ● Experimental reflectivity spectrum of SnTe film

——Fitted curve assuming that the reflectance is the one of a bulk material , see Table (D-4).

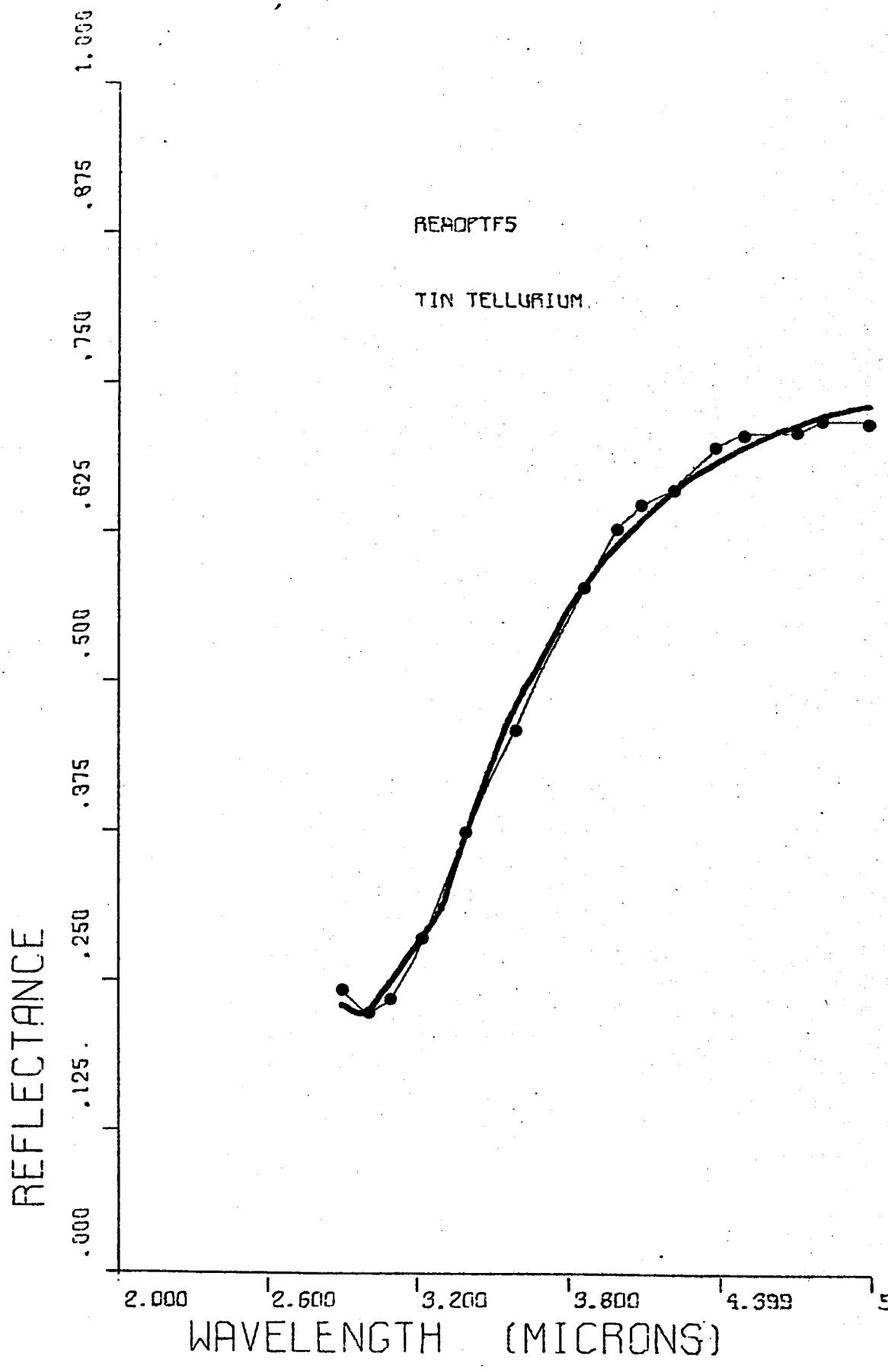

Fig.(D-9) • Experimental reflectivity spectrum of the SnTe film of fig. (D-8).

—— Fitted curve including the film thickness as a parameter.

Discrepancies in the values of ω_p and λ_p are due to differences in free carrier density. As far as the lattice dielectric constant is concerned, it has been calculated from a trial - and - error method. Unfortunately the previously described method does not always give optimum values for the parameters. It has been found that the objective function does not have a minimum for all the values of film thickness. In these cases approximate values can be calculated for the parameters by assuming that the reflectivity data are these of bulk. The reflectivity data of a thin tin - doped In_2O_3 film have been treated in that way.

Table (D-5) compares the classical oscillator parameters for a tin - doped indium oxide $\lambda/4$ film fabricated by THORN LIGHTING LTD., with experimental data obtained from the literature, Köstlin et al. (1974).

TABLE (D-5) (Sn - doped, In_2O_3 film)

	THE PRESENT METHOD (*)	DATA FROM THE LITERATURE
τ	3.85×10^{-15} sec	-
ε_L	8	4.0 (**)
ω_p	1.73×10^{15} sec^{-1}	1.57×10^{15} sec^{-1}
λ_p	1.1 μm	1.2 μm
m_r^*	-	0.54

(*) see fig. (D.10).

(**) This value has been calculated by neglecting τ .

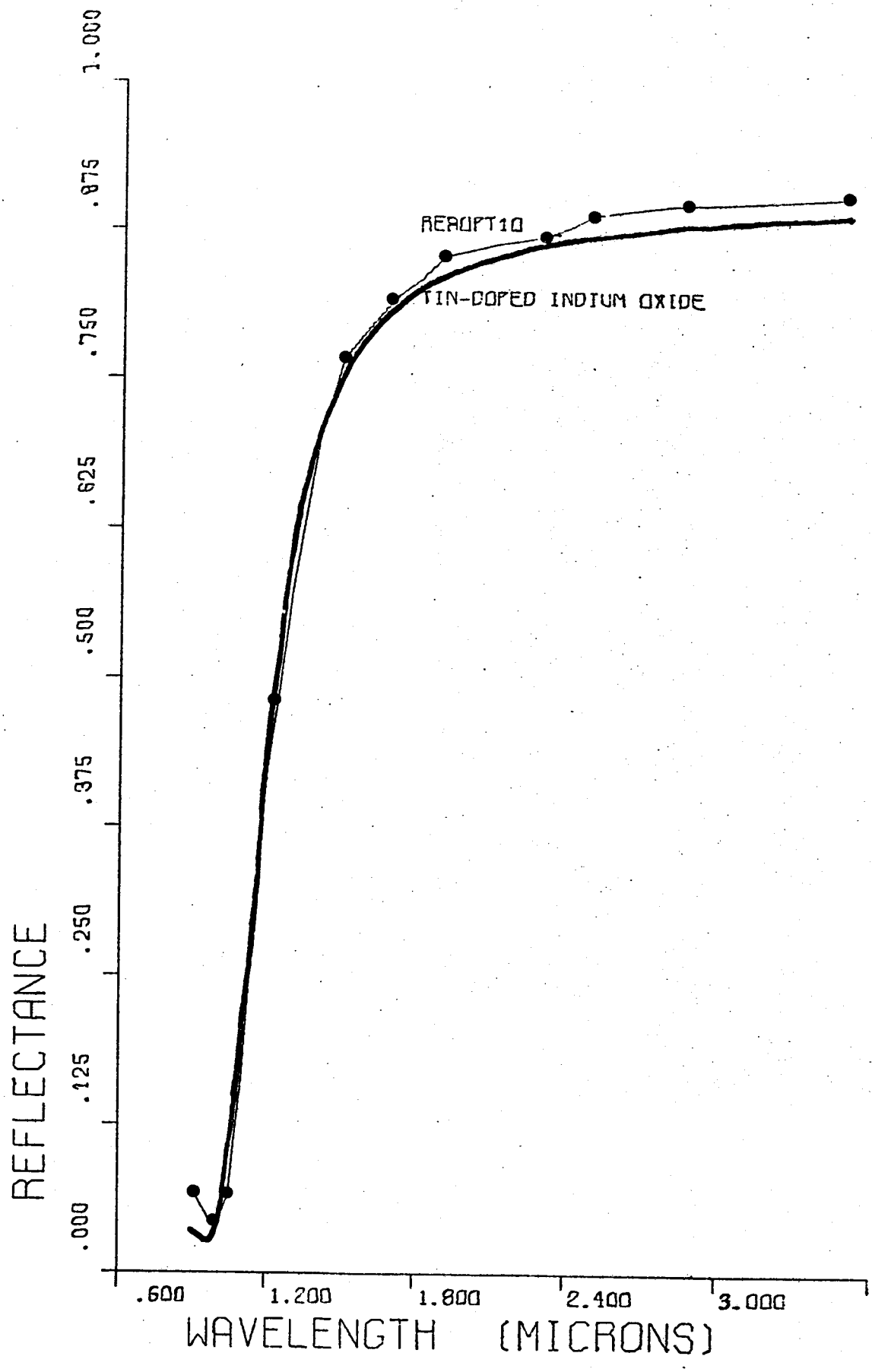

Fig. (D-10) ● Experimental reflectivity spectrum of a tin-doped indium oxide film.

—— Calculated reflectance according to the present method.

D.4 Remarks

Over - all errors in ε_L, ω_p, and τ are difficult to estimate but may be presented by the uncertainties associated with the curve fitting procedure.

Since we observed that the changes of each parameter has a rather unique effect on the reflectivity curve the sensitivity of the reflectivity to changes in the values of the parameters may give an estimate of the errors in the parameters. The sensitivity of the reflectance spectrum to changes in the parameters was checked by altering the optimum values until a change was monitored at the first decimal point of most of the reflectance values. In order to create such changes in the examples already worked, the following normalized changes of the values of the parameters were generally required:

$$\frac{\Delta \varepsilon_L}{\varepsilon_L} \simeq \pm 10\ \% \text{ to } 90\ \%$$

depending on whether ε_L is comparatively large (~ 90) or small (~ 8) respectively.

$$\frac{\Delta \omega_p}{\omega_p} \simeq \pm 10\ \%$$

and

$$\frac{\Delta \tau}{\tau} \simeq \pm 15\ \% \text{ to } \pm 30\ \%$$

depending on whether $\omega\tau \geq 1$ or $\omega\tau \ll 1$ respectively.
Thus, for a value of lattice dielectric constant equal to 8 a maximum

error of about $\pm$ 7 can be quoted to the optimum value given by the present method.

Also, the limitations of the present method are heavily depended on the accuracy of the experimental data used. It can be argued that when τ becomes negligible, i.e. $\omega\tau \ll 1$, the accuracy of the calculated values for τ becomes rather small.

However, in this case the same argument can be raised for most of the popular techniques. Moreover, it is obvious from the present results that the method is capable of giving accurate values for the relaxation time even when $\omega\tau$ is considerably small (GaAs) and it is not likely to find materials with much smaller values of $\omega\tau$ than the ones already examined.

As far as the computer time is concerned the total number of iterations did not exceed in any case the 500. This figure is equivalent to much more less than 1000 MILS, for the ICL 1900 computer.

Consequently this method can be used as a non - destructive technique for a quick evaluation of optical properties of a conducting material in the vicinity of its plasma edge. Moreover, the fact that this method makes use of a general purpose computer subroutine makes it suitable for application in a wide range of conducting materials for quick and rather accurate checks of relaxation time, lattice dielectric constant, and plasma frequency.

Finally, it is worth noting that the relative mass can be calculated from the effective number of free carriers (N / m_r^*) found by the present

method, if N is known, from Hall measurements for example. The accuracy of its value depends on the accuracy with which N has been measured.

The general type of computer programs written for the deduction of optical properties from reflectivity data will be shown in the following pages. The program shown assumes bulk-like optical behavior.

```
JOB FREAP100,P,JA1757
LUFORTRAN
JOBCORE 50000
VOLUME 15000
RUN ;,1000
****
DOCUMENT SOURCE
      LIBRARY(ED,SUBGROUPNAGF)
      LIBRARY (ED,SUBGROUPGRAF)
       PROGRAM(P001)
      INPUT 1 = CR0
       OUTPUT 2 = LP0
      COMPACT
      COMPRESS INTEGER AND LOGICAL
      TRACE 0
      END
```

```
      MASTER FREAP100
      INTEGER Q
      REAL L
      DIMENSION R(100),Y(100),L(100),SCONT(3),W(900),EN(100),EK(100),
     *EA(100),EB(100)
     *,EE1(50),EE2(50),TTR(50),TTN(50),TTK(50)
     *,G(100),OMEGAT(50),W1(50),W2(50),DRRR(50),DRR1(50)
     *,W11(50),W22(50),DRIRS(50)
     *,R1(30),R2(30),DELTA1(30),DELTA2(30)
      COMMON Y,L
      EXTERNAL SUMSQ,MONIT
      NO=1
      K=3
      IA=18
      J=IA
      IW=2*J*K+2*K*K+2*J+5*K
       ACC=0.1E-11
      H=0.1E-07
C    EXPERIMENTAL DATA OF  * * * *   GETE  * * * * *
      DMAX=10
      MAX=800
      IFAIL=1
C ------------------------------------------------------------------
C THIS PROGRAM MINIMIZES A SUM OF SQUARES USING A STRATEGY WHICH
CIS SIMILAR TO THAT APPLIED BY  POWELL (1968).
```

```
C ------------------------------------------------------------------
C ------------------------------------------------------------------
C    IA  IS EQUAL TO THE TOTAL NUMBER OF EXPERIMENTAL POINTS.
C  ------------------------------------------------------------------
      DO 102 I=1,IA
      READ(1,101) L(I),Y(I)
      WRITE(2,103) L(I),Y(I)
101   FORMAT(F3.1,2X,F5.3)
103   FORMAT(20X,'L= ',F5.2,5X,'REXP= ',F4.2)
102   CONTINUE
C ------------------------------------------------------------------
C  ESTIMATED OPTIMAL VALUES FOR T,EL,OMEGAP :
C SCONT(1) : T*CONSTANT1
C  SCONT(2) : EL
C  SCONT(3) : OMEGAP*CONSTANT3
      TINITIAL =6.0
      SCONT(1)=SQRT(TINITIAL)
      SCONT(2)=4.2
      SCONT(3)=5.24
C ------------------------------------------------------------------
C ------------------------------------------------------------------
      WRITE(2,44) TINITIAL,SCONT(2),SCONT(3)
44    FORMAT(//////////,30X,'INITIAL ESTIMATES OF SCONT : ',3X,
     *'T= ',E11.4,5X,'EL= ',E11.4,5X,'OMEGAP= ',E11.4)
      CALL E04FBF(IA ,3,SCONT,R,SSQ,ACC,H,DMAX,W,IW,SUMSQ,MONIT,1,MAX,
```

```
     *IFAIL)
       WRITE(2,55) SSQ
55     FORMAT(/////,30X,'SUM OF SQUARES =  ',E11.4)
       WRITE(2,66) IFAIL
66     FORMAT(/////,30X,'IFAIL= ',I1)
77      FORMAT(1H1)
       DO 4 I=1,25
4      WRITE(2,99) L(I),Y(I),R(I)
99     FORMAT(5X,'L= ',F5.2,5X,'RGIVEN= ',E14.6,5X,'DRFINAL= ',E14.6)
88      FORMAT(1H1)
       CC=0.3E+15
       VELOC=4*3.14*3.14*(CC**2)
       CONST1=0.1E-14
       CONST2=10.0
       CONST3=0.1E+15
       DO 313 I=1,IA
       EE1(I)  =SCONT(2)*CONST2*(1-((SCONT(3)**2)*(CONST3**2)/
     *(VELOC/(L(I)**2)+1./((SCONT(1)**4)*(CONST1**2)))))
       EE2(I)  =SCONT(2)*CONST2*(SCONT(3)**2)*(CONST3**2)*L(I)/
     *(SQRT(VELOC)*(SCONT(1)**2)*CONST1*(VELOC/(L(I)**2)+
     *1./((SCONT(1)**4)*(CONST1**2))))
       TTN(I)=SQRT(0.5*(SQRT(EE1(I)**2+EE2(I)**2)+EE1(I)))
       TTK(I)=EE2(I)/(2*TTN(I))
       TTR(I)=((TTN(I)-NO)**2+TTK(I)**2)/((TTN(I)+NO)**2+TTK(I)**2)
       WRITE(2,314) L(I),EE1(I),EE2(I),TTN(I),TTK(I),TTR(I)
```

```
314    FORMAT(1H ,'L= ',F5.2,3X,'E1= ',E14.6,3X,'E2= ',E14.6,3X,'N= ',
     *E14.6,3X,'K= ',E14.6,5X,' ROPT= ',E14.6)
313    CONTINUE
       DO 316 I=1,IA
 316   WRITE(2,315) L(I),TTR(I),Y(I)
315    FORMAT(20X,'L= ',F5.2,5X,'ROPT,= ',E14.6,5X,'REXP,= ',E14.6)
       SQ=0.1602E-18
C    FILM THICKNESS (IN MICR) :
       D1=0.15
       C=0.3E+09
       CC=0.3E+15
       CAPACITANCE=0.1
C    EFFECTIVE MASS
       FMR=0.14
C    REFRACTIVE INDEX OF SUBSTRATE:
       AN3=1.5
       EM=0.91091E-30
       T=(SCONT(1)**2)*CONST1
       EO=0.885416E-11
       VELOC=4*3.14*3.14*(CC**2)
       V=1.0
       NO=1
       CONS=4*NO*SQ*CAPACITANCE*V/(C*FMR*EM*EO)
       DO 211 I=1,IA
       OMEGAT(I)=2*3.14*CC*(SCONT(1)**2)*CONST1/L(I)
```

```
      G(I)=2*(OMEGAT(I)*(TTN(I)**2-TTK(I)**2-NO**2)+2*TTN(I)*TTK(I))/
     *(TTN(I)**2-TTK(I)**2-NO**2+2*TTN(I)*TTK(I)*OMEGAT(I))
211   WRITE(2,212)  OMEGAT(I),L(I),G(I)
212   FORMAT(5X,'OMEGAT= ',E11,3,5X,'L= ',F6.3,5X,'G= ',E11,3)
      DO 213 I=1, IA
      R1(I)=SQRT(((NO-TTN(I))**2+TTK(I)**2)/((NO+TTN(I))**2+TTK(I)**2) )
      R2(I)=SQRT(((TTN(I)-AN5)**2+TTK(I)**2)/((TTN(I)+AN3)**2+TTK(I)**2)
     *)
      BETA=4*3,14*TTK(I)*D 1 /L(I)
      DELTA=4*3,14*TTN(I)*D 1 /L(I)
      DELTA1(I)=ATAN(2*TTK(I)/((1-TTN(I))*(1+TTN(I))-TTK(I)**2))
      DELTA2(I)=ATAN(3*TTK(I)/((1,5-TTN(I))*(1+TTN(I))-TTK(I)**2))
      IF(DELTA1(I),LT,0) DELTA1(I)=DELTA1(I)+3,14
      IF(DELTA2(I),LT,0)  DELTA2(I)=DELTA2(I)+3,14
      FI=DELTA2(I)-DELTA1(I)-DELTA+3,14
      THETA=DELTA2(I)+DELTA1(I)-DELTA+3,14
      W1(I)=(1+(R2(I)/R1(I))*EXP(-BETA)*COS(FI)+G(I)*(R2(I)/R1(I))*EXP
     *(-BETA)*SIN(FI))/(1+(R2(I)**2/R1(I)**2)*EXP(-2*BETA)+2*(R2(I)/R1(I
     *))*EXP(-BETA)*COS(FI))
      W2(I)=((R1(I)**2)*(R2(I)**2)*EXP(-2*BETA)+R1(I)*R2(I)*EXP(-BETA)*
     *COS(THETA)+G(I)*R1(I)*R2(I)*EXP(-BETA)*SIN(THETA))/(1+(R1(I)**2)*
     *(R2(I)**2)*EXP(-2*BETA)+2*R1(I)*R2(I)*EXP(-BETA)*COS(THETA))
      DRR1(I)=CONS*(L(I)/(VELOC+(L(I)**2/T**2)))*
     *(+SQRT(VELOC)*TTN(I)*TTK(I)-L(I)*(TTN(I)**2-TTK(I)**2-NO**2)/T)/
     *((TTN(I)**2-TTK(I)**2-NO**2)**2+4*(TTN(I)**2)*(TTK(I)**2))
```

```
      DRRR(I)=(W1(I)-W2(I))*DRR1(I)
      WRITE(2,214)  L(I),DRR1(I),DRRR(I),W1(I),W2(I)
214   FORMAT(1H ,'L= ',F6.3,2X,'[DR1/R1]= ',E11.3,2X,'[DR/R]= ',E11.4,
     *10X,'W1= ',E11.4,2X,'W2= ',E11.4)
213   CONTINUE
C     ------- PLOTTING SUBROUTINES -*----  * * * * * * * * * * ** * *
      CALL UTPOP
      CALL UTP3(CHAR,4,0,4.0,-1)
      CALL UTP4A(3.4,5.4,0.011,0.023,5.0,6.0,
     *21HWAVELENGTH  (MICRONS) ,3,22H      [DR/R,V]  1/VOLTS ,3)
      CALL UTP6V(3HERS ,1,3,0.0,2.75,4.0,0.3)
      CALL UTP6V(4HGETE ,1,4,0.0,2.7,3.5,0.4)
      CALL UTP4B(L(7),DRRR(7),11,1)
      CALL UTPCL
C - - - - - - - - - - - - - - - - - - - - - - - - - - - - - - - - - - -
C----------------------   I,R,S,   --------------------------
      DO 824 I=1,IA
      BETA=4*3.14*TTK(I)*D 1 /L(I)
      DELTA=4*3.14*TTN(I)*D 1 /L(I)
      DELTA4=DELTA1(I)
      DELTA3=DELTA2(I)
      FI=DELTA4-DELTA3-DELTA+3.14
      THETA=DELTA4+DELTA3-DELTA+3.14
      R3=R2(I)
      R4=R1(I)
```

```
      W11(I)=(EXP(-BETA)+(R3/R4)*COS(FI)+(R3/R4)*G(I)*SIN(FI))/
     *((R3**2/R4**2)+EXP(-2*BETA)+2*(R3/R4)*EXP(-BETA)*COS(FI))
      W22(I)=((R3**2)*(R4**2)*EXP(-BETA)+R3*R4*COS(THETA)+
     *R3*R4*G(I)*SIN(THETA))/
     *(1+(R3**2)*(R4**2)*EXP(-2*BETA)+2*R3*R4*EXP(-BETA)*COS(THETA))
      DRIRS(I)=(W11(I)-W22(I))*EXP(-BETA)*DRR1(I)
      WRITE(2,823) L(I),DRIRS(I),W11(I),W22(I)
823   FORMAT(25X,'L= ',F5.3,5X,'[DR/R] IRS= ',E11.4,5X,'W11= ',E11.4,
     *3X,'W22= ',E11.4)
824   CONTINUE
      STOP
      END
```

```
      SUBROUTINE SUMSQ(J,K,SCONT,R)
      DIMENSION SCONT(K),R(J),Y(100),L(100)
      REAL L
      COMMON Y,L
      CC=0.3E+15
      CONST1=0.1E-14
      CONST2=10.0
      CONST3=0.1E+15
      VELOC=4*3.14*3.14*(CC**2)
      NO=1
      DO 1 I=1,J
      E1=SCONT(2)*CONST2*(1-((SCONT(3)**2)*(CONST3**2)/
     *(VELOC/(L(I)**2)+1./((SCONT(1)**4)*(CONST1**2)))))
      E2=SCONT(2)*CONST2*(SCONT(3)**2)*(CONST3**2)*L(I)/
     *(SQRT(VELOC)*(SCONT(1)**2)*CONST1*(VELOC/(L(I)**2)+
     *1./((SCONT(1)**4)*(CONST1**2))))
      TN=SQRT(0.5*(SQRT(E1**2+E2**2)+E1))
       TK=E2/(2*TN)
      TR=((TN-NO)**2+TK**2)/((TN+NO)**2+TK**2)
1     R(I)=TR-Y(I)
      RETURN
      END
```

```
      SUBROUTINE MONIT(J,K,SCONT,R,SSQ,ICALLS)
      DIMENSION SCONT(K),R(J)
      WRITE(2,100) ICALLS
100   FORMAT(/////,5X,'ICALLS=  ',I3)
       WRITE(2,200) SSQ
200    FORMAT(//,5X,'SUM OF SQUARES : ',E14.6)
      WRITE(2,300) (SCONT(I),I=1,K)
300    FORMAT(/////,5X,'VALUES OF TEL,OMEGAP ARE ACCORDINGLY : ',
     *3E14.6)
       RETURN
      END
```

REFERENCES

1. Abelès, F. and Thèye, M.L. Surf. Sci. 5 , 325 (1966).
2. Avaritsiotis J., M.Sc. Thesis, 1974 , Loughborough University of Tech.
3. Bennett, J.M. and Booty, M.J. Appl. Opt. 5, 41 (1966).
4. Bowlden H.J. and Wilmshurst, J.K. J.Opt.Soc.Am. 53, 1073 (1963).
5. Fox J.T., Howson and Emmony D.C. J.Appl. Phys. D, 7, 1864 (1974).
6. Harris L and Corrigan F.R. J.Opt. Soc.Am. 54, 143 (1964).
7. ———————————— Phys. Chem. Solids 26, 307 (1965).
8. Harris L. and Loeb A., J.Opt.Soc.Am, 45, 179 (1955).
9. Heavens, O.S., in Optical Properties of Thin Solid Films, Dover Publ. Inc. New York, 1965.
10. ———————— Physics of Thin Films Vol. 2 ,p. 193, 1964.
11. Köstlin H., Jost R.,Leims W., Philips Publications No 20/74 24.09.74/Ko
12. Rivory J., Optics Comm. 1, 334 (1970).
13. Robinson, T.S., Proc.Phys.Soc.(London) B65,910 (1952).
14. Simon I.,J. Opt. Soc.Am. 41, 336 (1951).
15. Ward, L.,Nag, A. and Dixon,L.C.W. Brit.J.Appl.Physics (J.Phys.D.), 2 , 301 (1969).
16. Wohlgemuth, J.H. and Brodie D.E. Canad.J.Phys., 53,1737 (1975).

APPENDIX E

A WAVELENGTH MONITOR FOR A SINGLE BEAM MONOCHROMATOR

It is often desirable with a single beam monochromator to scan through a band of wavelengths and produce a record of the output intensity against wavelength. The Hilger and Watts D310 double monochromator is provided with a motor drive which gives a wavelength output as a fraction of time, this letter shows a simple adaptation of this drive with no mechanical modifications to the instrument which provides a calibrated output voltage representing the wavelength.

Fig. (E-1) is a diagram of the mechanical parts of the attachment. An aluminium arm screwed on the side of the monochromator body, by the two existing screws, is the supporting frame of the whole mechanism. The rotation of the wavelength dialing drum is transmitted through a combination of coax-shafts (telescopic drive) to a 48DP 30 teeth Brass gear and a five lobe cam. A five lobe cam was used because five marks were needed, during one revolution of the wavelength dialing drum, each one corresponding to the 1/50 of the scale on the drum. The combination of the coax-shafts allows for the synchronous displacement of the micrometer drum. The inner shaft is connected to the drum by a pin, passed through an existing hole and it slides "in" and "out" inside the outer shaft applying on the latter torque at the same time.

A second 48DP 120 teeth Brass gear, which is engaged with the 30 teeth gear, rotates a 10-turn linear helipot (10KΩ). The combination of the two gears transforms the rotation of the wavelength dialing drum by a ratio of 4:1. This is necessary since the dialing drum rotates 40 times in order to scan the whole scale and there is no 40-turn helipot available on the market.

The helipot is electrically connected to a stabilized power supply through two potentiometers which are necessary for the initial calibration

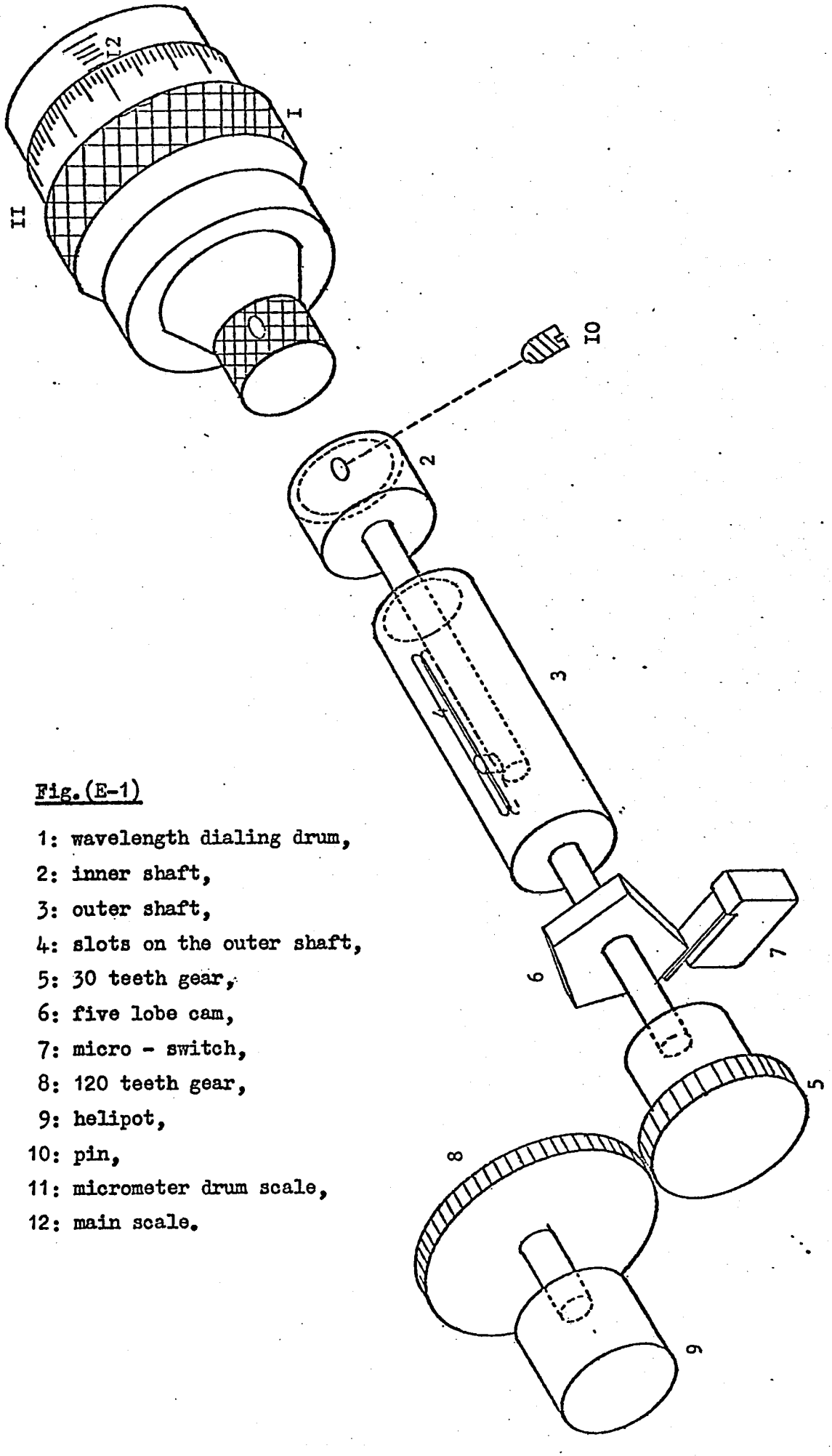

Fig.(E-1)

1: wavelength dialing drum,
2: inner shaft,
3: outer shaft,
4: slots on the outer shaft,
5: 30 teeth gear,
6: five lobe cam,
7: micro - switch,
8: 120 teeth gear,
9: helipot,
10: pin,
11: micrometer drum scale,
12: main scale.

of the d.c. voltage on the output of the pot. The output voltage of the pot is fed into a digital voltmeter, which is placed near the recorder, displaying the drum settings.

The five lobe cam operates a microswitch, the signal from which is processed to give a pulse of adjustable height which is subsequently recorded as a "pip" on the recorded spectrum. Preliminary adjustment of the position of the microswitch brought the reference "pips" in exact coincidence with certain divisions of the scale of the micrometer drum. The coincidence was exact for all the divisions of the main scale. The reference marks occured at 50 drum scale subdivision intervals; this was taken into consideration for the establishment of a convenient fiducial scale (in drum subdivisions) in step with the nominal wavelength. The final complete calibration of the instrument was then established by plotting the fiducial scale values of the calibrant lines as abscissa against the corresponding true wavelengths as ordinate. No special temperature or humidity control was employed for the room.

The motor control box, which allows for "forward" and "reverse" spectrum scanning, was removed from the monochromator and it was placed near the pen-recorder.

The described attachment has successfully been used and it has required no maintenance or re-calibration for more than one year.

Fig.(E-2) shows the actual wavelength monitor. Fig. (E-3) is the electronic circuit of the pen recorder marker unit used to control the height of the "pips".

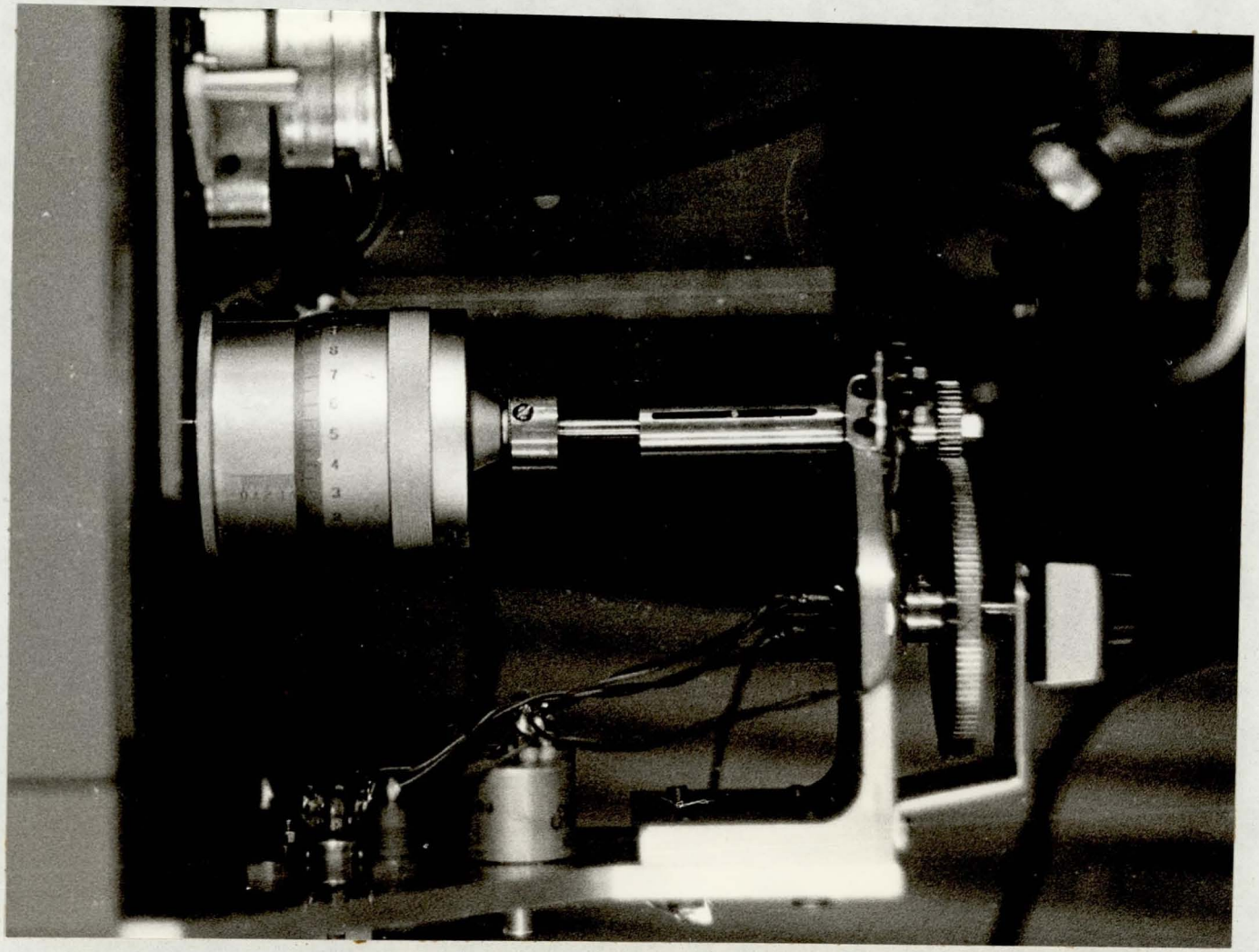

Fig.(E-2) Photograph of the wavelength monitor.

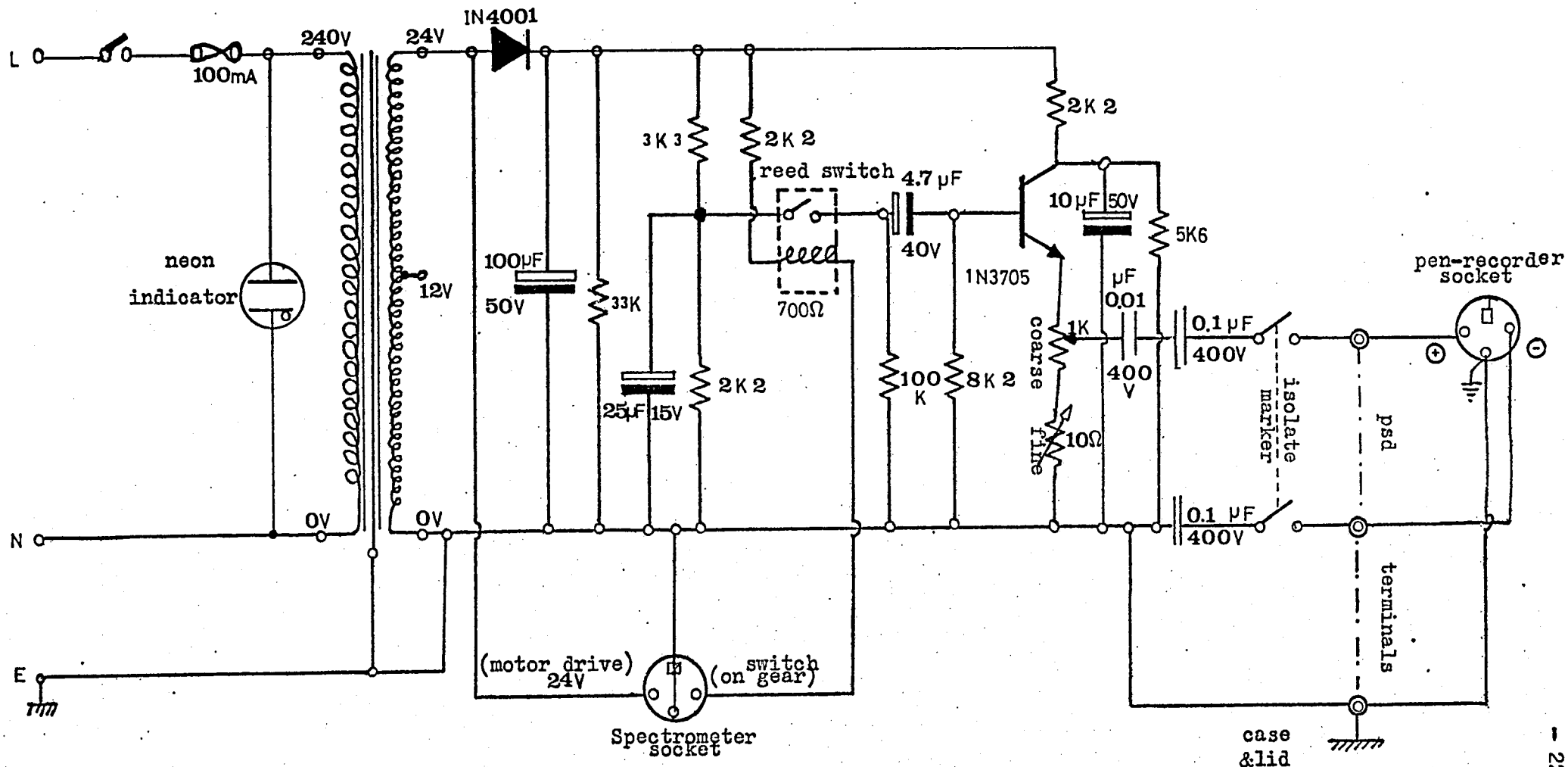

Fig.(E-3) Pen - recorder marker unit.